UNIVERSIDADE DO ALGARVE

Climatic variability and recent sedimentation in the Continental Shelf off the Guadiana River

Francisca Manuel Prudêncio Rosa

Dissertação para obtenção do Grau de Doutor em Ciências do Mar, da Terra e do Ambiente, Ramo Geociências, Especialidade Paleoceanografia

Trabalho efetuado sob a orientação de:

Prof. Doutor João Manuel Alveirinho Dias

Prof. Doutor Óscar Manuel Fernandes Cerveira Ferreira

2014

Climatic variability and recent sedimentation in the Continental Shelf off the Guadiana River

Declaração de autoria do trabalho

_____ Declaro ser a autora deste trabalho, que é original e inédito. Autores e trabalhos consultados estão devidamente citados no texto e constam da listagem de referências incluída.

Ser feliz é se tornar um autor da própria história…
É atravessar desertos fora de si, mas ser capaz de encontrar
Um oásis no recôndito da sua alma.

Pedras no caminho?
Guardo todas, um dia vou construir um castelo…

Fernando Pessoa

Aos meus avós,

e à minha mãe

Agradecimentos

A realização deste trabalho não teria sido possível sem o contributo e o apoio, quer diretos, quer indiretos, de uma série de pessoas e instituições, às quais quero deixar aqui o meu mais profundo agradecimento.

Em primeiro lugar, quero agradecer sinceramente aos meus dois orientadores, o Professor Doutor João Alveirinho Dias e o Professor Doutor Óscar Ferreira, que me acompanharam e incentivaram ao longo de todos estes anos dedicados à investigação científica. De igual forma, pela oportunidade que me ofereceram de crescer, como investigadora e como pessoa, no seio de um verdadeiro grupo de trabalho, onde a união fez sempre a força… Inclusive na concretização desta tese.

Ao Francisco Fatela, dedico um agradecimento muito especial e profundo, por me ter iniciado na carreira de micropaleontóloga, por ter cultivado em mim o gosto pelo debate saudável de ideias, e por todo o apoio e amizade que nunca deixou de me dedicar ao longo de todos estes anos.

Ao César Andrade, pelo mesmo apoio e pela mesma amizade genuína. Obrigada por todas as palavras e todos os conselhos que me ajudaram desde sempre a acreditar mais em mim, a acreditar mais na ciência, e a acreditar que nunca se desiste.

Ao Óscar, novamente, não como orientador, mas como pessoa e como amigo. Obrigada pela confiança e pelo apoio inabaláveis, os quais foram determinantes durante esta longa (e tantas vezes, árdua!) jornada.

Muito mais do que colegas, às queridas amigas Isabel, Ritinha, Ana Matias e Margarida, e ao André Pacheco, por todo o apoio, pelo companheirismo, pela aprendizagem, pela partilha e, sobretudo, pela amizade verdadeira construída ao longo dos anos.

Aos colegas do Ciacomar/CIMA, Carlos Loureiro, Mara Nunes, Sr. Cunha, Tiago Garcia, Simon Connor, João Horta e Sónia Oliveira. Em particular, às companheiras de gabinete, Sarita, Laura, Ana e Liliana, com quem partilhei o meu quotidiano, e as angústias e as vitórias do mundo da investigação, durante muito tempo.

Ao Paco Lobo, pela disponibilidade e pelo gosto em debater todas as ideias científicas!

Um agradecimento também a todas as pessoas que, antes da minha chegada à Universidade do Algarve, participaram no projeto CRIDA e contribuíram para a colheita das amostras que se tornaram no objeto de estudo deste trabalho.

À Selma, pela receção calorosa aquando a minha chegada ao Algarve, e pelos muitos momentos de amizade genuína que partilhámos desde então.

À Silvia Ortiz, colega e amiga da Petrostrat, pelo apoio moral na fase final de escrita e, sobretudo, pela disponibilidade que teve para rever na íntegra o capítulo maior e mais importante da tese.

À Marisa, por todo o apoio e generosidade naquele que foi um dos momentos mais difíceis que atravessei até hoje, o início da minha vida de emigrante. E depois, na fase final de escrita da tese, já em Gales, pela compreensão em todas as minhas 'ausências' forçadas por essa tarefa totalmente absorvente, em todas as noites de ansiedade, e em todos os dias de desalento!

Ao Severino, meu 'hermanito', pela amizade, pela paciência!, e pela partilha de dúvidas e incertezas ao longo das nossas respetivas teses, mas também de tantos momentos em que nos vingámos de todas elas e soubemos aproveitar a vida!

À Ana Gomes. Todos os obstáculos e todas as difíceis encruzilhadas se tornam mais leves quando podemos compartilhar tudo isso com uma companheira à altura da tarefa. Obrigada, minha linda amiga.

À Sara e à Catarina, companheiras de longa data e cuja amizade, insubstituível, ajudou a povoar de muitas gargalhadas e muitos momentos de pura comunhão, o caminho trilhado durante os últimos quinze anos.

À Sandra, amiga de uma vida inteira, literalmente!, e à Rita, a primeira pessoa com quem descobri todo o significado da palavra 'amizade'… Que venham, pelo menos, mais vinte anos!

À Sylvie. Amiga e companheira, transformada numa irmã desde que fui viver para o Algarve. Juntas, sobrevivemos a tantos obstáculos e tormentos mas, sobretudo, vivemos, e saboreámos!, outros tantos momentos de felicidade e de saudável alegria de viver.

À Sílvia. Amiga do meu coração, companheira na saúde e na doença, na alegria e na tristeza, nos bons e nos maus momentos… Em todas as despedidas e em todos os regressos. Os nossos braços dados são a construção mais sólida do mundo! Mais palavras, para quê?

À Fátima. Por todo o carinho, apoio e amizade sincera.

À minha família, os Prudêncios. Porque todos os rebentos que um dia deram fruto devem tanto a árvore e à sua raiz!

À minha mãe, que me apoiou, incentivou e, como sempre, me inspirou ao longo de toda esta jornada com o seu exemplo de dedicação, perseverança, coragem e profissionalismo. Sobretudo, pelo seu amor inabalável e pela confiança que soube transmitir-me em cada etapa do percurso.

À minha irmã. Criança que iluminou todos os meus dias e, agora, transformando-se em mulher, continua a acompanhar-me nesta maravilhosa viagem que é a vida.

Ao Bruno. Meu namorado, companheiro e amigo, que me ajudou a descobrir os profundos e múltiplos significados que cabem por dentro da palavra Amor.

Uma vez mais, e como sempre, aos meus avós, Manuel e Júlia... A quem julgo dever a melhor parte de mim mesma.

Finalmente, um reconhecimento muito especial, não a uma pessoa, mas a um lugar. Ao meu querido Algarve, terra de muito sol e muito mar, eternamente florido com os seus campos de amendoeiras e laranjeiras, com o seu manto infindável de estevas. Dele guardo o aroma fresco a hortelã e poejo das ribeiras, polvilhado pelo vermelho-vivo dos medronhais, o cheiro à maresia da Ria Formosa e ao sal dos areais infinitos. Horizonte claro e limpo, cuja luz marinha é alimento para a alma. Na cal das paredes e das chaminés rendilhadas, no oscilar dos botes em cada virar da maré… Casa é onde vive o coração.

APOIO INSTITUCIONAL E FINANCEIRO

- Fundação para a Ciência e a Tecnologia (FCT), através da bolsa de doutoramento com a referência SFRH/BD/46020/2008.

- Projeto CRIDA (Consequences for river discharge modifications on coastal zone and continental shelf) (Ref. POCTI/P/MAR/15289/99, FCT).

- Projeto IMCA (Impact of climatic and anthropic variations on the Northern continental shelf, Gulf of Cadiz) (Ref. POCI/CLI/60192/2004, FCT).

- Projeto CIRCO (Climate changes from isotopic records during the Holocene in Southwestern Iberia) (Ref. PTDC/CLI/66393/2006, FCT).

- Centro de Investigação Marinha e Ambiental (CIMA) da Universidade do Algarve.

RESUMO

O presente trabalho investiga os principais eventos deposicionais ocorridos na plataforma continental adjacente ao Rio Guadiana (norte do Golfo de Cádis, Sudoeste da Península Ibérica) durante o final do Pleistocénico e o Holocénico, e sua relação com os mecanismos forçadores, nomeadamente as variações climáticas, a subida do nível médio do mar e o impacte das ações antrópicas na região. Recorreu-se a uma abordagem integrada de vários indicadores em quatro testemunhos verticais de sedimentos (cores) recolhidos na plataforma, incluindo dados sedimentológicos (textura sedimentar, componentes da fração areia e morfoscopia do quartzo) e micropaleontológicos (foraminíferos bentónicos), integrados numa malha temporal construída com base em datações radiocarbono. Destes testemunhos, um localizou-se no ambiente da plataforma interna e os restantes no ambiente do corpo lodoso do Guadiana, a várias profundidades da plataforma média. A análise e integração dos dados permitiram reconhecer a evolução específica dos padrões deposicionais em cada um dos ambientes e fazer uma interpretação evolutiva do próprio corpo lodoso, cuja maior resolução temporal possibilitou, por sua vez, reconstruir mais detalhadamente a história evolutiva da região. Durante a fase mais acelerada da transgressão marinha pós-glaciar que caracterizou o final do Pleistocénico e o início do Holocénico, ambos os ambientes revelaram sequências com tendência transgressiva. A subida do nível do mar constituiu o principal fator condicionante do tipo e quantidade de sedimentos fornecidos à plataforma, bem como das espécies de foraminíferos colonizadoras desses sedimentos. Com o nível do mar a aproximar-se do atual por volta do Holocénico médio, os fatores climáticos revelaram-se preponderantes na evolução dos padrões depocicionais e ecológicos. Foram registadas profundas alterações durante os últimos cerca de 2,500-1,500 anos, com maiores quantidades de finos a serem fornecidos à plataforma e uma mudança clara nas faunas de foraminíferos do corpo lodoso. As ocupações Romana e Islâmica do sul da Península Ibérica terão tido grande importância no desenvolvimento destas alterações, provocando profundos impactes na paisagem e nas taxas de erosão ao longo da Bacia do Guadiana. Desde então, e até próximo da atualidade, o registo da plataforma e do corpo lodoso revelaram terem sido os impactos antrópicos aliados às oscilações mais recentes do clima, em grande parte modeladas pela Oscilação do Atlântico Norte (NAO), os principais agentes modeladores de toda a região em estudo.

Palavras-chave: Plataforma do Guadiana, Plistocénico/Holocénico, variações climáticas, sedimentos, foraminíferos bentónicos, reconstrução paleoambiental

ABSTRACT

The current work investigates the main depositional events that occurred on the continental shelf adjacent to the Guadiana River mouth (northern Gulf of Cadis, southwestern Iberian Peninsula) during the late Pleistocene and the Holocene, and relates them with main forcing mechanisms, namely climate change, mean sea-level rise and the impact of human activities in the region. An integrated approach based on several palaeoindicators was conducted in four sediment cores collected on the shelf, including sedimentological (sediment grain-size, sand fraction composition and morphoscopy of quartz grains) and micropalaeontological (benthic foraminifera) data, integrated into a temporal framework obtained from AMS (Accelerated Mass Spectometry) radiocarbon (^{14}C) datings. One of these cores was located on the inner shelf and the other three on the mid-shelf mud body. Data analysis and integration allowed to recognize the specific evolution of the depositional patterns in each one of these shelf domains and to interpret the evolution of the mud body. Moreover, the higher resolution of the muddy deposits enabled to reconstruct with greater detail the history of the region.

During the phase of fast sea-level rise that marked the late Pleistocene and the beginning of the Holocene, both shelf domains revealed a transgressive trend, with the rise in sea level constituting the main controlling factor of the type and amount of sediments that reached the shelf, and also of the main benthic foraminiferal species that colonized the middle shelf environment. As the mean sea level approached its present-day position around mid-Holocene, the climatic mechanisms became preponderant in determining the evolution of the depositional and ecological patterns across the shelf until ca. 2,500 years ago. Profound changes were observed during the last ca. 2,500-1,500 years, with higher amounts of sediments, mostly fine-grained, starting to reach the shelf and the onset of a clear modification on the benthic foraminifera of the mud body. The Roman and Islamic occupation of southern Iberia seemed to have been the main cause behind these changes, as they led to intensive land-use activities that enhanced soil erosion along the Guadiana Basin. Since then, and until modern times, the depositional record of the shelf and of the mud body, in particular, showed that the coupled-action of the anthropogenic impact with the more recent climate variations, these largely modulated by the North Atlantic Oscillation (NAO), has been the main forcing agent for the environmental changes occurring in the study area.

Keywords: Guadiana shelf, Pleistocene/Holocene, climate change, sediments, benthic foraminiferal, paleoenvironmental reconstruction

RESUMO ALARGADO

O presente trabalho teve como objetivo aprofundar os principais conhecimentos sobre os principais processos e eventos deposicionais ocorridos na plataforma continental adjacente ao Rio Guadiana (localizada no norte do Golfo de Cádis, Sudoeste da Península Ibérica) durante o período decorrente desde o final do Pleistocénico até à atualidade, e sua relação com os principais mecanismos forçadores, nomeadamente as variações climáticas, a subida do nível médio do mar e os impactes antrópicos na região. O Rio Guadiana drena uma vasta região com características semi-áridas, sendo o principal fornecedor de sedimentos e nutrientes à plataforma, sobretudo através de eventos de cheias. O regime fluvial deste rio, incluindo a generalidade da sua bacia hidrográfica, é altamente suscetível a alterações do clima. De igual forma, o intenso desenvolvimento humano que vem marcando toda a região da Bacia do Guadiana desde há milénios e, particularmente, após a Ocupação Romana da Península Ibérica, julga-se ter contribuído decisivamente para importantes alterações nos padrões erosivos dos solos, com consequências expectáveis ao nível do tipo e volume de sedimentos exportados pelo rio para o litoral e plataforma continental adjacente.

Tendo em vista o objetivo proposto, recorreu-se a uma abordagem integrada de indicadores presentes em quatro testemunhos verticais de sedimentos recolhidos na plataforma continental, incluindo dados sedimentológicos (textura sedimentar, composição da fração arenosa e morfoscopia dos grãos de quartzo) e micropaleontológicos (foraminíferos bentónicos), integrados numa malha temporal construída com base em datações radiocarbono. Destes testemunhos, um localizou-se no ambiente da plataforma interna, a cerca de 12 metros de profundidade e localizado a oeste da desembocadura do Rio Guadiana, e os outros três no corpo lodoso da plataforma adjacente à foz do Guadiana, na plataforma média, entre os 40 e os 90 metros de profundidade. A análise e integração de todos os dados permitiu, por um lado, reconhecer a evolução específica dos padrões deposicionais em cada um dos ambientes de plataforma e sua relação direta com as modificações nas descargas do rio e, por outro, fazer uma interpretação evolutiva do próprio corpo lodoso. A maior resolução temporal dos depósitos deste corpo sedimentar possibilitou, por sua vez, reconstruir mais detalhadamente os sucessivos paleoambientes e, por conseguinte, a história evolutiva da região.

Os padrões deposicionais ao longo da plataforma revelaram que ambos os ambientes foram sempre fortemente condicionados pelas variações no contributo sedimentar do Rio Guadiana e pela evolução geomorfológica do seu sistema estuarino, sendo que na área da plataforma interna foi também detetada uma forte influência dos processos de fornecimento e

redistribuição associados à deriva litoral. No caso específico do corpo lodoso, o registo sedimentar permitiu detetar esta tendência previamente ao Holocénico, isto é, desde o final do Pleistocénico e, em concreto, desde cerca dos 15,000 anos (cal. B.P.).

Durante o final do Pleistocénico e início do Holocénico, o impacto da rápida subida do nível médio do mar que marcou o período pós-glaciar sobrepôs-se claramente aos outros mecanismos forçadores, induzindo uma sucessão específica de paleoambientes à medida que ia submergindo extensas áreas da plataforma, com o local analisado da plataforma interna correspondendo então a um ambiente deltaico diretamente ligado à desembocadura do rio, enquanto os locais mais distais da atual plataforma média estariam situados num ambiente pouco profundo de plataforma interna. Esta sucessão ficou claramente registada nas sequências, quer da plataforma interna, quer do corpo lodoso, através da tendência transgressiva dos depósitos, bem como da diminuição gradual de componentes específicos da areia (outros terrígenos sem ser quartzo – OT, e fragmentos litoclásticos associados aos afloramentos rochosos da Bacia do Guadiana) e de grãos de quartzo pouco evoluídos (NU) que servem como indiciadores de maior proximidade à desembocadura do rio. O próprio processo de preenchimento sedimentar do estuário, intimamente ligado à transgressão marinha, reteve uma parte considerável do material transportado pelo rio. A partir de cerca dos 8,200-7,700 anos, a maior parte dos sedimentos mais grosseiros foi retido dentro do estuário e apenas os sedimentos em suspensão continuaram a ser transferidos para a costa e plataforma adjacente. De igual forma, as faunas de foraminíferos bentónicos do corpo lodoso foram ainda mais reveladoras desta evolução. As densidades faunísticas aumentaram significativamente, acompanhando a transição para ambientes mais profundos e estáveis, enquanto as espécies tipicamente adaptadas a ambientes costeiros – tais como *Asterigerinata mamilla*, *Cribrononion gerthi*, *Gavelinopsis praegeri* e *Bulimina elongata* – que dominaram os depósitos mais antigos, foram posteriormente substituídas de forma gradual por espécies com preferência ecológica por ambientes eutróficos menos hidrodinâmicos e substratos mais finos – tais como *Cassidulina laeviata*, *Bolivina ordinaria* e *Brizalina dilatata* – típicos das áreas mais profundas da plataforma. No entanto, é importante salientar que mesmo durante esta fase transgressiva, quantidades significativas de material fino já tinham começado a chegar à área onde entretanto se estabeleceu o corpo lodoso do Guadiana, querendo tal dizer que o abastecimentos fluvial de finos nunca foi interrompido, inclusive durante os estádios iniciais e mais acelerados de preenchimento estuarino.

Após a relativa estabilização do nível do médio no mar na região por volta dos 5,500 anos (cal. B.P.), e o processo de preenchimento sedimentar do estuário do Guadiana praticamente

concluído, as sequências sedimentares revelaram que outros fatores globais e regionais tornaram-se determinantes para o controlo do fornecimento de sedimentos e nutrientes à plataforma, nomeadamente as oscilações climáticas de escala milenar e centenária que caracterizaram o Atlântico Norte durante o Holocénico, e os impactes das ações antropogénicas à escala regional. Neste contexto, o facto das taxas médias de sedimentação na plataforma não terem aparentemente revelado nenhum incremento significativo até perto dos cerca de 2,500-2,000 anos (cal. B.P.), mesmo após o preenchimento do estuário estar praticamente concluído, pode ter resultado da combinação de dois fatores principais. Por um lado, o clima mais quente e húmido que terá caracterizado o início do Holocénico e que terá contribuído para o desenvolvimento de uma extensa cobertura vegetal, terá conferido proteção dos solos à erosão e ajudado a retardar o aumento expectável do transporte sedimentar fluvial e consequente ampliação das transferências para a plataforma. A tendência de aridificação que se terá verificado a partir de cerca dos 5,000-4,000 anos (cal. B.P.) em toda a bacia do Mediterrâneo e que também afetou o Vale do Guadiana, embora causando modificações no coberto vegetal, terá implicado simultaneamente uma redução importante do caudal fluvial e, com isso, redução do transporte sedimentar. Por outro lado, a estabilização do nível do mar próximo ao atual possibilitou o início da construção do delta submarino do Guadiana junto à sua desembocadura, num sistema onde os processos de fornecimento são tipicamente superiores aos de redistribuição devido às condições gerais de baixo hidrodinamismo da plataforma do Guadiana, o que terá sido responsável pela retenção continuada de uma parte considerável dos sedimentos transportados pelo rio. As faunas de foraminíferos do corpo lodoso constituíram o indicador que melhor registou esta tendência evolutiva do sistema deposicional, com flutuações nas abundâncias relativas de algumas espécies consideradas mais oportunistas – como *C. laevigata* and *B. dilatata* - a apontarem para um impacto reduzido de descargas excessivas de nutrientes fornecidos pelo rio.

Há cerca de 2,500-2,000 anos (cal. B.P.), registaram-se profundas alterações deposicionais e ecológicas nos dois ambientes da plataforma, apontando para transformações significativas na área-fonte, ou seja, na Bacia hidrográfica do Guadiana. Grandes quantidades de sedimentos começaram a chegar a plataforma e, em particular, verificou-se grande incremento de material fino. No local da plataforma interna, este aumento de finos traduziu-se por eventos deposicionais específicos intercalados nos sedimentos predominantemente arenosos, tendo sido interpretados como o registo de períodos marcados pela ocorrência de importantes cheias fluviais. No corpo lodoso, a fração fina passou a constituir mais de 90% dos depósitos e estendeu-se inclusive a outras zonas mais afastadas da linha direta de fornecimento do

Guadiana, o que claramente marcou o desenvolvimento definitivo deste corpo sedimentar na plataforma média. A causa principal do desencadeamento de tais mudanças estará ligada às Ocupações Romana e Islâmica da Península Ibérica, as quais envolveram grandes modificações nos padrões de uso do solo, em particular de toda a região sul da Península, onde extensas áreas foram convertidas ao cultivo intensivo, para além da intensificação da exploração mineira e da própria exploração dos recursos florestais para diversos fins comerciais. Todas estas atividades, embora tenham contribuído largamente para o desenvolvimento da região, envolveram a destruição significativa da cobertura vegetal, tendo desencadeado fenómenos erosivos sem precedentes que estarão na origem das mudanças ambientais registadas na plataforma, e no corpo lodoso em particular, ao serem responsáveis pelo aumento significativo da carga sedimentar transportada pelo rio. Por outro lado, este período poderá ter correspondido a uma fase particularmente húmida dentro do quadro geral de aridez que caracterizou a Península Ibérica nos últimos cerca de 5,000 anos, designado por alguns autores como Período Húmido Romano Ibérico. Uma oscilação climática no sentido de maiores níveis de precipitação, aliada à intensa erosão desencadeada na Bacia do Guadiana pelas atividades humanas já referidas, terá sido determinante na mudança dos padrões deposicionais da plataforma. Este impacto foi revelado igualmente pelas faunas de foraminíferos bentónicos, nas quais o estabelecimento ou aumento de determinadas espécies – tais como *Epistominella exigua*, *Valvulineria bradyana* e *Bulimina marginata* – traduziu de forma evidente a criação de novos nichos ecológicos dentro do corpo lodoso como resposta às alterações no fornecimento fluvial. Adicionalmente, este incremento nas descargas fluviais poderá ter acelerado a evolução geomorfológica natural da desembocadura do Guadiana e sido responsável pela colmatação de um antigo distributário oriental do rio, o qual é referenciado em fontes históricas de há pelo menos cerca de 2,000 anos. Tal processo terá conduzido, por sua vez, ao reforço do distributário ocidental, hoje correspondente ao canal principal do rio e que fornece diretamente a área da plataforma onde foram colhidas as sequências sedimentares analisadas.

Após o período húmido Romano, e até há cerca de 300 anos, os indicadores paleoambientais apontaram para a persistência do sinal climático de aridez na região da Bacia do Guadiana, o que é consistente com a informação disponível para outros locais do sul da Europa. A aridificação de toda esta região terá sido muito provavelmente forçada, em grande parte, pela ação da Oscilação do Atlântico Norte (NAO), a qual controla os trajetos do sistema de tempestades do Atlântico Norte e, por conseguinte, a maior ou menor humidade/precipitação disponibilizada à Península Ibérica. Tal justificaria a ausência do

registo de cheias nos depósitos da plataforma interna que foi verificado durante uma grande parte deste período. Não obstante, quantidades elevadas de sedimentos finos continuaram a ser fornecidas ao corpo lodoso, o que terá sido sintomático da continuação do impacte humano na região, pelo menos durante toda a Idade Média.

Os últimos 300 anos de deposição continuaram a ser fortemente marcados pelo intenso fornecimento de sedimentos finos, com um incremento particularmente significativo no local estudado da plataforma interna, e pela deposição de material terrígeno no corpo lodoso, indiciador do incremento dos impactes das cheias fluviais. Esta tendência foi atribuída a uma ligação ainda mais estreita entre os fatores climáticos e os antropogénicos. A ocupação humana prolongada da Bacia do Guadiana foi acentuada durante o século XIX, com um novo desenvolvimento da atividade mineira ao longo da Faixa Piritosa Ibérica (devido à lenha necessária para o processo de ustulação) e das práticas agrícolas, ambas com fortes impactes no uso do solo e nas taxas de erosão. Simultaneamente, este período correspondeu à fase mais acentuada do evento climático conhecido como 'Pequena Idade do Gelo', que afetou toda a região do Atlântico Norte e esteve associado com um índice negativo mais persistente da Oscilação do Atlântico Norte. Valores negativos persistentes do índice foram já reconhecidos como o principal mecanismo responsável por um aumento da humidade e da precipitação em toda a região sudoeste da Península Ibérica. A ação conjunta da amplificação dos processos erosivos derivados das atividades humanas com o aumento significativo dos caudais do Rio Guadiana devido à oscilação do clima, aparenta ter sido o mecanismo responsável pela maior exportação de sedimentos do continente para o domínio marinho e pelos padrões deposicionais mais recentes detetados na plataforma.

Contents

List of figures

List of tables

Chapter I

INTRODUCTION

II.1. Motivation and general setting of the study

Continental shelves have been assuming growing importance in palaeoclimatic and palaeoceanographic research studies as they constitute key-transfer areas between continental and marine environments (*e.g.*, Nittrouer and Wright, 1994; Kineke *et al.*, 1996; Jouanneau *et al.*, 1998; Sommerfield and Nittrouer, 1999; Araújo *et al.*, 2002; Dias *et al.*, 2002; Roussiez *et al.*, 2005; Dubrulle *et al.*, 2007), their deposits having high potential for registering past environmental changes such as sea-level variations, climatic events and the more recent anthropogenic impact on natural systems (*e.g.*, Rodero *et al.*, 1999; Lobo *et al.*, 2001; Edwards, 2002; Hanebuth and Stattegger, 2004; Abrantes *et al.*, 2005; Alt-Epping *et al.*, 2009). In particular, the mud deposits that can form in shelf areas adjacent to relevant sediment fluvial sources have become increasingly important to the understanding of Holocene environmental shifts. Their moderate to high sedimentation rates usually generate a more continuous record than other areas of the shelf and thus allow an interpretation of events with a millennial, centennial, and sometimes even decadal, time-scale resolution (*e.g.*, Lesueur *et al.*, 1996; Sommerfield and Wheatcraft, 2007; Burdloff *et al.*, 2008; Lantzsch *et al.*, 2009a; Nizou *et al.*, 2010; Rosa *et al.*, 2011; Mendes *et al.*, 2012b; Oberle *et al.*, 2014).

On the northern Gulf of Cadiz Margin, a number of studies have been conducted throughout the past years in order to try to understand the shelf main depositional patterns, and their past evolution in relation to several forcing mechanisms, including the postglacial sea-level rise, estuarine infilling, oceanographic shifts, changes in fluvial-sediment supply and climate (*e.g.*, López-Galindo *et al.*, 1999; Maldonado and Nelson, 1999; Nelson *et al.*, 1999; Rodero *et al.*, 1999; Sierro *et al.*, 1999; Gutiérrez-Mas *et al.*, 2003; González *et al.*, 2004; Lobo *et al.*, 2004; Lobo *et al.*, 2005; Mendes *et al.*, 2010; Rosa *et al.*, 2011). Additionally, the Holocene infilling of the Guadiana Estuary is well documented (Boski *et al.*, 2002; Boski *et al.*, 2008), which is crucial to understand past changes in the fluvial input onto the nearby shelf as the river is its main regional sediment source. The river runoff is itself extremely susceptible to variations in precipitation and to climatic oscillations such as those related with the North Atlantic Oscillation (NAO) (Dias *et al.*, 2004; Trigo *et al.*, 2004), whereas the narrow and bedrock-controlled morphology of the estuary determines a very efficient fluvial-export towards the coast (*e.g.*, Lobo *et al.*, 2003), with flood events being the main sediment-transfer mechanism from the continent to the shelf (Portela, 2004; González *et al.*, 2007). The majority of sediments that bypass the estuary mouth to the shelf correspond to suspended-load (Morales, 1997; Portela, 2004). This material tends to be re-suspended from the shallower

areas close to the river mouth and of the inner shelf by storm- and wave-activity, being transported offshore and eventually setting on the deeper middle shelf environment, where the lower hydrodynamic levels allow its deposition (González *et al.*, 2007). Here they have formed an important mud patch, which is part of the larger muddy deposits that cover a significant portion of the northern Gulf of Cadiz Margin, and constitute a highstand system track largely formed after the sea-level rise deceleration in mid-Holocene times (Nelson *et al.*, 1999; Lobo *et al.*, 2004; González *et al.*, 2004).

The Guadiana mud body has been part of the focus of a few investigations, mainly concerning its geochemical signature and relation to historical human-derived sources of pollutants along the river basin (Corredeira *et al.*, 2008), changes in the supply of organic carbon during the Holocene (Burdloff *et al.*, 2008), the coupling of natural and anthropogenic impacts in the overall shelf system (Mendes *et al.*, 2012b), and a first insight on the general mechanisms behind its formation on the middle shelf (Rosa *et al.*, 2011). However, an integrated study focusing specifically on the depositional mechanisms that led to its establishment and development on the middle shelf was yet lacking.

On the other hand, the recognition of the Iberian Peninsula as a region of strong climatic asymmetries due to its geographical position that places it under the combined influence of the Atlantic and the Mediterranean (*e.g.*, Castro-Díez *et al.*, 2002; Goodess and Jones, 2002; Martin-Vide and Lopez-Bustins, 2006), sets the Guadiana region itself as a key-location to try to understand the climatic complexity of the Holocene period in the context of the North Atlantic climate variability. Furthermore, the long-term human occupation of the Guadiana Basin has caused a profound and continued impact on the landscape (*e.g.*, Devy-Vareta, 1985; Chester and James, 1999; Boone and Worman, 2007), changing erosional processes and thus contributing to variations on the shelf sediment supply and amount of nutrients transported by the river to the ocean. As such, it is expectable that a strong interplay between natural and human forcing factors has helped to definitely shape the region throughout the past millennia.

Taking into account this overall scenario, and the high-potential of the Guadiana mud body to register in detail the past climatic and environmental anthropogenic changes that affected the region for the last millennia, urged an integrated approach that allowed understanding the formation and evolution of the mud body as a specific depositional and ecological shelf domain, and at the same time enabled its use as a high-resolution palaeoenvironmental tool to reconstruct the Holocene climatic and anthropogenic history of this semi-arid region within the North Atlantic.

II.2. Main goals

Hence considering the potential relevance that the sedimentary dynamics of the continental shelf off the Guadiana River assumes to understand the climatic contrasts along the North Atlantic, and of the middle shelf mud body as a high-resolution archive of past environmental changes, the main goals of the present work were the following:

1 - To identify the main depositional events occurred in the shelf environment during the late Pleistocene and Holocene and correlate them with sea-level changes and climatic oscillations that affected the region, based on a detailed sedimentological approach coupled with the analysis of the benthic foraminiferal faunas that colonized the middle shelf mud body, framed in a chronology obtained by radiocarbon dating (^{14}C);

2 – To determine variations in the sedimentary supplies of the Guadiana River onto the shelf system through the analysis of changes occurred in the apparent sedimentation rates, in the main compounds of the sand-sized sediments (coarse-fraction analysis), in the shape and surface texture of quartz grains and in the species composition of the benthic foraminifera. Link these variations to important climatic events, using the Guadiana-case as an example of the impact of fluvial systems on the adjacent coastal and marine environment in semi-arid regions of the North Atlantic;

3 - To relate the evolution of the Guadiana Estuary with modifications detected in the depositional patterns of the shelf, by comparing the data obtained in this study for the inner shelf and mid-shelf mud body sedimentary sequences with previous information obtained by other authors with the analysis of sequences collected inside the estuary;

4 – To evaluate the impact of Holocene climatic oscillations, particularly at an historical time-scale, in the overall sediment supply to the shelf and in the establishment of specific ecological niches for the benthic foraminiferal faunas, using the mud body deposits as the main tool. To identify the more recent anthropogenic impact on the shelf depositional system, and the role played by human-induced changes coupled with the late Holocene climatic events, including those related with the specific NAO-index signal, in the evolution of the natural systems of the region;

5 – To reconstruct the evolutional history of the mud body and relate it with the evolution of the Guadiana region itself, in the context of the North Atlantic postglacial climatic and environmental changes.

II.3. Thesis outline

The thesis has a structure composed by eight Chapters, preceded by two short Abstracts (one in English, the other in Portuguese) and an Extended Abstract (in Portuguese), and followed by the References section and three Appendices (A to C).

The content of each of those chapters is briefly summarized as follows.

Chapter I – Corresponds to a general introduction of the thesis itself, presenting the motivation for the study, the main aims and goals of the work, and its general outline.

Chapter II – Consists of a broad description and framing of the study area, focusing on its location, general climate and oceanography, main features of the continental shelf and postglacial evolution of its deposits, sea-level variations, Holocene climate change and the more recent human impact in the region.

Chapter III – Describes the materials and methods that were used in order to achieve the main goals established for the thesis work.

Chapter IV – Presents the sedimentological results of the inner shelf sedimentary sequence, its palaeoenvironmental interpretation, an approach on the climatic and anthropogenic forcing over the evolution of the deposits, and a summary which includes a synthesis-table of events.

Chapter V – Presents the sedimentological and micropalaeontological results of the middle shelf mud body sedimentary sequences, their palaeoenvironmental interpretation, an approach on the climatic and anthropogenic forcing over the evolution of the deposits, and a summary which includes a synthesis-table of events.

Chapter VI – Presents a general palaeoenvironmental reconstruction for the continental shelf based on the integration of the results and interpretation of the two previous chapters, with a main focus on the evolution and characterization of the mud body.

Chapter VII – Provides the main findings and conclusions obtained with the thesis research work.

Chapter VIII – Focuses on the taxonomy of the mud body benthic foraminifera, containing its detailed systematic and a set of five plates that feature scanning electron microscope (SEM) photographs of several important taxa, including of all the main benthic species used for multivariate statistical analysis and determination of the biofacies.

The Appendices correspond to the tables with general information on the counting and the relative abundances of the benthic foraminiferal species (taxa with more than one specimen in at least one sample) analysed in vibrocores 1 (Appendix A), 6 (Appendix B) and 14 (Appendix C).

Chapter II

STUDY AREA

II.1. General location

The study area is located on the inner- to middle-shelf adjacent to the Guadiana River Mouth, with the river and its estuary constituting a natural border between Portugal and Spain (Fig. II.1).

The continental shelf off the Guadiana River is located in the northern part of the Gulf of Cadiz, a large basin that is placed in the northeast Atlantic Ocean, along the southwestern margin of the Iberian Peninsula, extending from Cape São Vicente (on the west) to the Strait of Gibraltar (on the east), the latter setting the connection to the Mediterranean Sea (Fig. II.1).

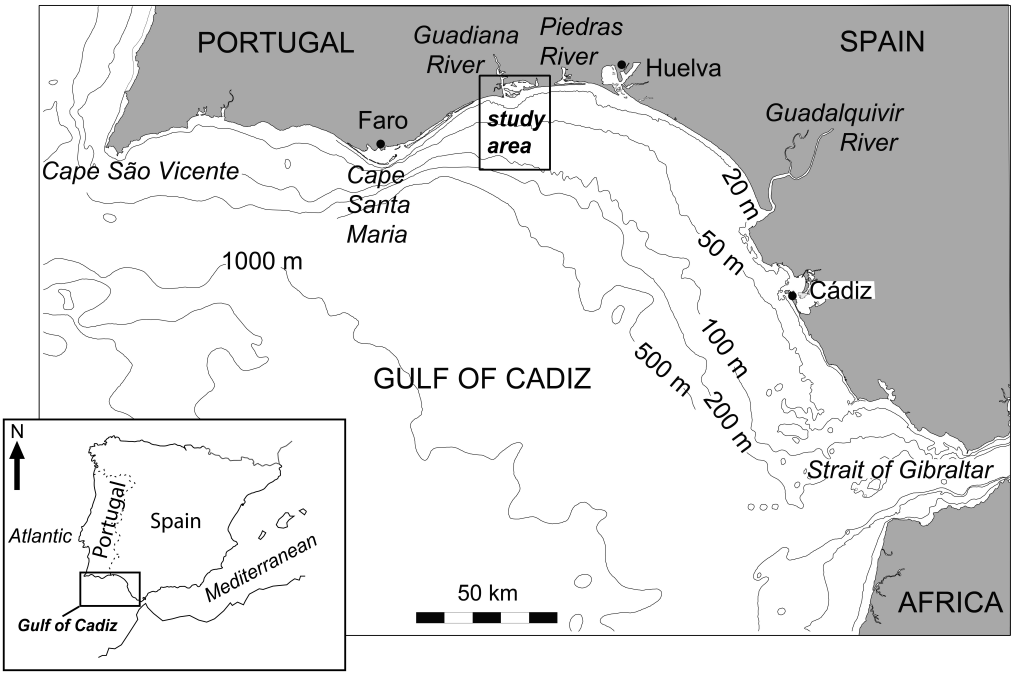

Figure II.1 – Map of the Gulf of Cadiz region and general location of the study area.

The basin is positioned near the eastern end of the Azores-Gibraltar Fracture Zone, which is part of the Eurasia-Africa plate boundary, and since late Miocene when N-S to NNW-SSE convergence movements took place between Iberia and Africa, the region has remained seismically-active, under convergence (*e.g.*, Torelli *et al.*, 1997; Gràcia *et al.*, 2003; Medialdea *et al.*, 2004).

Due to its geographic position and in terms of ecological setting, the Gulf of Cadiz basin is a transitional area that divides the North Atlantic Coastal Province into the European and the African sectors, constituting a relatively warm and oligotrophic pelagic system that interrupts the seasonal fringe of cold, nutrient-rich, upwelled waters coming from the west part of the basin (Garcia-Lafuente *et al.*, 2006; Garcia-Lafuente and Ruiz, 2007).

II.2. Regional climate

The Iberian Peninsula, together with the whole of the Western Mediterranean Basin, form a transitional climatic region where Atlantic and Mediterranean influences meet and imprint specific low-frequency variability patterns (*e.g.*, Ribeiro, 1945; Martin-Vide and Lopez-Bustins, 2006).

The climate that characterizes the study area is though clearly of Mediterranean influence (Ribeiro, 1945; Loureiro and Coutinho, 1995), with the Guadiana River draining a semi-arid region and its runoff being characterized by high seasonal and inter-annual variability (Cunha, 1983; Loureiro *et al.*, 1986; Dias *et al.*, 2004; Trigo *et al.*, 2004). The mean annual rainfall in the Algarve along the hydrological year has been further described as distributed by three different periods, namely rainy (October-February), transitional (March-May) and dry (June-September) (Loureiro and Coutinho, 1995).

These general climate trends have been found to be further defined by the North Atlantic Oscillation (NAO), which is the leading pattern of climate and winter surface variability over the North Atlantic (Hurrell, 1995; Visbeck *et al.*, 2001) (Fig. II.2).

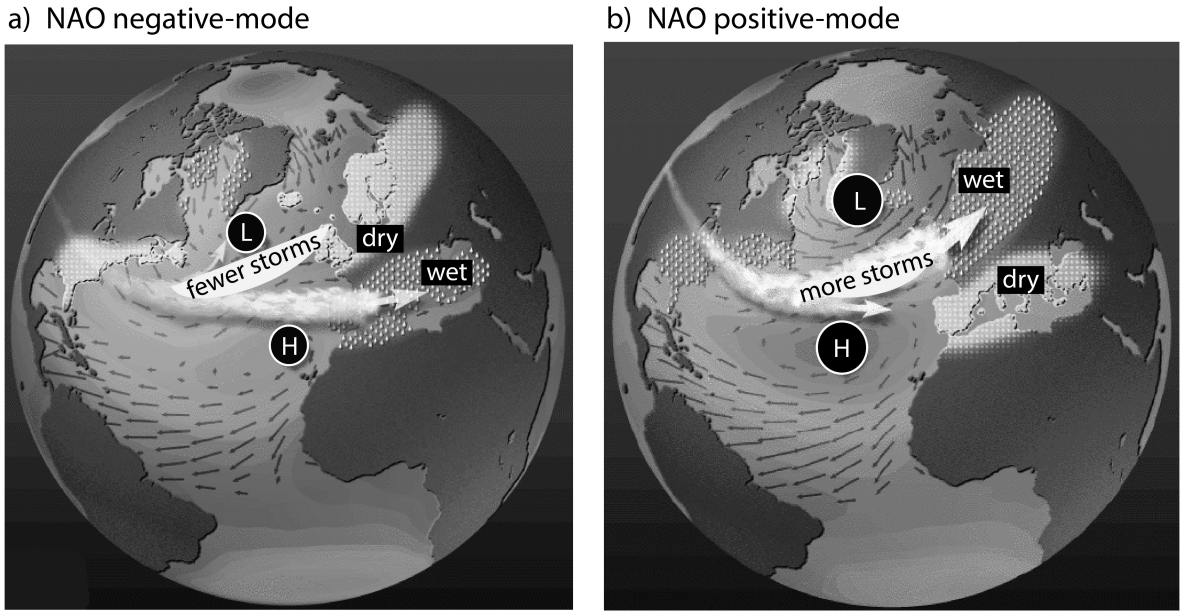

Figure II.2 – Model of the two modes of the North Atlantic Oscillation (NAO), associated storminess activity and distribution of moisture over the North Atlantic: **a)** negative and **b)** positive NAO index phases. H – Subtropical High Pressure Centre, L – Icelandic Low Pressure Centre (adapted from http://www.ldeo.columbia.edu/res/pi/NAO/).

The winter (December-March) station-based index of the NAO is frequently calculated on basis of the difference of normalized sea-level pressure between Lisbon (Portugal) (although Ponta Delgada-Azores and Gibraltar have also been used) and Stykkisholmur/Reykjavik (Iceland) since 1864 (*e.g.*, Hurrell and Van Loon, 1997; Hurrell and Deser, 2010). In general

terms, the NAO refers to a redistribution of atmospheric mass between the Arctic and the subtropical Atlantic basin, and shifts from one phase to another, producing large changes in surface air temperature, winds, storminess and precipitation over the Atlantic (*e.g.*, Hurrell and Deser, 2010) (Fig. II.2). Anomalies in precipitation, including dry wintertime conditions over southern Europe and the Mediterranean, and wetter-than-normal conditions over northern Europe and Scandinavia, have also been linked to the behavior of the NAO (Hurrell and Van Loon, 1997) (Fig. II.2). Positive values of the NAO index are typically associated with stronger-than-average westerlies over the middle latitudes, more intense weather systems over the North Atlantic and wetter/milder weather over western Europe, whereas negative index values usually associate with stronger westerlies and enhanced moisture over low-latitudes and the Mediterranean (*e.g.*, Hurrell and Deser, 2010) (Fig. II.2).

In the Iberian Peninsula, the winter precipitation and moisture availability are indeed largely modulated by the NAO index (Corte-Real *et al.*, 1998; Rodriguez-Puebla *et al.*, 1998; Goodess and Jones, 2002; Trigo *et al.*, 2004; Martin-Vide and Lopez-Bustins, 2006). Specifically, in the Guadiana River Basin, pervasive NAO negative-phases are known for inducing higher precipitation and stronger river flows whereas the opposite occurs during pervasive NAO positive-phases (Dias *et al.*, 2004; Trigo *et al.*, 2004).

II.3. Continental shelf off the Guadiana River

II.3.1. Physiography

The Guadiana shelf stands in a transitional zone between the narrow and relatively steep West Portuguese shelf, with a mean width of 5 km and a slope of ca. 0.5º, and the north-eastern corner of the Gulf of Cadiz where the shelf is more than 30 km wide off the Guadalquivir River mouth and has gentle slopes of less than 0.2º (*e.g.*, Lobo *et al.*, 2001).

The study area can be divided into three main morphological provinces, namely the inner shelf, the smooth middle shelf and the outer shelf (Nelson *et al.*, 1999).

Off the Guadiana River, the shelf break lies at around 140–150 m water depth (Baldy, 1977; Vanney and Mougenot, 1981) and the mean slope is 0.32º (Roque, 1998; Lobo *et al.*, 2001). The middle shelf is located between ca. 30-50 and 90-100 m water depths with slopes of 0.35º to 0.49º (*e.g.*, Nelson *et al.*, 1999; González *et al.*, 2004).

II.3.2. Oceanographic setting

II.3.2.1. Hydrodynamics

The surface circulation in the Gulf of Cadiz is integrated into the general circulation of the Northeast Atlantic, having the Azores current, which feeds the Canary Current, frequently forming meanders that separate from the main flow (Alves *et al.*, 2002). The circulation within the Gulf of Cadiz thus constitutes the last meander of the Azores current, part of which enters the Mediterranean Sea through the Strait of Gibraltar to balance evaporation and buoyancy losses within this sea (Criado-Aldeanueva *et al.*, 2006).

In general terms, the surface circulation is anticyclonic with short, meteorologically-induced, variations, and the North Atlantic Central Water (NACW) occupies the water masses of the upper 1,000 m of the water column (Criado-Aldeanueva *et al.*, 2006). Two surface coastal variations of the NACW have been furthermore identified, the Atlantic Water (SAW) and the Warm Shelf Waters (SW), the first being originated in shallow waters that are modified by air-sea interactions, and the latter being detected mainly over the continental shelf and characterized by the influence of continental processes, including heating and freshwater inputs from land (Criado-Aldeanueva *et al.*, 2006).

The anticyclonic gyre is permanent in the open sea but interrupted on the continental shelf during the spring-summer season, when a more complex circulation pattern is established, with two different cells of cyclonic circulation forming both to the east and to the west of Cape Santa Maria (García-Lafuente *et al.*, 2006; García-Lafuente and Ruiz, 2007) (Fig. II.3). In the western sector the cell is linked to open-sea and upwelling processes, whereas in the eastern sector coastal processes dominate (García-Lafuente *et al.*, 2006; García-Lafuente and Ruiz, 2007). As a consequence, on the Guadiana shelf, the south-eastward Atlantic inflow currents that control the dislocation of water masses over the continental margin are opposed by a counter-current flowing westwards along the inner shelf and close to the coast (Folkard *et al.*, 1997; Relvas and Barton, 2002; García-Lafuente *et al.*, 2006) (Fig. II.3). On the western sector, oceanographic conditions are strongly influenced by the almost permanent upwelling phenomena occurring off Cape São Vicente, triggered by the wind-stress curl (Fiúza, 1983; Vargas *et al.*, 2003). Westerly winds are the main driven-mechanism for this upwelling and can occasionally create a second upwelling core off Cape Santa Maria, which weakens and even disappears when wind-stress shifts to easterlies (*e.g.*, Vargas *et al.*, 2003). These upwelling events may also be responsible for further primary production by vertical advection of nitrogen, which can be up to two orders of magnitude higher than production

maintained by vertical diffusion (Ruiz and Navarro, 2006). On the eastern sector, easterly winds favour the seasonal appearance of the previously mentioned warm costal counter current, which may in some cases, when wind-stress is strong enough, extend and invade the western sector, connecting both sectors and often turning poleward around Cape São Vicente (*e.g.*, Relvas and Barton, 2002; Garcia-Lafuente *et al.*, 2006; Garcia-Lafuente and Ruiz, 2007; Relvas *et al.*, 2007).

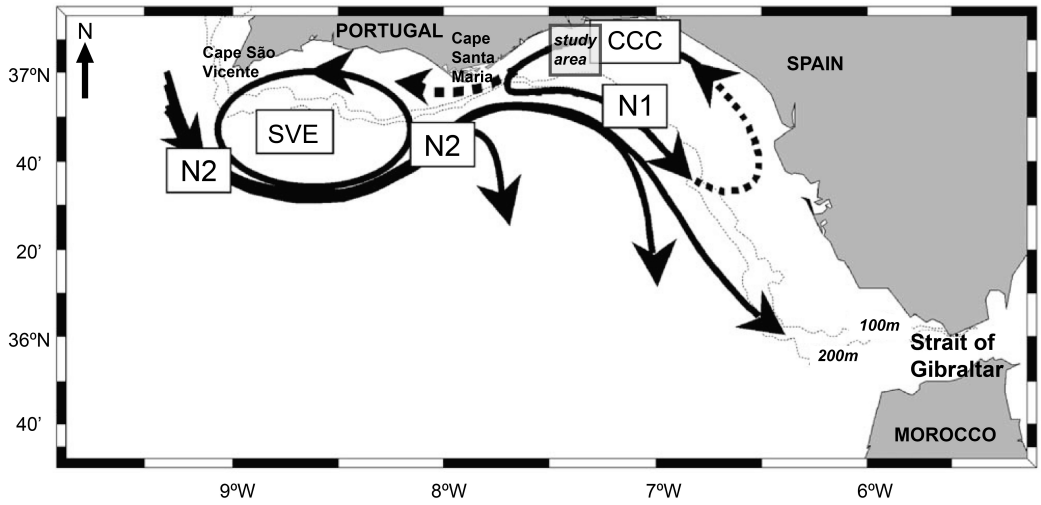

Figure II.3 – Surface water mass circulation on the continental shelf of the Gulf of Cadiz. N1 was identified with the Huelva Front, N2 as a branch of the Portuguese-Canary eastern boundary current, CVE as the cyclonic eddy off Cape São Vicente, and CCC as the coastal counter current active to the east of Cape Santa Maria (adapted from García-Lafuente *et al.*, 2006).

Concerning the hydrodynamic regime, the study area is characterized by semi-diurnal tides with average ranges of 1.3 m and 2.8 m for neap and spring tides, respectively, although maximum ranges of 3.5 m can be reached during the latter. Wave climate is moderate to high (Ciavola *et al.*, 1997), with an average offshore significant wave height of 0.92 m (Costa *et al.*, 2001). Incident waves from the W-SW are dominant, representing 71% of occurrences (Costa *et al.*, 2001) and generating an eastward directed longshore transport. 'Levante' conditions (short period waves generated by SE Mediterranean wind) represent 23% of the total occurrences (Costa *et al.*, 2001). Storm events in the area have been defined as events with offshore significant wave heights greater than 3 m (Pessanha and Pires, 1981). The establishment of return periods for the main incident wave directions indicates that SW storms are more energetic than SE storms for the same return period (Pires, 1998). However, the cuspate shape of the Portuguese coast generates different areas in terms of exposure to wave action, with the eastern section that extends beyond the Guadiana River Mouth being relatively protected from the more energetic W-SW waves, and more exposed to 'Levante' waves.

II.3.2.2. Primary production

The highest concentrations of chlorophyll along the Gulf Cadiz region are observed in the coastal zone between the Guadiana and the Guadalquivir river mouths, mainly driven by the nutrient-enriched fluvial discharges (Ruiz and Navarro, 2006). Additionally, local wind forces also play a role in biological production, with westerlies enhancing chlorophyll concentration and easterlies decreasing it (Ruiz and Navarro, 2006; Prieto *et al.*, 2009). In the coastal and shelf areas adjacent to the Guadiana River, the impact of suspended-particulate matter (SPM) and nutrients was observed particularly around the mouth of the estuary, involving the development of a fingerprint plume that represents a net export of SPM and nutrients to the coastal area recorded both horizontally and vertically (Cravo *et al.*, 2006). The plume has a mean width of about 10-15 km and despite being centred slightly east of the mouth of the Guadiana River, tended to migrate westward, extending down to ca. 20 m water depth, probably influenced by the coastal counter current that flows along the eastern shelf sector, in what seems to constitute a recurring event (Cravo *et al.*, 2006). In general, during wintertime, when phytoplankton activity is reduced, the plume nutrient concentrations are much higher than in the adjacent open sea (Cravo *et al.*, 2006).

II.3.3. Sediment supply and surficial distribution of sediments

The main regional sediment source to the study area is the Guadiana River (González *et al.*, 2004; Martins *et al.*, 2012), with sediment supply from the river basin being dominated by suspended load relative to bed load material (Morales, 1997). The second most important regional source to the shelf is the littoral drift, involving largely bed load transport (González *et al.*, 2004).

Mean river flows of the Guadiana River obtained at Pulo do Lobo Station (covering 91% of the drainage basin) for the period 1946/47 to 1999/2000 were of about 142 m^3 s^{-1}, with distinct seasonal (winter maximum) and inter-annual variations (Portela, 2004). However, comparison with data obtained after the construction of several dams and irrigation schemes showed that this pattern has been disturbed. For the more recent period between 1980/81 and 1999/2000, Alves *et al.* (2001) estimated that the river runoff was since then reduced to ca. 82 m^3 s^{-1}). Also, Dias *et al.* (2004) concluded that the negative correlation of a negative NAO-index with flood frequency was r=0.81 for the period 1946-1964, and was then reduced to r=0.72 for the subsequent period 1964-1998. The estimated sediment supply from the river basin onto the shelf for almost the same period (1946-1990) was of about 43.96×10^4 m^3 yr^{-1} in

terms of bed-load material and of about 57.90x10^4 m^3 yr^{-1} for suspended material (Morales, 1997). However, more recent studies pointed out that for low river flows the net bed-load transport was down-estuary at spring tides, yielding an estimate of 5,400 m^3 yr^{-1} of export seaward (Garel and Ferreira, 2011). The bulk of bed-load sediment exported by the estuary is deposited within the 15 m bathymetric line (González *et al.*, 2007). Winter floods, although episodic, play a crucial role in the supply of both coarse- and fine-grained sediments from the river to the continental shelf (Morales, 1997; Portela, 2004). In the winter of 2000/2001, field measurements showed that ca. 7.5-9.5x10^5 m^3 of sand were exported from the estuary onto the inner shelf, and at the same time fines were re-suspended on the inner shelf and re-deposited at the upper limit of the middle shelf (González *et al.*, 2007). The estuary itself is prolonged offshore by a submerged sandy delta (Morales, 1997), where fluvial-supplied sediments are mixed with the marine material supplied by longshore drift (González *et al.*, 2004).

The longshore transport of mostly sandy sediments is eastward-direct under the influence of onshore conditions that produce a net annual littoral drift around 180x10^3 m^3 yr^{-1}, from the southern Portuguese coast towards the eastern sector of the Gulf of Cadiz (González *et al.*, 2001)

Depositional patterns indicate a predominant eastward transport of sediments under the influence of south-eastward Atlantic inflow currents and the littoral drift (*e.g.*, Gutierrez-Mas *et al.*, 1994; Nelson *et al.*, 1999; González *et al.*, 2007), although the counter-current flowing westward along the inner shelf and close to the coast (Folkard *et al.*, 1997; Relvas and Barton 2002; García-Lafuente *et al.*, 2006) generates a weaker westward component (González *et al.*, 2007).

The surficial sediment distribution on the inner shelf area down to water depths of ca. 25 m is mostly dominated by sands (Moita, 1985; Fernandez-Salas *et al.*, 1999; Nelson *et al.*, 1999; Magalhães, 2001; González *et al.*, 2004; Martins *et al.*, 2012) (Fig. II.4). This pattern is interrupted only by the sandy muds and muds of the prodeltaic wedge just eastward off the Guadiana Estuary mouth, and by some patches of sandy muds and muddy sands located around the bathymetric of 10-15 m, in front and deviated to the west of the river mouth (González *et al.*, 2004; González *et al.*, 2007; Rosa *et al.*, 2013) (Fig. II.4). Most of the inner shelf is dominated by terrigenous components, largely quartz, although locally bioclasts can form larger accumulations (González *et al.*, 2004). Specifically in the vicinity of the Guadiana mouth, fluvial-supplied other terrigenous particles and molluscs concentrate down to ca. 5 m

water depth whereas micas settle around the 10-15 m-bathymetric lines (Rosa *et al.*, 2013). The maximum concentrations of quartz are found mainly in the prodeltaic area, to the south of the fluvial deltaic bulge and near the coast to the east, whilst other terrigenous accompanied by ca. 2-4% of metaschists and greywacke are very abundant on the deltaic bulge (González *et al.*, 2004 and 2007).

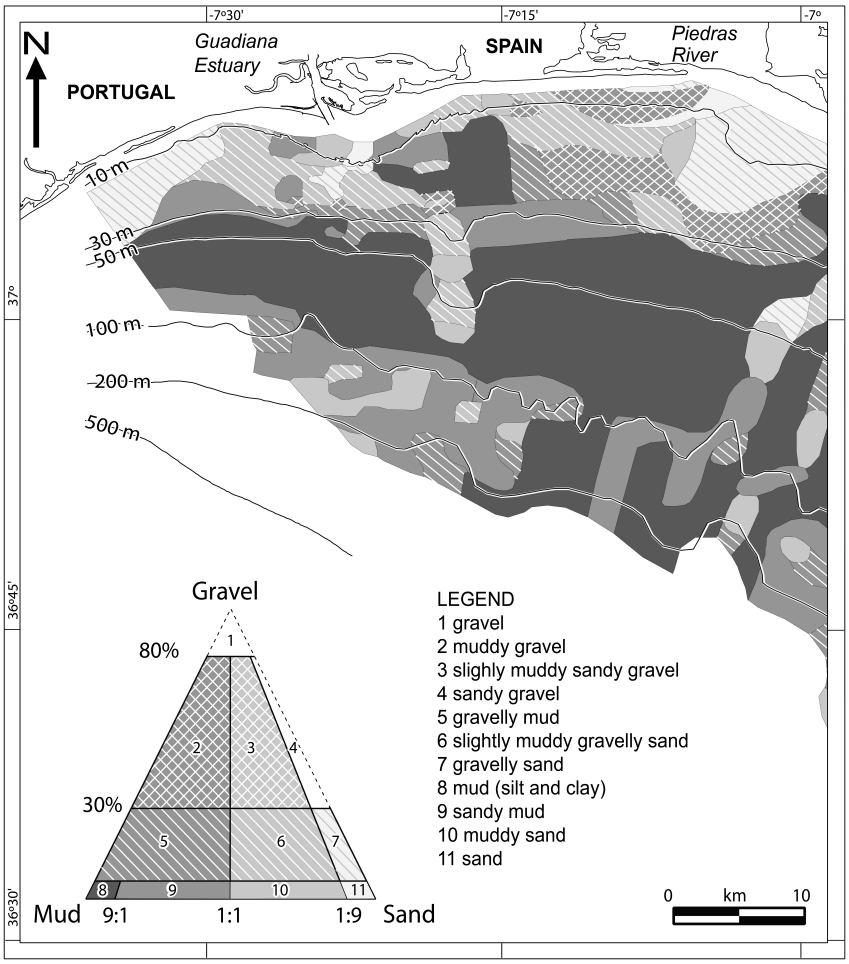

Figure II.4 – Modern distribution of surficial sediments on the Guadiana Shelf (sediments of type 1 and 4 do not occur on the mapped area). Classification of sediments according to Folk (1954). (Adapted from González *et al.*, 2004).

The distribution of morphoscopic quartz shows that the inner shelf areas to the south and east of the Guadiana River mouth down to ca. 10 m water depth, including the deltaic bulge, contain large quantities of not-worn (NU) grains, followed by smooth-shining (EL) grains that increase with water depth (González *et al.*, 2004 and 2007) (Fig. II.5). Small patches of rounded-frosted (RM) grains occur only at transition from the inner to the middle shelf, around the bathymetric of 30 m, both to the south and to the east of the river mouth, probably associated with subaerial exposure on the shelf during lowstand conditions (González *et al.*, 2004 and 2007) (Fig. II.5).

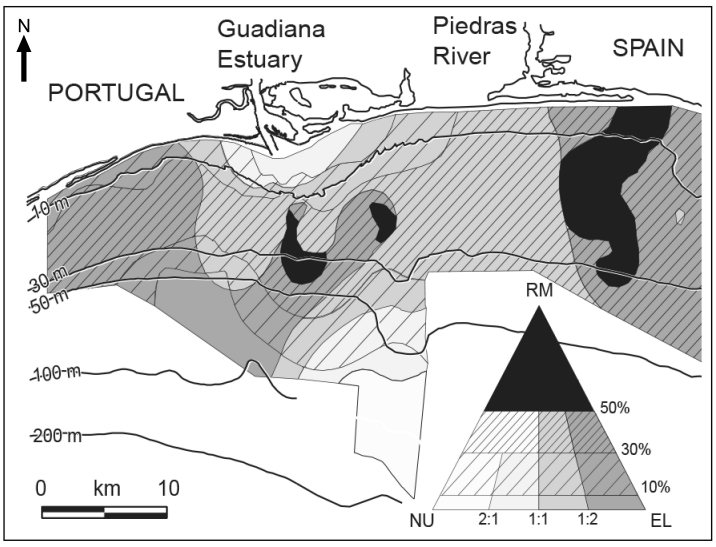

Figure II.5 – Modern distribution of morphoscopic types of sandy quartz on the Guadiana shelf. NU – not-worn, EL – smooth-shining, RM – rounded-frosted (adapted from González *et al.*, 2004).

The middle shelf is dominated throughout by the very fine silt and clay deposits that form the Guadiana mud belt, extending from ca. 30-40 to 90-100 m water depths (Fernandez-Salas *et al.*, 1999; Nelson *et al.*, 1999; Magalhães, 2001; González *et al.*, 2004; González *et al.*, 2007; Martins *et al.*, 2012) (Fig. II.4). East of the Guadiana River Mouth, these deposits are cut by a N-S oriented bulge of transgressive coarser deposits that is composed of muddy gravelly sands and muddy sands, and stretches from ca. 20 to 100 m water depth (González *et al.*, 2004 and 2007) (Fig. II.4). At the outer shelf sediments are usually an heterogeneous mixture of sands and silty clays, but some coarser deposits of sand and gravelly sand also occur near the shelf edge (Nelson *et al.*, 1999; González *et al.*, 2004; González *et al.*, 2007) (Fig. II.4). Most of the sand on the middle and outer shelf is composed of grains of bioclastic origin, where foraminifera dominate but locally on the outer shelf larger amounts of mollusc shells remain, particularly in the area of the transgressive bulge (González *et al.*, 2004 and 2007). Quartz is however the dominant sand compound throughout the mid-shelf area occupied by the mud belt, in front and to the east of the Guadiana River mouth, down to ca. 90 m water depth (González *et al.*, 2004 and 2007). The morphoscopy characteristics of sandy quartz show that grains with a blunt-shining (EL) signature predominate on the middle shelf, with varying amounts of not-worn (NU) and rounded-frosted (RM) that are higher at shallower and deeper areas, respectively (González *et al.*, 2004; González *et al.*, 2007) (Fig. II.5).

In general terms, the surficial distribution of sediments along the Gulf of Cadiz Margin indicate that the predominant sand- to mud-facies are in equilibrium with present-day bottom currents, except for the outer shelf transgressive sand facies (Nelson *et al.*, 1999).

II.3.4. Postglacial evolution of deposits

The late Quaternary general pattern of sedimentary facies on the Gulf of Cadiz continental shelf results from the interaction of several controlling factors that are dominated by the Atlantic inflow currents flowing southeastward across the shelf towards the Strait of Gibraltar (Nelson *et al.*, 1999).

The evolution of deposits in the Gulf of Cadiz Margin after the last glacial maximum has been controlled mainly by changes in mean sea level, with sediments accumulated on the Guadiana shelf featuring related transgressive (TST) and highstand (HST) system tracks (*e.g.*, Somoza *et al.*, 1997; Nelson *et al.*, 1999; Lobo *et al.*, 2001 and 2004). The main consequence of relative sea-level variations upon the development of shelf and slope facies was the formation of the lowstand prograding slope wedge off major rivers, transgressive sand deposits across the shelf and highstand prograding mud layers on the mid-shelf (*e.g.*, Gutierrez-Mas *et al.*, 1996; Rodero *et al.*, 1999; Lobo *et al.*, 2001; González *et al.*, 2004).

These distributional patterns have been further influenced by the full development of Atlantic inflow currents over the continental shelf and of Mediterranean outflow currents over the slope, during the late Quaternary, when the postglacial transgression resulted in maximum water depths over the Gibraltar sill (Nelson *et al.*, 1999). As a result, both the shelf prodeltaic deposits and the mid-shelf mud layers have prograted southeastward from the major river sources, forced by the inflow current system (Nelson *et al.*, 1999). Throughout the Holocene highstand period, sediment dispersal also seems to have been controlled by an intermittent counter current system that depends on the wind regime (Lobo *et al.*, 2004), as described previously in sub-section II.3.2 (Oceanographic setting).

The transgressive deposits correspond to four parasequences that are exposed on the middle to the outer Guadiana shelf (Lobo *et al.*, 2001), namely in the area of the transgressive bulge (González *et al.*, 2004), downlapped by shelf prograding subaequous deltaic and pro-deltaic facies of the Holocene HST (Maldonado and Nelson, 1999; Rodero *et al.*, 1999). However, on the middle shelf to the south of the Guadiana Estuary, these transgressive deposits are poorly developed and usually covered by the highstand mud deposits (González *et al.*, 2004). At the outer shelf edge, underlying the mid-shelf mud and inner shelf sand facies, lays this late Pleistocene to Holocene transgressive sand sheet that was formed by the eustatic shoreline advance (Nelson *et al.*, 1999).

The highstand deposits on the Guadiana shelf form a prodeltaic wedge on the inner shelf area eastward of the river mouth, and the extensive mud belt that covers most of the middle

shelf (Nelson *et al.*, 1999; González *et al.*, 2004; Lobo *et al.*, 2004). The mid-shelf mud layer begins inshore at ca. 40-50 m water depth and extends offshore to about 100 m water depth, with the thickest part setting offset southeast of the river mouth and being well developed in-between the Guadiana and Guadalquivir river mouths (Nelson *et al.*, 1999). All the margins of the extensive mud deposits are interrupted by non-depositional areas, except for the southeast margin (Nelson *et al.*, 1999).

The development of the shelf depositional patterns throughout the late Pleistocene and Holocene has also been strongly influenced by the evolution of the Guadiana Estuary, and its infilling process. Similar to the evolution of several other estuarine systems along the Gulf of Cadiz Margin, both in the Spanish (Dabrio *et al.*, 2000; Lario *et al.*, 2002; Zazo *et al.*, 2008) and in the Portuguese (Boski *et al.*, 2008; Zazo *et al.*, 2008; Schneider *et al.*, 2010) coast sectors, the Guadiana Estuary infilling was closely related to the postglacial sea-level changes (Boski *et al.*, 2002; Lobo *et al.*, 2003). A first phase of accelerated infilling was identified between ca. 13,000 and 7,500-7,300 cal. years B.P. (Boski *et al.*, 2002 and 2008), which trapped mostly clay sediments inside the estuary until ca. 8,200-7,800 cal. years B.P. (Boski *et al.*, 2002). After this date, the central part of the estuary started to accumulate coarser material that was being partly introduced by the continental shelf (Boski *et al.*, 2002). The second phase of infilling developed at a much slower rate between ca. 7,500-7,300 and 5,700 cal. years B.P. and since then predominantly sandy sedimentation was initiated inside the estuary (Boski *et al.*, 2002). Since the sea level has been nearly stabilized in the region, after ca. 5,500 cal. years B.P., and with the estuarine accommodation space much reduced, prograding processes started to develop at the river mouth (Morales, 1997; Morales *et al.*, 2006). The estuary late Holocene geomorphological evolution included the construction of the submerged fluvial delta and the progradation of both the western and eastern margins, which started to retain an important part of the sediments being supplied by the river to the coast and shelf domains (Morales, 1997).

II.4. Late Quaternary sea-level variation

During the Quaternary, the main control on sea-level change was the exchange of mass between ice sheets and oceans, with ice sheet growth contributing to induce sea-level lowstands (*e.g.*, Lambeck and Chappell, 2001). In the course of the Last Glacial Maximum (LGM) the eustatic sea level was around 125 +/- 5 m lower than the present day mean level and there is evidence for a non-uniform rise from the LGM to the end of the deglaciation.

Using worldwide sea-level data from several sites, improved constraints on the global rate of rise have been attempted (Fleming *et al.*, 1998), pointing to an initial slow rise that lasted from ca. 21 to 17 ka cal. B.P. with an average rate of ca. 6 m ka^{-1}, followed by an increased average rate of ca. 10 m ka^{-1} for the next 10,000 years until most of the decay of the large ice sheets was completed by 7 ka cal. B.P.

Furthermore, it has been recognized that sea-level changes caused by glacial cycles have both a global and a regional character (*e.g.*, Fleming *et al.*, 1998; Leorri *et al.*, 2012), with the associated meltwater discharges playing a significant role on rapid climatic change in western Europe (*e.g.*, Fairbanks, 1989). It has been indeed demonstrated that the climate of the last glacial period was extremely unstable, with such variability that ranged from full glacial to nearly interglacial conditions, being first observed in the $d^{18}O$ record of Greenland ice cores (Dansgaard *et al.*, 1993; Grootes *et al.*, 1993). These cycles were named as Dansgaard–Oeschger (D–O) Stadials and Interstadials, corresponding to cold and warm periods, respectively (Bond *et al.*, 1993) (Fig. II.6). Some of the D–O Stadials were further related to episodes of massive iceberg discharges into the North Atlantic Ocean (Bond *et al.*, 1993), named Heinrich events (HE) and which have occurred six times along the last glacial period (60,000–15,000 calendar years B.P.) (Fig. II.6). Since then, during late Pleistocene, the Northern Hemisphere was marked by a succession of major deglacial climatic events that preceded the Holocene period, namely the Oldest Dryas (ca. 18,000-14,700 cal. years B.P.; the Bølling/Allerød warm period (ca. 14,600 to 12,900 cal. years B.P.) and the Younger Dryas cold event (ca. 12,900 to 11,700 cal. years B.P.) (*e.g.*, Alley and Clark, 1999) (Fig. II.6).

Worldwide studies focusing on global and regional mean sea-level trends after the LGM, are also quite consensual in that the sea level was fast rising by the time of the Oldest Dryas, driven by the huge meltwater release from decaying ice masses during the deglaciation (*e.g.*, Fleming *et al.*, 1998; Dias *et al*., 2000; Hanebuth *et al.*, 2000; Bard *et al.*, 2010; Smith *et al.*, 2011). Accordingly, the sea-level rise curve established by Dias *et al.* (2000) (Fig. II.7a) for the northern Portuguese Margin placed the mean sea level around 80-75 m below its present-day position at around 13,000 years B.P. (ca. 15,400 cal. years B.P.). During the Bølling/Allerød period and the Younger Dryas, the sea level continued to rise and global sea-level reconstructions agree in that there was very fast acceleration in the rates of rise around 14,000 cal. years B.P., due to an important meltwater pulse that released great volumes of polar ice into the ocean (Fairbanks, 1989; Fleming *et al.*, 1998; Hanebuth *et al.*, 2000; Bard *et al.*, 2010). This pulse, which occurred during the Bølling/Allerød period, is known as MWP 1A, and although different studies attribute slightly different time-spans for its occurrence, in

general terms they all point to a sea-level rise of about 20 m in less than ca. 500 years (Fairbanks, 1989; Fleming *et al.*, 1998; Hanebuth *et al.*, 2000; Bard *et al.*, 2010).

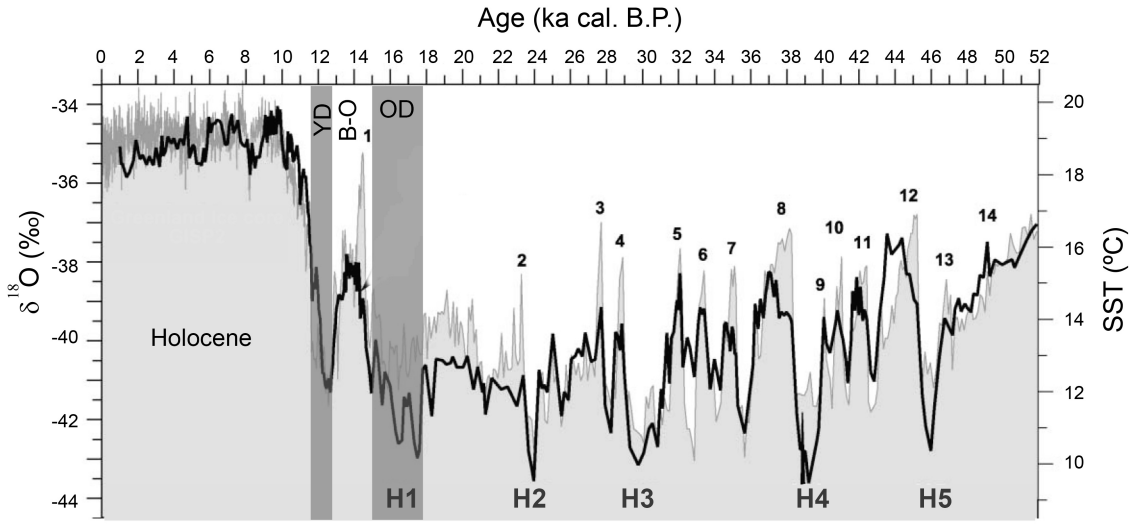

Figure II.6 – Climate variability since the last glacial period: grey line marker is the atmospheric temperature record of the Greenland ice core GISP2 reconstructed from oxygen stable isotope data (Grootes *et al.*, 1993), black line marker represents a case-study of reconstructed surface temperatures of the Alboran Sea (Cacho *et al.*, 2002). Dansgaard–Oeschger (D–O) Interstadial cycles correspond to the numbers on top of the grey line marker (Dansgaard *et al.*, 1993), Heinrich events are signalized on the bottom (Bond *et al.*, 1993), YD – Younger Dryas, B-O - Bølling/Allerød, OD – Oldest Dryas (adapted from Cacho *et al.*, 2002).

According to the same studies, although with great regional and latitudinal variability, the sea-level rise decelerated but in general continued to rise after the MWP 1A, reaching around 60-55 m below present until ca. 12,000 cal. years B.P. In the curve established by Dias *et al.* (2000), the sea level on the northern Portuguese Margin was reconstructed as being already at ca. 45-40 m below present around 12,000 years B.P. (ca. 14,000 cal. years B.P.) (Fig. II.7a). It was followed by a phase of sea-level rise deceleration, and in some mid-latitude areas even a slight sea-level drop (*e.g.*, Dias *et al.*, 2000), associated with the onset of the colder Younger Dryas (YD) that is believed to have slowed down the deglacial melting of the ice sheets (Fairbanks, 1989; Fleming *et al.*, 1998; Hanebuth *et al.*, 2000; Bard *et al.*, 2010). This process of deceleration in the rate of rise during the YD has been further detected in the records of the SE Gulf of Cadiz margin (Rodero *et al.*, 1999) and of the Guadiana Estuary (Delgado *et al.*, 2012) (Fig. II.7b). In the transition to the Holocene period there was another noticeable acceleration in the global rise of sea level due to a second major meltwater pulse (MWP 1B) that affected the ice caps, linked with the transition from the colder YD to the warmer early Holocene (*e.g.*, Fleming, 1989; Bard *et al.*, 2010). The sea level is thought to have rapidly reached ca. 30 m below present mean level around the beginning of the Holocene in many regions (Fleming, 1989; Hanebuth *et al.*, 2000; Bard *et al.*, 2010), and the curves established

for several locations throughout the Iberian Margin (Dias *et al.*, 2000; Lario *et al.*, 2002; Vis *et al.*, 2008; Delgado *et al.*, 2012) and for the Bay of Biscay (Leorri *et al.*, 2012) are likewise in close agreement with such scenario (Fig. II.7).

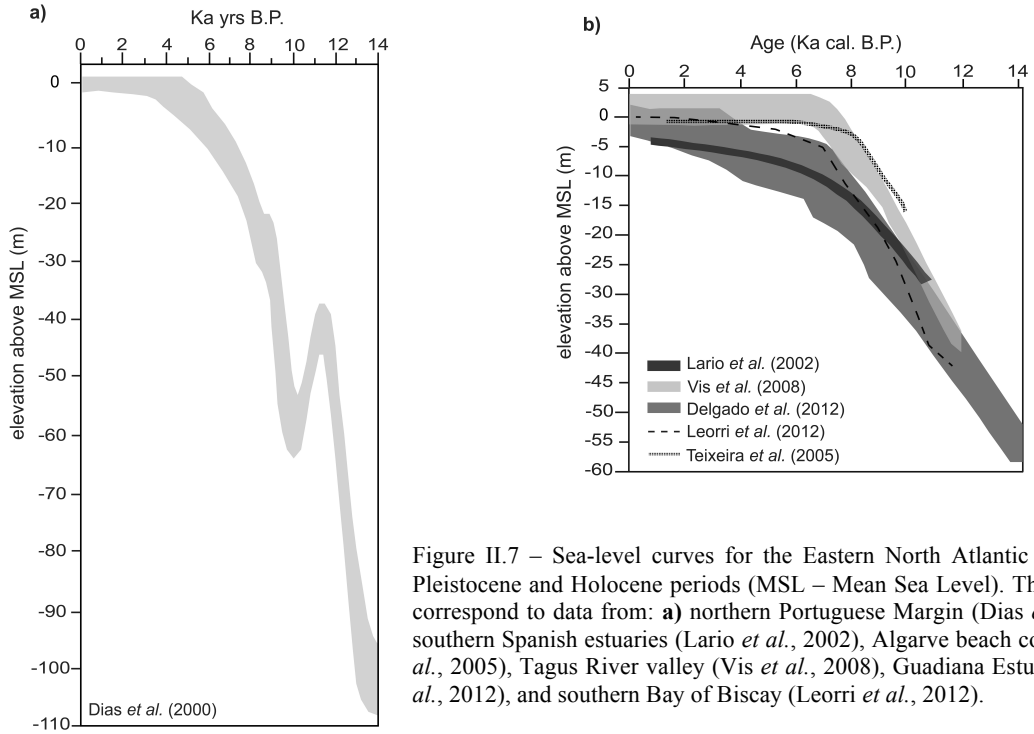

Figure II.7 – Sea-level curves for the Eastern North Atlantic during the late Pleistocene and Holocene periods (MSL – Mean Sea Level). The model curves correspond to data from: **a)** northern Portuguese Margin (Dias *et al.*, 2000); **b)** southern Spanish estuaries (Lario *et al.*, 2002), Algarve beach coast (Teixeira *et al.*, 2005), Tagus River valley (Vis *et al.*, 2008), Guadiana Estuary (Delgado *et al.*, 2012), and southern Bay of Biscay (Leorri *et al.*, 2012).

The sea-level reconstructions for the western European margin point to persistent sea-level rise throughout early- to mid-Holocene times (*e.g.*, Hijma and Cohen, 2010), including those conducted in different areas along the Iberian Margin (Dias *et al.*, 2000; Lario *et al.*, 2002; Teixeira *et al.*, 2005; Moura *et al.*, 2007; Zazo *et al.*, 2008; Vis *et al.*, 2008; Delgado *et al.*, 2012) and in the Bay of Biscay (Leorri *et al.*, 2012) (Fig. II.7). The first phase was characterized by a fast rate of rise of ca. 7-8.5 mm yr^{-1} (700-850 cm/ka) that lasted from the beginning of the Holocene until ca. 7,500-7,000 cal. years B.P. It was followed by a deceleration in the pace of marine transgression, which progressed at ca. 3 mm yr^{-1} (300 cm/ka) until around 5,500 cal. years B.P., when it reached its near stabilization. This is in accordance with the data obtained by other authors, who also pointed to the sea level reaching close to its present-day position at around 6,000-5,500 cal. years B.P. (Dabrio *et al.*, 2000; Dias *et al.*, 2000; Long, 2001; Lario *et al.*, 2002; Moura *et al.*, 2007; Zazo *et al.*, 2008; Leorri *et al.*, 2012) (Fig. II.7).

The most recent data concerning the infilling of the Guadiana Estuary indicated that since ca. 7,500 cal. years B.P. the sea level has continued to oscillate, slowly rising at a rate of ca. 0.9-1.8 mm yr^{-1} (9-18 cm/ka) (Boski *et al.*, 2008; Delgado *et al.*, 2012) (Fig. II.7b).

II.5. Holocene climate control and the recent anthropogenic impact

It has long been recognized that the Holocene was a time of important climate oscillations, and abrupt cyclic-climatic changes have been identified in particular for the North Atlantic during this period (*e.g.*, Bond *et al.*, 1997; Wanner *et al.*, 2008).

Holocene climate variability and instability is to a large extent driven by centennial- and millennial-scale fluctuations in the North Atlantic thermohaline circulation (*e.g.*, Chapman and Shackleton, 2000), and seems to have been characterized by diverse climatic responses at different latitudes of the North Atlantic region (*e.g.*, Ruddiman and McIntyre, 1981; Mörner, 1993; deMenocal *et al.*, 2000; Magny *et al.*, 2003).

Several records from across the Mediterranean and the Iberian Peninsula are consensual in that the early- to mid-Holocene was a period characterized by moisture conditions, occurring within the context of a generalized warmer and wetter climate designated as the Holocene Thermal Maximum (*e.g.*, Wanner *et al.*, 2011; Désprat *et al.*, 2003; Naughton *et al.*, 2007a; Fletcher and Sánchez Goñi, 2008; Kaal *et al.*, 2011; Giraudi *et al.*, 2012). Particularly in the southern part of Iberia, increased precipitation records and an optimum of forest development have been identified by several authors between the beginning of the Holocene and ca. 5,500-4,500 cal. years B.P. (*e.g.*, Dorado Valiño *et al.*, 2002; Zazo *et al.*, 2008; Anderson *et al.*, 2011), including in the Guadiana Lower Valley, where the pollen record revealed an exceptional expansion of the forest cover until ca. 5,000 cal. years B.P. (Fletcher *et al.*, 2007). An important dry and cold event seems however to have occurred within this time-interval at ca. 8,000 cal. years B.P. (Fletcher *et al.*, 2007), which was also detected in other areas of the Mediterranean Basin and Iberia (*e.g.*, Cacho *et al.*, 2002; Dorado Valiño *et al.*, 2002; Magny *et al.*, 2003; Eynaud *et al.*, 2009; Giraudi *et al.*, 2012) and probably can be correlated with the widely known 8.2 ka cal. B.P. cooling event (*e.g.*, Bond *et al.*, 1993; Barber *et al.*, 1999). It was much smaller and brief than the previous glacial swings, and sedimentological and glaciological research suggest that it was caused by a significant freshwater input into the North Atlantic (*e.g.*, Bard, 2002).

From mid- to late-Holocene onwards, a generalized climate change seems to have been set at around 5,500-4,500 cal. years B.P. mainly driven by orbital forcing that caused a shift in insolation and the installation of the present atmosphere circulation in the northern hemisphere (Jalut *et al.*, 2009), with most studies recognizing the progressive widespread of drier conditions (*e.g.*, Fletcher and Sánchez Goñi, 2008; Morellón *et al.*, 2008; Kaal *et al.*, 2011; Giraudi *et al.*, 2012). Along the Mediterranean Basin, the climate change that began at

this date resulted in changes in the seasonal pattern of precipitation and several arid phases were identified as a regional response to global climatic oscillations (Jalut *et al.*, 2000). In the western Mediterranean area, including southern Iberia, such trend also forced the establishment of an arid, Mediterranean-like, climate (*e.g.*, Dorado Valiño *et al.*, 2002; Carrión *et al.*, 2004; Carrión *et al.*, 2007; Zazo *et* al., 2008; Jalut *et al.*, 2009; Gil-Romera et al., 2010). The pollen-based record for the Guadiana Lower Valley further agrees with this scenario, with a generally drier climate being detected in the region after ca. 5,000 cal. years B.P. (Fletcher *et al.*, 2007). However, within this general scenario of enhanced dryness for the mid- to late-Holocene period, several decadal- to centennial-scale climate oscillations with a more regional extent also seem to have occurred and events of enhanced humidity were detected throughout Europe and the Mediterranean (*e.g.*, Carrión *et al.*, 2001; Faust *et al.*, 2004; Mayewski *et al.*, 2004; González-Álvarez *et al.*, 2005; Bernárdez *et al.*, 2008; Casana, 2008; Marquer *et al.*, 2008; Alt-Epping *et al.*, 2009; Büngten, 2011). One of the most prominent of these events detected in the Iberian Peninsula took place around 2,600-1,600 cal. years B.P. as the most humid phase of the last 4,000 years in southern Spain, roughly coinciding with the Roman occupation of the Peninsula, thus being denominated as the Iberian-Roman Humid Period (Martín-Puertas *et al.*, 2009).

Furthermore, at a sub-orbital timescale, the influence of North Atlantic climatic variability and of its main synoptic mode of atmosphere circulation, the NAO, is widely recognized and has been linked by many authors to climate and environmental changes inferred during the main climatic events that marked the late Holocene (*e.g.*, Abrantes *et al.*, 2005; Gil *et al.*, 2006; Wanner *et al.*, 2008; Trouet *et al.*, 2009; Moreno *et al.*, 2012), including the more recent Medieval Warm Period and the Little Ice Age (*e.g.*, Hughes, 1994; Mann, 1999; Mann and Jones, 2003). Instrumental data concerning the winter NAO-index variability only go further back until the mid-19th century, but recent studies have been making an effort to reconstruct the NAO patterns as far as the 16th-17th centuries (Cook *et al.*, 2002; Luterbacher *et al.*, 2002) and even spanning for the last ca. 1,000 years (Bard *et al.*, 2007; Trouet *et al.*, 2009; Trouet *et al.*, 2012), highlighting its influence over the European climate at multidecadal and centennial time-scales. In southern Iberia, coastal records of climatic oscillations during the last ca. millennia detected a decadal periodicity that seemed related to fluctuations of the NAO index (Zazo *et al.*, 2008), whereas in the specific case of the Guadiana Valley climatic oscillations that were detected at a submillennial-scale throughout the Holocene have also been associated with variations in the North Atlantic ocean-atmosphere system and with the NAO index (Fletcher *et al.*, 2007).

Superimposed on the Holocene climate change, the more recent impact of anthropogenic development and land-use activities has been widely investigated throughout European territories, and a positive correlation seems clear between both forcing mechanisms in the shape and transformation of the natural systems (*e.g.*, Berglund, 2003; Büngten, 2011).

In southern Iberia, the influence of human activity has been detected in some areas as far back as ca. 5,500 cal. years B.P. (*e.g.*, Carrión and Dupré, 1997), and studies focusing on the mineral extraction of the Iberian Pyrite Belt dated it from around the third millennium B.C. (Nocete et al., 2005), which is consistent with that date. In the Guadiana Valley, the first signs of human intervention in the vegetation cover (Fletcher *et al.*, 2007) and of mining exploitation (Delgado *et al.*, 2012) also date back to around 4,500-4,000 cal. years B.P. Yet, the investigations carried out specifically in the Guadiana Basin influence area also seem to agree in that more significant transformations occurred later, with the emergence of a semi-forested cultural landscape and the intensification of mining activities only after ca. 3,300 cal. years B.P. (Fletcher *et al.*, 2007; Delgado *et al.*, 2012). This matches quite well with the beginning of the Iberian Period (3,200 cal. years B.P.) that was identified in the neighboring region of Sierra Baza (southern Spain) as a time of advance in agriculture and irrigation, with the widespread cultivation of vines and of fig and almond trees (Carrión *et al.*, 2007).

However, the first major significant changes to the landscape were brought by the Roman Rule of Iberia that followed (ca. 200 years B.C. to 500 years A.D. – ca. 2,200 to 1,450 cal. years B.P.), with historical and archaeological sources clearly denouncing an intensification of human impact on woodland resources during this period, mainly for agricultural, domestic use and mining purposes (*e.g.*, Alarcão, 1987; Alarcão, 1990; Fabião, 1993). The more recent pollen and multiproxy investigations carried out in the Guadiana area are in agreement with such scenario (Fletcher *et al.*, 2007; Delgado *et al.*, 2012), as are several studies developed in other areas of southern Iberia that unravelled the onset of strong human intervention in the vegetation cover only after ca. 2,000 cal. years B.P. (*e.g.*, Zazo *et al.*, 2008; Gil-Romera *et al.*, 2010). Moreover, the coupling of Roman development with a contemporaneous climate shift towards more humidity has been pointed out as the main mechanism for enhanced impacts on the landscape throughout the Mediterranean (Casana, 2008; Zielhofer *et al.*, 2002; Faust *et al.*, 2004) and in other areas of Iberia (Désprat *et al.*, 2003; Dinis *et al.*, 2006; Mighall *et al.*, 2006; Carrión *et al.*, 2010b), as the human interventions created the pre-conditions for soil erosion but it only occurred when unusually high precipitation levels were originated.

The Medieval Islamic Rule of Iberia, after the 8th century A.D. (ca. 1,200 cal. years B.P.), constituted the second major pulse of human intervention in the study area. It was responsible

for further impacts on the southern regions of Iberia, including along the Guadiana Basin, initiating an unprecedent population growth and an extraordinary maximization of the natural resources of the region (*e.g.*, Devy-Vareta, 1985; Ribeiro, 1987; Oliveira Marques, 1993; Chester and James, 1999, Boone and Worman, 2007), which eventually led to the occurrence of even more severe erosional processes (Chester and James, 1999; Boone and Worman, 2007; Chester, 2012).

Although the human-induced transformations along the Guadiana Basin that were irreversibly put in motion during the Roman and Islamic times, persisted to some extent throughout the Middle Ages and beyond (*e.g.*, Ribeiro, 1987; Mattoso, 1995; Chester and James, 1999), the human impact in the region only witnessed another significant increase for the last ca. 200-150 years. New agricultural developments and, particularly, the reactivation and expansion of several important mines along the Iberian Pyrite Belt during the 19th century A.D., contributed to the enhancement of the long-term anthropogenic impacts in the region (e.g., Serrão, 1986; Corredeira *et al.*, 2008; Chester, 2012; Delgado *et al.*, 2012). As a consequence, soil erosion increased along the watersheds and there was an increment in the sediment supply from the river basin onto the coast and shelf domains (González *et al.*, 2001; Dias *et al.*, 2004; González and Dias, 2006).

Chapter III

MATERIALS AND METHODS

III.1. Vibrocores

III.1.1. Collection

The four sediment vibrocores chosen to integrate this study were collected on the continental shelf off the Guadiana River mouth, situated in the Northern Gulf of Cadiz, near the Portuguese-Spanish southern border (Fig. III.1).

The collection was carried out onboard the vessel *Aguayo* during campaigns CRIDA0702 and CRIDA0405, in July 2002 and April 2005, respectively, in the frame of Project CRIDA (POCTI/P/MAR/15289/99). The cores were retrieved using a light-weighted vibrocorer with water injection, characterized by a core barrel of 4 m length and an inner diameter of 9 cm.

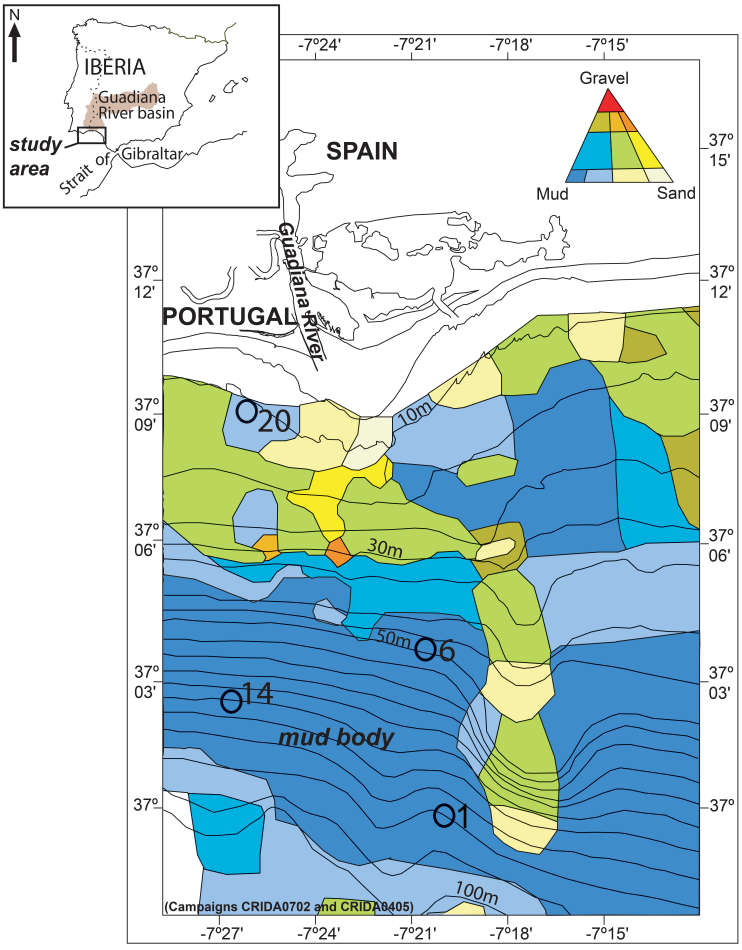

Figure III.1 – General setting of the study area, location of the vibrocores (CRIDA0702, CRIDA0405) and modern sediment cover of the Guadiana Shelf (adapted from Gonzalez *et al.*, 2004). Classification of sediments according to Folk (1954).

The cores were afterwards transported to the Ciacomar/CIMA (UAlg) facilities, where they were opened, described and sampled in the laboratory following standard procedures.

III.1.2. Location and water depth

Three of the vibrocores set for analysis (namely cores 1, 6 and 14) were placed on the middle shelf and within the Guadiana mud body, whilst one vibrocore (core 20) was situated on the inner shelf (Fig. III.1; Table III.1).

Core 1 (376.5 cm length) was collected in the deepest and most offshore area of the central mud body, at a water depth of ca. 92 m and positioned at -7º 19' 58.94'' W; 36º 59' 59.93'' N. Core 6 (299 cm length) was retrieved from a shallower area of the central mud body, at a water depth of ca. 40 m and positioned at -7º 20' 45.31'' W; 37º 3' 48.28'' N. Core 14 (241.5 cm length) was collected in the western part of the mud body, at a water depth of ca. 80 m and positioned at -7º 26' 40.45'' W; 37º 2' 39.77'' N. Finally, core 20 (342 cm length) was taken from the inner shelf at a water depth of ca. 12.8 m, and positioned at -7º 26' 3.55'' W; 37º 9' 9.65'' N. All this information is summarized in Table III.1.

Table III.1 – Reference, length (cm), water depth (m) and location (WGS84 geographical coordinates, UTM grid 29) of the analysed vibrocores.

Core	Campaign	Length (cm)	Depth (m)	Latitude (N)	Longitude (W)
1	CRIDA0702	376.5	92	36º 59' 59.93''	-7º 19' 58.94''
6	CRIDA0702	299	40	37º 3' 48.28''	-7º 20' 45.31''
14	CRIDA0405	241.5	80	37º 2' 39.77''	-7º 26' 40.45''
20	CRIDA0405	342	12.8	37º 9' 9.65''	-7º 26' 3.55''

III.1.3. Sampling

In the laboratory, the cores were opened and split lengthwise into two halves. One half was preserved for archive and frozen, whereas the second half was set for analysis and sampled immediately.

Sampling of the three cores from the mud body followed identical procedures. Core 1 was sampled sequentially in intervals of 1 cm-thick slices from the top (0 cm) down to 20 cm, and of 2 cm-thick slices from this level to the base of the sequence. Core 6 was sampled at the top in a 2 cm-thick slice (0-2 cm), and sequentially from there to level 40 cm in 1 cm-thick slices, and in 2 cm-thick slices between that level and the base. Core 14 was sampled sequentially in 1 cm-thick slices from the top (0 cm) down to 50 cm, and from this level to 239 cm in 2 cm slices, with the base level sampled in a 2.5 cm-thick slice (239-241.5 cm).

Sampling of the inner shelf core was also performed sequentially but with a more irregular grid, adjustable to the variations in grain-size and sediment composition along-core.

Vibrocore 20 was sampled at the top in a 2 cm-thick slice (0-2 cm), as well as for core-depth intervals 3-19 cm, 22-36 cm, 40-94 cm, 97-99 cm, 104-142 cm, 205-222 cm and 316-318 cm. Sampling consisted on 1 cm-thick slices for core-depth intervals 2-3 cm and 36-40 cm; on 1.5 cm-thick slice between 102.5 cm and 104 cm; and on 3 cm-thick slices for core-depth intervals 19-22 cm, 94-97 cm, 99-102 cm, 142-205 cm, 222-316 cm, and from level 318 cm down to the base of the core (342 cm).

Each level of cores 1, 6 and 14 was sub-sampled for grain-size, geochemical and benthic foraminiferal analyses. In core 20, the same was done for most of the sequence, except in the basal section (222-342 cm), where levels were sub-sampled only for grain-size and benthic foraminiferal analyses due to the coarser nature of sediments that disabled future geochemical analyses.

III.2. Dating

III.2.1. AMS radiocarbon analyses

Sample levels selected for dating analysis were first chosen based on the presence of significant changes observed along the vibrocores in the dominant type of sediments, which had already been identified through the grain-size analyses. Whenever possible, complementary datings were further obtained to help validate the previous set and to establish a higher resolution for the temporal framework of the sequences.

A total of 15 radiocarbon analyses were processed for the four vibrocores. Accelerated mass spectrometry (AMS) radiocarbon (^{14}C) dating was performed at Beta Analytic Inc. (U.S.A.), using 20 to 40 mg of mixed benthic foraminiferal tests for levels of the mud body vibrocores, and a minimum of 30 mg of mollusc shells for levels of the inner shelf vibrocore. Almost all samples corresponded to 2 cm-thick intervals, except for level 132-136 cm of core 14, in which the low abundance of foraminiferal tests compelled the use of 4 cm, and levels 151-154 cm and 286-289 cm of core 20 that had been previously sampled for grain-size at 3 cm-thick slices.

Samples of the mud body vibrocores were first washed with tap water through a 63-µm sieve. The retained sediment was dried in an oven at ca. 50 ºC and then analysed under the binocular microscope for collection of the benthic foraminiferal tests, with special attention for avoiding re-worked tests that could disturb the dating results. As for the inner shelf samples, the mollusc shells were chosen from the coarse fraction (-6 Φ to 4 Φ / 64 mm to 0.063 mm) according to their preservation state, in order to avoid remobilized material. They

were furthermore identified, based on specialized bibliography (Fischer *et al.*, 1987; Macedo, 1999), to assure the individuals matched species with an ecological distribution compatible with the inner shelf environment, from where vibrocore 20 was collected.

The obtained radiocarbon ages were calibrated with programme CALIB 5.1 (Stuiver *et al.*, 2005), using the MARINE04 curve and the global ocean reservoir correction of ca. 400 years (Stuiver and Reimer, 1993). Local reservoir effect (delta *R*) was furthermore applied according to Soares and Martins (2010), specifically a correction of 0±100 years for dates older than 2,000 radiocarbon years and of -135±20 years for dates younger than that age.

Conventional radiocarbon ages will be reported as years 'before present' (B.P., 'present' = 1,950 A.D.). Calendar calibrated ages will be reported as years 'before Christ' and 'Anno Domini' (B.C./A.D.) and calibrated ages as years 'before present' (B.P.).

III.2.2. Age models and sedimentation rates

The age models were created for all vibrocores based on ^{14}C calibrated (2 sigma) ages, core depth (cm) and sedimentation rates (cm per thousand of years).

The age-depth model adopted in this study was based on a linear interpolation, which assumes a stable sediment accumulation between the dated levels. The calibrated ages (cal. years B.P.) were plotted against core depths (cm) and the gradients of the lines connecting each adjacent pair of points corresponded to an estimate of the sedimentation rates. In the linear interpolation approach, interpolated ages are calculated for intermediate depths between each of the adjacent pair of points. The changes that are thus identified in the sedimentation rates along-core make the interpolation model the most appropriate fit to our data (Telford *et al.*, 2004). Moreover, although linear interpolation remains as a basic approach to derive an age-depth model, as it does not account for errors on the calibrated ages nor makes corrections for sediment compaction, it has been proven to provide good estimates for both ages and gradients, which are usually in agreement with results produced by more complex models (Blaaw and Heegaard, 2012).

Sedimentation rates (cm/ka cal. B.P.) that were obtained for all the shelf sedimentary sequences translate the velocity of sediment build-up (van Andel *et al.*, 1975). Zero validation was applied to the age model created for each sediment core.

III.3. Sedimentology

III.3.1. Grain-size

Downcore grain-size analyses were carried out sequentially in all four vibrocores using 2 cm-thick sample slices, or 3–4 cm slices for coarser sediments. Firstly, samples were treated with hydrogen peroxide to eliminate organic matter. Coarse (sand and gravel) and fine (silt and clay) grained sediments were then separated by wet sieving using a 63-μm sieve. The grain-size distribution (at phi scale intervals, Φ) of the coarse fractions was determined by dry sieving, and of the fine fractions by the pipette method. In addition, the dominant textural classes (gravel, sand, silt, and clay; silt and clay corresponding to 'mud' as defined by the classification of Folk, 1954) were determined in each case.

III.3.2. Determination of sand fraction compounds

For determination of the sand (–1 Φ to 4 Φ / 2 mm to 0.063 mm) compounds, a sampling grid of regular 10 cm intervals was established along-core in each one of the sedimentary sequences. A total of 39 samples were analysed for vibrocore 1, of 31 samples for vibrocore 6, of 25 samples for vibrocore 14 and of 36 samples for vibrocore 20.

The terrigenous and biogenic compounds were identified and quantified under a binocular microscope by counting 100 grains in each sand phi class (-1 to 0 Φ, 0 to 1 Φ, 1 to 2 Φ , 2 to 3 Φ and 3 to 4 Φ), giving a total of 500 grains for each sample. Within the terrigenous compounds, quartz, mica, charcoal, carbonate lithoclasts, schist/greywackes, sandstones, aggregates (poly-mineralic grains) and other terrigenous grains (mono-mineralic grains, such as feldspars and heavy minerals) were distinguished. The biogenic compounds were divided into molluscs, benthic foraminifera, planktonic foraminifera, ostracods and other bioclasts (such as fragments of echinoderms and corals). The results were statistically analysed and the weighted mean for all compounds was calculated after Sarnthein (1971), corresponding to the total sum of grains in each sand 'phi' class multiplied by their weight and divided by the total weight of the sand fraction.

The same procedure was adopted for the gravel fraction of vibrocore 20, whenever it was found to be statistically representative (≥100 grains in each sample) in more than one half of the analysed samples.

In order to maintain regional consistency, the identification scheme followed the classification established by Dias (1987) for the superficial sediments of the northern Portuguese continental shelf.

III.3.3. Quartz shape and surface texture

In the same samples that had been analysed for identification of the sand compounds, 100 quartz grains were additionally selected from each 1–2 Φ size fraction for surface texture and shape analyses. This investigation was also conducted under the binocular microscope, and the results were statistically evaluated with the calculation of the relative abundances for all variables that integrated the analysis.

Grains were classified according to the morphoscopic groups defined in Schneider and Cailleux (1959): not worn ('non-usés', NU, indicative of weak transport), rounded-frosted ('rond-mats', RM, indicative of aeolian transport), and smooth-shining ('emoussés-luisants', EL, indicative of transport in water). A fourth group was proposed for grains evidencing a mixed EL/RM signature, suggestive of initial water and subsequent aeolian transport.

Shape analyses were based on the roundness and sphericity of grains, indicators for erosion and transport (Powers 1953). The degree of roundness was classified from very angular (VA), angular (A), and subangular (SA) - indicative of weak transport - to subrounded (SR), rounded (R), and well rounded (WR), indicative of more vigorous transport. The degree of sphericity was classified as either high or low, indicative of both the transport intensity and the dominant transport mechanism that could correspond to a multidirectional (*e.g.*, tides, waves, wind) or to a unidirectional (*e.g.*, river currents) flow, respectively.

III.4. Benthic foraminifera

III.4.1. Sample preparation

The study of benthic foraminifera in the mud body deposits followed a 10 cm interval sampling grid for each core, and the core-base samples were considered for analysis. A total of 31 samples were analysed in vibrocore 1, of 30 samples in vibrocore 6, and of 25 samples in vibrocore 14.

All selected samples were dried in the oven at ca. 50 ºC and weighted, in order to obtain the weight (g) of the total sediment. Dry samples were then washed through the 2,000-μm and 63-μm sieves under tap water, to separate the gravel and sand sediments, and to remove the

fine material, respectively. The sieves went through Methylene Blue dye in-between the wash of each sample, to avoid their contamination with previously washed material. Both gravel and sand fractions were dried in the oven (ca. 50 ºC) and weighted, to attain the weight (g) of the total coarse-fraction of the dry sediment samples.

III.4.2. Counting and identification

The > 63-µm material was divided into aliquots with the help of an Otto micro-splitter, the size of the split for each sample being determined according to the number of expected individuals. The goal was to obtain at least 300 foraminiferal tests for identification in each sample, the number most widely considered as minimum necessary when a more detailed approach on the overall distribution of species is intended for the assemblages. Although for dead/fossil assemblages (time-averaged accumulations), the counting of 100 individuals may suffice to record all the important species, it often does not allow to distinguish more specific features such as which of the main species is dominant (Fatela and Taborda, 2002; Murray, 2006).

The study of the benthic foraminiferal microfaunas was carried out under a binocular microscope MEIJI Techno EMZ3, with a maximum magnification of up to 140x. In each aliquot, all well-preserved benthic foraminiferal tests were picked from a tray, mounted on lightly glued cardboard slides, and the individuals counted and identified up to the *species*, whenever possible. The generic classification of benthic foraminifera followed the taxonomy proposed by Loeblich and Tappan (1987) for the *Genera* level, except *Textularia*, *Quinqueloculina* and *Discorbis* for which the original species names found in the Ellis and Messina Catalogue of Foraminifera (1942-2009) were kept. Species identification was furthermore determined on basis of specialized bibliography, namely the Ellis and Messina catalogue (1942-2009), Murray (1971), Colom (1974), Boltovskoy *et al.* (1980), Jones (1994), Levy *et al.* (1995), Debenay *et al.* (2001), Murray (2003), Martins and Gomes (2004), Milker and Schmiedl (2012), among others.

Relative abundances (%) of all the identified species were calculated in all samples of the three cores. Taking into consideration counts of ca. 300 individuals, and although only abundances of < 1% are found to be close to confidence limits and cease to be significant (Buzas, 1990), the abundance variations of occurrences up to 5% are generally not considered meaningful (Murray, 2006). Hence, species distribution and assemblages of main benthic

foraminiferal species were established for each sedimentary sequence considering only species with more than 5% in at least one sample of the core.

All the main benthic foraminiferal species, and several other, were documented by means of scanning electron microscope (SEM) photographs, which were obtained with a JEOL, JMS-5200 LV microscope at the Faculty of Sciences of the University of Lisbon.

III.4.3. Population density and diversity measures

The population density (or faunistical density, FD) was calculated for each sample, corresponding to the number of benthic foraminifera per gram of dry sediment (nº/g of dry sediment). The number of species, designated by Species Richness (S), was also determined for each sample. The population diversity measures of Shannon-Wiener Index (Hs) and Evenness (J) were calculated using the PAST (PAlaentological Statistics, ver. 1.81) software (Hammer *et al.*, 2008), with species richness (S*i*) and the total number of individuals (*ni*) of each sample (*i*) as data entries. The Shannon-Wiener diversity index (values ranging from 0 to infinite) uses the proportion *p* of species *x* (*px*) and the ln(*px*), being *p*=100%. This implies that the contribution of each species *x* to the index value Hs(*i*) depends on its proportion within the sample *i*, and as a consequence rare species make little contribution. Evenness (values ranging from 0 to 1) is used to describe how individuals are distributed amongst species in each sample, meaning that the greater the dominance of one species, the lower will be the value of J.

III.4.4. Cluster analysis (multivariate statistics)

Cluster analysis was applied to the assemblages of main foraminiferal species (species with > 5% in at least one sample of each core), determined for the mud body sequences.

Cluster analysis stands as one of the most widely used techniques of multivariate statistics in foraminiferal studies, segregating variables (such as samples and species) into naturally occurring groups and quantifying the between-group relationships (Sen Gupta, 1999). A cluster corresponds to a group of objects of the considered variable that are sufficiently similar to be recognized as members of the same group, resulting from the analysis of the similarities/dissimilarities among those objects (Blaaw and Heegaard, 2012). The most frequently used clustering methods are both hierarchical and agglomerative, meaning they start with all objects in separate groups and proceed iteratively to cluster by merging pairs of groups from previous iterations, until all objects are grouped into a single cluster (Sen Gupta,

1999). The advantage of hierarchical clustering is that it allows for the local determination of group boundaries along a sedimentary sequence, evidencing the relationships among groups, whilst agglomerative clustering is also more satisfactory for zonation because the clusters are built up locally (Grimm, 1987).

Cluster analysis of the assemblages defined in each vibrocore was performed with the PAST software (ver. 1.81; Hammer *et al.*, 2008) for R-Mode clustering (grouping of foraminiferal species) and the TILIA software (ver. 2.0.2; Grimm, 2004) for Q-Mode clustering (grouping of samples).

For R-Mode clustering, analyses were stratigraphically unconstrained, as the grouping of species does not intend to join them on basis of their stratigraphic relationships. The PAST software allowed the performance of several algorithms and therefore a number of analyses were run with the foraminiferal data of the three vibrocores, as it is advisable to discard or distrust any results that are fundamentally different from the others (Sen Gupta, 1999). The algorithms tested were Ward's Method, also known as the 'incremental sum of squares' method, and UPGMA (Unweighted Pair-Group Method using Arithmetic averages) using as measure indices of goodness-to-fit either the 'Gower Distance' (dissimilarity measure) or the 'Matrix Correlation' (similarity measure). Ward's Method operates on a dissimilarity matrix of Euclidian distances (0-infinity) and follows a zonation criterion that diminishes the total within-zone dispersion, which means the clusters are joined such that the increase in within-group variance is minimized. In the unconstrained analysis, the method searches for the minimum value between objects in the entire dissimilarity matrix at each stage of the clustering process (Grimm, 1987). The UPGMA method proceeds by step-wise condensation of the cophenetic similarity/dissimilarity matrix. Each step starts by the identification of the next pair of objects that has the largest similarity or the smallest dissimilarity, followed by a condensation of all the measures of resemblance involving that pair which calculates the arithmetic means of the similarities/dissimilarities (Blaaw and Heegaard, 2012). Clusters are therefore joined based on the average distance between all members of two groups. As for the UPGMA measure indices that compare the original data matrix with the cophenetic similarity/dissimilarity matrix, 'Matrix Correlation' is Pearson's linear correlation coefficient r (0-1) computed between the values in the two half-matrices of similarities, whilst the 'Gower Distance' is the sum of the squared differences between the original and the cophenetic values (Blaaw and Heegaard, 2012). Although one method is not necessarily better than the other, attention should be paid to assure the best choice is made accordingly to the specificities of the analysed data. Correlation coefficients, for example, may prove to be

undesirable measures of similarity in high-diversity communities, because they are strongly affected by sample size (Krebs, 1989). Several studies based on the comparison of the various clustering techniques also seem to suggest that, in many cases, the Ward's Method may show some superiority to UPGMA algorithms (Sen Gupta, 1999). A good approach to quantify the success of a specific cluster analysis and compare the results given by different algorithms, is the obtainment of the cophenetic correlation value. It compares the between-object similarity values in the original matrix with a similar test derived from the clustered results, in which values approaching 1 indicate less distortion of the original similarities by the clustering process and thus correspond to the most adequate algorithm (Sen Gupta, 1999). After applying the three different algorithms of R-Mode clustering to the mud body foraminiferal microfaunas, Ward's Method proved indeed to be the best-fit to the foraminiferal data of the vibrocores. Although its cophenetic correlation value was not the highest for any of the cores, it proved still to perform quite satisfactory with high mean values, always above 0.86. But more importantly, the further comparison of the species assemblages suggested by its dendrograms and by those of the UPGMA indices with the natural distribution of the species abundances within each core, proved that the Ward's Method was the algorithm which reflected best the natural tendencies evidenced by the mud body microfaunas.

For Q-Mode clustering analysis, TILIA software uses the program CONISS that performs stratigraphically constrained clustering (clusters contain only stratigraphically adjacent samples) based on Ward's Method, which has proven to perform very satisfactorily on frequency data of fossil stratigraphic data (Grimm, 1987). For frequency data (*e.g.*, pollen data, foraminifera), transformation before calculation of the matrix of squared Euclidian distances, is usually advised (Grimm, 1987). This is particularly recommended when a few species are excessively common or rare in the samples and these extreme values distort the overall picture (Krebs, 1989), as was the case of the mud body foraminiferal assemblages. The square-root transformation, which produces the chord distance of Edwards and Cavalli-Sforza and up-weights rare variables relative to abundant ones, has been the best attested for this type of data (Grimm, 1987) and was thus applied to our foraminiferal data.

The cluster analyses produce results under the form of dendrograms, which illustrate the hierarchical relationships of the clusters defined by the analysis. The recognition of significant clusters within a dendrogram is largely a subjective process, with clusters being graphically designated by simply constructing a 'phenon' line that marks a level of similarity/dissimilarity at which the clusters are presumed to represent meaningful aggregations (Sen Gupta, 1999). A good strategy is to delimit zones using a straight cut across

the dendrogram and then, according with the specific distribution of the clusters for each set of data and if it requires so, to divide certain zones further into sub-zones that have interpretive value (Hedberg, 1976). In the specific case of the CONISS program (TILIA software) that was used, various criteria to define the heights of nodes connecting clusters in dendrograms for the 'incremental sum of squares' (Ward's) method, are available. The 'total within-cluster dispersion' was the criterion chosen for our foraminiferal data, as it usually generates zones similar to those the researcher would select by inspection, with just a straight cut across the dendrogram, therefore providing the most useful and realistic information (Grimm, 1987).

Chapter IV

INNER SHELF ENVIRONMENT

IV.1. Results

IV.1.1. Lithological description and profile

The lithological description of the sedimentary sequence was based on the direct observation of the sediments, taken place immediately after the vibrocore was opened and before sampling. According to this preliminary description, a log profile of the sequence was constructed for the present study (Fig. IV.1), in order to help visualize the general aspect of the main sedimentological features and fossiliferous content that characterized vibrocore 20.

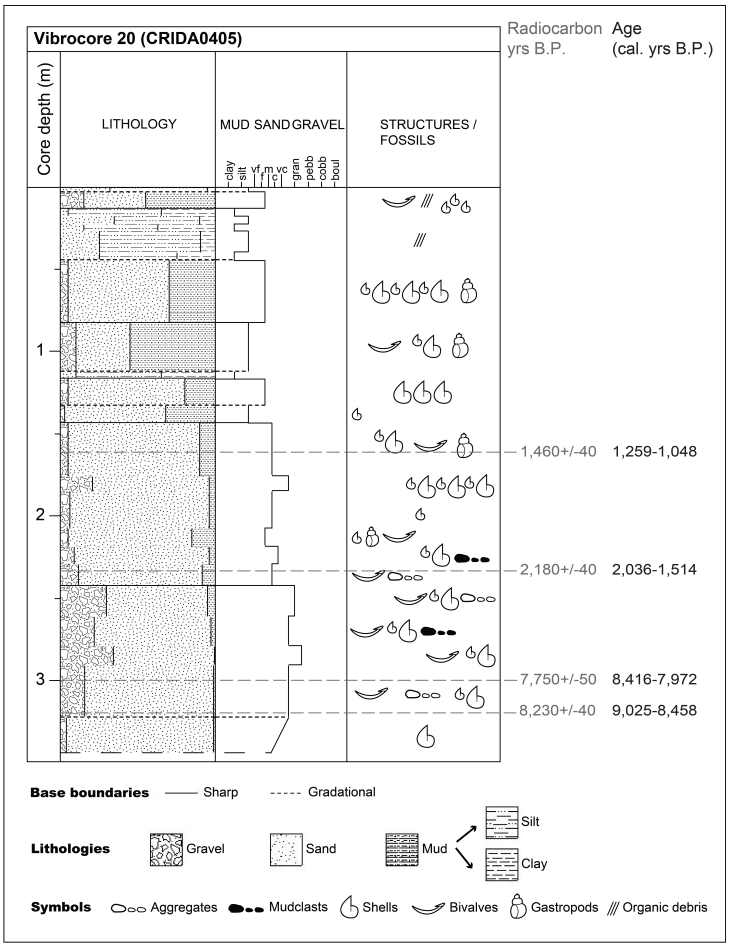

Figure IV.1 – Log profile of vibrocore 20. Fine sediments (silt and clay) stand as 'mud' whenever deposits were a mixture of gravel, sand and fines, or separately as 'silt' and 'clay' when deposits were composed only by sand and fines. 'Shells' represent mixed and mainly broken bioclastic content, with different symbol sizes attesting for the dimensional variability of the bioclasts found within the sediment layers.

From the base of the sequence until close to core level 241 cm, sediments corresponded to coarse sands with very abundant small to large bioclastic remains (mostly molluscs), and unbroken bivalve shells. Two depositional intervals (289-277 cm and 259-241 cm) within this core section were marked by enhanced coarse sedimentation, which was due to the particularly high accumulation of big-sized bivalve shells. Aggregates (rock fragments) were

also present in this section of the core, tending to become smaller towards its upper limit, together with some mudclasts that appeared between levels 277 cm and 259 cm.

A sharp boundary separated the base section of the upper one (comprised between levels 241 cm and 143 cm), indicating an abrupt change in sedimentation that occurred between both depositional phases. Deposition continued to be dominated by sands but these became medium- to coarse-grained, and with a clear higher contribution of fine material ('mud') throughout the section. The bioclastic content became more diversified, with still significant amounts of bioclastic remains of several dimensions but also more abundant unbroken bivalve shells and gastropods. Some mudclasts were detected between core levels 228 and 217 cm. A thin layer of ca. 10 cm of much coarser sands was identified at core depth 184-175 cm, characterized by a strong increase of the bioclastic content.

The transition to the upper section (from core depth 143 cm to 44 cm) was again marked by a rapid shift in sedimentation. Sediments became increasingly finer, with mainly fine-grained sands dominating the record and accompanied by an important mud component that increased as much as two-fold. The bioclastic content continued to be abundant and almost entirely dominated by broken mollusk shells. A very thin and well individualized mud layer was identified between levels 116 cm and 112 cm, apparently setting the definitive establishment of a fine-dominated deposition at the site of vibrocore 20 on the inner shelf.

Around core depth 44 cm, a gradational boundary translated a more or less gradual variation, with a depositional change towards even finer sediments. Predominantly silt and clay that were almost absent of visible bioclastic content, deposited at this site of the inner shelf until recent times (top of the sequence). This type of sedimentation was however interrupted during a specific event, recorded in the sedimentary sequence (core depth 13-3 cm) as a layer of coarser deposits. It corresponded to a mixture of sand and silt, with many bioclastic remains, some unbroken shells of bivalves and high amounts of organic debris. This organic material was only further registered at the core-depth interval 39-26 cm.

IV.1.2. Age model

The age model for vibrocore 20 was constructed based on four AMS radiocarbon datings, obtained at selected depth levels along-core. All information concerning the dated levels, sample laboratory codes, radiocarbon and calibrated dating results, is summarized in Table IV.1.

Table IV.1 – AMS Radiocarbon (^{14}C) dating of selected levels from vibrocore 20.

Core	Level (cm)	Lab. code	Conventional radiocarbon age (years B.P.)	Delta *R* (Local reservoir effect)	Calendar age B.C./A.D. (2σ calibrated)	Calibrated age (cal. years B.P.)
20	151-154	Beta-235174	1,460±40	-135±20	691-902 A.D.	1,259-1,048
20	215-217	Beta-244437	2,180±40	0±100	86 B.C.-436 A.D.	2,036-1,514
20	286-289	Beta-244438	7,750±50	0±100	6,466-6,022 B.C.	8,416-7,972
20	316-318	Beta-235175	8,230±40	0±100	7,075-6,508 B.C.	9,025-8,458

The oldest date was obtained at core level 316-318 cm, attributing an age of 9,025-8,458 cal. years B.P. near the base of the sedimentary sequence (Fig. IV.2). At core level 286-289 cm, dating results provided an age of ca. 8,416 to 7,972 cal. years B.P. for the sediments, corresponding to a coarser deposition (Fig. IV.2). An age of 2,036 and 1,514 cal. years B.P. was obtained at level 215-217 cm, where a peak (ca. 20%) of silt and clay deposition occurred (Fig. IV.2). Finally, the youngest date obtained for the sequence corresponded to an age between 1,259 and 1,048 cal. years B.P. at level 151-154 cm, which sets the beginning of fine sedimentation episodes on the inner shelf (Fig. IV.2).

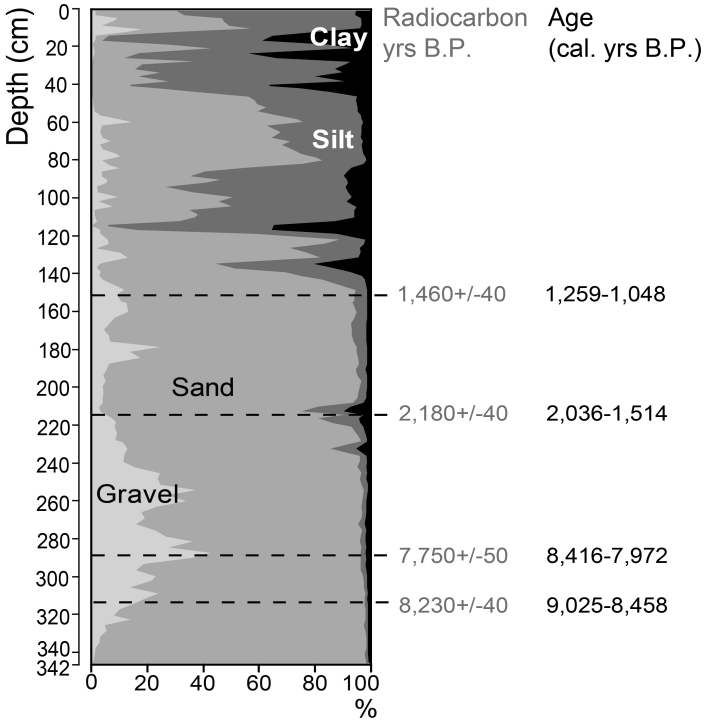

Figure IV.2 – Depth (cm), grain-size and dated levels along vibrocore 20. Dating results are given in radiocarbon years B.P. and calibrated ages (cal. years B.P.).

Sedimentation rates on the inner shelf location of vibrocore 20 showed a general increase trend along time (Fig. IV.3). In early Holocene, during the period between ca. 9,200 and 8,400-7,900 cal. years B.P., rates were about 54 cm/ka. For the period that lasted from ca. 8,400-7,900 cal. years B.P. until ca. 2,000-1,500 cal. years B.P., the rates decreased and reached their lowest values on the inner shelf, of around 11 cm/ka. During the late Holocene, the velocity of sediment build-up greatly increased. Sedimentation rates reached around 102 cm/ka during the period from ca. 2,000-1,500 until 1,260-1,050 cal. years B.P., and around 132 cm/ka from this last date until recent times.

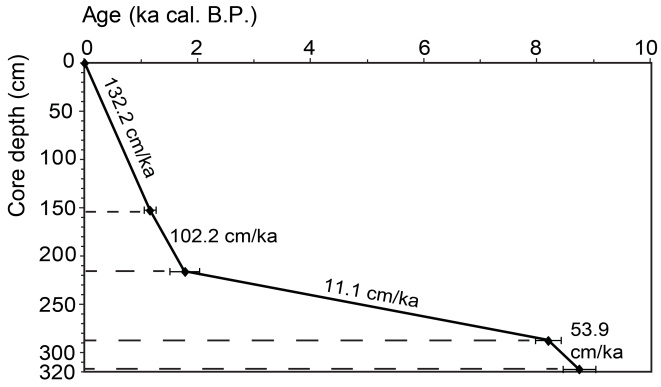

Figure IV.3 – Age model and sedimentation rates (cm/ka) of vibrocore 20. The error-bars in the control-points of the age model curve represent the uncertainty (2σ) of the calibrated dates (ka cal. B.P.).

In what concerns the lowermost ca. 20 cm of the vibrocore (from 318 to 342 cm core-depth), in which no dating was possible to obtain, the same sedimentation rate that was calculated for the oldest dated period of the sequence (between 9,025- 8,458 cal. years B.P. and 8,416 to 7,972 cal. years B.P.) was assumed for constructing the core age model. Based on these calculations, an age of 9,178 cal. years B.P. was estimated for the base-level (339-342 cm) of the sequence.

IV.1.3. Sediment characterization

IV.1.3.1. Grain-size

The grain-size composition (sedimentary texture) of vibrocore 20 showed that coarser sediments (gravel and mostly sand) dominated this inner shelf location until ca. 1,000 cal. years B.P., and from this age until present-day deposition became finer with enhanced content of silt and clay (Fig. IV.4a). Concomitantly, the mean grain-size of sediments was typical of coarse to medium sands until the same date, and afterwards increased to values that characterize fine sands and fines (Fig. IV.4b).

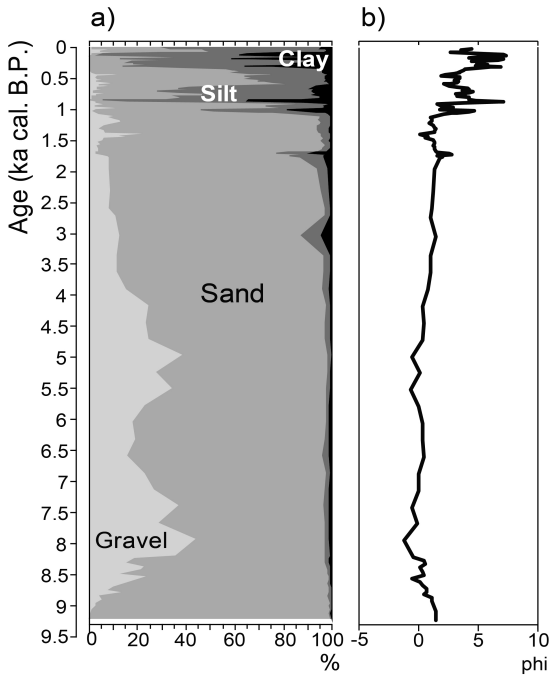

Figure IV.4 – **a)** Sediment grain-size composition (%) and **b)** mean grain-size (phi - Φ), along vibrocore 20.

Sand was the most abundant type of sediment from the base of the sequence until ca. 1,000 cal. years B.P., persistently comprising more than 50% of total sediments (Fig. IV.4a). Until ca. 3,500 cal. years B.P. it was escorted by significant amounts of gravel, together consistently comprising more than 95% of total sediments (Fig. IV.4a). Enhanced gravel deposition occurred between ca. 8,200 and 7,300 cal. years B.P., and again between ca. 5,600 and 4,700 cal. years B.P., with abundances ranging from 30% to 40%. These depositional events were intercalated by a period (ca. 6,800-6,000 cal. years B.P.) when gravel decreased, reaching minimum values of ca. 20% of total sediment and this gravel depletion being compensated by an increase of sand content up to almost 80%.

Between ca. 4,800 and 1,600 cal. years B.P., a gradual decrease of the gravel content was verified. From ca. 4,800 until 3,900 cal. years B.P. it comprised around 25% of total sediments, between ca. 3,900 and 2,700 cal. years B.P. it dropped to 10-15%, and between ca. 2,700 and 1,600 cal. years B.P. it persistently attained less than 10%. This was consentaneous with an increase of sand, which was always above 72.5% during the same period and reaching more than 85-90% between ca. 3,900 cal. years B.P. and 1,000 cal. years B.P. Within this period, fines exhibited peaks of abundance around 3,000 cal. years B.P. and 1,700-1,800 cal. years B.P., of ca. 15% and 20%, respectively. As for gravel, it showed two significant abundance peaks, at ca. 1,450-1,380 cal. years B.P. with 15-25% of total sediment, and around 1,200-1,100 cal. years B.P. with 10.5-13% (Fig. IV.4a).

The last ca. 1,000 years were characterized by a significant change in the depositional patterns (Fig. IV.4). Episodes of enhanced fine sedimentation (silt and clay) alternated with mostly sand depositional events, spanning for periods of more or less 100 to 300 years. During the period that lasted from ca. 1,060 to 930 cal. years B.P., silt increased to values of 15-35%, escorting sand that roughly spanned from ca. 70% to 80%. A short event of finer deposition took place around 1,020-1,000 cal. years B.P., with enhanced clay sedimentation (ca. 12-20%) and sand content dropping to 40-50%. It was followed by a sand peak of 70-85% between ca. 980 and 900 cal. years B.P., accompanied by a slight decrease of silt and clay to less than 5%. The period of ca. 870-840 cal. years B.P. corresponded to an episode of high silt and clay sedimentation, ca. 60% and 35%, respectively. From ca. 820 to 350 cal. years B.P., deposition exhibited very low clay contents and was dominated mostly by sand and silt, which alternated as the most abundant type of sediment along time. Hence, the period between ca. 820 and 620 cal. years B.P. was controlled by finer deposition, whilst from ca. 600 to 320 cal. years B.P. sand content ousted silt. Silt and clay again dominated sedimentation from ca. 310 to 90 cal. years B.P., and from this age until present-day clay became almost absent, with sand increasing again to values close to 30-40%. However, during these last ca. 100 years that were marked by a tendency for finer deposition, an episode of enhanced coarser sedimentation occurred. It was evidenced by a significant increase of both sand and gravel at around 90-75 cal. years B.P., which show a sharp peak of abundance in a single event, with sand reaching 40% and gravel almost 20%.

IV.1.3.2. Sand and gravel fraction compounds

The sand and gravel fractions of vibrocore 20 exhibited different distribution patterns for their terrigenous and biogenic compounds, but nonetheless both fractions showed a clear and steady trend of increasing biogenic content from the base to the top of the sequence (Fig. IV.5). Sand-sized sediments were persistently dominated by terrigenous particles until ca. 2,200 cal. years B.P., which showed particular high abundances (of ca. 80%) from the base of the sequence (at ca. 9,200 cal. years B.P.) up to ca. 5,700 cal. years B.P. (Fig. IV.5.a). From ca. 2,200 cal. years B.P. until the top of the sequence, deposition alternated episodes of terrigenous-dominated sand with biogenic-dominated sand (Fig. IV.5.a). Gravel-sized sediments revealed predominance of biogenic compounds throughout the sequence, except for a specific depositional event centered at ca. 8,600 cal. years B.P. (Fig. IV.5.b). However, the magnitude of the difference between the proportions of each type of gravel compounds was

quite variable along time (Fig. IV.5.b). From the base of the sequence until ca. 3,800 cal. years B.P., biogenic overcame terrigenous compounds but with smaller margins of difference, whilst from that age until recent times they increased substantially and became consistently 80% to almost 100% of the total gravel fraction (Fig. IV.5.b).

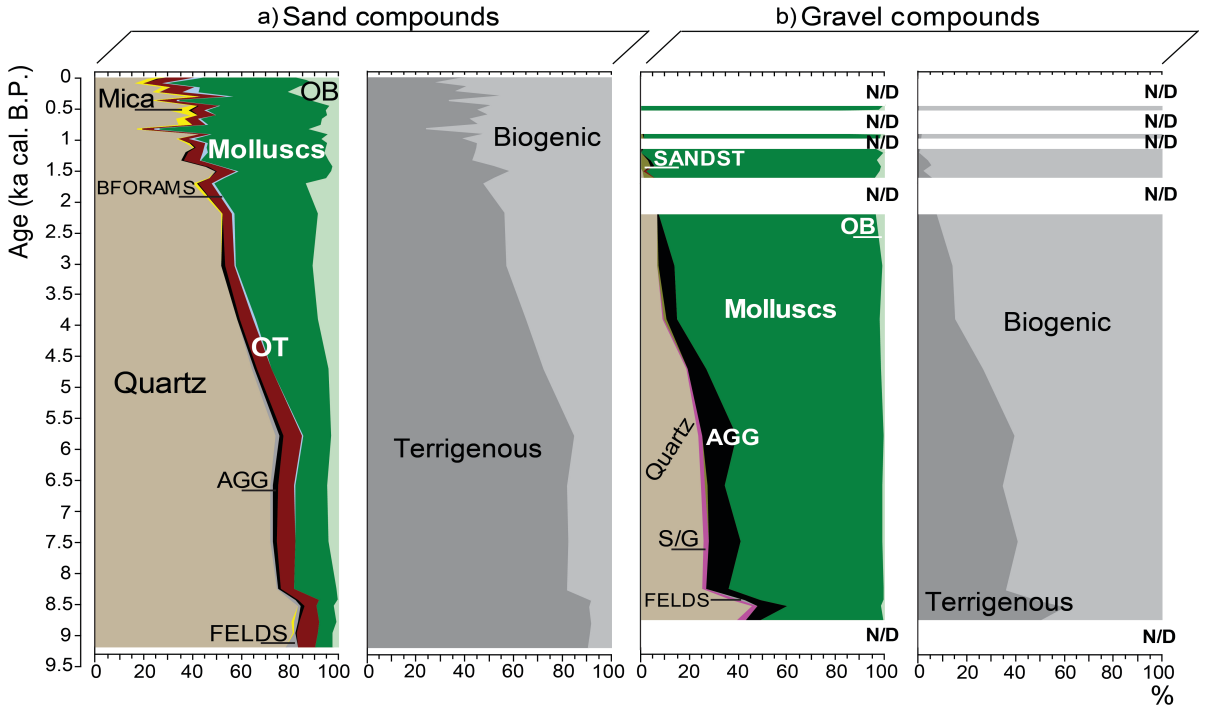

Figure IV.5 – Relative abundances (%) of terrigenous and biogenic compounds along vibrocore 20 for: **a)** sand fraction, **b)** gravel fraction. N/D ('no-data') refers to sections of the sedimentary sequence where the number of grains for counting was not statistically representative and no identification was obtained. Legend: FELDS - feldspars, S/G - schist/greywackes, AGG - aggregates, OT - other terrigenous, BFORAMS - benthic foraminifera, OB - other bioclasts, SANDST - sandstones.

Within the sand fraction (Fig. IV.5.a), the oldest recorded period spanned from ca. 9,200 to 8,400 cal. years B.P., and it was characterized by the highest amounts of quartz (ca. 80%) and lowest of biogenic compounds (ca. 7-9.5%). Within the terrigenous compounds, feldspars were present up to 5% and other terrigenous (OT) particles contributed with up to almost 9%. The biogenic component was constituted mainly by molluscs, which represented ca. 6-8% of the total sand fraction, and some fragments (< 2.5%) of other bioclasts (OB). During the period that lasted from ca. 8,400 cal. years B.P. until ca. 5,800 cal. years B.P., the proportions of both aggregates and OT were maintained, whilst feldspars decreased substantially to less than 1.5%. At the same time, the biogenic compounds increased twofold, with molluscs reaching almost 20% of total sand. From ca. 5,800 cal. years B.P. until 3,000 cal. years B.P., there was a gradual and steady increase of molluscs up to almost 32%, accompanied by an increase (up to ca. 10%) of OB particles from around 4,700 cal. years B.P. Feldspars became totally absent from the record during this period. Between 3,000 and ca. 2,100 cal. years B.P.,

sand became also devoid of aggregates. From ca. 2,100 and 1,700 cal. years B.P., OB increased to a maximum of ca. 13%, simultaneously with a fall in quartz abundance values down to ca. 40%. A new peak of terrigenous, mainly quartz, occurred at ca. 1,600-1,500 cal. years B.P., and it was contemporaneous with a decrease of OB particles. From this age until ca. 900 cal. years B.P., quartz decreased, while OB increased. Benthic foraminifera increased, although remaining with very low abundances of ca. 1-2.5%. At around 820 cal. years B.P., the highest amount of molluscs was verified, composing ca. 60% of the sand, concurrently with the lowest abundance of quartz, which was less than 20%. The phase between ca. 760 and 520 cal. years B.P. witnessed enhanced sedimentation of mica, which was up to almost 7.5%. Also, quartz increased again to ca. 30-40% and molluscs decreased from 60% to less than 50%. Another event of reduced terrigenous contribution took place at around 370 cal. years B.P., with less amounts of both quartz (25%) and mica (ca. 2.5%), attended by an increase of all biogenic compounds, in particular molluscs (ca. 55%) and OB (ca. 10%). It was followed by an episode of some reverse tendency, centered at ca. 300 cal. years B.P., characterized by an enhancement of quartz and mica deposition (ca. 40% and 6.5%, respectively), concomitant with a decrease in molluscs down to 25%. From this age until recent times, the abundances of terrigenous and biogenic compounds fluctuated around the same range of values. Quartz remained with lower abundances of 17% to less than 30%, mica around 3-4%, OT roughly 10%, benthic foraminifera between 2% and 5.5%, molluscs from 35% to 45% and OB from ca. 13% up to 20%. In general, deposition of sand was always dominated by quartz and molluscs, which alternated as the predominant component along time. They were accompanied by a more or less stable contribution of OT and OB particles, and by increased abundances of benthic foraminifera and mica from ca. 1,800 and 850 cal. years B.P., respectively, up to the top of the sequence.

Concerning the gravel fraction (Fig. IV.5.b), its abundance was not significant from the base of the sequence until close to 8,800 cal. years B.P. and thus the oldest considered period for its analysis was from ca. 8,800 to 8,500 cal. years B.P. It was characterized by the highest amount of terrigenous in the entire sedimentary sequence. Quartz (which included low amounts of quartzite) reached almost 50% of the total gravel fraction, whilst schist/greywackes also presented their highest abundances within the sequence (ca. 2-4.5%) and aggregates were 12.5%. The biogenic compounds were dominated almost exclusively by molluscs, with about 38% of total gravel. Between ca. 8,500 and 4,700 cal. years B.P., gravel was dominated by molluscs, which increased gradually from 50% until close to 72%, and the whole biogenic compound started to increase significantly from around 5,800 cal. years B.P.

onwards. During this period, quartz decreased gradually from ca. 37% to 19% and schist/greywackes also diminished to 1-2%. Feldspars were present only at ca. 8,400 cal. years B.P. with 2% abundance. As for aggregate particles, their quantity was constantly around 7-9%, except for two peaks at ca. 7,500 cal. years B.P. and 5,800 cal. years B.P., with 12.7% and 14.5%, respectively. Sandstones were constricted to around 6,600 cal. years B.P. with only 1.4%. The roughly 1,000 years-period that spanned from ca. 4,700 to 3,900 cal. years B.P. was marked by a further increase of molluscs up to ca. 83%, and a concomitant decrease of quartz down to ca. 9%. Aggregates also fell to values of 7.5-4.7% and schist/greywackes became less than 1%. During the next ca. 1,500 years, until ca. 2,400 cal. years B.P., the gravel fraction became much reduced. It witnessed an increase of the biogenic compounds, with molluscs reaching almost 90%, together with a decrease of quartz to values below 7%, and the total disappearance of schist/greywackes and sandstones. Gravel became again statistically representative at ca. 1,600 cal. years B.P. and lasting until ca. 1,100 cal. years B.P. The first hundred years of this period (ca. 1,600-1,500 cal. years B.P.) witnessed a drop in quartz to less than 1% and a return of sandstones that reached 4.5%, with both compounds representing the total contribution of terrigenous to the gravel fraction. As for the biogenic, molluscs surpassed 90% and OB particles were around 3.5-1.5%. From ca. 1,500 to 1,100 cal. years B.P., quartz became totally absent and sandstones the predominant terrigenous compound (up to 4.5%). Molluscs clearly dominated gravel during this time with ca. 93-99%. From ca. 980 to 900 cal. years B.P., they were accompanied by vestigial amounts of OB particles, sandstones and aggregates (ca. 1.5%). A hiatus in gravel deposition occurred again from ca. 800 to 600 cal. years B.P., followed by more or less one hundred years (ca. 520-440 cal. years B.P.) of fully biogenic gravel-sized particles, almost exclusively composed by molluscs (98-100%). From ca. 440 cal. years B.P. to present-day, gravel became once more statistically non-representative.

IV.1.3.3. Quartz shape and surface texture

The shape (morphometry) and surface texture (morphoscopy) analyses of sandy quartz along vibrocore 20 revealed that high sphericity, rounded (SUBR, R and WR) and simultaneously smooth-shinning grains dominated sediments at this site of the inner shelf for most of the studied period (Fig. IV.6).

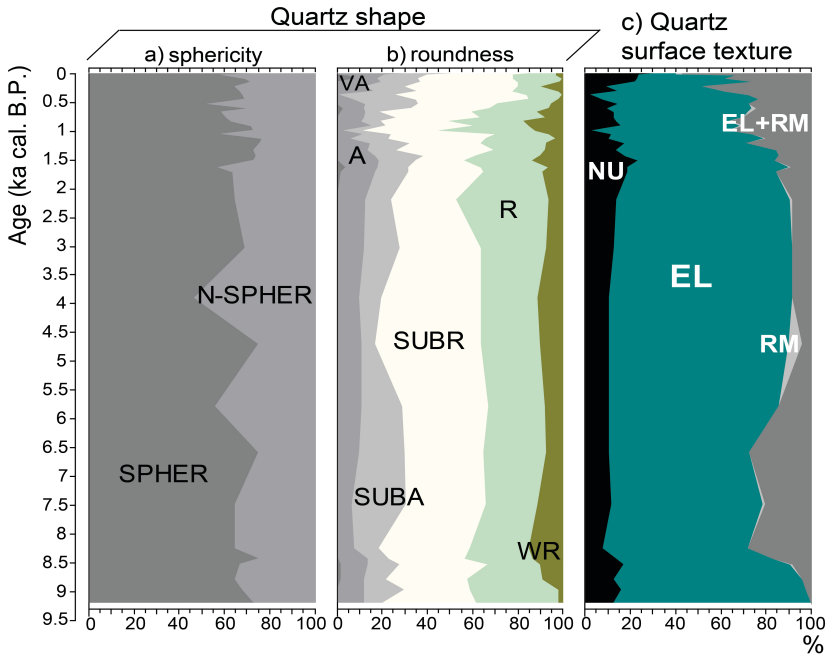

Figure IV.6 – Distribution (%) of sandy quartz grains along vibrocore 20 in relation to shape as **a)** sphericity and **b)** roundness, and to **c)** surface texture. Legend: SPHER – high sphericity, N-SPHER – low sphericity, VA – very angular, A – angular, SUBA – sub-angular, SUBR – sub-rounded, R – rounded, WR – well rounded, NU – not-worn, EL – smooth-shining, RM – rounded-frosted, EL+RM – mixed EL and RM signatures.

Sphericity characterization of the quartz grains (Fig. IV.6.a) indicated that the oldest recorded period (ca. 9,200-7,500 cal. years B.P.) was marked by predominance of high sphericity quartz with ca. 65-70%. Within this period, a localized event around 8,400 cal. years B.P. occurred, with high-sphericity grains reaching 76% of total sandy quartz. In the period between ca. 6,600 and 3,900 cal. years B.P., high and low sphericity grains alternated as the predominant quartz type. Two events with high sphericity quartz composing as much as 75% of total grains took place at ca. 6,600 cal. years B.P. and 4,700 cal. years B.P. They were intercalated by other two events, at around 5,800 and 3,900 cal. years B.P., in which the abundances of low sphericity grains greatly increased to ca. 45% and 53%, respectively. From ca. 3,000 to 1,600 cal. years B.P., the proportions of sphericity types were rather stable and high sphericity quartz dominated with ca. 60-70%. A phase evidenced by the highest abundance values of high sphericity quartz (73-77%) along the sequence took place from ca. 1,500 cal. years B.P. until ca. 1,100 cal. years B.P. It was followed by a peak (ca. 40%) of low sphericity grains at ca. 1,000 cal. years B.P., and again by a short period (980-900 cal. years B.P.) of input of high sphericity grains (ca. 72-73%). The time between 760 and 520 cal. years B.P. was characterized by another increase of low sphericity quartz, which ranged from 39% to 46%, although a peak of high sphericity (72%) was centered at ca. 590 cal. years B.P. From ca. 440 cal. years B.P. until recent times, high sphericity grains increased with

abundances ranging from 65% to 72%, except for a drop to 60% very close to the top of the sedimentary record (at ca. 20 cal. years B.P.).

The analysis of the roundness of quartz grains (Fig. IV.6.b) revealed that from ca. 9,200 to 8,400 cal. years B.P., the record was dominated by rounded forms (SUBR, R and WR) but there were also significant proportions of angular forms (mainly A with 10-13% and SUBA with 10-18%). Subrounded (SUBR) quartz generally oscillated between ca. 35% and 40%, whilst rounded (R) quartz fluctuated between around 30% and 40%. Well rounded (WR) grains were practically absent from the record until ca. 8,800 cal. years B.P., and from that age until ca. 8,400 cal. years B.P. increased up to 10-13%. A specific event was registered at ca. 8,200 cal. years B.P., with angular (A) grains dropping to below 10%, SUBR reaching 40% of total quartz and WR grains reaching a peak of 15%. From ca. 8,200 until 5,800 cal. years B.P. the abundance of SUBA grains increased to ca. 20-25% and conversely the R grains decreased to 23-28%, as well as the WR grains that were reduced to less than 10%. At the same time, A quartz was reduced to less than 10%. Between ca. 5,500 and 3,600 cal. years B.P., rounded forms again increased with SUBR grains reaching almost 50% of total quartz. The phase from around 3,600 cal. years B.P. to 1,800-1,700 cal. years B.P. witnessed a further increase of rounded (R) quartz up to 40%. The time interval 1,800-1,300 cal. years B.P. evidenced another rise of all angular forms, which constituted nearly 35% of total grains. From ca. 1,200 until 760 cal. years B.P. this tendency was reverted, with SUBA and A quartz diminishing to less than 10%. At the same time, SUBR grains reached abundances of up to almost 50%, R grains of up to ca. 40% and WR grains attained their highest value within the sedimentary sequence, of almost 20%. The next ca. 700 years, lasting until recent times, were distinguished by a gradual return to angular forms as SUBA and A quartz increased up to 20-30%, and particularly R grains diminished to below 20%. Specifically VA quartz reached ca. 10% in a single depositional episode centered at ca. 75 cal. years B.P, coincident with the total disappearance of WR grains.

Regarding the study of quartz surface texture (Fig. IV.6.c), from the base of the sequence until ca. 8,500 cal. years B.P. there were significant amounts (up to 17%) of not-worn (NU) quartz reaching this area, along with smooth-shining (EL) grains that dominated sands with ca. 75-85%. From ca. 8,400 to 5,800 cal. years B.P., grains with a mixed signature of smooth-shining and rounded-frosted (EL+RM) gained expression, composing between ca. 15% and almost 30% of total quartz. Contemporaneously, both NU and EL decreased to mean values of ca. 10% and 65%, respectively. The period ranging from ca. 5,500 to 3,800 cal. years B.P. was marked by a higher contribution of RM quartz (ca. 6%). A subsequent phase lasting ca.

300 years (from ca. 1,700 to 1,400 cal. years B.P.) was marked by an increase of NU grains up to ca. 25%, which then dropped to less than 5% at ca. 1,000 cal. years B.P., coincident with a peak of EL+RM grains of ca. 35%. A period of ca. 400 years followed, in which the contribution of NU again augmented to 10-16% and EL quartz decreased to ca. 50-60%. A well marked episode centered around 450-370 cal. years B.P. was determined by a drop in NU abundance to its lowest values within the sedimentary sequence (ca.3-8%). At the same time, EL grains increased to almost 70% and EL+RM quartz disappeared from the record. The next ca. 300 years witnessed a gradual recovery of NU, in parallel with a decrease of EL grains to values below 50% and an increase of EL+RM grains to ca. 35-45%. This period culminated with an event at ca. 75 cal. years B.P., characterized by the highest values of NU (ca. 30%) and mixed EL+RM (57%) grains along the entire sequence. Simultaneously, EL dropped to their lowermost abundance within the sequence, of ca. 10%.

IV.2. Discussion

The multi-proxy sedimentological analysis conducted in vibrocore 20 unravelled a succession of different depositional environments on this location of the Guadiana inner shelf for the period spanning from ca. 9,200 cal. years B.P until present-day. These depositional domains were distinguished by key sedimentological features (or evolutionary trends of such features), identified on basis of significant variations occurring within the set of the analysed proxies. For the last ca. 2,000, the higher resolution of the sedimentary record allowed a more detailed interpretation of events and the direct comparison with Historical information. This enabled the evaluation of the combined action of anthropogenic and recent climate impacts, which was one of the main aims of the present work.

IV.2.1. Depositional environments

Based on the previously mentioned key sedimentological features and trends, four main depositional stages were identified along the sedimentary record of vibrocore 20 for the evolution of this area throughout the analysed period (Fig. IV.7).

Stage 1: from ca. 9,200 until 8,500-8,200 cal. years B.P.

The first stage developed during the early Holocene (Fig. IV.7) and was characterized by apparently low sedimentation rates of about 54 cm/ka cal. B.P. (Fig. IV.3). This period corresponded to a time when the postglacial sea-level rise that marked the beginning of the Holocene was already in motion, as has been recognized since about 13,000-10,000 cal. years

B.P. in several other regional coastal and marine archives for the same region (Dabrio *et al.*, 2000; Lario *et al.*, 2002; Boski *et al.*, 2002, Teixeira *et al.*, 2005; Boski *et al.*, 2008; Zazo *et al.*, 2008) (Fig. II.7b). The sea-level rise certainly explains in part the inferred low sedimentation rates, as the sediments transported by the Guadiana River were partially retained inside the estuary. On the other hand, the existing lower sea level implied that this location was in a different environmental setting than today, and under a distinct sediment-supply regime as our data seem to suggest. Sand clearly dominated deposition at this time, whilst silt and clay were absent from the record (Figs. IV.4a and IV.7). The terrigenous compounds exhibited their highest contribution to this area during this stage, dominating the sand and gravel fractions (Figs. IV.5 and IV.7). Within terrigenous sand, the highest amounts of quartz and lowest of biogenic compounds were verified, together with the highest content of feldspars in all of the sequence, and a significant content of OT particles (Figs. IV.5a and IV.7). Within terrigenous gravel, the most noticeable feature was the presence of Paleozoic schists/greywacke (S/G), which exhibited their highest abundances of the record, and also a noteworthy contribution of aggregates (Figs. IV.5b and IV.7). The biogenic component of both coarse fractions was composed almost exclusively by mollusc shells throughout this stage (Figs. IV.5 and IV.7). In what concerns sandy quartz, there was a predominance of smooth-shinning, rounded (mostly SUBR and R) and of spherical grains, although significant proportions of angular forms and an important contribution of not-worn grains also characterized this site during this time (Figs. IV.6 and IV.7).

The clear dominance of sand, coupled with the absence of silt and clay material (Figs. IV.4a and IV.7), speaks in favor of a depositional environment where the prevailing conditions didn't allow for the settling of fluvial-derived fine sediments. Present-day depositional patterns at identical depths of the inner shelf indicate that it is currently under the influence of the Guadiana River suspended load discharges (González *et al.*, 2004; González *et al.*, 2007; Rosa *et al.*, 2013). Although sand typically dominates sediments at almost all depths of the inner shelf, continental-derived fine material has been found to be quite significant at the deepest areas of the inner shelf in the vicinity of the Guadiana River mouth, specifically below ca. 10 m water depth (Rosa *et al.*, 2013). The absence of this riverine imprint during the beginning of the Holocene at this site is most probably linked with the lower sea levels that prevailed prior to and during the initial phases of the postglacial Flandrian marine transgression. Several studies conducted worldwide, including in the North Atlantic and more specifically in the Algarve coast and the Gulf of Cadis, have established sea-level rise curves for this period and are consensual in that the sea level was by then many

meters below its present-day position. In general, these curves seem to place the site of vibrocore 20 above sea level (Fig. II.7) but almost any of them agree on the exact magnitude of the lowered sea level, in some cases differing for more than 10 meters (Fig. II.7), thus reflecting the high degree of uncertainty that can be inherent to such reconstructions. Namely the two curves established specifically for the Algarve region, those of Teixeira *et al.* (2005) and of Delgado *et al.* (2012), indicate quite different sea levels for this period (Fig. II.7b; from ca. -11 to -4 m and from ca. -27 to -15 m, respectively, for the period 9,200 until 8,500-8,200 cal. years B.P.). The latter puts indeed the current site of vibrocore 20 some meters above sea level at the beginning of the Holocene transgression, but its margin of error is rather high. On the contrary, the previous points to a different situation, in which this site would be very close to the coastline, and by the end of the present stage already ca. 10 m under the sea level. Considering this last scenario, the actual site of vibrocore 20 would have stand in an even shallower domain, probably transitional, or where deposition would be more identical to what has been detected in modern proximal areas above ca. 10 m that exhibit almost no muddy sediments and a strong domination of continental-derived terrigenous compounds (González *et al.*, 2004 and 2007; Rosa *et al.*, 2013). The bed-load exported by the Guadiana River into the coast (Portela *et al.*, 2004) that concentrates mainly in the proximal areas near the river mouth (González *et al.*, 2004), and the contribution of the littoral drift, which is mainly composed of sand and stands as a crucial regional sediment source into the Guadiana shelf (González *et al.*, 2004), would dominate deposition in this area. Furthermore, data regarding the early Holocene evolution of the Guadiana Estuary (Boski *et al.*, 2002) point to an accelerated phase of estuarine infilling by clayey sediments, between ca. 11,000 cal. years B.P. and 8,200-7,800 cal. years B.P. Consequently, it is expectable that the fluvial exports to the coast were by then deprived of a great amount of its suspended load. This in turn would facilitate the remobilization of this material from the shallow areas in the vicinity of the river mouth and the deposition would chiefly correspond to coarser sediments, as it seems to have been recorded in this location at this time.

Concurrently, the most significant presence within the record of several fluvial-originated terrigenous compounds, both in the gravel and in the sand fractions (Figs. IV.5 and IV.7), seems to confirm the existence of such a depositional setting in this location. Coastal depositional processes in areas close to fluvial sediment sources have been acknowledged as accumulation spots for continental-derived coarse terrigenous particles (*e.g.*, López-Galindo *et al.*, 1999; González *et al.*, 2004 and 2007; Rosa *et al.*, 2013). In particular, the contribution of feldspars and the high contents of OT particles clearly reveal the strong influence of the

Guadiana bed-load discharges. The OT particles are generated by the dismantling of igneous and metamorphic rocks along the Guadiana River basin and don't resist during long transport paths, thus concentrating in proximity to the sediment source where the system is able to preserve less these stable elements, namely in the deltaic bulge just off the river mouth and down to 5m water depth where sediments are coarser (González *et al.*, 2004; Rosa *et al.*, 2013). The same studies concluded that the fluvial-supplied OT tend to escort highly abundant marine shells (molluscs) at shallower waters just off the river mouth, which reflects quite well the general composition of sediments during this stage. Accordantly, the presence of feldspars has also been signalized at shallower depths under close continental sediment supplies, in neighbouring shelf areas of the Gulf of Cadis (López-Galindo *et al.*, 1999). As for the gravel-sized S/G particles that are exclusively originated in the outcrops of the Guadiana River basin, they have been related with the direct fluvial exportations onto the inner shelf and reported to peak out immediately off the river mouth, always escorting local OT depocenters (González *et al.*, 2004 and 2007). The lowermost content of both the gravel- and sand-fraction biogenic compound, almost exclusively mollusc shells (Figs. IV.5 and IV.7), it is also indicative of a very proximal coastal domain. Transgressive deposits previously identified on the Guadiana shelf, characterized as well by high amounts of quartz and OT particles associated with S/G particles and comparatively low amounts of bioclasts, have been associated with a higher-energy and more proximal domain impacted by floods in the Guadiana Basin, namely a detritical fan (González *et al.*, 2004). This study raised possibility that the lower sea levels implied the existence of an older detritical system at the beginning of the transgression, transporting sediments southward from the present-day Guadiana River mouth (González *et al.*, 2004). The long term export patterns disclosure by sandy quartz seem to support this hypothesis. Although it cannot be disregarded the importance of reworking processes associated with coastal and littoral drift currents that are attested by predominant smooth-shinning and tended rounded spherical grains (Figs. IV.6 and IV.7), the significant contribution of angular and not-worn grains (Figs. IV.6 and IV.7) corroborates the scenario of enhanced impact of the fluvial bed-load discharges during this period. Modern distribution of quartz on the Guadiana shelf features larger quantities of not-worn grains in the vicinity of the river mouth, namely in the deltaic bulge area, directly associated with sediment input from the Guadiana basin (González *et al.*, 2007). In the same way, angular quartz usually points to weak reworking and low remobilization that indicate proximity to the sediment sources.

Chapter V

MIDDLE SHELF MUD BODY

V.1. Results

V.1.1. Lithological description and profiles

The lithological description of the mud body sedimentary sequences was based on the direct observation of the deposits. This was carried out immediately after the vibrocores were opened and before sampling. The preliminary description of these deposits allowed the construction of log profiles for vibrocores 1, 6 and 14, aimed for the present study (Figs. V.1, V.2 and V.3). They have been intended to help visualize the general aspect of the main sedimentological features and fossiliferous content that characterized the three sequences retrieved from the Guadiana mud body.

The sequence of **vibrocore 1** (Fig. V.1) started at ca. 15,345 cal. B.P. (376-378 cm core depth) with the deposition of sandy muds escorted by small contents of gravel. The visible bioclastic content was very reduced and limited to some small-sized mollusc shell fragments. Close to the base of the core, this unit was characterized by more enhanced mud contents. They gradually decreased upwards in detriment of sand and gravel, until ca. 292 cm core depth, where an abrupt change in sedimentation set the terminus of this unit.

The above unit went from ca. 292 cm until ca. 243 cm core depth and represented a period of finer sedimentation in this area. Deposits became clearly dominated by compact mud (silt and clay), as sand decreased to half and gravel became absent. No visible bioclastic content was detected within these deposits.

The unit from ca. 243 cm until ca. 186 cm core depth showed again a gradual coarsening of sediments, with sand becoming dominant towards the top of the unit. Bioclastic remains appeared as rare near the base of the unit but small fragments of shells became much more abundant from ca. 205 cm core depth upwards.

The overlaying unit that corresponded to the core depth-interval 186-128 cm, was marked by an increase of fine sediments, with mud content surpassing sand. Visible bioclasts were absent from this entire section of the core, except for one isolated bivalve shell found in the transition between the previous unit and the current one.

A thin semi-liquid horizon (128-124 cm core depth) overlaid the preceding unit and was characterized by higher contents of sand and gravel. From here up to ca. 80 cm core depth, sediments consisted on a monotonous sequence of dark silty clays with no visible bioclasts. At the top of this unit, a thin anoxic layer marked the transition to the overlaying unit.

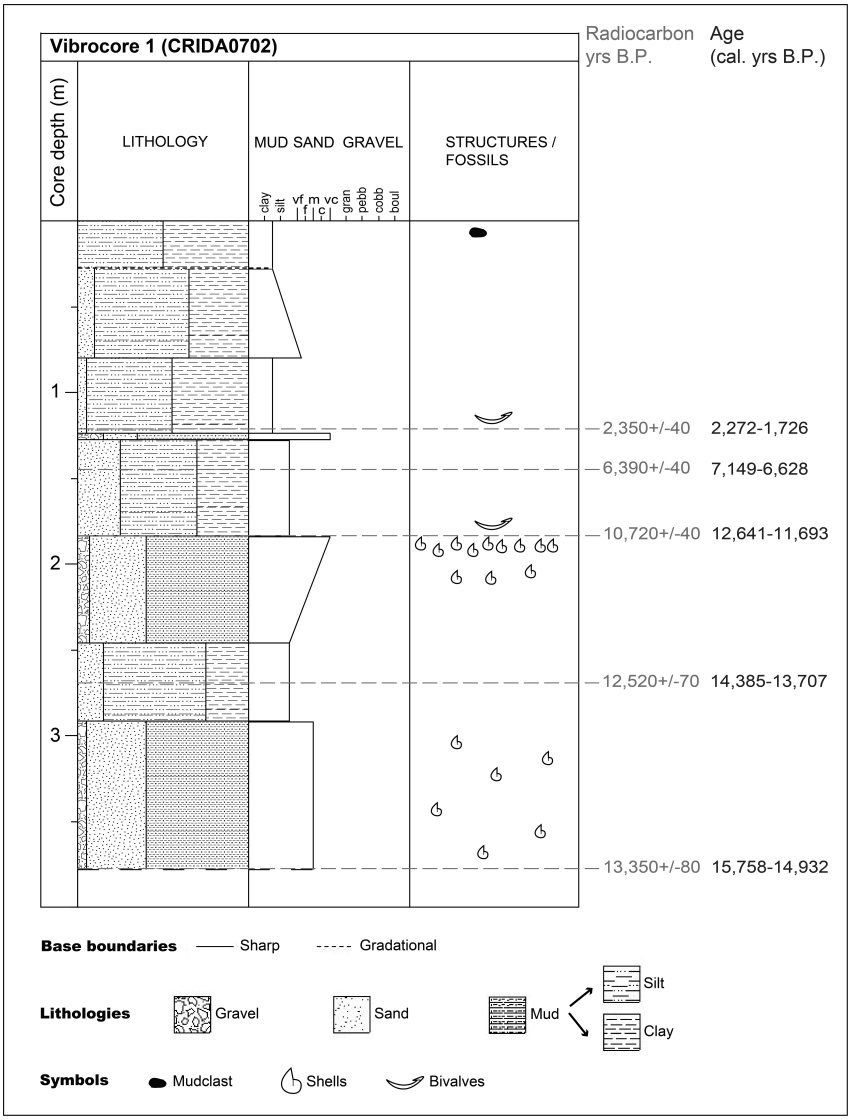

Figure V.1 – Log profile of vibrocore 1. Fine sediments (silt and clay) stand as 'mud' whenever deposits were a mixture of gravel, sand and fines, or separately as 'silt' and 'clay' when deposits were composed only by sand and fines. 'Shells' represents mixed and mainly broken bioclastic content, with different symbol sizes attesting for the dimensional variability of the bioclasts found within the sediment layers.

At ca. 80 cm core depth, sediments became slightly coarser due to another increase of sand-sized particles. Upwards, from this level until around 26 cm core depth (top level of the unit) deposition returned steadily and gradually to finer sediments.

The top-most unit of vibrocore 1 (ca. 26-0 cm core depth) was composed almost exclusively of muds, mainly due to the enhancement of clayey sedimentation.

The sequence of **vibrocore 6** (Fig. V.2) started around 12,500 cal. B.P. (297-299 cm core depth) with the deposition of uniform clayey silts showing some content of sands, which characterized sedimentation until ca. 243 cm core depth. To the top of the unit, a few larger mollusc shells were present.

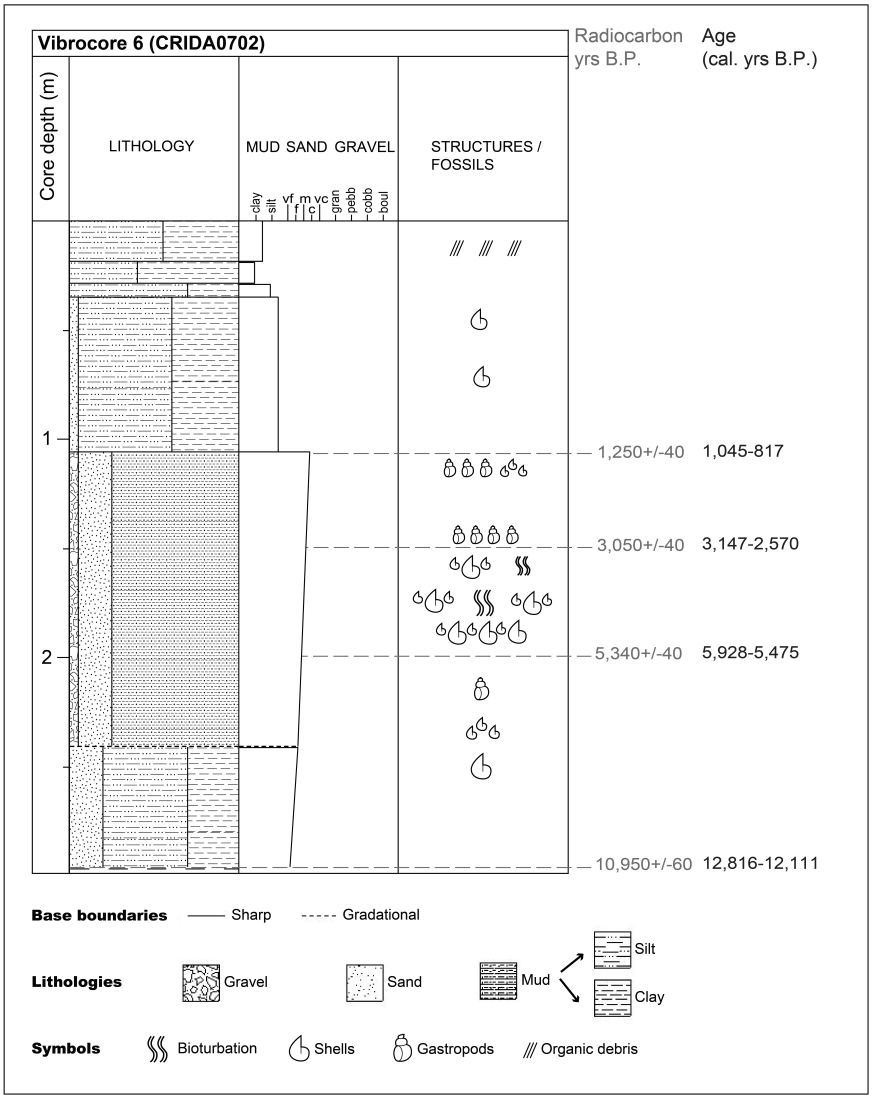

Figure V.2 – Log profile of vibrocore 6. Fine sediments (silt and clay) stand as 'mud' whenever deposits were a mixture of gravel, sand and fines, or separately as 'silt' and 'clay' when deposits were composed only by sand and fines. 'Shells' represent mixed and mainly broken bioclastic content, with different symbol sizes attesting for the dimensional variability of the bioclasts found within the sediment layers.

Between core levels 243 cm and 106 cm, deposition was dominated by a thick unit of muds with enhanced sand content and small amounts of gravel-sized particles. The dimensional composition of sediments remained rather constant with only small fluctuations, but some important variations of the bioclastic content were observed. Until ca. 223 cm core depth, sediments were devoid of visible bioclasts, except for some very small fragments of mollusc shells and one larger gastropod shell found at level 219 cm. The section ranging from ca. 223 cm to ca. 153 cm continued to present small fragments of shells and specifically the interval 170-153 cm evidenced several marks of bioturbation. Between ca. 153 cm core depth and the top of the unit (at 106 cm) most deposits were devoid of visible bioclasts, except for

two specific thin layers with concentrated small fragments of shells and gastropods, at levels 142-138 cm and 116-112 cm, respectively.

A thick unit developed between core levels ca. 106 cm and 39 cm, corresponding to a monotonous succession of clayey silts with much reduced sand content and almost total absence of visible bioclasts, although a few small fragments were identified at ca. 70-80 cm core depth and near the top of the unit.

Upwards, from ca. 39 cm to 31 cm core depth a ca. 10 cm-thick horizon was deposited. Sediments consisted of even more abundant silt with significant clay content, whilst sand disappeared from the record.

The overlaying unit comprised about 14 cm (from ca. 31 to 17 cm core depth) and evidenced a turn in the dominant size-fraction, with sediments becoming finer as clay content exceeded silt.

The upper-most unit, going from ca. 17 cm core depth until the top of the sequence, consisted of once again silt-dominated sediments, with an important clay contribution. Close to the bottom of the unit, a black anoxic thin layer rich in organic debris was detected. Bioclasts continued to be absent from the deposits.

The sequence of **vibrocore 14** (Fig. V.3) started around 2,500 cal. B.P. (239-241.5 cm core depth) with the deposition of a very coarse layer (ca. 8.5 cm-thick), dominated by sandy sediments with important gravel content. Mud was present but in very low amounts. No visible bioclasts were detected.

The above unit corresponded to the depth interval 233-225 cm and consisted on much finer sediments that were dominated by muds. Fine sands and gravel-sized particles were also present but in small amounts, whilst visible bioclasts remained absent.

A thin horizon between 225 cm and 221 cm was again composed of coarser sediments, with gravel content surpassing mud. Small fragments of shells began to appear within these deposits.

A new shift in deposition occurred between core levels 221 cm and 209 cm, with enhanced mud contribution and small quantities of both gravel and sand. Larger fragments of mollusc shells were present, together with a few unbroken bivalve shells.

The unit established at the core depth-interval 209-197 cm corresponded to another coarser depositional event due to higher input of gravel, despite muds continuing to dominate sediments. Fragments of shells of various dimensions were identified.

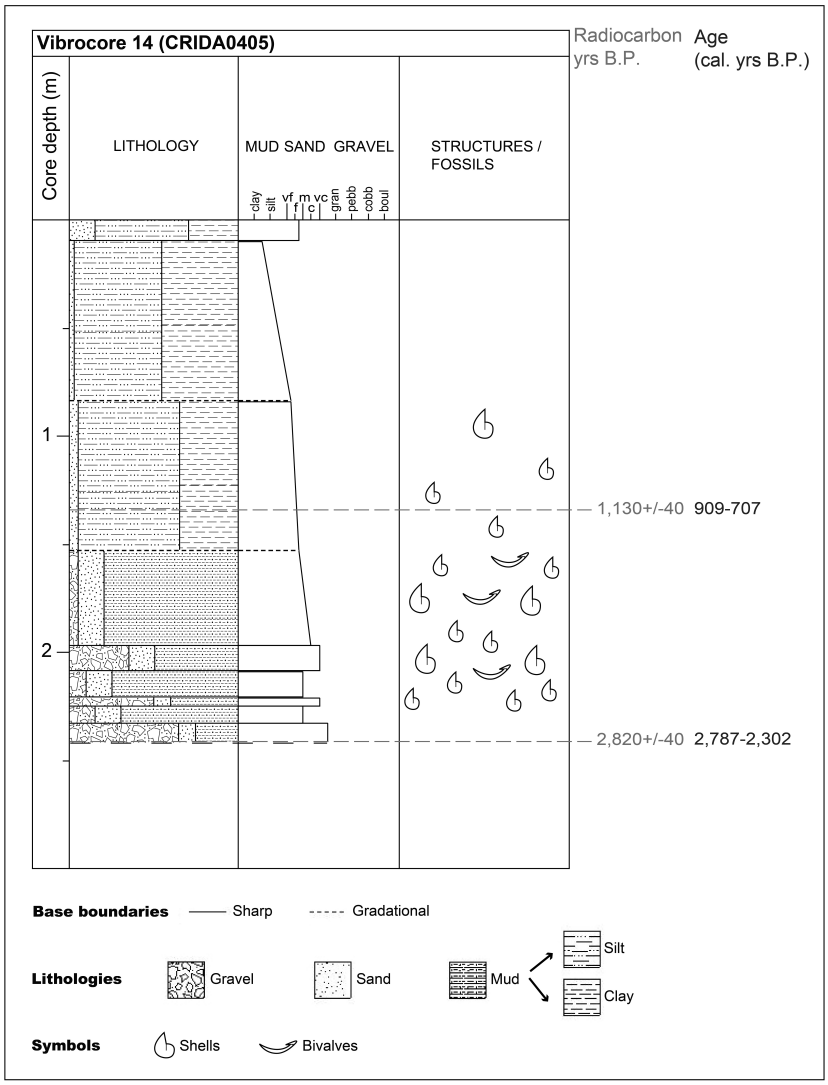

Figure V.3 – Log profile of vibrocore 14. Fine sediments (silt and clay) stand as 'mud' whenever deposits were a mixture of gravel, sand and fines, or separately as 'silt' and 'clay' when deposits were composed only by sand and fines. 'Shells' represent mixed and mainly broken bioclastic content, with different symbol sizes attesting for the dimensional variability of the bioclasts found within the sediment layers.

A thick unit developed between core levels 197 cm and 153 cm, dominated by muds but with a significant contribution of sands. The bioclastic content was abundant, consisting of medium-large fragments of mollusc shells and several unbroken bivalves. From the base to the top of the unit, a slight and gradual fining tendency of the sediments was observed.

The transition from the previous unit to the above one, at the core depth-interval of 153-84 cm, was gradational and the upwards fining trend previously observed was maintained. This unit was dominated by silt and clay, although a small contribution of sand-sized sediments persisted. The visible bioclastic content diminished and was sparse, consisting only on small mollusc fragments.

Another very thick unit developed between ca. 84 cm and 14 cm core depth. The transition was again gradational with an even more pronounced domination of fine sediments, as the deposits were composed almost exclusively of silts and clays. There was no visible bioclastic content.

The uppermost unit (last ca. 14 cm of deposition) marked another return to a somewhat coarser trend, as muds continued to clearly dominate sediments but there was an increase of the sand content. Again, no visible bioclasts were identified within the topmost unit of the sequence.

V.1.2. Age models

Age models were constructed for the three mud body vibrocores, based on a total of eleven AMS radiocarbon datings obtained at selected depth levels along-core. In all vibrocores, the oldest dating was obtained near the base of the sequences, allowing in each one to establish an age for the oldest recorded sediments. Conventional radiocarbon ages are reported as years 'before present' (B.P., 'present' = 1,950 A.D.). Calendar calibrated ages are reported as years 'before Christ' or 'Anno Domini' (B.C./A.D.), and calibrated ages as years 'before present' (B.P.). All information concerning the dated levels, sample laboratory codes, radiocarbon and calibrated dating results, is summarized in Table V.1.

In the case of **vibrocore 1** (Fig. V.4a), the base-level dating attributed an age of 15,758-14,932 cal. years B.P. to the sedimentary sequence, making it the oldest of the three vibrocores. At core level 272-274, an age of ca. 14,385-13,707 cal. years B.P. was estimated. Where a transition to more muddy sediments occurred, level 182-184 cm was dated as being ca. 12,641-11,693 cal. years B.P. Age estimation attained at level 146-148 cm provided a date of 7,149-6,628 cal. years B.P. for these sediments. At level 120-122 cm, close to a further increase of muds towards the top of the sequence, the youngest age obtained for the record corresponded to 2,272-1,726 cal. years B.P.

For **vibrocore 6** (Fig. V.4b), the oldest date was obtained at core level 297-299 cm and corresponded to an age of ca. 12,816-12,111 cal. years B.P. At level 199-201 cm, dating results revealed an age of 5,928-5,475 cal. years B.P. Around a small peak of sand and gravel, dating analyses performed at 149-151 cm core depth indicated an age of 3,147-2,570 cal. years B.P. Finally, the most recent age acquired for this sequence was of 1,045-817 cal. years B.P. at level 108-110 cm, when a clear shift to enhanced mud deposition was set.

Table V.1 – AMS Radiocarbon (^{14}C) dating of selected levels from vibrocores 1, 6 and 14.

Core	Level (cm)	Lab. code	Conventional radiocarbon age (B.P.)	Delta *R* (Local reservoir effect)	Calendar age B.C./A.D. (2σ calibrated)	Calibrated age (cal. years B.P.)
1	120-122	Beta-211321	2,350±40	0±100	322 B.C.-224 A.D.	2,272-1,726
1	146-148	Beta-342488	6,390±40	0±100	5,199-4,678 B.C	7,149-6,628
1	182-184	Beta-221035	10,720±40	0±100	10,471-9,743 B.C.	12,421-11,693
					10,691-10,484 B.C.	12,641-12,434
1	272-274	Beta-260012	12,520±70	0±100	12,435-11,751 B.C.	14,385-13,707
1	376-378	Beta-194503	13,350±80	0±100	13,808-12,982 B.C.	15,758-14,932
6	108-110	Beta-275573	1,250±40	-135±20	905-1,133 A.D.	1,045-817
6	149-151	Beta-204307	3,050±40	0±100	1,197-620 B.C.	3,147-2,570
6	199-201	Beta-221036	5,340±40	0±100	3,978-3,525 B.C.	5,928-5,475
6	297-299	Beta-194505	10,950±60	0±100	10,201-10,161 B.C.	12,151-12,111
					10,866-10,216 B.C.	12,816-12,166
14	132-136	Beta-282269	1,130±40	-135±20	1,041-1,243 A.D.	909-707
14	238-241.5	Beta-282268	2,820±40	0±100	837-352 B.C.	2,787-2,302

Concerning **vibrocore 14** (Fig. V.4c), the first two datings revealed that the sedimentation was much more recent and for that reason no additional analyses were performed. The age of 2,787-2,302 cal. years B.P. attributed to the base-level of the core (238-241.5 cm) revealed it to be the youngest sedimentary sequence of the three that were analysed. The second dating was carried out at level 132-136 cm, coincident with a depositional change towards enhanced silt contents that determined a definitive fining-up trend of sediments, and revealed an age of 909-707 cal. years B.P.

Sedimentation rates on the mud body evidenced an apparent generalized rising tendency along time, although vibrocore 1 seemed to reveal a long period with very low values that lasted from the beginning of the Holocene until around late Holocene (Fig. V.5).

The sequence of **vibrocore 1** (Fig. V.5a) exhibited mean sedimentation rates ranging between ca. 80 cm/ka and 48 cm/ka for the late Pleistocene- early Holocene period of the record, lasting from ca. 15,500 cal. years B.P. (at the base of the vibrocore) until ca. 12,000

cal. years B.P. Roughly coincident with the onset of the Holocene (11,700 cal. years B.P.), at ca. 12,000 cal. years B.P., there was an apparent accentuated drop of the rates, down to ca. 5 cm/ka. These values seem to have persisted until close to 6,000 cal. years B.P. and then slightly increased to around 6.8 cm/ka, which apparently was maintained throughout the mid- and until late-Holocene. Around 2,000 cal. years B.P., the rates increased to values more close to those prior to the beginning of the Holocene, reaching ca. 60.5 cm/ka.

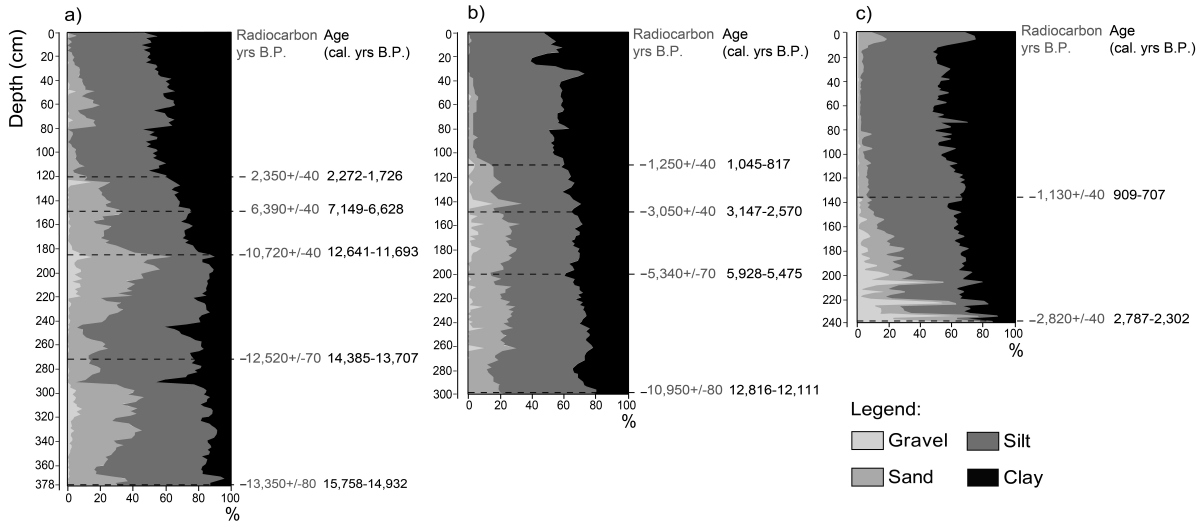

Figure V.4 – Depth (cm), grain-size composition and levels selected for dating analysis along: **a) vibrocore 1**, **b) vibrocore 6** and **c) vibrocore 14**. Dating results are given in radiocarbon years B.P. and calibrated ages (cal. years B.P.).

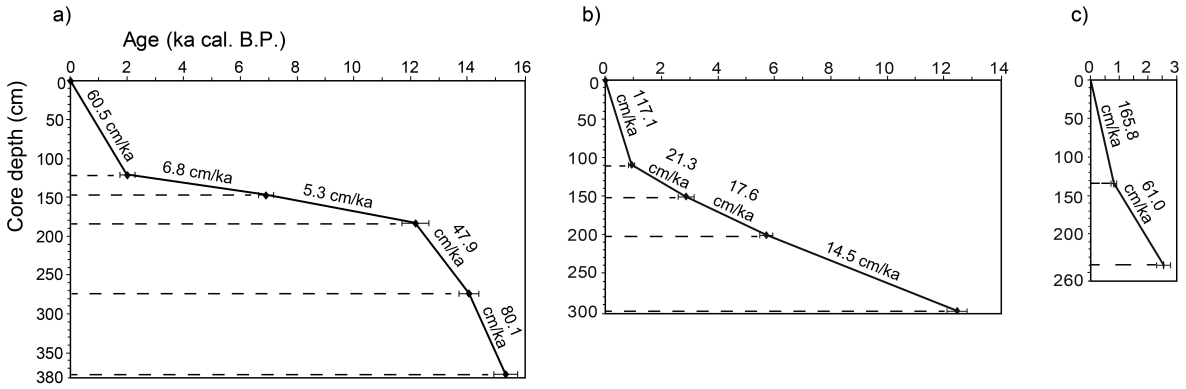

Figure V.5 – Age models and sedimentation rates (cm/ka) on the mud body: **a) vibrocore 1**, **b) vibrocore 6**, and **c) vibrocore 14**. The error-bars in the control-points of the age model curves represent the uncertainty (2σ) of the calibrated dates.

The sequence of **vibrocore 6** (Fig. V.5b) appeared to have presented lower sedimentation rates for the oldest deposits, followed by a persistent increase throughout the Holocene. From ca. 12,500 cal. years B.P. until close to 6,000 cal. years B.P., the apparent mean rates were of ca. 14.5 cm/ka. Between this date and around 3,000 cal. years B.P. they slightly increased to ca. 17.5 cm/ka, and again for the period that lasted until ca. 1,000 cal. years B.P., reaching ca.

21 cm/ka. The last 1,000 years apparently recorded a significant increment of the mean rates that reached close to 120 cm/ka.

The sequence of **vibrocore 14** (Fig. V.5c), which comprised only the late Holocene, provided a similar evolutionary trend of the sedimentation rates. The almost two first millennia that have been recorded at this site, from ca. 2,500 cal. years B.P. until ca. 800 cal. years B.P., were characterized by rates of about 60 cm/ka. During the last ca. 800 years, the rates increased more than twofold and reached values of ca. 165 cm/ka.

V.1.3. Sediment characterization

V.1.3.1. Grain-size

The grain-size composition (sedimentary texture) of the mud body sequences (Fig. V.6) revealed a persistent dominance of fines (usually > 60-70% of total sediments) and a generalized fining-up tendency, with particularly enhanced silt and clay deposition from around 2,000 cal years B.P. (vibrocore 1) and 1,000 cal. years B.P. (vibrocores 6 and 14). It is also worth of noting that the three sequences exhibited very identical grain-size compositional and mean patterns for the same periods along the time record (Fig. V.6).

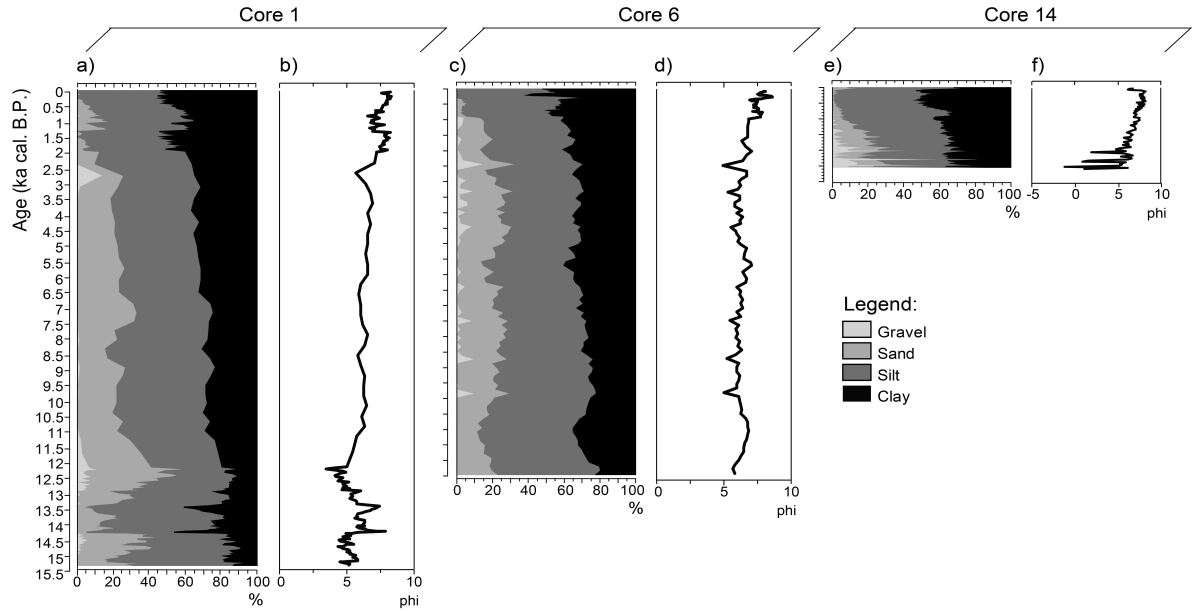

Figure V.6 – Sediment grain-size composition (%) and mean grain-size (phi - Φ) on the mud body: **a)** and **b) vibrocore 1**; **c)** and **d) vibrocore 6**; **e)** and **f) vibrocore 14**.

The sequence of **vibrocore 1** (Fig. V.6a-b) initiated at ca. 15,345 cal. years B.P. with a series of depositional cycles that alternated enhanced coarse-sized sediments, particularly sand, with greater inputs of fine material to the mid-shelf. These cycles started as shorter

episodes of about 500 year-depositional periods from ca. 15,500 until 14,250 cal. years B.P., and became longer towards the beginning of the Holocene, close to 12,000-11,500 cal. years B.P. The early Holocene around 12,000 cal. years B.P. was marked by an increase of fines, noticeably of silt, and a concurrent decrease of sands. This depositional pattern was maintained relatively constant throughout most of the Holocene, with only some fluctuations mainly around the relative proportions of sand- and clay-sized sediments. Around 3,000-2,500 cal. years B.P. an episode of enhanced gravel input occurred, setting the transition to a new depositional phase. It started at about 2,200 cal. years B.P. with silt-dominated deposition accompanied by ca. 40% of clay and almost 10% of sand, which gradually passed to a clay-dominated environment (almost 60% of clay). Simultaneously, sand content diminished upwards until it became absent at ca. 1,250 cal. years B.P. Around this date, another rapid change in sedimentation determined a shift to the next phase, as sands reappeared with ca. 15% in detriment of clay material. From 1,250 cal. years B.P. until close to 300 cal. years B.P., sand was always significant within the deposits but slowly decreasing towards the top. At ca. 300 cal. years B.P., sand disappeared from the record, concomitantly with an increase of clay content that persisted until recent times.

The sequence of **vibrocore 6** (Fig. V.6c-d) was permanently dominated by muddy sediments from the base until the top of the record but evident oscillations on the abundances of all the textural classes did occur. The record started in early Holocene at ca. 12,500 cal. years B.P. with an abundant deposition of silt-dominated muds to which sand contributed with ca. 10-15%, lasting until ca. 10,000 cal. years B.P. The time interval 10,000-6,500 cal. years B.P. was marked by a slight increase of the coarse-grained fraction. Although always in vestigial amounts, gravel appeared in the record with successive small peaks, whilst sand was persistently around 20%. Between ca. 6,500 cal. years B.P. and 5,000 cal. years B.P., the deposition became again finer due to a small rise in the abundance of both the silt and clay fractions. The period ranging from ca. 5,000 cal. years B.P. until ca. 2,300 cal. years B.P. set a return to slightly coarser conditions, with gravel increasing and clay contents diminishing. This phase terminated with a specific event centred at about 2,400 cal. years B.P. that was characterized by a peak of abundance of the gravel-size fraction (ca. 15% of total sediments), correspondent to the highest gravel content within the entire record. From 2,300 cal. years B.P. until close to 800 cal. years B.P. gravel contents dropped and silt increased. The time spanning from ca. 800 cal. years B.P. up to ca. 300 cal. years B.P. witnessed a further increase of fine sedimentation, in particular of silt, as gravel disappeared completely and sand became vestigial. At around 300 cal. years B.P., an episode of enhanced clay deposition that reached

about 60% of total sediments marked the transition to the most recent depositional phase. This last phase was characterized by persistent very high clay contents, with sediments being entirely composed of silt and clay until recent times.

The sequence of **vibrocore 14** (Fig. V.6e-f) started with several well pronounced, short-lived coarser- and finer-alternated depositional cycles that took place between the base of the vibrocore at around 2,550 cal. years B.P. and ca. 1,950 cal. years B.P. The first cycle presented more than 50% of gravel content, escorted by small amounts of sand and silt, and by ca. 20% of clay. At around 2,500 cal. years B.P. a new cycle of reverted tendency was set with gravel dropping to nearly 10%, whilst clay and silt increased to almost 40% and to 35%, respectively. Another coarse-enhanced depositional cycle occurred at around 2,480 cal. years B.P., with gravel peaking close to 70% and both silt and clay diminishing to less than half-content. It was succeeded by a longer depositional cycle between ca. 2,450 and 2,320 cal. years B.P., which was characterized by gravel content below 20%, increased sand up to ca. 15% and enhanced silt and clay that made up 40% and 35% of the deposits, respectively. At ca. 2,300 cal. years B.P. another important peak of gravel (of ca. 60%) was accompanied by a great decrease of all the other grain-size fractions. From ca. 2,280 cal. years B.P. until ca. 2,050 cal. years B.P. mud sediments dominated deposition with ca. 85%, except for a localized event at 2,150 cal. years B.P. when gravel reached almost 15%. The last significant gravel contribution within the sequence took place at about 2,000 cal. years B.P. with ca. 35%. At around 1,950 cal. years B.P. an important shift in the depositional pattern was put into motion, with the end of the short depositional cycles. A longer depositional phase commenced and lasted until ca. 1,100 cal. years B.P., featuring reduced gravel content that was always below 15% and gradually decreased together with sand. At the same time, clay continued contributing with ca. 35% while silt progressively increased. From ca. 1,100 cal. years B.P. until ca. 500 cal. years B.P. the sedimentation became even finer, with sand contents of around 5% and muds composing the remaining ca. 95% of total sediments. The time interval of ca. 500-200 cal. years B.P. witnessed the complete disappearance of the coarse-fraction and the deposits were fully mud-composed. From ca. 200 cal. years B.P. until the top of the record, sand was again present but with just 5-10%. The exception was an event centred at ca. 45-25 cal. years B.P., in which sand increased to 15-18%.

V.1.3.2. Sand fraction compounds

All the three sequences of the mud body exhibited specific evolutionary trends concerning their terrigenous and biogenic composition of sand (Fig. V.7). However, the overall distribution of compounds along time revealed a generalized domination of terrigenous and an increase in the diversity of the bioclasts towards the top of the sequences (Fig. V.7). Within terrigenous quartz was almost always the most abundant compound, whereas bioclasts were dominated by molluscs, except the last 7,000 years of vibrocore 1, usually dominated by benthic foraminifera (Fig. V.7).

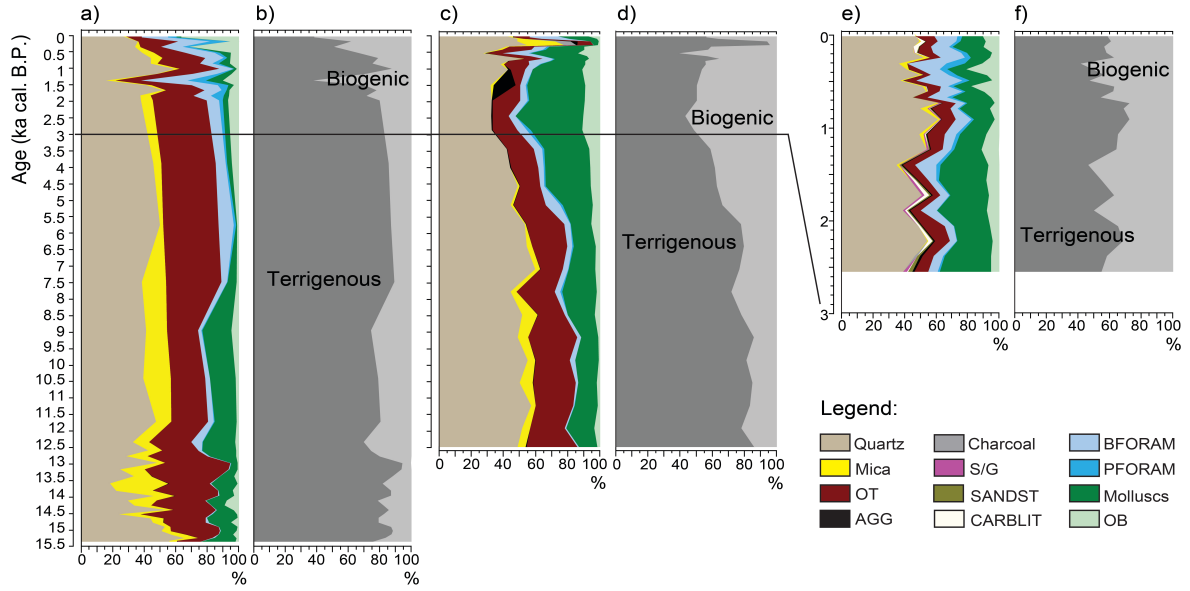

Figure V.7 – Relative abundances (%) of sand compounds and proportion (%) of terrigenous versus biogenic compounds on the mud body: **a)** and **b) vibrocore 1**; **c)** and **d) vibrocore 6**; **e)** and **f) vibrocore 14**. Legend: OT – other terrigenous, AGG – aggregates, S/G – schist/greywackes, SANDST – sandstones, CARBLIT – carbonate lithoclasts, BFORAMS – benthic foraminifera, PFORAMS – planktonic foraminifera, OB – other bioclasts.

The record of **vibrocore 1** (Figs. V.7a-b) started in the late Pleistocene, at ca. 15,500 cal. years B.P., with enhanced sandy terrigenous contents of almost 90%, to which quartz contributed with 50-65%, being escorted by ca. 15% of other terrigenous (OT) particles and vestigial mica, whilst molluscs dominated the biogenic compound. The next phase went from ca. 14,800 cal. years B.P. to ca. 13,000-12,900 cal. years B.P. and showed the same proportion of terrigenous versus biogenic compounds but an accentuated decrease of quartz to values oscillating between 20% and 40%, in favour of enhanced contents of mica (ca. 5-35%) and particularly of OT (ca. 25-40%). Mollusc shells continued to dominate the biogenic compound with ca. 15-20% of total sand. The phase from ca. 13,000-12,900 until 11,800 cal. years B.P. was characterized by a shift in the composition of sand, evidenced by an important increase of the bioclasts due to higher mollusc content and the appearance of benthic

foraminiferal tests that attained ca. 5%. At the same time there was a significant decrease of the OT down to ca. 20-25% and of mica down to ca. 5-10%. Between ca. 11,800 and 9,000 cal. years B.P., roughly coincident with the beginning of the Holocene, mica deposited again with up to ca. 15-20% and there was a slight decrease of the biogenic compound, more noticeably of the mollusc content. The time interval of ca. 9,000 cal. years B.P. until ca. 7,500 cal. years B.P. translated an evident change in the characteristics of sand. There was a strong terrigenous increase driven mainly by higher abundances of OT particles in detriment of much lower abundances of mollusc shells, leading to the almost full domination of the biogenic compound by benthic foraminifera. During the period that followed, from ca. 7,500 until 5,700 cal. years B.P., the relative proportions of terrigenous and bioclasts remained rather constant but there was a significant change within the first, as mica gradually decreased to about 5%, and quartz and the OT were much enhanced to nearly 50% and more than 20%, respectively. A long depositional period succeeded between 5,700 cal. years B.P. and ca. 1,800 cal. years B.P., in which all sand compounds and the terrigenous/biogenic proportions were generally maintained, although quartz steadily decreased upwards in detriment of mica and planktonic foraminifera that made their first appearance and rapidly reached nearly 8%. Afterwards, the late Holocene was distinguished by some accentuated depositional changes. The first significant phase was centred around 1,700 to 1,200 cal. years B.P., with a fast turn in sedimentation that led to the highest abundance peak (> 60% of total sand) of the biogenic along the entire sequence. Both benthic and planktonic foraminifera increased twofold to ca. 30% and 11%, respectively, and molluscs and other bioclasts (OB) tripled up to around 10%. Within terrigenous, quartz evidenced the most pronounced drop from ca. 40% to 18%, but OT particles were also reduced from ca. 25% to 15%. A depositional episode then occurred around 1,100 cal. years B.P., with another rise in terrigenous, namely quartz that dominated sand with ca. 60% and OT. Concurrently, benthic foraminiferal content dropped to half and all other biogenic compounds practically disappeared. Starting at around 900-800 cal. years B.P. and until close to present-day, the last depositional phase saw a general increase of all biogenic and also of mica, whilst quartz and OT progressively diminished. A specific event centred at ca. 180 cal. years B.P. is worth noting, when OT again showed an abundance peak in detriment of decreased mica and OB, which became almost absent from the record.

The record of **vibrocore 6** (Figs. V.7c-d) showed that from the base of the sequence, at ca. 12,500 cal. years B.P., until around 9,200 cal. years B.P. the sand fraction was clearly dominated by ca. 80-85% of terrigenous material. Within it, quartz was predominant with about 50% of total sand, escorted by an important contribution of OT particles (ca. 20-30%)

and by ca. 2.5-8% of mica. Regarding the biogenic compounds, mollusc shells dominated these older deposits. The phase between ca. 9,200 cal. years B.P. and 7,200 cal. years B.P. witnessed an increase of the biogenic up to ca. 30%, mainly due to more abundant mollusc contents and increasing benthic foraminifera (up to ca. 5%) that were concomitant with a decrease in quartz. The period lasting until ca. 5,700 cal. years B.P. was marked by a rise in terrigenous, with the increase of quartz and OT particles, and reduced biogenic contents that were driven mainly by less amounts of mollusc shells. The 5,700-5,500 cal. years B.P. timeline then set a definitive turn within the record, with the older sediments being clearly dominated by terrigenous and sediments deposited after that date becoming gradually enriched in bioclasts until the top of the sequence. Hence, the period from 5,700 until ca. 2,500-2,200 cal. years B.P. witnessed a gradual and significant increase of the whole biogenic compound, particularly of molluscs that composed almost 40% of total sand, and of benthic foraminifera that doubled to ca. 8%. At the same time, quartz diminished to a minimum of ca. 35% and mica became vestigial. The depositional phase between ca. 2,500-2,200 cal. years B.P. and 1,100 cal. years B.P. exhibited a moderate but steady trend of increasing and diversifying terrigenous, mainly due to an important contribution of aggregates that composed almost 15% of sand, in detriment of mollusc content. Although vestigial, it is worth noting that mica reappeared in the deposits, escorting the aggregate particles. The last ca. 1,000 years were characterized by fast, short-phased oscillations of almost all terrigenous and biogenic compounds. Between ca. 1,100 and 600 cal. years B.P. terrigenous peaked out with almost 70% of total sand, as quartz attained ca. 55%. However, aggregates disappeared during this time. The following depositional phase, lasting from ca. 600 until 300 cal. years B.P., showed a reverse tendency. Bioclasts made their highest contribution within the record (almost 60%), with benthic foraminifera reaching a peak of 14%, molluscs increasing to ca. 25-30% and other bioclasts (OB) to ca. 9-12%. Within the terrigenous, quartz dropped to ca. 36% and OT also decreased. From ca. 300 cal. years B.P. until ca. 100 cal. years B.P. an important depositional shift determined the highest abundance of terrigenous compounds in the whole sequence, which peaked out with 95% of total sand. Amongst terrigenous, quartz contributed with 50% and aggregates reappeared with about 5%, whilst the most noticeable features were an input of mica of ca. 23% and the arise of charcoal particles (ca. 7.5-9.5%) that were present only during this period. Contemporaneously, the much reduced biogenic contribution was limited to mollusc shells. The last ca. 100 years witnessed a gradual recovery of all biogenic compounds, in particular of benthic foraminifera and molluscs (ca. 15-20% and 17.5%, respectively), whilst mica returned to abundances below 5%.

The record of **vibrocore 14** (Figs. V.7e-f) began at ca. 2,600 cal. years B.P. and the oldest depositional phase lasted from this date until ca. 2,300 cal. years B.P., with terrigenous sand (ca. 55%) slightly surpassing biogenic sand (c. 45%). It was characterized by high diversity of terrigenous compounds that were dominated by ca. 40% of quartz and included ca. 2% of fragments of schist/greywackes (S/G), of sandstones and of aggregates, together with ca. 8% of OT. Bioclasts were dominated by molluscs that composed ca. 30% of sand, but had also an important contribution of benthic foraminifera with ca. 5-10%. From 2,400 cal. years B.P. until ca. 2,000 cal. years B.P. there was a further enhancement of terrigenous up to 70% of total sand, mainly due to the increase of quartz up to ca. 55% and of OT up to ca. 20%, in detriment of reduced mollusc content. However, and despite the abundance rise of carbonate lithoclasts (CARBLIT) during this time, terrigenous became less diversified as S/G and sandstones disappeared from the record. Between ca. 2,000 and 1,500 cal. years B.P. bioclasts generally increased to ca. 50% of total sand, mostly driven by increased contents of mollusc shells. At the same time, there was a significant decrease of OT particles, which dropped from ca. 14% to 6.5%, but S/G contributed again to sedimentation. The short phase lasting from ca. 1,500 cal. years B.P. until 1,300 cal. years B.P. witnessed a further enhancement of bioclasts, especially due to an important increase of benthic foraminifera up to 13%. Molluscs also increased and planktonic foraminifera, although vestigial (ca. 3%), slightly increased in this period. Terrigenous were reduced to ca. 35% of quartz, 10% of OT and the first contribution of mica that was nonetheless vestigial. Between ca. 1,300 cal. and 700 cal. years B.P. there was a gradual recovery of terrigenous with increased abundances of quartz, mica and OT, against an impoverishment in molluscs and benthic foraminifera. In the period ranging from ca. 700 to 250 cal. years B.P., the composition of sand oscillated several times, chiefly due to alternated higher and lower quartz abundance in opposition to decreased or increased biogenic contribution. Notwithstanding, in general this period was marked by much more abundant benthic and planktonic foraminifera (ca. up to almost 30% and 5%, respectively), together becoming more abundant than molluscs, and by much lower amounts of OT that accompanied a general decrease in quartz. The last ca. 250 years of deposition featured another increase of terrigenous up to ca. 65% until the top of the sequence, mostly because of enhanced OT supplies. CARBLIT reappeared in very small amounts, and simultaneously mica became absent. Within bioclasts, benthic foraminifera were co-dominant with molluscs, escorted by OB fragments and planktonic foraminifera.

V.1.3.3. Quartz shape and surface texture

The shape and surface texture characterization of sandy quartz was possible only for vibrocores 6 and 14, because the sand fraction 1-2Φ in most of the samples from vibrocore 1 did not provide the minimum number of quartz grains required for this analysis. The quartz shape and surface characteristics revealed quite common features and trends at both mid-shelf sites for most of the studied period (Fig. V.8). Namely, the very similar proportions of high and low spherical quartz, together with the predominance of rounded forms and smooth-shinning textures, coupled with an important contribution of not-worn grains (Fig. V.8). However, somewhat distinctive patterns were also observed along the sequences (Fig. V.8).

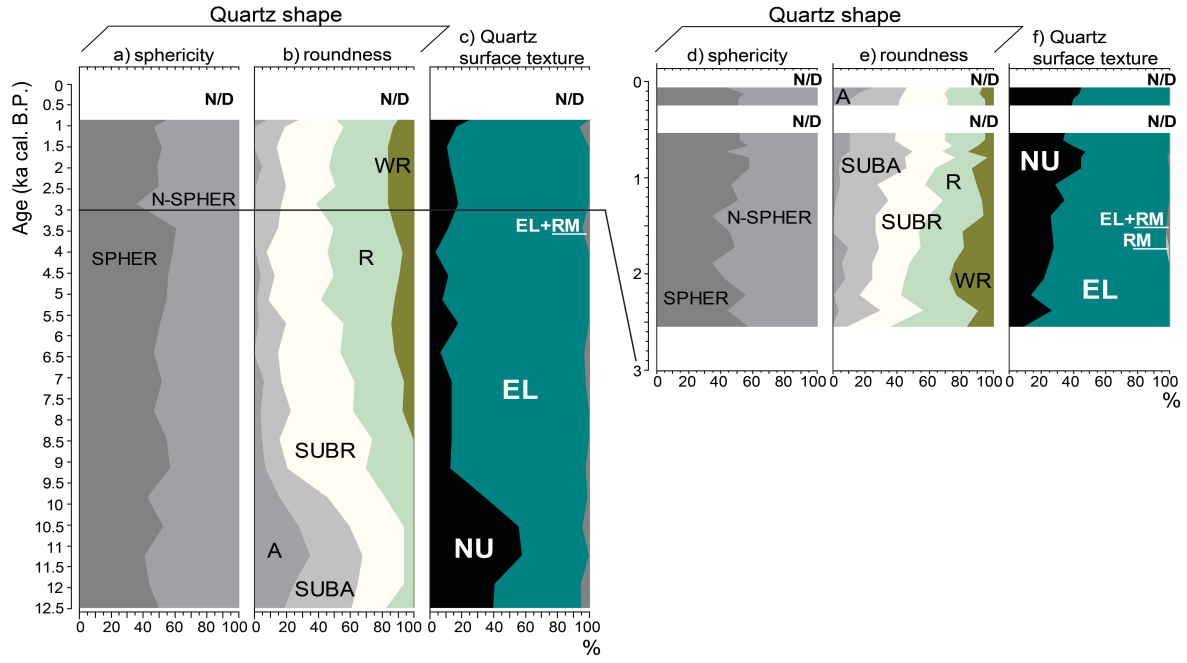

Figure V.8 – Distribution (%) of sandy quartz grains in relation to: **a)** and **d)** sphericity, along **vibrocore 6** and **vibrocore 14**; **b)** and **e)** roundness, along **vibrocore 6** and **vibrocore 14**; **c)** and **f)** surface texture, along **vibrocore 6** and **vibrocore 14**. N/D ('no-data') refers to sections of the sedimentary sequences where the number of quartz grains was insufficient for counting. Legend: SPHER – high sphericity, N-SPHER – low sphericity, A – angular, SUBA – sub-angular, SUBR – sub-rounded, R – rounded, WR – well rounded, NU – not-worn, EL – smooth-shining, RM – rounded-frosted, EL+RM – mixed EL and RM signatures.

Along **vibrocore 6** (Figs. V.8a-c), the oldest period (from the base of the sequence at ca. 12,500 cal. years B.P. until ca. 9,200 cal. years B.P.) was characterized by the highest proportions of angular forms found within the entire record, reaching ca. 55-60% of total quartz, and concurrently by the highest amounts of not-worn quartz (particularly after ca. 11,800 cal. years B.P.) that reached up to 60% of all the grains. At ca. 9,200 cal. years B.P. the quartz characteristics changed rapidly, translated by a great increase of rounded forms and smooth-shining grains that became dominant with ca. 80%-90%. After this date and throughout early- to late-Holocene until ca. 3,800 cal. years B.P., these characteristics

remained rather stable but with a slight gradual increase of all rounded forms (sub-rounded, rounded and well rounded). Indeed it is worth mentioning the appearance of well rounded (WR) quartz around 8,400 cal. years B.P. and its steady increase up to almost 15%. Between ca. 3,800 cal. years B.P. and 1,700-1,600 cal. years B.P. there was some increase of not-worn (NU) quartz that showed a peak of abundance (nearly 20%) around 3,000 cal. years B.P. It was coincident with a peak of low sphericity quartz (ca. 60%) that corresponded to the highest contribution of this type of grains within the sequence. Around 1,700-1,600 cal. years B.P., at the transition to the last and most recent phase, NU quartz exhibited a significant drop down to ca. 5% that was contemporaneous with the highest amounts of WR grains (ca. 20% of total quartz). From ca. 1,700-1,600 cal. years B.P. upwards, SUBA and NU quartz gradually increased, the latter reaching 25% at around 860 cal. years B.P. From this date onwards and until the top of the sequence, it was not possible to obtain information on sandy quartz due to insufficient material for analysis.

Along **vibrocore 14** (Figs. V.8d-f), the first phase lasted from ca. 2,500 cal. years B.P. until ca. 2,200 cal. years B.P. and corresponded to abundance peaks of low sphericity, angular (A) and NU quartz. The time interval of 2,200-1,200 cal. years B.P. continued with the dominance of all rounded forms but showing a gradual decreasing trend towards the top, accompanied by the gradual increase of NU grains in detriment of blunt-shining (EL) quartz. The period between ca. 1,200 and 900 cal. years B.P. was marked by an enhancement of all rounded forms that constituted 70% of total quartz, simultaneously with a small increase of EL grains. From ca. 900 until 550 cal. years B.P., there was another peak of NU quartz, which reached ca. 50% and constituted its highest abundance value in the entire record. It was concomitant with an enrichment of angular forms that had an identical contribution. For the time interval 550-250 cal. years B.P. it was not possible to characterize sandy quartz due to the lack of sufficient grains for analysis. From ca. 250 to 80 cal. years B.P., quartz grains revealed a dominance of rounded forms with ca. 55%, whilst NU grains slightly decreased but maintained high values of ca. 40-45%. The last ca. 80 years of deposition revealed insufficient material for analysis.

V.1.4. Benthic foraminiferal community

V.1.4.1. Faunistical density, species richness, diversity measures and species distribution

The faunistical density (FD), species richness (S), Shannon-Wiener diversity index (Hs), evenness (J) and distribution of the main benthic foraminiferal species with the respective Q-

mode clusters along the three mud body vibrocores, are represented in Figures V.9, V.10 and V.11. In vibrocore 1, core levels 360-362 cm, 350-352 cm, 340-342 cm, 300-302 cm, 260-262 cm, 250-252 cm, and 230-232 cm did not present the minimum number (300) of foraminiferal specimens for counting and identification. The same was verified in vibrocore 6 for core levels 19-20 cm and 31-32 cm. These samples were excluded from the statistical analysis.

A total of 21 species with abundance >5% in at least one sample, all calcareous, were identified in the three vibrocores. Amongst them, 7 species were present in all vibrocores, namely *Bolivina ordinaria*, *Brizalina dilatata*, *Bulimina marginata*, *Cassidulina laevigata*, *Cassidulina minuta*, *Cribrononion gerthi* and *Epistominella exigua*. With the opposite behaviour, eight species were found only in one of the vibrocores (five in vibrocore 1 and three in vibrocore 6), namely *Bulimina aculeata*, *Gavelinopsis praegeri*, *Hyalinea balthica*, *Nonionella stella*, *Rectuvigerina phlegeri*, *Stainforthia fusiformis*, *Trifarina carinata* and *Valvulineria bradyana*. The remaining six species were present in two of the three vibrocores, namely *Asterigerinata mamilla*, *Ammonia beccarii*, *Bolivina pseudoplicata*, *Bulimina elongata*, *Bolivina striatula* and *Nonion fabum*. R-mode cluster analysis results for all the main 21 benthic foraminiferal species of the three sequences are represented in Figure V.12.

Vibrocore 1

The FD varied between 13 and 6,434 specimens per gram of dry sediment (specimens/g) with a clear increasing trend from the base towards the top of the sequence (Fig. V.9). Between the base at ca. 15,300 cal. years B.P. and ca. 12,600 cal. years B.P., the FD persistently exhibited the lowest values, of about 13 to 790 specimens/g. From 1,800-1,700 cal. years B.P. until close to present-day the values showed great oscillations, with a maximum of 6,434 specimens/g at around 1,300 cal. years B.P. Species richness (S) and the diversity index Hs showed very similar trends along time (Fig. V.9), their highest values being observed at the base of the core, 78 species and Hs of 3.5, respectively. High variability of values occurred from ca. 15,200 until 11,500 cal. years B.P., with S between 60 and 43, and Hs between 2.77 and 3.1. As for evenness (J), it exhibited persistently constant mean values of ca. 0.725-0.813 (Fig. V.9).

A total of 17 main benthic foraminiferal species were identified (Appendix A) and the Q-mode cluster analysis revealed two main periods correspondent to Clusters I1 and II1, which grouped sample levels with different proportions of benthic species (Fig. V.9).

- The period between ca. 15,300 and 8,000-7,800 cal. years B.P. (Cluster I1) was characterized by high abundances (ca. 30%) of *B. ordinaria* and also by up to 30% of *A.*

mamilla (decreasing values upwards), ca. 20-30% of *C. gerthi*, and ca. 20% of *A. beccarii* (decreasing values upwards), *C. laevigata* (increasing values upwards) and *B. dilatata* (increasing values upwards). They were escorted by much smaller percentages (ca. 5-10%) of almost all the other species, except *H. balthica*, *B. marginata* and *B. striatula* that were practically absent from the record. From ca. 15,300 until 12,600 cal. years B.P., *B. ordinaria* and *A. mamilla* co-dominated (ca. 20% and 30%, respectively) and were accompanied by ca. 10% of *B. pseudoplicata* and *B. elongata*, and ca. 5% of *G. praegeri*, *T. carinata*, *S. fusiformis*, *N. stella*, *E. exigua* and *C. minuta*. From ca. 12,600 until 10,600 cal. years B.P., the most abundant species was *C. gerthi* that increased to ca. 30%, whilst *B. ordinaria* and *A. mamilla* decreased to less than 15%; *C. laevigata* and *B. dilatata* gradually increased to ca. 10%, and also *C. minuta* to more than 5%; at the same time, *B. elongata*, *G. praegeri*, *T. carinata*, *S. fusiformis* and *N. stella* became practically absent. From ca. 10,600 until 8,000 cal. years B.P., *C. laevigata* and *B. dilatata* further increased to ca. 15% and were co-dominant with *B. ordinaria*, whereas *C. gerthi, A. beccarii* and *A. mamilla* gradually decreased, the latter becoming almost absent.

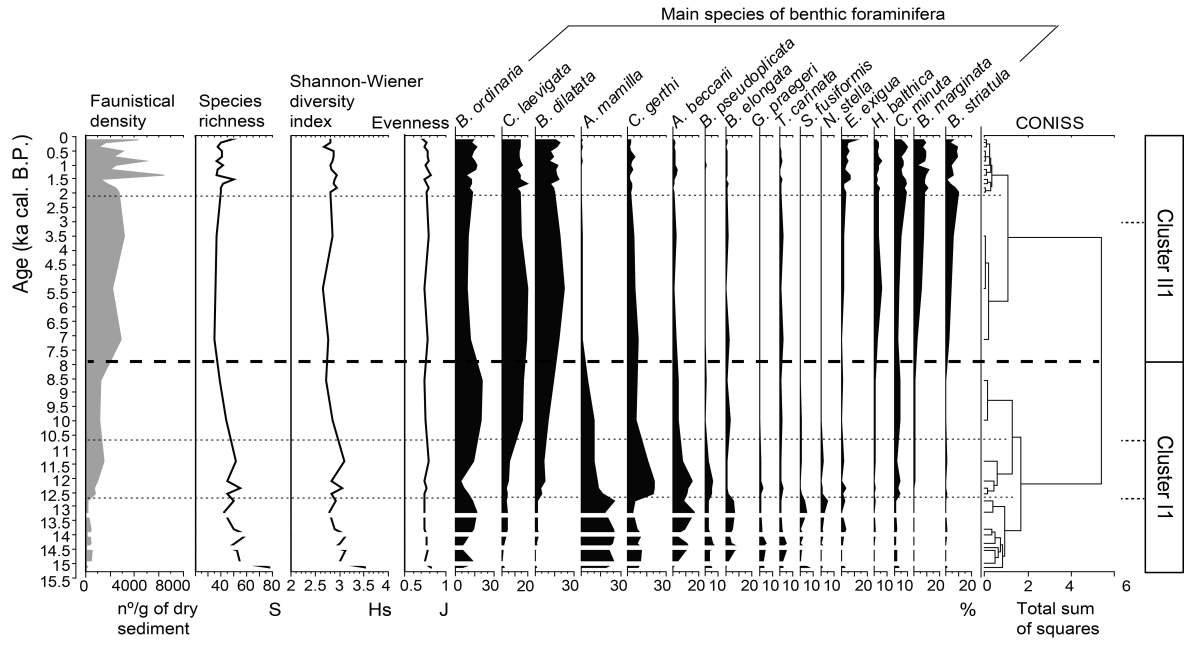

Figure V.9 – Variation along time of the faunistical density, species richness, Shannon-Wiener diversity index, evenness and relative abundances of the main benthic foraminiferal species (abundance >5% in at least one sample) for **vibrocore 1**. Q-mode cluster analysis performed by CONISS with definition of clusters based on the record of relative abundances of the benthic foraminiferal species: the black dashed line separates the two main stratigraphically constrained zones (Clusters I-II); thin punctuated lines represent sub-divisions within the main zones. Thin blanked bands on the basal part of the record correspond to levels where no data was obtained due to insufficient specimens for counting.

- The period between ca. 8,000-7,800 cal. years B.P. until the present (Cluster II1) was co-dominated by species *C. laevigata* and *B. dilatata* (with ca. 15-20%) and still significant

abundances of *B. ordinaria* (ca. 10-15%). Following these, the most representative species (with ca. 5-10%) were *C. gerthi* that decreased towards the top, and *E. exigua*, *H. balthica*, *C. minuta*, *B. marginata* and *B. striatula* that increased towards the top. From ca. 8,000-7,800 until 2,000 cal. years B.P., these abundance values remained rather constant, although *C. gerthi* continued to decrease whereas *B. marginata* and *B. striatula* gradually increased. From ca. 2,000 cal. years B.P. until the present, these species presented the same mean abundance values but exhibiting more pronounced oscillations.

Vibrocore 6

The FD varied between 269 and 1,659 specimens/g with the highest values obtained for the middle part of the sequence, between ca. 9,500 and 2,500 cal. years B.P. (Fig. V.10). Species richness (S) was more or less constant around 40-50 from the base of the core until ca. 3,500 cal. years B.P., except for a small peak (54 species) registered at ca. 10,600 cal. years B.P. (Fig. V.10). At ca. 860 cal. years B.P. the highest S value (63 species) was verified but this date simultaneously marked a transition to the period with the lowest S values (38 to 47) of the sequence, which lasted until close to present. The diversity index Hs and evenness (J) showed low variability throughout most of the sequence, in particular from the core base until ca. 1,000 cal. years B.P. (Fig. V.10). Between ca. 12,200 and 1,000 cal. years B.P. Hs was around 2.5 to 3 and J was around 0.7 to 0.8. At about 750 cal. years B.P. the lowest diversity of less than 2.5 and lowest J of ca. 0.66 were verified. Afterwards and until present-day, Hs slightly increased to around 2.8 and J to around 0.75.

A total of 15 main benthic foraminiferal species were identified (Appendix B) and the Q-mode cluster analysis revealed two main periods correspondent to Clusters I6 and II6, which grouped sample levels with different proportions of benthic species (Fig. V.10).

- The period between ca. 12,500 and 3,000-2,800 cal. years B.P. (Cluster I6) was characterized by high abundances of ca. 25-30% for species *B. ordinaria* and *A. mamilla* that co-dominated the foraminiferal record. *Nonion fabum*, *A. beccarii*, *R. phlegeri*, *C. minuta*, *B. elongata*, *B. pseudoplicata*, *C. gerthi*, *C. laevigata* and *B. dilatata* were the other most important species with abundance values around 5-10%. From 12,500 until ca. 9,200 cal. years B.P., dominant *B. ordinaria* and *A. mamilla* were mainly escorted by *N. fabum*, *B. elongata*, *B. pseudoplicata* and *C. gerthi*. From ca. 9,200 until 3,000 cal. years B.P., *A. mamilla* steadily decreased down to vestigial abundances (ca. 1%) whereas *B. elongata* and *B. pseudoplicata* also gradually decreased from ca. 10% to less than ca. 5%. Conversely, *A. beccarii*, *R. phlegeri*, *C. gerthi*, *C. laevigata* and *B. dilatata* increased from ca. 5% to ca. 10%.

V. bradyana, *B. aculeata* and *E. exigua* made their first appearance with small but increasing amounts of less than 5%.

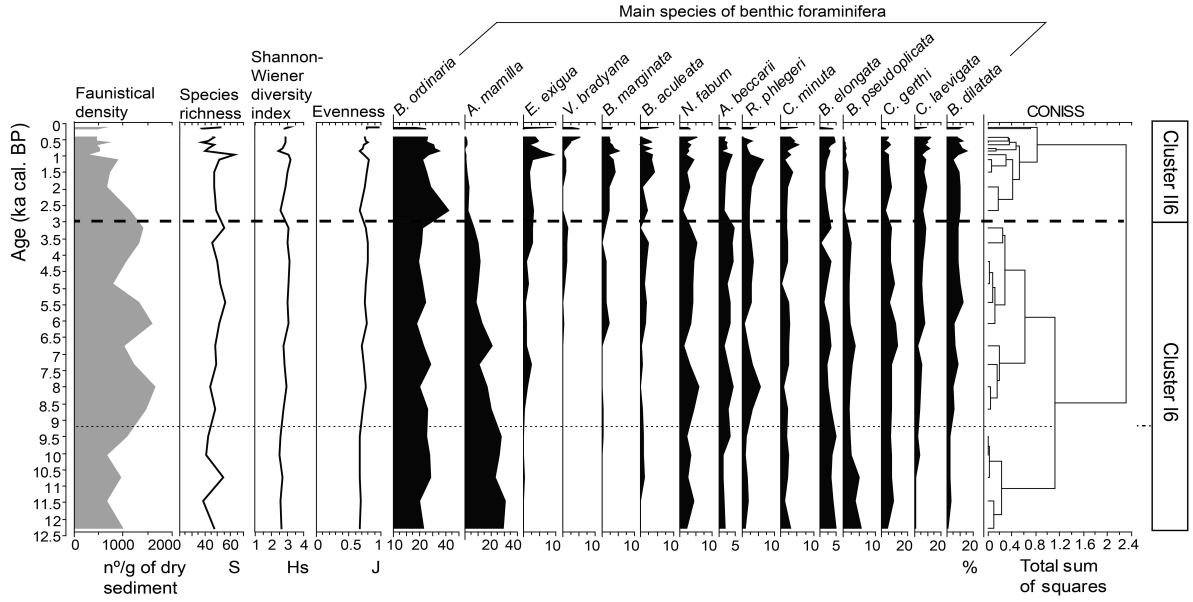

Figure V.10 – Variation along time of the faunistical density, species richness, Shannon-Wiener diversity index, evenness and relative abundances of the main benthic foraminiferal species (abundance >5% in at least one sample) for **vibrocore 6**. Q-mode cluster analysis performed by CONISS with definition of clusters based on the record of relative abundances of the benthic foraminiferal species: the black dashed line separates the two main stratigraphically constrained zones (Clusters I-II) along the vibrocore; the thin punctuated line represents a subdivision within Cluster I6. Thin blanked band on the top of the record corresponds to levels where no data was obtained due to insufficient specimens for counting.

- The period ranging between ca. 3,000-2,800 cal. years B.P. and present-day (Cluster II6) witnessed even greater abundances of *B. ordinaria* that dominated the record with 30-40%. Almost all the other species showed a general increase during this time interval, *E. exigua*, *B. elongata*, *C. minuta* and *B. dilatata* particularly after ca. 1,200-1,000 cal. years B.P., and *V. bradyana* after ca. 500 cal. years B.P. *Asterigerinata mamilla* and *B. pseudoplicata* showed a reverse tendency, becoming practically absent.

Vibrocore 14

The FD varied between 361 and 7,069 specimens/g and showed the most pronounced variation from the core base, around 2,500 cal. years B.P., until ca. 1,400 cal. years B.P. (Fig. V.11). At the base of the sequence, FD registered a very high abundance of 6,290 specimens per gram of dry sediment, followed by a drop to ca. 770 specimens/g at around 2,100 cal. years B.P. At ca. 1,600 cal. years B.P., FD reached the highest value within the sequence, of ca. 7,069 specimens/g. From ca. 1,500-1,400 until 600 cal. years B.P. the FD was lower with mean values of ca. 1,900-2,900 specimens/g. The period between ca. 600 and 100 cal. years B.P. witnessed a further decrease to mean values of 351-858 specimens/g. In the last 100 years the FD increased up to ca. 2,835-4,060 specimens/g. Species richness (S) also oscillated

throughout time, showing a general trend for higher values from the core base until ca. 1,400 cal. years B.P. (around 50-60 species) and for lower values from this date until the present (around 40-50 species) (Fig. V.11). The lowest S value of 29 species occurred around 300 cal. years B.P. Diversity index Hs and evenness (J) were rather constant and evidenced similar trends throughout time (Fig. V.11). Slightly higher values for both Hs and J were obtained from the core base until ca. 1,500 cal. years B.P., of ca. 2.8-3.2 and 0.75, respectively. Between this date and modern times values were around 2.5 for Hs and 0.7 for J.

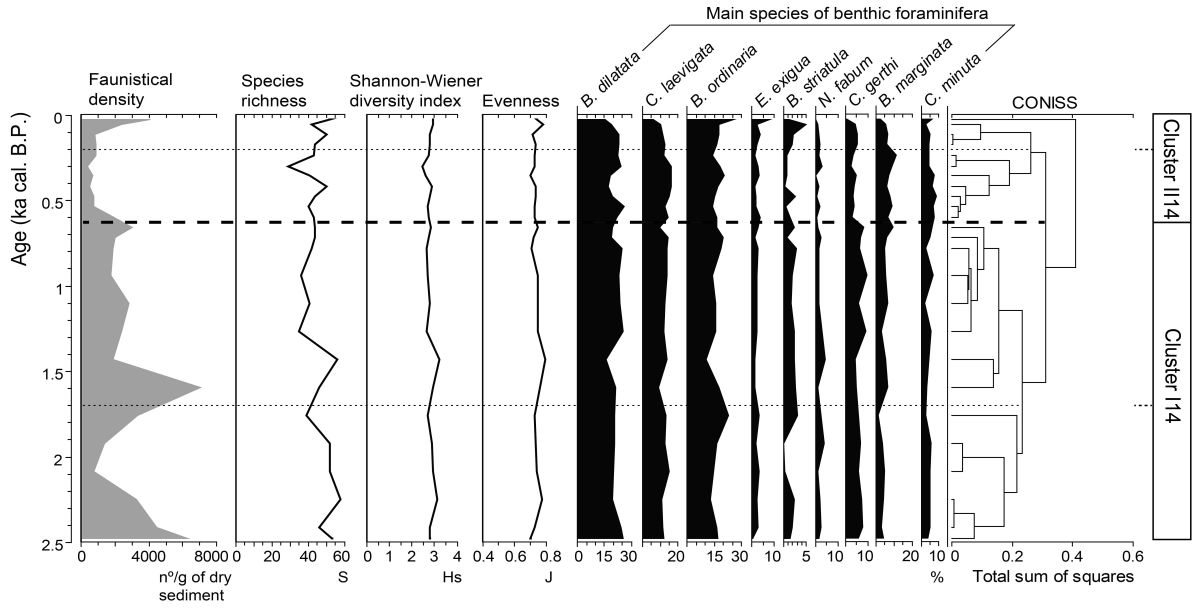

Figure V.11 – Variation along time of the faunistical density, species richness, Shannon-Wiener diversity index, evenness and relative abundances of the main benthic foraminiferal species (abundance >5% in at least one sample) for **vibrocore 14**. Q-mode cluster analysis performed by CONISS with definition of clusters based on the record of relative abundances of the benthic foraminiferal species: the black dashed line separates the two main stratigraphically constrained zones (Clusters I-II) along the vibrocore; thin punctuated lines represent subdivisions within the main zones.

A total of 9 main benthic foraminiferal species were identified (Appendix C) and the Q-mode cluster analysis revealed two main periods correspondent to Clusters I14 and II14, which grouped sample levels with different proportions of benthic species (Fig. V.11).

- The period between ca. 2,500 and 600 cal. years B.P. (Cluster I14) was characterized by the dominance of *B.dilatata*, *C. laevigata* and *B. ordinaria* that presented persistent mean values of about 15% to 25%, followed by *C. gerhti* with ca. 10%, whereas all the remaining species showed lower abundances of around 5%. From ca. 2,500 until 1,700 cal. years B.P., *B. ordinaria* increased and reached a peak of almost 25%, *B. striatula* oscillated significantly, *N. fabum* showed an increasing trend, whereas *B. marginata* and *C. minuta* slightly decreased. From ca. 1,700 until close to 600 cal. years B.P., *E. exigua* was the only decreasing species, whilst the others generally increased, in particular *B. striatula*, *C. gerthi* and *B. marginata*.

- The period between ca. 600 cal. years B.P. and the top of the sequence (Cluster II14) continued to present the same general tendencies, but witnessed an important decrease of *C. gerhti* and conversely an increase of *E. exigua* and *B. marginata*. From ca. 600 until 200 cal. years B.P., *C. gerthi* decreased to less than 5% and *B. marginata* and *C. minuta* increased to ca. 10%. From 200 cal. years B.P. until the present, *C. laevigata* dropped to about 10%, *E. exigua*, *B. striatula* and *C. gerthi* increased, whilst the opposite trend was observed for *B. marginata* and *C. minuta*.

V.1.4.2. R-mode clustering

The R-mode cluster analysis performed on the three cores (Fig. V.12) was intended to evaluate the differences and similarities amongst the evolutionary trends of each individual species along time, thus allowing the identification of different clusters (groups) of species in each core.

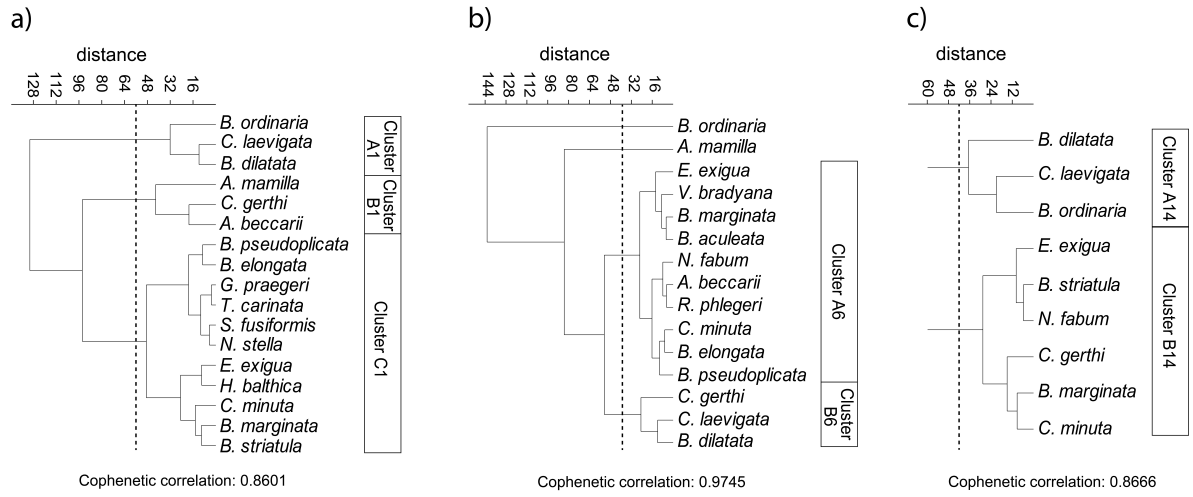

Figure V.12 – Foraminiferal groups produced by R-mode cluster analyses (Ward's Method) and dendrogram classification based on a total of 21 benthic foraminiferal species with relative abundance >5% in at least one sample of the three vibrocores: **a) vibrocore 1**; **b) vibrocore 6**; **c) vibrocore 14**. Clusters A-C correspond to the main groups of species in each core and the dashed line marks the distance that individualized the different groups.

Three main groups were established in vibrocore 1 (Fig. V.12a), two main groups in vibrocore 6 (Fig. V.12b), and two main groups in vibrocore 14 (Fig. V.12c). The cophenetic correlation obtained for the clustering of the three vibrocores were very high, showing the strong inter-relation between the distribution trends of the different species (Fig. V.12). Correlation values were ca. 0.86 for vibrocore 1 (Fig. V. 12a), 0.97 for vibrocore 6 (Fig. 12b) and 0.87 for vibrocore 14 (Fig. 12c).

V.1.4.3. Comparison of R-mode and Q-mode clustering: Biofacies

Comparing the results of Q-mode clustering (Figs. V.9, V.10 and V.11) with the information obtained from the R-mode clustering (Fig. V.12), it was possible to establish the main trends of the species distributional patterns along time and in relation to each other (Fig. V.13). As such, the Q-mode clusters determined along each sequence will be further on designated as 'Biofacies' (Fig. V.13), as they correspond to different benthic environments inhabited by typical groups of species and thus have specific ecological meaning.

Dominant species *B. dilatata*, *C. laevigata* and *B. ordinaria* were grouped together in the same R-mode cluster of vibrocores 1 and 14 (Groups A1 and A14) (Figs. V.12a, c and V.13a, c). In vibrocore 6 (Figs. V.12b and V.13b) *B. ordinaria* exhibited a specific distributional pattern, usually dominating the benthic community (Fig. V.13b). *Asterigerinata mamilla* was the other important species in vibrocore 6 (Fig. V.13b), co-dominating the benthic community with *B. ordinaria* until ca. 9,200 cal. years B.P. (Fig. V.13b).

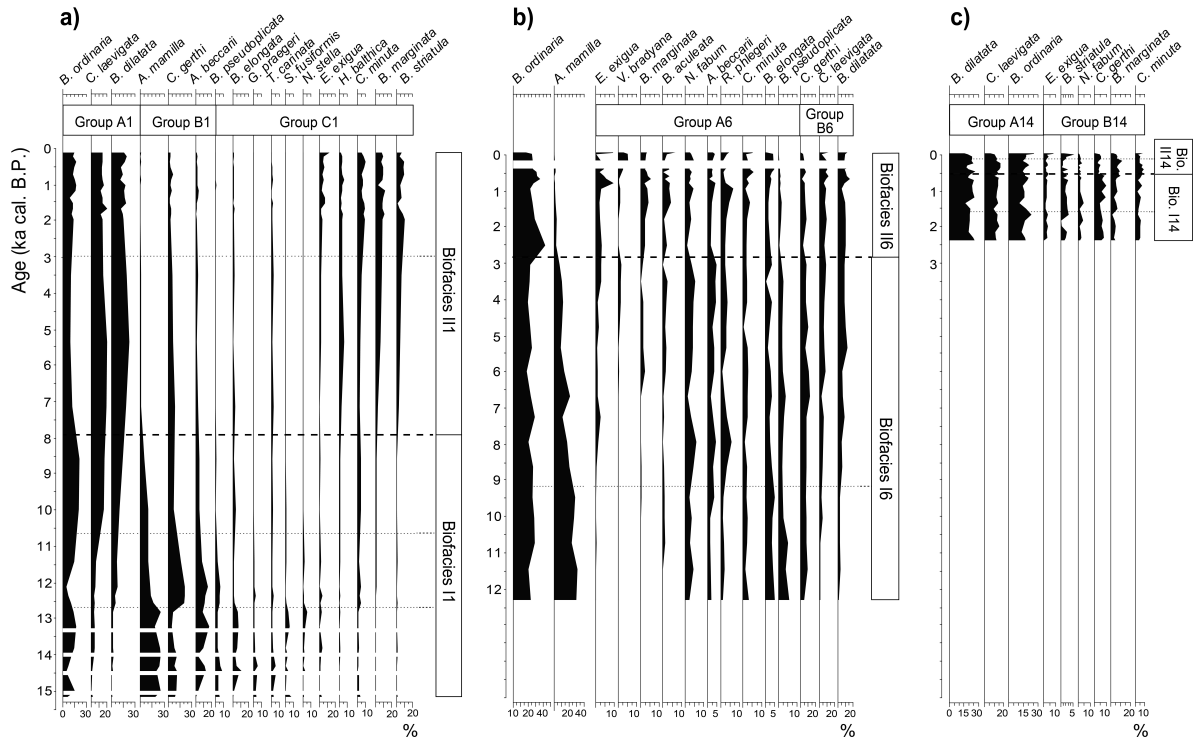

Figure V.13 – Comparison of foraminiferal groups produced by R-mode (Ward's Method) clustering and of biofacies produced by Q-mode (stratigraphically constrained) clustering along **a) vibrocore 1**; **b) vibrocore 6**; **c) vibrocore 14**. Thin blanked bands in vibrocores 1 and 6 correspond to the levels where no data was obtained due to insufficient specimens for counting.

In **vibrocore 1** (Fig. V.13a), Biofacies I1 characterized the benthic community from ca. 15,300 until 8,000-7,800 cal. years B.P. and was dominated by species belonging to Groups A1 and B1. However, during this period, the proportions of these species varied. Until ca.

10,600 cal. years B.P., Group B1 was dominant, with *A. mamilla* being the most abundant species until ca. 12,600-12,500 cal. years B.P. and *C. gerthi* from this date until close to 10,600 cal. years B.P. Until ca. 12,600-12,500 cal. years B.P., species *B. pseudoplicata*, *B. elongata*, *G. praegeri*, *T. carinata*, *S. fusiformis* and *N. stella* of Group C1 were also present but in very small abundances. From ca. 10,600 until 8,000-7,800 cal. years B.P., Biofacies I1 was dominated by Group B1, with *B. ordinaria* as the most abundant species and *B. dilatata* and *C. laevigata* significantly increasing in abundance upwards. Biofacies II1 characterized the record from ca. 8,000-7,800 cal. years B.P. until today, being dominated by species *B. ordinaria*, *B. dilatata* and *C. laevigata* of Group A1, together with an increasing contribution of species *E. exigua*, *H. balthica*, *C. minuta*, *B. marginata* and *B. striatula* of Group C1 that became particularly significant after ca. 3,000-2,000 cal. years B.P.

In **vibrocore 6** (Fig. V.13b), Biofacies I6 characterized the benthic faunas from ca. 12,500 until 3,000-2,800 cal. years B.P., with *B. ordinaria* dominating the community and *A. mamilla* co-dominating until ca. 9,200 cal. years B.P., after which its abundance gradually decreased until almost disappearance close to ca. 3,000-2,800 cal. years B.P. Species *N. fabum*, *A. beccarii*, *R. phlegeri*, *C. minuta*, *B. elongata* and *B. pseudoplicata* of Group A6 were also present throughout this biofacies, whilst species of Group B6 became more important after ca. 9,200 cal. years B.P. Biofacies II6 characterized the record after ca. 3,000-2,800 cal. years B.P. until present-day, being dominated by *B. ordinaria* and characterized by species *E. exigua*, *V. bradyana*, *B. marginata* and *B. aculeata* of Group A6 that became more representative. The remaining species of Groups A6 and species of Group B6 persistently showed identical contributions.

In **vibrocore 14** (Fig. V.13c), species of Group A14 were persistently dominant (*B. dilatata* slightly more abundant), and the two Biofacies I14 and II14 were determined on basis of different contributions of the species belonging to Group B14. Biofacies I14 dominated the record from ca. 2,500 until 600 cal. years B.P. and was characterized by higher abundances of *B. striatula*, *N. fabum* and *C. gerthi*. After ca. 600 cal. years B.P. until present-day, Biofacies II14 was marked by an abundance decrease of these species in favour of more abundant *B. marginata*.

V.2. Discussion

The multi-proxy study conducted in the sedimentary sequences of the Guadiana mud body, based on their main sedimentological and benthic foraminiferal features, unravelled a

succession of different depositional environments for the period spanning from ca. 15,300 cal. years B.P. (late Pleistocene) and throughout the Holocene, until close to present-day. Furthermore, the full correspondence of the last ca. 2,500 with the entire record of vibrocore 14, coupled with the higher resolution of the sedimentary record of vibrocores 1 and 6 attained for this time interval, enabled a more detailed interpretation of recent climatic events and its direct comparison with Historical information concerning the anthropogenic forcing.

V.2.1. Depositional environments

Based on the features and trends of the key-proxies, four main depositional stages were identified for the evolution of this mid-shelf area (Figs. V.14, V.15 and V.16). The first main depositional stage (Stage 1), from ca. 15,300 until 12,500-12,000 cal. years B.P., elapsed during the late Pleistocene and was registered only in vibrocore 1 (Fig. V.14). The following main depositional stage (Stage 2) lasted from ca. 12,500-12,000 until 8,000 cal. years B.P., including a part of the Younger Dryas (ca. 12,900-11,700 cal. years B.P.) and the early phases of the Holocene (onset at ca. 11,700 cal. years B.P.), whilst Stage 3 covered mainly the mid- to late-Holocene, spanning from ca. 8,000 until 3,000-2,500 cal. years B.P., both stages being registered in vibrocores 1 and 6 (Figs. V.14 and V.15). Finally, the most recent depositional stage (Stage 4) corresponded to the late Holocene, covering the last ca. 2,500 years, and was registered in the three cores (Figs. V.14, V.15 and V.16).

Stage 1: from ca. 15,300 until 12,500-12,200 cal. years B.P.

The first stage was characterized at the site of vibrocore 1 by apparent moderately high sedimentation rates that ranged from ca. 80 to nearly 50 cm/ka (Fig. V.5a). Sediments were usually a combination of dominant silt with important but variable contents of sand and a significant clay input, plus a very reduced and intermittent contribution of gravel (Figs. V.6a and V.14). Within sand, quartz was generally the most abundant compound (Figs. V.7a-b and V.14). Other terrigenous particles (OT) were almost as abundant as quartz, and mica was also of some significance, whereas the biogenic compound consisted almost exclusively of mollusc shells (Figs. V.7a and V.14). In what concerns the benthic foraminiferal community, the most evident feature were the very low faunistical densities (FD) that persisted throughout this period (Figs. V.9 and V.14). The diversity index Hs was slightly higher and seemed to exhibit important fluctuations (Figs. V.9 and V.14). This phase was dominated by Biofacies I1 (Figs. V.13a and V.14).

Chapter VI

PALEOENVIRONMENTAL EVOLUTION OF THE GUADIANA CONTINENTAL SHELF AND RECONSTRUCTION OF THE MUD BODY

The multi-proxy study performed in the sedimentary sequences of the Guadiana inner shelf and mid-shelf mud body allowed an integrated interpretation of the main depositional and environmental events taken place during the last ca 15,300 cal. years B.P., from late Pleistocene and throughout the Holocene until close to present-day. The post-glacial transgression that was initiated after the Last Glacial Maximum (LGM) was recorded at both shelf domains by a generalized fining-up tendency of sediments (transgressive sequence) and on the middle shelf by a succession of different benthic foraminiferal faunas. Here, this process eventually led to the establishment of the fine to very fine deposits that constitute the Guadiana mud body. They functioned as a crucial marine archive of the climatic and recent anthropogenic impacts on the natural systems of the region, and its evolutionary history will now be further analysed in the present chapter.

As was already discussed in the previous chapters, the Guadiana River is the main regional source for the sediments that are deposited on the adjacent continental shelf (González *et al.*, 2004). The estuarine system plays a crucial role in the type and amount of the sedimentary material that is transferred from the river to the coastal ocean and episodic flood events have been found to be the main mechanism for sediment discharge (fine- and coarse-grained) from the river basin onto the shelf (González *et al.*, 2004; Portela, 2004; González *et al.*, 2007).

The sediment supply from the basin is however clearly dominated by suspended load relative to bed load material (Morales, 1997). Apparently, the estuary retains only a minor share (about 10%) of the total amount of fine-grained sediments produced in the drainage basin, the rest being transported onto the shelf as part of plumes of riverborne suspended material that initially deposits at the inner shelf domain (Portela, 2004) (Fig. VI.1). Re-suspension and remobilization processes occurring at this energetic area of the shelf are afterwards responsible for the redistribution of the fine sediments onto the deeper and less hydrodynamic setting of the middle shelf, where they eventually accumulate (*e.g.*, González *et al.*, 2004 and 2007). The same mechanism of initial deposition of fluvially-supplied fine material on shallower shelf areas, followed by post-remobilization and transport onto deeper middle shelf areas where they eventually settle, has been identified in several other continental margins (*e.g.*, Lesueur *et al.*, 1996; Jouanneau *et al.*, 1998, Dias *et al.*, 2002a; Edwards, 2002; Roussiez *et al.*, 2005; Dubrulle *et al.*, 2007).

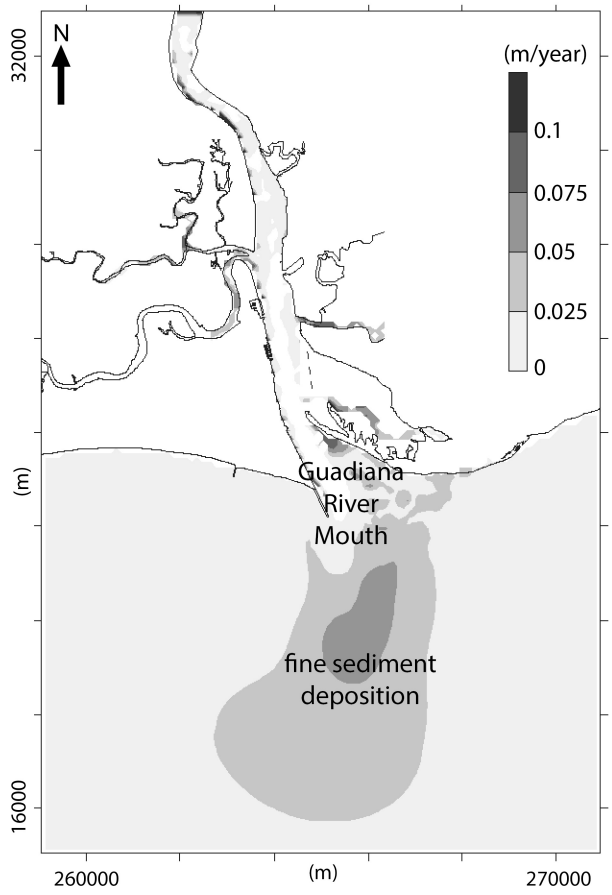

Figure VI.1 – General simulation of modern fine (cohesive) sediment deposition (m year^{-1}) in the Guadiana lower estuary and on the adjacent inner shelf (adapted from Portela, 2004).

At a long-term scale, such process is believed to have generated the fine-grained deposits that cover an important area of the shelf adjacent to the Guadiana Estuary Mouth (*e.g.*, Nelson *et al.*, 1999; González *et al.*, 2004; Lobo *et al.*, 2005). These deposits are part of the extensive highstand prograding mud facies that covers mid-shelf depths throughout the Gulf of Cadiz Margin (Gutiérrez-Mas *et al.*, 1996; Rodero *et al.*, 1999), formed when the Holocene sea-level rise resulted in maximum water depth over the Gibraltar sill and in the full development of the Atlantic inflow and Mediterranean outflow currents (Nelson *et al.*, 1999).

Our record from the Guadiana mud body showed though that significant deposition of fine material started as early as the late Pleistocene, during earlier stages of the Flandrian transgression (Fig. VI.2a), when over 60% of silt-dominated muds mixed with sand accumulated at the deeper and more distal site of vibrocore 1, around 15,000 cal. years B.P. (Figs. V.4a and V.6a). This tendency persisted throughout the final stages of the Pleistocene sea-level rise (Fig. VI.2b), and close to the beginning of the Holocene, around 12,000 cal. years B.P., mud deposition had already increased up to ca. 80% of total sediments at this site, with similar values also being observed for the same period in the shallower mid-shelf vibrocore 6 (Figs. V.4a-b and V.6a-d).

When comparing these results with information obtained for shelf mud deposits in other areas of the Iberian Margin, namely the important Galicia Mud Belt, on NW Iberia, it is clear that the evolution of the Guadiana mud body followed a somewhat different pattern. Just as is verified for the latter, the fine-grained deposits of the Galicia Mud Belt are originated from regional fluvial input, mainly the discharges of the Douro River (Araújo *et al.*, 2002; Portela, 2008), storing ca. 70% of the total detritical fluxes that are transferred from the continent to the shelf (Jouanneau *et al.*, 2002). They first settle on the inner shelf but post-remobilization caused essentially by winter wave and storm action transports a major part offshore onto the deeper middle shelf, which becomes their main depositional site (Dias *et al.*, 2002a and 2002b). Studies focusing on the evolution of the Galicia Mud Belt have however pointed out that the first onset of major mud deposition in the area was forced by the last phases of the postglacial transgression and subsequent sea-level near stabilization (Drago *et al.*, 1999; Lantzsch *et al.*, 2009a, 2009b and 2010). The flooding of the Douro Estuary during the late Pleistocene to early Holocene sea-level rise led first to accumulation of fine sediments inside the river valley, whereas the posterior export of terrigenous material to the shelf was initiated only during the Holocene, between ca. 8,370 and 5,249 cal. years B.P. (Lantzsch *et al.*, 2009a). It was caused by a shift in the balance between the rate of sea-level rise and the amount of fluvial sediment supply, which provided the prerequisite for initiation and further expansion of the mid-shelf mud depocentre, when a transition occurred from pure fine sands towards mud contents of more than 25% (Lantzsch *et al.*, 2009a). This contrasts with the record of the Guadiana mud body sequences that, although showing an identical fining-up trend forced by postglacial sea-level rise and drowning of the shelf, revealed a much higher content of mud even since before the Holocene times (Figs. V.4a-b and V.6a-d). Although the Guadiana Estuary was also retaining a significant part of the fluvial sediment-load in the course of its estuarine infilling during the early Holocene sea-level rise (Boski *et al.*, 2002 and 2008), the transfer of sediments seems to have always been significant enough to allow the deposition of fine material on the shelf, even at shallower depths than those characterizing the modern sites of the studied sequences.

It is likely that differences in the regional climate and associated fluvial runoff of the major rivers supplying both mud depocentres, in the nature of source rocks along the two river basins, as well as on the hydrodynamic regime that characterizes each of the shelf systems, have all contributed to such diverse evolutional trends of the mud depocentres, and to what

appears to be the specific case of the Guadiana deposits, characterized by a stronger predominance of fine sediments at a much earlier stage.

Variations in the lithology of the continental bedrock sources have strong effects on the sediment composition and grain-size distribution patterns of shelf deposits (*e.g.*, Monteiro *et al.*, 1982; Dias and Nittrouer, 1984; Paiva *et al.*, 1997; Alves *et al.*, 2003; Machado *et al.*, 2005; Mil-Homens *et al.*, 2006). The outcropping formations along the Douro River Basin, mainly consisting of plutonic and granitoid rocks, contribute with high amounts of coarser material to the drainage system, as attested by the volumes of sand that reach and bypass the Douro Estuary Mouth (Portela, 2008). Conversely, the weathering of the metamorphic schist and greywacke formations that dominate extensive areas of the Guadiana Basin contributes to the much more significant quantities of fine, rather than coarse, material which constitutes the sediment-load transported by the fluvial system (Morales, 1997; González *et al.*, 2004; Portela, 2004; González *et al.*, 2007). Additionally, the influence of fluvial input and of regional coastal/shelf hydrodynamism has already been indicated as a major factor in controlling the textural composition of shelf sediments along the Portuguese Margin (*e.g.*, Martins *et al.*, 2012). Precipitation and topography have a strong impact on river flow and discharge rates, with rainfall being much heavier in the highlands of northern Iberia than in the low lying areas of the southern part of the Peninsula (*e.g.*, Martins *et al.*, 2012). In part this probably also explains the coarser nature of riverborne sediments reaching the northwestern shelf, as the transport-capacity of the Douro River is therefore much higher. In what concerns shelf hydrodynamics, whereas the northwestern margin is characterized by high energetic conditions which difficult the setting of muds and allows their re-suspension (*e.g.*, Lantzsch *et al.*, 2009a; Martins *et al.*, 2012), the southern shelf corresponds to a low energy environment that favours the accumulation of the fluvially-derived fine sediments (*e.g.*, González *et al.*, 2007; Martins *et al.*, 2012).

By the time of the early Holocene and after the last global major pulse of sea-level rise MWP 1B, significant fine sedimentation continued to occur at the two mid-shelf sites in front of the Guadiana River, and coarse-grained deposits, possibly related with an ancient delta of the Guadiana, started to accumulate at the much shallower site of vibrocore 20 (Fig. VI.2b). The high amounts of mud mixed with an important contribution of terrigenous sand material (of ca. 20%) persisted on the mid-shelf deposits throughout most of the Holocene (Figs. V.4a-b and V.6a-d), whereas on the inner shelf the record of vibrocore 20 showed that coarser terrigenous sediments dominated deposition closer to the river mouth during all this time. No

major changes in terms of fine deposition were observed on the mid-shelf sites during this extended period (Figs. V.4a-b and V.6a-d), not even after sea-level near stabilization at ca. 5,000 cal. years B.P., which seems to indicate that the infilling of the Guadiana Estuary did not cause immediate impact on the adjacent middle shelf domain. A significant change was observed though on the inner shelf record, with sediments becoming less coarse, as gravel was reduced and sand became the main sediment type particularly after the sea level was almost stabilized (Fig. IV.4a).

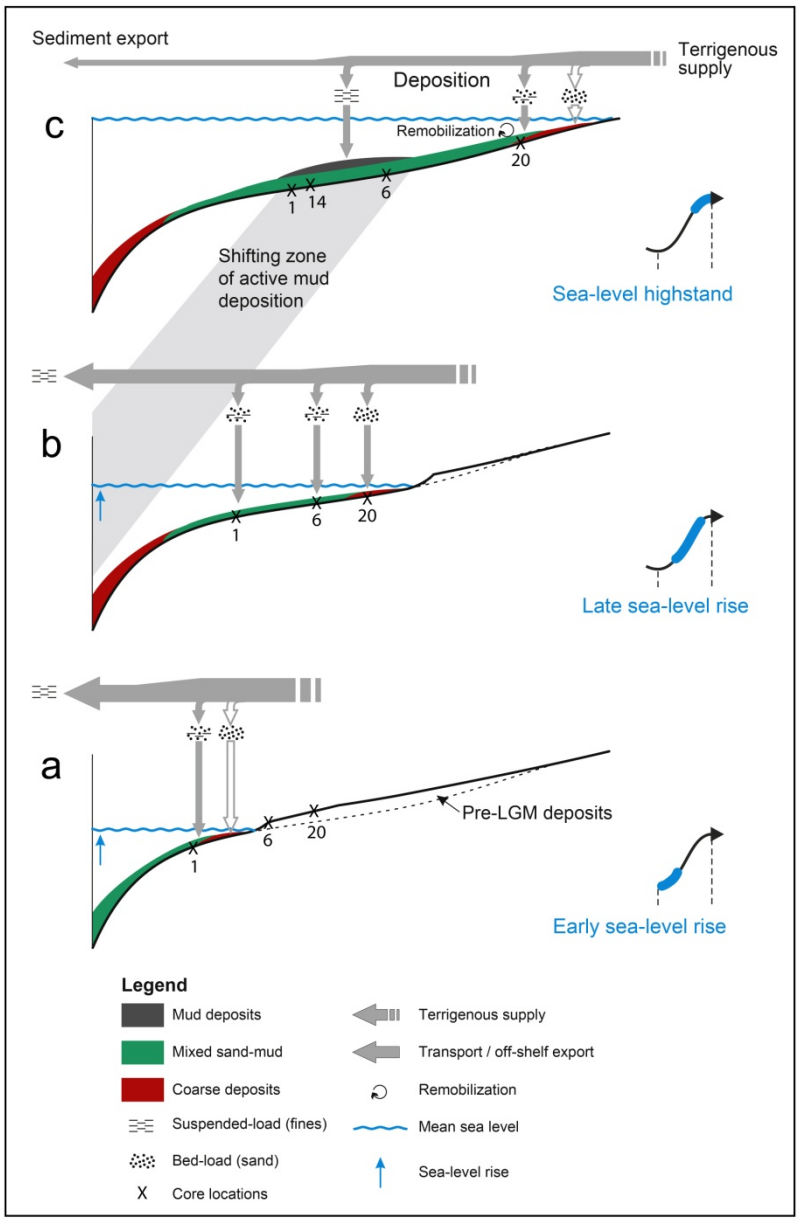

Figure VI.2 – Evolutional scheme of the Guadiana shelf and of the establishment of the mid-shelf mud body, since the late Pleistocene sea-level rise (**a** and **b**) until the formation of the highstand deposits that translate modern conditions on the shelf environment (**c**). Contour grey arrows represent possible sedimentation patterns in shelf areas not covered by the set of vibrocores analysed in this study.

Both inner and middle shelf sequences also evidenced an apparent lower rate of sediment supply during this period, again even after the sea level had approached its present day position around mid-Holocene, and the infilling of the Guadiana Estuary was practically complete (Boski *et al.*, 2002 and 2008). It was considered as a possible explanation that climate forcing, namely enhanced dryness across the Mediterranean Basin and southern Europe (*e.g.*, Jalut *et al.*, 2000; Fletcher *et al.*, 2007; Fletcher and Goñi, 2008; Magny *et al.*, 2009; Carrión *et al.*, 2010a; Fletcher *et al.*, 2012), could have contributed to reduced river flows and consequently to a lessen capacity of sediment-transfer of the Guadiana River. Such a climate scenario would refrain sediment export onto the shelf, specially because soils would still be protected from erosional processes by the well developed vegetation cover that had previously expanded in the Guadiana Basin under the early Holocene moisture conditions (*e.g.*, Fletcher *et al.*, 2007), even though the bypass of fluvially-supplied sediments was probably favoured by the progressively more stable sea levels and decreased retention of sediments inside the estuary. At the same time, after the maximum flooding of the Guadiana Estuary (Morales, 1997; Boski *et al.*, 2002), the prograding phase of the river mouth was put in motion (Morales, 1997; Lobo *et al.*, 2003; Morales *et al.*, 2006) and probably started to retain a part of the fluvial-supplied sediments for deltaic construction. This means that the supply mechanisms surpassed the distributional processes, which is consistent with the low-energy characteristics of the Guadiana margin, and particularly in comparison with the Douro Estuary case where the higher energetic levels prevented the development of such depositional system associated with the river mouth.

By late Holocene, around 2,000 cal. years B.P., the shelf depositional environment witnessed major changes. At the most distal and deeper site of vibrocore 1, fine sedimentation was enhanced to more than 90% (Figs. V.4a and V.6a) and apparently much higher amounts of sediments started to reach the area (Fig. V.14), the same being verified for the inner shelf (Fig. IV.7). At the same time, fine sediments started to accumulate at the deep site of vibrocore 14 (Figs. V.4c and V.6e), which seemed to translate the onset of mud deposition in this area, westward deviated from the Guadiana River Mouth. It is thus clear that important transformations related with the sediment sources were by then taking place, namely along the Guadiana Basin, increasing significantly both the sediment-load of the river and its transport-capacity. The timing of these changes matches well with one of the most crucial historical periods of recent times, the expansion of the Roman Empire. Throughout most of Europe and in particular across the Mediterranean Basin, the Roman rule was responsible for massive

human development and consequent major impacts on the natural systems, including in southern Iberia and along the Guadiana Basin (*e.g.*, Alarcão, 1987; Alarcão, 1990; Fabião, 1993). Many palaeoenvironmental studies have already unravelled the effects that land-use activities such as intensive agricultural practices, mining exploitation and the constructions of dams have had in soil erosion and sedimentations patterns, both in continental and in marine systems, during the Roman Period (*e.g.*, Zielhofer *et al.*, 2002; Désprat *et al.*, 2003; Faust *et al.*, 2004; Mighall *et al.*, 2006; Carrión *et al.*, 2007; Casana, 2008; Gil-Romera *et al.*, 2010; Anderson *et al.*, 2011; Kaal *et al.*, 2011; Delgado *et al.*, 2012). Furthermore, it has been proposed that this period also corresponded to a time of enhanced humidity across the Mediterranean, amplifying the human-induced erosional processes (*e.g.*, Désprat *et al.*, 2003; Thorndycraft and Benito, 2006; Bernárdez *et al.*, 2008; Casana, 2008; Martín-Puertas *et al.*, 2009; Mohamed *et al.*, 2010; Dermody *et al.*, 2012; Corella *et al.*, 2013). As such, it is likely that the changes detected in the shelf depositional patterns at this time, with enhanced sediment-supply and higher amounts of fine-grained material reaching the mid-shelf, were mainly driven by human forcing but further enhanced by a climate shift towards more humidity and higher river-runoff. It determined an even more pronounced fining-up trend within the mud body depocentre and the onset of mud deposition in a location deviated from the main sediment-pathway of the Guadiana Mouth, marking a clear expansion of the mud body beyond its depocentre, as had been previously observed (Rosa *et al.*, 2011), and clearly setting new conditions on the shelf (Fig. VI.2c). A very similar process of mud-enhancement on the shelf domain due to the coupling of climatic changes and strong human impact during Roman times has also been recognized on the Northern Aquitaine shelf (Lesueur *et al.*, 1996; 2001 and 2002). Major changes on erosional processes along the catchment areas of the Gironde and Loire rivers, the main regional sediment-suppliers to the shelf, were detected since ca. 2,000 cal. years B.P. and modified drastically the shelf depositional patterns by introducing large amounts of fine-grained material onto the system, which led to the final establishment and expansion of the Gironde and 'La Grande Vasière' mud fields on the middle shelf.

After ca. 1,000 cal. years B.P., another high input of fine material started to reach the shelf, determining almost fully mud deposition at the mud body sites of vibrocores 6 and 14 (Figs. V.4a, V.4c, V.6c and V.6e), as well as the preservation of important mud layers at the inner shelf site (Figs. IV.2 and IV.4a). Again, anthropogenic causes seemed to be behind this evolutionary trend, as it was contemporaneous with another phase of notable human

development in southern Iberia, the Islamic Medieval Period (*e.g.*, Ribeiro, 1987). During the Muslim rule, and particularly after the 8th century A.D. (ca. 1,350 cal. years B.P.), there was an unprecedent population growth (*e.g.*, Oliveira Marques, 1993; Boone and Worman, 2007) and the exceptional conditions of the region for agriculture were largely maximized (*e.g.*, Devy-Vareta, 1985; Ribeiro, 1987; Magalhães, 2002; Gamito, 2007; Borges Coelho, 2008). This eventually had consequences on erosion, which is likely to have become more severe, leading to enhanced sediment-load being transported by the river and transferred onto the shelf. Furthermore, the evolution of the Guadiana River Mouth itself, including the narrowing of its eastern margin tidal inlets (Morales, 1997), was most certainly further contributing for the observed patterns of deposition on the shelf and within the mud body. As was already discussed in the previous chapter, the intensification of erosion processes due to human land-use was probably one of the main reasons that led to the silting-up of the Guadiana eastern distributary. Consequently, there was a reinforcement of the western distributary and a continuous deviation of most of the river sediment-load towards what is today the main channel of the estuary, which became the chief transfer-pathway between the estuarine system and the shelf, discharging directly onto the area where the cores were located. This was probably the main mechanism that changed once more the depositional patterns in the mid-shelf, and contributed to the full establishment of the mud body deposits at their present-day position (Fig. VI.2c). It is interesting to notice that identical evolutional trends were again unravelled for the Northern Aquitaine shelf (Lesueur *et al.*, 1996; 2001 and 2002), where significant morphological changes of the Gironde River Mouth partially driven by the influence of human activity were responsible for controlling the further increase of supply of suspended sediment to the shelf after ca. 1,000 cal. years B.P. These authors concluded that the bulk of the mud accumulated on the Aquitaine mid-shelf over the last two millennia and an important part of the fine-grained sedimentation has occurred since Medieval Age, with the Gironde shelf mud fields corresponding to the final phase of a highstand deposit sequence.

The fine deposits today forming the Guadiana mud body can thus be interpreted in terms of their genesis and general configuration according to the schematic model proposed by Lantzsch *et al.* (2009a) (Fig. VI.3), as belonging to type 2a.

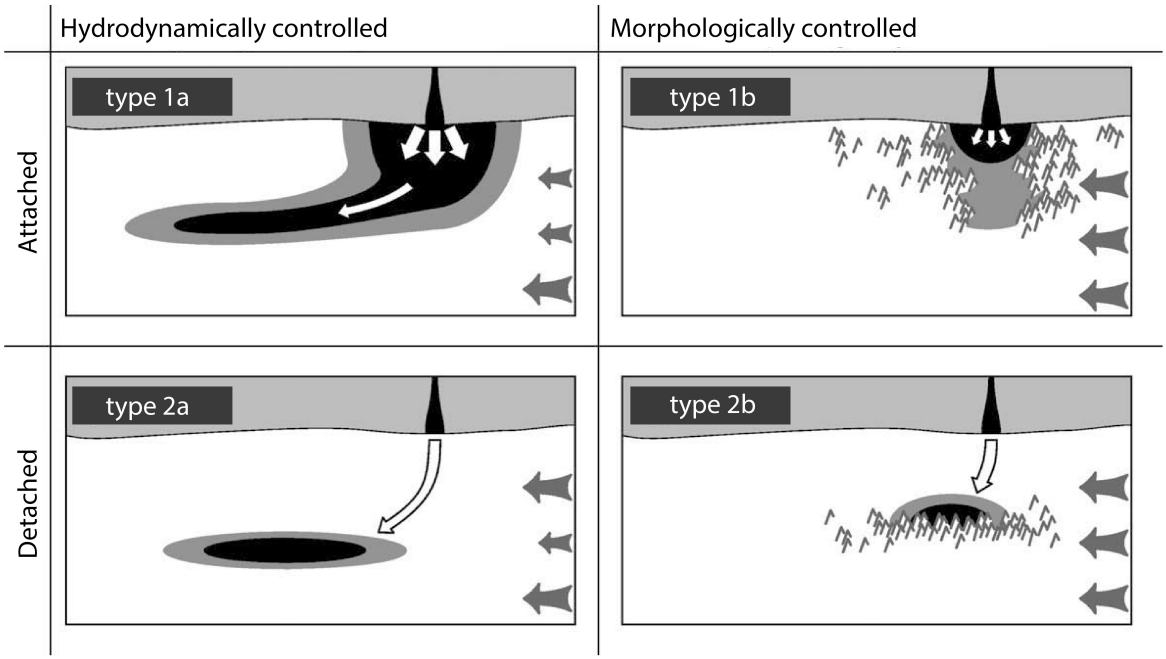

Figure VI.3 – Classification of Holocene mud depocentres as proposed by Lantzsch *et al.* (2009a). Type **1:** depocentres attached to the main sediment source; Type **2:** detached depocentres. Sub-types **a** and **b** are related to the main forcing mechanism for mud deposition: **a** - hydrodynamically-favouring conditions on the mid-shelf; **b** - favouring morphological features. White arrows indicate sediment input and transport, grey arrows the strength of the hydrodynamic regime on the inner, middle and outer shelf.

In general terms, their formation has been mainly controlled by the moderate sediment supplies of the Guadiana River and the hydrodynamic regime across the shelf, which determines re-suspension of the fine sediments from the more energetic coastal and inner shelf domain, and its transport offshore where they eventually settle and accumulate at the less hydrodynamic environment of the middle shelf, detached from their main sediment source (Fig. VI.3).

On the mid-shelf these deposits have formed the Guadiana mud body, which constitutes an important regional fine-grained deposit that started to build-up as early as the late Pleistocene sea-level rise. However, it only developed into an almost fully mud deposit during the last phases of the Holocene highstand, forced by the conjoint action of recent climatic events and the intensive human occupation of the region that has transformed irreversibly the Guadiana Basin landscapes since Roman and Islamic times, until present-day.

Chapter VII

MAIN FINDINGS AND CONCLUSIONS

Main findings: depositional stages and shelf evolution

The multi-proxy sedimentological and micropaleontological study conducted in the four sequences retrieved from the Guadiana inner- to mid-shelf unravelled a succession of different depositional environments for the period spanning from late Pleistocene (for the record of the middle shelf mud body) and from early Holocene (for the record of the inner shelf), until close to present-day. These paleoenvironments were established across the shelf as a response to global and regional forcing mechanisms, namely climate change, the postglacial sea-level rise and the more recent impact of human development. Their reconstruction allowed to rebuild the evolutionary history of the Guadiana region throughout the analysed period, and to assess the role of the interplay between climatic and anthropogenic forces in shaping the natural systems. Furthermore, the insight on the evolution of the Guadiana mid-shelf mud body as a specific depositional and ecological domain is presented in detail for the first time and enabled a higher-resolution interpretation of the events occurred at a millennial- to centennial-scale, including those that took place during Historical times.

On the inner shelf location of vibrocore 20, four main depositional stages were identified throughout the last ca. 9,200 years, evolving from a proximal setting that was probably part of the submerged deltaic system associated with the Guadiana River mouth into a shallow inner shelf domain. On the mid-shelf mud body, four depositional stages were recognized since the late Pleistocene from ca. 15,300 cal. years B.P. The different ages obtained for the three analysed sequences implied that the four depositional stages could only be identified in the older record of vibrocore 1, whereas the younger vibrocores 6 and 14 did not register all stages. The deeper vibrocore 1 and the shallower vibrocore 6, both located in front of the Guadiana River mouth and on the modern depocentre of the mud body, evolved from a shallow inner shelf setting towards a mud-dominated middle shelf environment, following a diachronic process due to their differences in water depth. The site of vibrocore 14, situated at an intermediate depth between vibrocores 1 and 6 but deviated to the west of the main sediment source, the Guadiana River, registered only the last ca. 2,000 years and translated the more recent expansion of the mud body towards other areas outside its depocentre. All shelf sequences revealed a clear fining-up trend of sediments, corresponding to a transgressive record associated with the global postglacial rise of the mean sea level, which was almost fully stabilized in the region around 5,500 cal. years B.P.

Mud body first depositional stage

The oldest sediments correspond to the mud body first depositional stage (ca. 15,300 to 12,500-12,200 cal. years B.P.) and constitute transgressive deposits registered only at the more distal site (vibrocore 1) in a context of lowstand, but already forced by fast sea-level rising. Deposition occurred in a much shallower environment than today, probably in a proximal, more energetic, inner shelf domain standing at ca. 10-15 m below water depth. Sediments corresponded to a combination of dominant silt with alternating amounts of clay and sand that translate pulses of sea-level rise at different rates, together with significant continental-derived terrigenous material that reflected the proximity to the Guadiana bed-load discharges. The benthic foraminiferal species clearly confirmed this environmental scenario. They were dominated by typical coastal taxa, such as *Asterigerinata mamilla*, *Cribrononion gerthi*, *Gavelinopsis praegeri* and *Bulimina elongata*, whereas the very low faunistical densities pointed to some degree of ecological instability due to the higher impact of coastal currents and fast changing conditions arising from the fast sea-level rise. By the time of the Younger Dryas (ca. 12,900-11,700 cal. years B.P.), the sea had already rise several meters and the site of vibrocore 1 would have been in a deeper marine setting (ca. 30-50 m water depth), approximately in the transition from the inner to the middle shelf.

Second mud body and first inner shelf depositional stages

The second depositional stage registered on the mud body, from ca. 12,500-12,200 until 8,000 cal. years B.P., corresponds to the final part of the Younger Dryas (YD) and to the early Holocene, and was recorded at the two mid-shelf sites of vibrocores 1 and 6. At the beginning of this stage, the sea had already drowned a significant part of the shelf, placing the location of vibrocore 1 probably at ca. 60 m water depth and of vibrocore 6 around 10 m water depth. With the mean sea level continuing to rise and accelerating at the beginning of the Holocene, there was a further deepening of the shelf environments during this time. This acceleration was probably the cause for the apparently low sedimentation rates registered at both sites, as it continued to promote the Guadiana Estuary fast infilling and retention of fluvial sediments. The two locations evidenced evolutionary trends that translate their further transition into deeper conditions, characterized by the continuous deposition of high amounts of fine material that corresponded to the setting of the mud body on the middle shelf. However, they exhibited different sedimentary and ecological features that are consistent with their location at different water depths and distance to the river mouth, with the site of vibrocore 1 reaching near 75-85 m water depth and vibrocore 6 around 25-35 m water depth. The most evident

changes were observed within the benthic foraminiferal communities, as the species typical of more energetic shallow environments still dominated the site of vibrocore 6, but were gradually replaced in the deeper site of vibrocore 1 by opportunistic species with preference for finer sediments and lower energetic conditions, namely *Bolivina ordinaria*, *Cassidulina laevigata* and *Brizalina dilatata*.

During this time-interval, the first depositional stage of the inner shelf was identified between ca. 9,200 and 8,500-8,200 cal. years B.P. The sand and gravel composition of sediments, together with the morphoscopy and shape of sandy quartz, revealed a strong signature of the Guadiana direct bed-load input with the significant presence of fluvially-derived feldspars and Paleozoic schists/greywacke, and poorly reworked quartz grains, which today can only be found in the proximal area of the river mouth. By early Holocene, this site would stand in a shallower and more proximal environment that was probably part of the submerged detritic delta just off the river mouth.

Third mud body, second and third inner shelf depositional stages

The first phase of the mud body third depositional stage (ca. 8,000 to 6,000-5,800 cal. years B.P.) correspond to the time when the sea was evolving to near stabilization, at around 5,500 cal. years B.P. Both mid-shelf sites were approaching water depths similar to the present ones, already in a fully marine shelf environment, and this process was again better evidenced by the benthic foraminiferal faunas. Although revealing quite diverse trends at each site as a differentiated bathymetric response to evolving water depths and distance to the river mouth, the increased faunistical densities and rather constant diversity values highlight the establishment of more stable ecological conditions in a eutrophic deeper environment, continuously favoured by the high influx of fluvially-supplied nutrients. On the other hand, the Guadiana Estuary was by then reaching an advanced state of infilling but no increased sediment bypass towards this area seems to have occurred, the same being detected for the inner shelf site. Here, the evolutional patterns during this time-interval, which corresponds to its second depositional stage, also revealed the crucial influence of the Holocene sea-level rise. Until close to 5,800 cal. years B.P., the environment gradually shifted from a transitional/coastal setting to a clear inner shelf domain, as is attested by the increase of marine-derived biogenic compounds and of better reworked (blunt-shining) quartz, and by the decrease of the fluvial-originated bed-load compounds. These were used as proxies for increased water depth and distance to the river mouth, which led to an enhancement of marine processes in the area over the continental-derived imprint. Moreover, they seem to attest for

the existence of a warmer and moisture climate, which had been previously identified in the region during early Holocene times and that offered soil protection to erosion due to vegetation cover expansion along the Guadiana Basin, thus contributing to reduce sediment-input from the river to the shelf.

During the second phase of the middle shelf third depositional stage, until ca. 2,500-2,000 cal. years B.P., the sedimentological patterns remained very similar but with a persistent sediment fining-up trend, which further evidenced the growing stability of this mid-shelf area under the continuous influence of the Guadiana suspended-load supplies. However, a shift in the benthic foraminiferal communities of vibrocore 1 seemed to indicate less changeable ecological conditions, as there was a decrease of the highly opportunistic *C. laevigata* and *B. dilatata* in favour of other species, like *Hyalinea balthica*, *Bulimina marginata* and *Bolivina striatula*. These are also related to fine-grained bottom-sediments, in intermediate to deep environments with high primary productivity, and usually occupy the same ecological niches as *C. laevigata* and *B. dilatata*, but do not exhibit the same opportunistic behaviour. Such trend was interpreted as the response to a decreasing impact of more direct and excessive nutrient supplies from the river that resulted from a combination of two major forcing factors, namely the post-transgression evolution of the Guadiana Estuary mouth and changes in regional climate towards increased aridity. Consistently, on the inner shelf location, the third depositional stage that lasted from ca. 5,800 until around 2,000 cal. years B.P. witnessed a further increase of the marine signature of the deposits, coupled with indicators of continuous, but reduced, river sediment-supply, despite the almost completion of the Guadiana Estuary infilling that was expected to have reversed such trend. This was attributed to the combined action of the two previously mentioned main factors. The prograding processes occurring on both margins of the estuary and the construction of the fluvial deltaic system led to sediment imprisonment on the terminal part of the estuary, whereas the increased aridity that is recognized for the Guadiana River Valley during this period, although also impacting on the vegetation cover and soil erosion rates, must have reduced river-activity. Together, both mechanisms seem to have been responsible for a diminished fluvial input of sediments and nutrients onto the adjacent shelf.

Fourth mud body and inner shelf depositional stages

The onset of the fourth depositional stage took place at around the same approximate dates on the inner and middle shelf, at around 2,000 cal. years B.P., and was marked by much enhanced sediment supply onto both shelf areas.

On the middle shelf sequences of vibrocores 1 and 6, it corresponded mainly to fine-grained material, accompanied by important changes in the sand fraction compounds. Also, the increase of specific benthic foraminiferal species and the appearance of other, namely *Bulimina aculeata*, *B. marginata*, *H. balthica*, *Rectuvigerina phlegeri*, *B. striatula* and, in particular, *Epistominella exigua*, represented a definitive turn-over of the ecological niches within the mud body. At the same time, high amounts of fine sediments started to accumulate at the site of vibrocore 14, initiating the mud body record in this location of the middle shelf. On the inner shelf, the increased amount of sediments reaching the site was also followed by the first major deposition of muds at ca. 1,000 cal. years B.P., generating a record of alternating sand-dominated and fine-dominated deposits that were interpreted as phases of dryer climate and reduced floods, and phases of wetter climate and enhanced flood-events, respectively.

The onset of these changes was probably the consequence of the first major impact of anthropogenic activities along the Guadiana River Basin, related with the Roman occupation of Iberia and a possible wetter phase in the region. The strong human-forced soil erosion due to new agricultural practices and widespread wood exploitation for construction, domestic use and mining activities, eventually associated with higher precipitation and river runoff, increased sediment load and seemed to have caused major modifications on the shelf depositional environment, leading also to the final phase of fining-trend in the mid-shelf mud deposits. Furthermore, the coupled human-climate forcing upon the river export capacity probably enhanced progradation at the estuary mouth, leading to the silting-up process of an ancient eastern distributary of the estuary, and the reinforcement of the western main estuarine channel that discharges directly onto this area of the shelf. After ca. 1,500 cal. years B.P., a higher impact of bed-load fluvial discharges was regarded as an even stronger human impact in the landscape of the Guadiana region, associated with the Islamic Rule of southern Iberia. The further human-induced increase of the river sediment-load might have also been the main cause for the definitive colmatation of the Guadiana eastern distributary, and final reinforcement of the transfer-capacity of the main western channel. This time-interval, until ca. 800 cal. years B.P., has been identified as a more severe dry period in southern Europe, largely forced by the effects of the atmospheric NAO (North Atlantic Oscillation) system and specifically by a more persistent positive signal of its index, which means river-activity must have been reduced. However, on the inner shelf, the occurrence of an initial wetter phase was not recorded, as the absence of flood-like mud deposits until ca. 850 cal. years B.P. seemed to suggest a persistent dry climate, or at least that the moisture conditions were not strong

enough to generate a significant deposition of fine material in this shallower location, and its preservation as flood-layers.

The general enhanced aridity seems to have persisted until close to ca. 300 cal. years B.P., with human impacts during the Middle Ages probably continuing to be the main forcing factor behind the persistent high amounts of sediments that reached the shelf, almost fully suspended-load in the case of the middle shelf area. Here, this process contributed to the further development of the mud body depositional system, and to ecological conditions that continued to favour opportunistic benthic foraminiferal species under high nutrient inputs from the Guadiana River. On the inner shelf site, there was however a signal for enhanced river runoff between ca. 850 and 600 cal. years B.P., translated by the first significant input of fine material to the site, mostly silt. It could be a record of higher precipitation and occurrence of floods due to a shorter wetter period in the region, perhaps linked to a fluctuation of the NAO index towards negative values. Afterwards and until close to 350 cal. years B.P., the decline of fines signalizes the reduction of flood-impact events on the inner shelf, in the already mentioned context of a dry climate, possibly modulated in part by a phase of more persistent NAO-positive values.

The last ca. 300 years of deposition in the mud body continued to be strongly dominated by fluvially-supplied fine sediments and indicated a clear enhancement of the Guadiana River runoff, with a specific sedimentological imprint of continental-derived terrigenous that reflected an even more intensive coupling of anthropogenic and climate forcing mechanisms. Moreover, the accumulation of abundant charcoal particles registered around 100 cal. years B.P. that were probably originated in the mining activities along the Guadiana Basin, seem to correspond to the depositional imprint on the shelf of major floods that were described for the Guadiana River within this time-interval, such as the one recorded in 1876 A.D. New ecological niches were also established within the mud body that translate these changes in fluvial-supply, with species that profit from very abundant nutrient input clearly increasing, such as *E. exigua* and *Valvulineria bradyana*, both emerging as characteristic species of this period. The long-term human occupation and transformation of the region since as early as ca. 2,500-2,000 cal. years B.P. was indeed accentuated after the 19th century by strong-impact activities such as intensive mining exploitation and agricultural practices, which led to an even greater exposure of soils to erosion. Simultaneously, this time corresponds to the most pronounced phase of the LIA (Little Ice Age), clearly associated with a persistent negative-like mode of the NAO index that is the main responsible for increased moisture and winter precipitation in SW Iberia. This is in accordance with what was detected for the inner shelf

during this period, where the last ca. 350 years witnessed a strong return to enhanced fine deposition that clearly revealed higher precipitation levels and the establishment of a wetter climate in the region.

Coupled with the stronger human-induced erosion along the river basin, the climate-driven increased runoff hence seems to have been the main responsible for the significant enhancement of the Guadiana River export capacity of sediments and nutrients from the continent to the shelf, and to the new depositional patterns established both on the inner shelf and in the mid-shelf mud body.

Final remarks

The depositional patterns of the inner shelf site throughout the Holocene were closely associated with the inputs from the Guadiana River and the geomorphologic evolution of its estuarine system, coupled with a strong imprint of the longshore drift supplies. The coarse and very coarse terrigenous-dominated material that constitute much of the older deposits until close to 3,500 cal. years B.P. revealed the importance of early- to mid-Holocene sea-level variations and the retention of sediments inside the Guadiana Estuary during its infilling. Superimposed on this fluvial-forced variability, the dominance of well-reworked (spherical, rounded and blunt-shinning) quartz within sand attests the continued importance of coastal processes at this site throughout time. On the mid-shelf mud body, depositional patterns also reveal that the evolution of this area was closely tied to the sediment supplies of the Guadiana River, since as early as the late Pleistocene. The impact of the postglacial sea-level rise that characterized the early Pleistocene and the beginning of the Holocene overruled other forcing mechanisms during the first depositional stages of the mud body, as it submerged large areas of the shelf. Simultaneously, it controlled the infilling of the Guadiana Estuary, with consequences for the type and amount of sediments that were transferred from the river basin onto the adjacent shelf. After the near stabilization of the mean sea level and with the estuarine infilling almost complete around mid-Holocene, sediment retention seems to have further continued until late Holocene due the prograding processes that began in the Guadiana River Mouth, but other global and regional factors became determinant in the control of sediment supply to the shelf system, namely the millennial- to centennial-scale North Atlantic climatic oscillations, and the more recent impact of human development in the region.

Further work needs however to be conducted in order to clarify some issues that require a better understanding, namely: the integration of all the data based on the analysis of the cores

with high-resolution seismic profiles to obtain an improved stratigraphical definition on the depositional processes occurred on the continental shelf, and to help reconstruct the paleo-drainage system of the river; detail the temporal framework based on the radiocarbon datings with additional dating analyses that would allow a better accuracy on the calculation of the sedimentation rates, and specifically for the more recent deposits of the cores, in which the radiocarbon method lacks accurateness, such as amino acid racemisation (AAR) or radioisotopic measurements of ^{210}Pb; investigate the isotopic record of the shelf deposits to determine more accurately oceanographic changes that were linked to variations in climate and in primary production, through the analysis of oxygen and carbon stable isotopes; and explore the problematic concerning the compaction of sediments along the cores, which influences the correct assessment of past sedimentation rates.

Chapter VIII

TAXONOMY OF BENTHIC FORAMINIFERA

VIII.1. Systematic

The systematic taxonomy of benthic foraminifera from the Guadiana mud body is presented in this chapter for all the species that were found with at least two specimens in at least one of all the analysed samples (Appendixes A, B and C).

In the current study, the commonly accepted systematic hierarchy established by Loeblich and Tappan (1988) was followed, placing foraminifers in the Order Foraminiferida (Eichwald, 1930). Following the 1960's publications from the same authors, most of systematisits have accordingly classified foraminifers as belonging to the Kingdom Protista, more recently also designated as Kingdom Protoctista, which englobes eukaryotic unicellular organisms. The taxonomic rank of foraminifera was raised from order to class also by Loeblich and Tappan (1992) according to the characteristics of the organisms, organized as follows: 1) granuloreticulose pseudopodia; 2) outer cover, usually a test; 3) alternation of haploid and diploid generations; 4) the presence of a test constructed from non-oriented calcareous or siliceous crystals.

The classification of the foraminifers' genera and all their successive higher classes (subfamilies, families, superfamilies and suborders) established in the present study was based on the work by Loeblich and Tappan (1988), except for the genera Textularia and species *Discorbis williamsoni* that were kept with the original names taken from the Ellis and Messina catalogue of Foraminifera (1942-2009). For each identified species, the taxonomic references were organized according to the following schematics: 1) the name of the species as was used in the present work, together with the name of the author and the date of its first identification; 2) the plate and figure numbers for the species that were photographed with the scanning electron microscope (SEM), which included all the main species (> 5% abundance in at least one sample) and several other whenever it was possible to obtain their photographic record; 3) the original generic classification and species name obtained with the Ellis and Messina catalogue of Foraminifera (1942-2009); 4) a synonymy list, whenever existing; 5) examples obtained from the literature (*e.g.*, Murray, 1971; Colom, 1974; Boltovskoy *et al.*, 1980; Jones, 1994; Levy *et al.*, 1995; Debenay *et al.*, 2001; Murray, 2003; Martins and Gomes, 2004; Mendes *et al.*, 2004; Milker and Schmiedl, 2012; Holbourn *et al.*, 2013).

ORDER FORAMINIFERIDA Eichwald 1830

SUBORDER TEXTULARIINA Delage and Hérouard 1896

Superfamily SPIROPLECTAMMINACEA Cushman 1927

Family SPIROPLECTAMMINIDAE Cushman 1927

Subfamily SPIROPLECTAMMININAE Cushman 1927

Genus SPIROPLECTINELLA Kisel'man 1972

***Spiroplectinella wrighti* (Silvestri 1903)**

Spiroplecta wrighti Silvestri, 1903, Accad. Pont. Romana Nuovi Lincei, Atti, Roma, Italy, tom. 56, p. 59-60, text-figs. 1-6.

Spiroplectinella wrighti (Silvestri), Loeblich and Tappan, 1988, p. 112, pl. 120, figs. 1-16; Jones, 1994; p. 47, pl. 42, figs. 17-18; Debenay and Redois, 1997, pl. 1, fig. 7.

Superfamily TROCHAMMINACEA Schwager 1877

Family TROCHAMMINIDAE Schwager 1877

Subfamily TROCHAMMININAE Schwager 1877

Genus AMMOGLOBIGERINA Eimer and Fickert 1899

***Ammoglobigerina globigeriniformis* (Parker and Jones 1865)**

Lituola nautiloidea Lamarck var. *globigeriniformis* Parker and Jones, 1865, Roy. Soc. London, England, vol. 155, p. 407, pl. 15, figs. 46-47, pl. 17, figs. 96-98.

Trochammina globigeriniformis (Parker and Jones), De Stigter *et al.*, 1998, pl. 1, fig. 5; Duchemin *et al.*, 2007, p. 28, pl. 2, figs. 13-14.

Ammoglobigerina globigeriniformis (Parker and Jones), Martins and Gomes, 2004, p. 26-27, fig. 2.10; Abu-Zied et al., 2008, p. 64, pl. I, figs. 4-5; Milker and Schmiedl, 2012, p. 35, fig. 9.25-9.26.

Superfamily TEXTULARIACEA Ehrenberg 1838

Family EGGERELLIDAE Cushman 1937

Subfamily EGGERELLINAE Cushman 1937

Genus EGGERELLOIDES Haynes 1973

***Eggerelloides scaber* (Williamson 1858)**

Bulimina scabra Williamson, 1858, Ray Soc., London, England, p. 65, pl. 5, figs. 136-137.

Eggerella scabra (Williamson), Murray, 1971, p. 45, pl. 15, figs. 1-6; Levy *et al.*, 1995, p. 19, pl. 2, fig. 9.

Eggerelloides scaber (Williamson), Murray, 2003, p. 13, fig. 2.11; Martins and Gomes, 2004, p. 36-39, fig. 2.17.

Eggerelloides scabrus (Williamson), Milker and Schmiedl, 2012, p. 37, fig. 10.9.

Family TEXTULARIIDAE Ehrenberg 1838

Subfamily TEXTULARIINAE Ehrenberg 1838

Genus BIGENERINA d'Orbigny 1826

***Bigenerina nodosaria* d'Orbigny 1826**

Plate I, fig. 1

Bigenerina nodosaria d'Orbigny, 1826, Ann. Sci. Nat., Paris, ser. 1, t. 7, p. 261, pl. 11, figs. 9-12.

Bigenerina nodosaria d'Orbigny, Colom, 1974, p. 79 and 87, fig. 6a-n; Levy *et al.*, 1995, p. 20, pl. 3, fig. 1; Martins and Gomes, 2004, p. 42-43, fig. 2.19.

Genus TEXTULARIA Defrance 1824

***Textularia agglutinans* d'Orbigny 1839**

Textularia agglutinans d'Orbigny, 1839, Hist. Phys. Polit. Nat. Cuba, Paris, p. 144, vol. 8, pl. 1, figs. 17-18 and 32-34.

Textularia agglutinans d'Orbigny, Colom, 1974, p. 80 and 87, fig. 7w-a'; Boltovskoy *et al.*, 1980, p. 51, pl. 32, figs. 5-7; Jones, 1994, p. 48, pl. 43, figs. 1-3; De Stigter *et al.*, 1998, p. , pl. 2, fig. 5; Duchemin *et al.*, 2005, p. 217, pl. 1, fig. 7; Mojtahid *et al.*, 2009, pl. III, figs. 43-44; Milker and Schmiedl 2012, p. 36, figs. 10.15 and 10.16.

***Textularia candeiana* d'Orbigny 1839**

Textularia candeiana d'Orbigny, 1839, Hist. Phys. Polit. Nat. Cuba, Paris, p. 143, pl. 1, figs. 25-27.

Textularia cf. *candeiana* d'Orbigny, Colom, 1974, p. 82 and 88, fig. 9a-g.

Textularia candeiana d'Orbigny, Ellis and Messina, 1942-2009, nº 21.639; Boltovskoy *et al.*, 1980, p. 51, pl. 32, figs. 8-11.

***Textularia conica* d'Orbigny 1840**

Plate I, fig. 2

Textularia conica d'Orbigny, 1840, Hist. Phys. Polit. Nat. Cuba, Paris, p. 143, vol. 8, pl. 1, figs. 19-20.

Textularia conica d'Orbigny, Levy *et al.*, 1995, p. 20, pl. 3, fig. 5; Martins and Gomes, 2004, p. 44-45, fig. 2.20; Milker and Schmiedl, 2012, p. 39, fig. 10.18.

***Textularia deltoidea* Reuss 1850**

Plate I, fig. 3

Textularia deltoidea Reuss, 1850, K. Akad. Wiss. Wien, Math.-Nat. Cl., Denksch., Wien, Österreich, Bd. 1, p. 381, pl. 49, fig. 4.

Textularia deltoidea Reuss, Levy *et al.*, 1995, p. 20, pl. 3, fig. 6; Martins and Gomes, 2004, p. 45-46, fig. 2.21; Mendes *et al.*, 2013, p. 108, pl. 1, fig. 2.

***Textularia sagittula* (Defrance 1824)**

Textularia sagittula Defrance, 1824, Dictionaire des Sciences Naturelles, Paris, France, Levrault, tom. 32, p. 177, pl. 13, fig. 5.

Spiroplectinella sagittula (Defrance), Martins and Gomes, 2004, p. 23-24, fig. 2.8; Milker and Schmiedl, 2012, p. 34, fig. 9.19-9.21.

Textularia sagittula Defrance, Murray, 1971, p. 31, pl. 8, figs. 1-9; Colom, 1974, p. 80 and 89-90, fig. 7i-l; Debenay and Redois, 1997, pl. 1, fig. 9; De Stigter *et al.*, 1998, pl. 1, fig. 7; Murray, 2003, p. 15, figs. 3.12-3.14.

SUBORDER MILIOLINA Delage and Hérouard 1896

Superfamily MILIOLACEA Ehrenberg 1839

Family SPIROLOCULINIDAE Wiesner 1920

Genus ADELOSINA d'Orbigny 1826

***Adelosina* cf. *granulocostata* (Germeraad 1946)**

Quinqueloculina granulocostata Germeraad, 1946, Amsterdam: J. H. de Bussy, ser. 3 (Geol.), nº 2, p. 63. Figure in Brady, op. cit., pl. 6, figs. 15-20.

Quinqueloculina granulocostata Germeraad, Ellis and Messina, 1942-2009, nº 36.656.

Adelosina granulocostata (Germeraad), Jones, 1994, p. 23, pl. 6, figs. 15-20.

***Adelosina laevigata* d'Orbigny 1826**

Plate I, fig. 4

Adelosina laevigata, d'Orbigny, 1826, Ann. Sci. Nat., Paris, France, ser. 1, tom. 7, p. 304. Figures in Parker, Jones and Brady, Ann. Mag. Nat. Hist., London, England, 1871, ser. 4, vol. 8, pl. 8, fig. 12, and in d'Orbigny, 1846, pl. 20, figs. 22-24.

Quinqueloculina (Adelosina) laevigata (d'Orbigny)*,* Colom, 1974, p. 187 and 189, fig. 52a-j.

Adelosina laevigata d'Orbigny, Loeblich and Tappan, 1988, p. 328-329, pl. 337, figs. 5-12; Milker and Schmiedl, 2012, p. 48, figs. 12.18-12.19.

Family HAUERINIDAE Schwager 1876

Subfamily HAUERININAE Schwager 1876

Genus QUINQUELOCULINA d'Orbigny 1826

***Quinqueloculina lata* Terquem 1876**

Plate I, fig. 5

Quinqueloculina lata Terquem, 1876, Mém. Soc. Dunkerquoise, Dunkerque, vol. 20, p. 173, pl. 11, fig. 8.

Quinqueloculina lata Terquem, Murray, 1971, p. 63, pl. 23, figs. 1-3; Levy *et al.*, 1995, p. 23, pl. 4, fig. 2; Debenay *et al.*, 2001, pl. II, fig. 2; Milker and Schmiedl, 2012, p. 58, figs. 15.30-15.31.

***Quinqueloculina seminulum* (Linné 1758)**

Serpula seminulum Linné, 1758, Holmiae, Sweeden, impensis L. Salvii, tom. 1, p. 786, pl. 2, fig. 1.

Quinqueloculina seminula (Linné), Levy *et al.*, p. 23, pl. 4, fig. 3; Debenay *et al.*, 2001, pl. II, figs. 11-12; Milker and Schmiedl, 2012, p. 59, figs. 15.30-15.31.
Quinqueloculina seminulum (Linné), Murray, 1971, p. 65, pl. 24, figs. 1-6; Boltovskoy *et al.*, 1980, p. 47, pl. 29, figs. 7-13; Jones, 1994, p. 21, pl. 5, fig. 6; Martins and Gomes, 2004, p. 53-54, fig. 2.26;

***Quinqueloculina stalkeri* Loeblich and Tappan 1953**

Plate I, fig. 6

Quinqueloculina stalkeri Loeblich and Tappan, 1953, Smithsonion Inst., Misc. Coll., Washington, D. C., vol. 121, nº 7, p. 40, pl. 5, figs. 5-9.
Quinqueloculina stalkeri Loeblich and Tappan, Boltovskoy *et al.*, 1980, p. 47, pl. 29, figs. 14-16; Martins and Gomes, 2004, p. 55, fig. 2.27.

***Quinqueloculina venusta* Barrer 1868**

Quinqueloculina venusta Barrer, 1868, K. Akad. Wiss. Wien, Math.Naturw. Cl., Sitzber., Wien, Österreich, Bd. 58, Abt. 1, p. 147, pl. 2, fig. 6.
Quinqueloculina venusta Barrer, Jones, 1994, p. 21, pl. 5, fig. 7; Martins and Gomes, 2004, p. 56-57, fig. 2.28.

Subfamily SIGMOILINITINAE Luczkowska 1974

Genus SIGMOILINITA Seiglie 1965

***Sigmoilinita tenuis* (Czjzek 1848)**

Quinqueloculina tenuis Czjzek, 1848, Naturw. Abh., Wien, Österreich, Bd. 2, Abth. 1, p. 149, pl. 13, figs. 31-34.
Sigmoilinita tenuis (Czjzek), Jones, 1994, p. 26, pl. 10, figs. 7-8 and 11; Levy *et al.*, 1995, p. 25, pl. 5, fig. 1; Martins and Gomes, 2004, p. 60. Fig. 2.30.

Subfamily SIGMOILOPSINAE Vella 1957

Genus SIGMOILOPSIS Finlay 1947

***Sigmoilopsis schlumbergeri* (Silvestri 1904)**

Plate I, fig. 7

Sigmoilina schlumbergeri Silvestri, 1904, Accad. Pont. Romana Nuovi Lincei, Mem., Roma, Italy, vol. 22, p. 267 and 269, pl. 7, figs. 12-14; p. 481, text-fig. 6; p. 482, text-fig. 7.

Sigmoilopsis schlumbergeri (Silvestri), Levy *et al.*, 1995, p. 25, pl. 5, fig. 2; Martins and Gomes, 2004, p. 61-63, fig. 2.31; Abu-Zied *et al.*, 2008, p. , pl. I, figs. 18-19; Milker and Schmiedl, 2012, p. 69-70, fig. 18.7-18.8; Holbourn *et al.*, 2013, p. 506-507; figs. 1-2.

SUBORDER LAGENINA Delage and Hérouard 1896

Superfamily NODOSARIACEA Ehrenberg 1838

Family VAGINULINIDAE Reuss 1860

Subfamily LENTICULININAE Chapman, Parr and Collins 1934

Genus NEOLENTICULINA McCulloch 1977

***Neolenticulina peregrina* (Schwager 1866)**

Cristellaria peregrina Schwager, 1866, Geol. Thiel, Wien, Österreich, vol. 2, p. 245, pl. 7, fig. 89.

Neolenticulina variabilis (Reuss), Jones, 1994, p. 80, pl. 68, figs. 11-16.

Lenticulina peregrina (Schwager), Murray, 1971, p. 89, pl. 35, figs. 3-5; Levy *et al.*, 1995, p. 27, pl. 5, fig. 5; Mojtahid *et al.*, 2009, pl. II, fig. 24.

Neolenticulina peregrina (Schwager), Martins and Gomes, 2004, p. 64-65, fig. 2.33; Milker and Schmiedl, 2012, p. 73, fig. 18.21; Holbourn *et al.*, 2013, p. 368-369, figs. 1-2.

Subfamily MARGINULININAE Wedekind 1937

Genus AMPHICORYNA Schlumberger 1881

***Amphicoryna catesbyi* (d'Orbigny 1839)**

Nodosaria catesbyi d'Orbigny, 1839, Hist. Nat. Cuba, Paris, p. 16, vol. 8, pl. 1, figs. 8-10.

Amphicoryna catesbyi (d'Orbigny), Levy *et al.*, 1995, p. 27, pl. 5, fig. 9.

Amphicoryna catesbyi (d'Orbigny), Debenay and Redois, 1997, p. 28, pl. 2, fig. 14.

***Amphicoryna scalaris* (Batsch 1791)**

Nautilus (Orthoceras) scalaris Batsch, 1791, Jena, Univ. Press, pp. 1, 4, pl. 2, fig. 4a-b.

Amphicoryna scalaris (Batsch), Murray, 1971, p. 77, pl. 29, figs. 1-4; Jones, 1994, p. 77, pl. 65, figs. 7-9; Levy *et al.*, 1995, p. 27, pl. 5, fig. 10; Martins and Gomes, 2005, p. 65-66, fig. 2.34.

***Amphicoryna separans* (Brady 1884)**

Nodosaria scalaris (Batsch) var. *separans* Brady, 1884, Rept. Challenger Exped., London, England, Zool., pt. 22, vol. 9, p. 510, pl. 64, figs. 16-19.

Amphicoryna separans (Brady), Jones, 1994, p. 76, pl. 64, figs. 16-19.

Family LAGENIDAE Reuss 1862

Genus LAGENA Walker and Jacob 1798

***Lagena semistriata* Williamson 1848**

Lagena striata (Walker) var. B, *semistriata* Williamson, 1848, Ann. Mag. Nat. Hist., ser. 2, vol. 1, p. 14, pl. 1, figs. 9-10.

Lagena semistriata Williamson, Murray, 1971, p. 85, pl. 33, figs. 4-8; Jones, 1994, p. 64, pl. 57, figs. 14 and 16; Debenay *et al.*, 2001, pl. III, fig. 15.

***Lagena sulcata* (Walker and Jacob 1798)**

Serpula (*Lagena*) *sulcata* Walker and Jacob, 1798, Kanmacher, Ed. 2, p. 634, pl. 14, fig. 5.

Lagena sulcata (Walker and Jacob), Murray, 1971, p. 87, pl. 34, figs. 5-8; Jones, 1994, p. 64, pl. 57, figs. 23, 25-27 and 33-34; Debenay *et al.*, 2001, pl. III, fig. 7; Holbourn *et al.*, 2013, p. 324-325, fig. 1.

Family ELLIPSOLAGENIDAE Silvestri 1923

Subfamily OOLININAE Loeblich and Tappan 1961

Genus OOLINA d'Orbigny 1839

***Oolina hexagona* (Williamson 1848)**

Plate 1, fig. 8

Entosolenia squamosa (Montagu) var. *hexagona* Williamson, 1848, Ann. Mag. Hist., London, England, ser. 2, vol. 1, p. 20, pl. 2, fig. 23.

Oolina hexagona (Williamson), Murray, 1971, p. 93, pl. 37, figs. 4-6; Levy *et al.*, 1995, p. 29, pl. 6, fig. 3; Martins and Gomes, 2004, p. 69-70, fig. 2.38; Holbourn *et al.*, 2013, p. 382-383, fig. 1.

Subfamily ELLIPSOLAGENINAE Silvestri 1923

Genus FISSURINA Reuss 1850

***Fissurina annectens* (Burrows and Holland 1895)**

Lagena annectens Burrows and Holland, 1895, Paleontogr. Soc., London, England, p. 203, pl. 7, fig. 11a-b.

Fissurina annectens (Burrows and Holland), Jones, 1994, p. 67, pl. 59, figs. 7 and 15.

***Fissurina fimbriata* (Brady 1881)**

Plate I, fig. 9

Lagena fimbriata Brady, 1881, Quart. Jour. Micr. Sci., London, n. s., vol. 21, p. 61. Figure in Brady, 1884, Rept. Voy. Challenger, Zool., vol. 9, pl. 60, figs. 26-28.

Fissurina fimbriata (Brady), Jones, 1994, p. 70, pl. 60, figs. 26-27.

***Fissurina globosocaudata* Albani and Yassini 1989**

Fissurina globosocaudata Albani and Yassini, 1989, *in* Albani and Yassini (1995), p. 124, figs. 392-393, 409-410.

Fissurina globosocaudata Albani and Yassini, Martins and Gomes, 2004, p. 73, fig. 2.41.

***Fissurina laevigata* Reuss 1850**

Fissurina laevigata Reuss, 1850, K. Akad. Wiss. Wien, Math. Nat. Cl., Denkschr., Wien, Österreich, Bd. 1, p. 366, pl. 46, fig. 1.

Fissurina laevigata Reuss, Boltovskoy *et al.*, 1980, p. 32, pl. 15, figs. 14-16; Jones, 1994, p. 113, pl. 114, fig. 8; Martins and Gomes, 2004, p. 74, fig. 2.42.

***Fissurina lucida* (Williamson 1848)**

Entosolenia marginata (Montagu) var. *lucida* Williamson, 1848, Ann. Mag. Hist., London, England, p. 17, pl. 2, fig. 7.

Fissurina lucida (Williamson), Murray, 1971, p. 97, pl. 39, figs. 1-3; Boltovskoy *et al.*, 1980, p. 32, pl. 15, figs. 17-20; Alve and Murray, 2001, p. 24, pl. I, figs. 6-7; Debenay *et al.*, 2001, pl. III, fig. 27; Martins and Gomes, 2004, p. 75-76, fig. 2.43.

***Fissurina marginata* (Montagu 1803)**

Vermiculum marginatum Montagu, 1803, J. S. Hollis, Romsey, England, p. 524. Figured by Walker and Boys, 1784, *Testacea minuta rariora*, pl. I, fig. 7.

Fissurina marginata (Montagu), Murray, 1971, p. 97, pl. 39, figs. 4-6; Murray, 2003, p. 17, figs. 5.3-5.4; Martins and Gomes, 2004, p. 76-77, fig. 2.44; Milker and Schmiedl, 2012, p. 78-79, fig. 19.12.

***Fissurina orbignyana* Seguenza 1862**

Plate I, fig. 10

Fissurina orbignyana Seguenza, 1862, *Descrizione dei Foraminiferi Monotalamici delle Marne Mioceniche de Distretto di Messina*. Messina, p. 66, pl. 2, figs. 19-20.

Fissurina orbignyana Seguenza, Murray, 1971, p. 99, pl. 40, figs. 1-5; Jones, 1994, p. 68, pl. 59, fig. 18; Murray, 2003, p. 17, figs. 5.5-5.6; Martins and Gomes, 2004, p. 78, fig. 2.45; Holbourn *et al.*, 2013, p. 250-251, fig. 1.

***Fissurina staphyllearia* Schwager 1866**

Fissurina staphyllearia Schwager, 1866, Geol. Theil, Wien, Österreich, Bd. 2, Abt. 2, p. 209, pl. 5, fig. 24.

Fissurina staphyllearia Schwager, Ellis and Messina, 1942-2009, nº 6.605; Jones, 1994, p. 67-68, pl. 59, figs. 8-11.

***Fissurina* sp**

SUBORDER ROBERTININA Loeblich and Tappan 1984

Superfamily CERATOBULIMINACEA Cushman 1927

Family CERATOBULIMINIDAE Cushman 1927

Subfamily CERATOBULIMININAE Cushman 1927

Genus LAMARCKINA Berthelin 1881

***Lamarckina haliotidea* (Heron-Allen and Earland 1911)**

Plate II, fig. 1

Pulvinulina haliotidea Heron-Allen and Earland, 1911, Roy. Micr. Soc. Jour., London, England, p. 338, pl. 11, figs. 6-11.

Pulvinulina haliotidea Heron-Allen and Earland, Ellis and Messina, 1942-2009, nº 17.927.

Lamarckina haliotidea (Heron-Allen and Earland), Murray, 1971, p. 205, pl. 86, figs. 1-6; Debenay *et al.*, 2001, pl. IV, fig. 22; Murray, 2003, p. 24, figs. 8.12-8.13; Diz *et al.*, 2004, p. 273, fig. 2.2; Martins and Gomes, 2004, p. 80-81, fig. 2.47.

Genus RUBRATELLA Grell 1956

***Rubratella intermedia* Grell 1956**

Plate II, fig. 2

Rubratella intermedia Grell, 1956, Archiv Protistenk., Jena, Germany, vol. 102, nº 3/4, p. 291; p. 293, tf. 1, figs. 1-14; p. 295, tf. 2a-d; p. 304, tf. 3a-d, a'-d'; pls. 22-23, figs. 1-45.

Rubratella intermedia Grell, Loeblich and Tappan, 1988, p. 442, pl. 475, figs. 15-18; Debenay *et al*., 2001, p. 92, pl. IV, fig. 25.

SUBORDER ROTALIINA Delage and Hérouard 1896

Superfamily BOLIVINACEA Glaessner 1937

Family BOLIVINIDAE Glaessner 1937

Genus BOLIVINA d'Orbigny 1839

***Bolivina albatrossi* Cushman 1922**

Plate II, fig. 3

Bolivina albatrossi Cushman, 1922, U. S. Nat. Mus., Washington, D. C., nº 104, p. 31, pl. 6, fig. 4.

Bolivina albatrossi Cushman, Ellis and Messina, 1942-2009, nº 72.704; Martins and Gomes, 2004, p. 85, fig. 2.49; Abu-Zied *et al.*, 2008, p. 65, pl. I, fig. 26.

***Bolivina difformis* (Williamson 1858)**

Textularia variabilis Williamson var. *difformis* Williamson, 1858, Ray. Soc., p. 77, pl. 6, figs. 166, 167. Type 96.8.13.43.

Brizalina difformis (Williamson), Murray, 1971, p. 109, pl. 44, figs. 1-2; Milker and Schmiedl 2012, p. 81, figs. 19.28 and 19.29

Bolivina difformis (Williamson), Boltovskoy *et al.*, 1980, p. 17, pl. 2, fig. 17; Levy *et al.*, 1995, p. 30, pl. 6, fig. 11; Martins and Gomes, 2004, p. 87-88, fig. 2.51.

***Bolivina inflata* Heron-Allen and Earland 1913**

Bolivina inflata Heron-Allen and Earland, 1913, Roy. Irish Acad., Proc., Dublin, Ireland, vol. 31, sect. 3 (1911-1915), p. 68, pl. 4, figs. 16-19.

Bolivina inflata Heron-Allen and Earland, Ellis and Messina, 1942-2009, nº 1.741-1.742.

***Bolivina ordinaria* Phleger and Parker 1952**

Plate II, fig. 5

Bolivina ordinaria Phleger and Parker, 1952, Geol. Soc. Amer. Mem., New York, nº 46, pt. 2, p. 14, pl. 7, figs. 4-6.

Bolivina variabilis (Wiliamson 1858), Debenay *et al.*, 2001, p. 92-93, pl. IV, figs. 3-4.

Bolivina dilatata Reuss 1850, Mojtahid *et al.*, 2009, pl. II, fig. 16.

Bolivina ex. gr. dilatata, Duchemin *et al.*, 2007, pl. 1, figs. 14-16.

Bolivina ordinaria Phleger and Parker, Boltovskoy *et al.*, 1980, p. 18, pl. 3, figs. 1-3; Martins and Gomes, 2004, p- 90-91, fig. 2.53; Mendes *et al.*, 2012, p. 38, fig. 2.8a-f.

***Bolivina pseudoplicata* Heron-Allen and Earland 1930**

Plate II, fig. 6

Bolivina pseudoplicata Heron-Allen and Earland, 1930, Roy. Micr. Soc., Jour., London, England, ser. 3, vol. 4, p. 81, pl. 3, figs. 36-40.

Bolivina pseudoplicata Heron-Allen and Earland, Murray, 1971, p. 107, pl. 43, figs. 1-7; Boltovskoy *et al.*, p. 18, pl. 3, figs. 4-8; Debenay *et al.*, 2001, p. 92-93, pl. IV, fig. 6; Murray, 2003, p. 19, fig. 6.17; Martins and Gomes, 2004, p. 92-94, fig. 2.54.

***Bolivina seminuda* Cushman 1911**

Plate II, fig. 7

Bolivina seminuda Cushman, 1911, U. S. Nat. Mus., Bull., Washington, D. C., U. S. A., nº 71, p. 34, tf. 55.

Bolivina seminuda Cushman, Martins and Gomes, 2004, p. 95-97, fig. 2.55.

***Bolivina striatula* Cushman 1922**

Plate II, fig. 11

Bolivina striatula Cushman, 1922, Carniege Inst., Publ. nº 311, Washington, D. C., U. S. A., p. 27, pl. 3, fig. 10.

Bolivina striatula Cushman, Colom, 1974, p. 106 and 120-121, fig. 17a-g; Levy *et al.*, 1995, p. 32, pl. 7, fig. 3; Martins and Gomes, 2004, p. 100-101, fig. 2.57; Duchemin *et al.*, 2007, p. 28, pl. I, figs. 12-13; Mendes *et al.*, 2012, p. 38, fig. 3.1.

***Bolivina subspinescens* Cushman 1922**

Plate II, fig. 8

Bolivina subspinescens Cushman, 1922, U. S. Nat. Mus., Bull., Washington, D. C., U. S. A., nº 104, p. 48, pl. 7, fig. 5.

Brizalina variabilis (Williamson 1858), Murray, 1971, p. 113, figs. 1-3.

Bolivina spinescens Cushman 1911, Debenay and Redois, 1997, pl. 3, fig. 1.

Bolivina italica Cushman 1936, Mendes *et al.*, 2012, p. 38, fig. 2.7.

Brizalina subspinescens (Cushman), Holbourn *et al.*, 2013, p. 84-85, figs. 1-4.

Bolivina subspinescens Cushman, Ellis and Messina, 1942-2009, nº 1.983-1.984; Levy *et al.*, 1995, p. 32, pl. 6, fig. 13; Milker and Schmiedl, 2012, p. 81, fig. 19.24.

***Bolivina tortuosa* Brady var. *atlantica* Cushman 1936**

Bolivina tortuosa Brady var. *atlantica* Cushman, 1936, Cushman Lab. Foram. Res., Spec. Publ., Sharon, Mass., U. S. A., nº 6, p. 57, pl. 8, fig. 8.

Bolivina tortuosa Brady var. *atlantica* Cushman, Ellis and Messina, 1942-2009, nº 2.009.

Bolivina tortuosa Brady 1881, Boltovskoy *et al.*, 1980, p. 18, pl. 3, figs. 14-17.

Sigmavirgulina tortuosa (Brady), Jones, 1994, p. 58, pl. 52, figs. 31-34; Milker and Schmiedl 2012, p. 91, fig. 21.12.

***Bolivina* cf. *acerosa* Brady 1936**

Bolivina acerosa Brady, 1936, Cushman Lab. Foram. Res., Spec. Publ., Sharon, Mass., U.S.A., nº 6, p. 54, pl. 8, fig. 1.

Bolivina acerosa Brady, Ellis and Messina, 1942-2009, nº 1.543.

***Bolivina* cf. *plicata* d'Orbigny 1839**

Bolivina plicata d'Orbigny, A. d', *Voyage dans l'Amérique Méridionale; Foraminfères*, Strasbourg, France: Levrault, t. 5, pt. 5, p. 62, pl. 8, figs. 4-7.

Bolivina plicata d'Orbigny, Ellis and Messina, 1942-2009, nº 73.630-73.631.

***Bolivina* cf. *robusta* Brady 1881**

Bolivina robusta Brady, 1881, Quart. Jour. Micr. Sci., London, n. s., vol. 21, p. 57.

Bulimina (Bolivina robusta) Brady, Ellis and Messina, 1942-2009, nº 38.279.

Bolivina robusta Brady, Jones, 1994, p. 58, pl. 53, figs. 7-9; Hayward *et al.*, 2013, p. 442, fig. 6.6.

Bolivina cf. *robusta* Brady, Debenay *et al.*, 2001, pl. IV, fig. 5.

***Bolivina* cf. *skagerrakensis* Qvale and Nigam 1985**

Bolivina skagerrakensis Qvale and Nigam, 1985, Journ. Foram. Res., Washington, vol. 15, nº 1, p. 6, pl. 1-2.

Bolivina skagerrakensis Qvale and Nigam, Ellis and Messina, nº 73.633-73.639.

Bolivina skagerrakensis Qvale and Nigam, Levy *et al.*, 1995, p. 31, pl. 7, fig. 1; Martins and Gomes, 2004, p. 97-98, fig. 2.56.

***Bolivina* sp**

Genus BRIZALINA O. G. Costa 1856

***Brizalina alata* (Seguenza 1862)**

Vulvulina alata Seguenza, 1862, Accad. Gioenia Sci. Nat. Catania, Atti., ser. 2, t. 18, p. 115, pl. 2, fig. 5.

Bolivina alata (Seguenza), Colom, 1974, p. 106 and 119, fig. 17u-z; Levy *et al.*, 1995, p. 30, pl. 6, fig. 12; Abu-Zied *et al.*, 2008, p. 65, pl. I, fig. 25.

Brizalina alata (Seguenza), Jones, 1994, p. 58, pl. 52, figs. 2-4; Holbourn *et al.*, 2013, p. 76-77, figs. 1-5.

***Brizalina dilatata* (Reuss 1850)**

Plate II, fig. 4

Bolivina dilata Reuss, 1850, K. Akad. Wiss. Wien, Math.-Nat. Cl., Denkschr., Wien, Österreich, Bd. 1, p. 381, pl. 48, fig. 15a-c.

Bolivina dilata Reuss, Colom, 1974, p. 107 and 120, fig. 18j-n; Jannink *et al.*, 1998, pl. 1, fig. 1; Martins and Gomes, 2004, p. 88-90, fig. 2.52; Duchemin *et al.*, 2007, p. 28, pl. I, fig. 17.

Brizalina dilata (Reuss), Mendes et al., 2012, p. 38, fig. 3.2; Milker and Schmiedl, 2012, p. 81-82, fig. 19.30.

***Brizalina spathulata* (Williamson 1858)**

Plate II, fig. 9

Textularia variabilis Williamson var. *spathulata* Williamson, 1858, Ray Soc., p. 76, pl. 6, figs. 164, 165. Type 96.8.13.42.

Bolivina spathulata (Williamson) Mojtahid *et al.*, 2009, pl. II, fig. 17.

Brizalina spathulata (Williamson), Murray, 1971, p. 111, pl. 45, figs. 1-4; Colom, 1974, p. 107 and 121, fig. 18h-i; Martins and Gomes, 2004, p. 108-110, figs. 2.61 and 2.62; Mendes *et al.*, 2012, p. 38, fig. 3.3; Milker and Schmiedl, 2012, p. 82, figs. 20.1 and 20.2.

***Brizalina subaeraniensis* (Cushman 1922)**

Plate II, fig. 10

Bolivina subaeraniensis Cushman, 1922, U. S. Nat. Mus., Bull., Washington, D. C., U. S. A., nº 104, p. 46, pl. 7, fig. 6.

Bolivina subaeraniensis Cushman, Ellis and Messina, 1942-2009, nº 1.979-1.980.

Brizalina subaeraniensis (Cushman), Murray, 1971, p. 111, pl. 45, figs. 5-7; Colom, 1974, p. 106 and 121, fig. 17h-n; Martins and Gomes, 2004, p. 111-112, fig. 2.63; Duchemin *et al.*, 2007, p. 28, pl. I, fig. 18; Mojtahid *et al.*, 2009, pl. II, fig. 14.

***Brizalina translucens* (Phleger and Parker 1951)**

Bolivina translucens Phleger and Parker, 1951, Geol. Soc. Amer., Mem., New York, nº 46, pt. 2, p. 15, pl. 7, figs. 13-14.

Bolivina translucens Phleger and Parker, Ellis and Messina, 1942-2009, nº 39.782.

Brizalina translucens (Phleger and Parker), Martins and Gomes, 2004, p. 113-114, fig. 2.64.

Superfamily BOLIVINITACEA Cushman 1927

Family BOLIVINITIDAE Cushman 1927

Genus ABDITODENTRIX Patterson 1985

***Abditodentrix asketocomptella* Patterson 1985**

Abditodentrix asketocomptella Patterson, 1985, J. Foram. Res., vol. 15, nº 2, p. 138-140, pl. 1.

Abditodentrix asketocomptella Patterson, Ellis and Messina, 1942-2009, nº 73.544-73.547; Martins and Gomes, 2004, p. 115, fig. 2.65.

Superfamily CASSIDULINACEA d'Orbigny 1839

Family CASSIDULINIDAE d'Orbigny 1839

Subfamily CASSIDULININAE d'Orbigny 1839

Genus CASSIDULINA d'Orbigny 1826

***Cassidulina crassa* d'Orbigny 1839**

Cassidulina crassa d'Orbigny, 1839, Strasbourg, France, Levrault, tom. 5, pl. 5, p. 56, pl. 7, figs. 18-20.

Cassidulina crassa d'Orbigny, Jones, 1994, p. 60, pl. 54, fig. 4; Debenay *et al.*, 2001, p. 92-93, pl. IV, fig. 18; Martins and Gomes, 2004, p. 118-119, fig. 2.67; Abu-Zied *et al.*, 2008, p. 65, pl. II, figs. 3-4.

***Cassidulina laevigata* d'Orbigny 1826**

Plate II, fig. 12

Cassidulina laevigata d'Orbigny, 1826, Ann. Sci. Nat., ser. 1, vol. 7, p. 282, pl. 15, figs. 4-5.

Cassidulina carinata Silvestri, Levy *et al.*, 1995, p. 32-33, pl. 7, fig. 4; Mojtahid *et al.*, 2009, pl. I, fig. 3.

Cassidulina laevigata Boltovskoy *et al.*, 1980, p. 22, pl. 7, figs. 4-6; Murray, 2003, p. 21, figs. 6.8-6.10; Milker and Schmiedl, 2012, p. 84, fig. 20.6.

***Cassidulina minuta* Cushman 1933**

Plate II, fig. 13

Cassidulina minuta Cushman, 1933, Contr. Cushman Lab. Foram. Res., Sharon, Mass., U. S. A., vol. 9, pt. 4, nº 137, p. 92, pl. 10, fig. 3.

Cassidulina minuta Cushman, Boltovskoy *et al.*, 1980, p. 22-23, pl. 7, figs. 7-11; Martins and Gomes, 2004, p. 123, fig. 2.69; Mendes et al., 2004, p. 189, pl. 2, fig. 9.

Cassidulina obtusa Williamson, Jones, 1994, p. 60, pl. 54, fig. 5; Levy *et al*., 1995, p. 33, pl. 7, fig. 5; Murray, 2003, p. 21, figs. 6.11-6.12.

***Cassidulina teretis* Tappan 1951**

Cassidulina teretis Tappan, 1951, Cushman Found. Foram. Res., Contr., Washington, D. C., vol. 2, pt. 1, p. 7, fig. 30.

Cassidulina teretis Tappan, Jones, 1994, p. 59, pl. 54, fig. 1; Martins and Gomes, 2004, p. 124-125, fig. 2.70; Holbourn *et al.*, 2013, p. 138-139, figs. 1-5.

Genus CASSIDULINOIDES Cushman 1927

***Cassidulinoides bradyi* (Norman 1881)**

Cassidulina bradyi Norman, 1881, Quart. Jour. Micr. Sci., London, n. s., vol. 21, p. 59; fig. in Brady, 1884, Rept. Challenger Expedit., London, Zool., pt. 22, vol. 9, pl. 54, figs. 6-10.

Cassidulinoides bradyi (Norman), Jones, 1994, p. 60, pl. 54, figs. 6-9; Levy *et al.*, 1995, p. 33, pl. 7, fig. 6; Martins and Gomes, 2004, p. 126, fig. 2.71; Abu-Zied *et al.*, 2008, p. 65, pl. II, figs. 5-6.

Genus GLOBOCASSIDULINA Voloshinova 1960

***Globocassidulina subglobosa* (Brady 1881)**

Cassidulina subglobosa Brady, 1881, Quart. Journ. Micr. Sci., London, vol. 21, p. 60. Figure in Brady, 1884, Rept. Challenger Expedit., London, Zool., pt. 22, vol. 9, pl. 54, fig. 17.

Globocassidulina subglobosa (Brady), Jones, 1994, p. 60, pl. 54, fig. 17; Levy *et al.*, 1995, p. 33, pl. 7, fig. 7; Debenay and Redois, 1997, pl. 3, fig. 11; Murray, 2003, p. 24, fig. 8.7; Martins and Gomes, 2004, p. 128-130, fig. 2.73; Milker and Schmiedl, 2012, p. 85-86, figs. 20.13-20.14; Holbourn *et al.*, 2013, p. 264-265, figs. 1-2.

Superfamily TURRILINACEA Cushman 1927

Family STAINFORTHIIDAE Reiss 1963

Genus HOPKINSINA Howe and Wallace 1932

***Hopkinsina atlantica* (Cushman 1944)**

Hopkinsina pacifica Cushman var. *atlantica* Cushman, 1944, Cushman Lab. Foram. Res., Sharon, Mass., U. S. A., nº 12, p. 30, pl. 4, fig. 1.

Hopkinsina pacifica (Cushman), Debenay *et al.*, 2001, pl. IV, fig. 14; Diz and Francés, 2008, p. 185, pl. II, fig. 6; Mendes *et al.*, 2012, p. 38, fig. 3.5.

Genus STAINFORTHIA Hofker 1956

***Stainforthia feylingi* Knudssen and Seidenkrantz 1993**

Stainforthia feylingi Knudssen and Seidenkrantz, 1993, Contr. Cushman Found. Foram. Res., Special Pub., nº 32, p. 5-13. Figure in Blais-Stevens and Patterson, 1998, p. 217, pl. 2, fig. 1.

Stainforthia feylingi Knudssen and Seidenkrantz, Martins and Gomes, 2004, p. 133-134, fig. 2.75.

***Stainforthia fusiformis* (Williamson 1858)**

Plate II, fig. 14

Bulimina pupoides d'Orbigny var. *fusiformis* Williamson, 1858, Ray Soc., London, England, p. 63, pl. 5, figs. 129-130.

Fursenkoina fusiformis (Williamson), Murray, 1971, p. 185, pl. 77, figs. 1-5.

Stainforthia fusiformis (Williamson), Alve and Murray, 2001, p. 24, pl. 1, fig. 13; Debenay *et al.*, 2001, pl. IV, fig. 13; Gooday and Hughes, 2002, p. 106, pl. II, fig. n; Murray, 2003, p. 26, figs. 10.1-10.4; Martins and Gomes, 2004, p. 135-137, fig. 2.76; Diz and Francés, 2008, p. 185-186, pl. II, figs. 11-12; Mendes *et al.*, 2013, p. 108, pl. 1, fig. 13.

***Stainforthia* sp**

Superfamily BULIMINACEA Jones 1875

Family SIPHOGENERINOIDIDAE Saidova 1981

Subfamily TUBULOGENERININAE Saidova 1981

Genus RECTUVIGERINA Mathews 1945

***Rectuvigerina phlegeri* Le Calvez 1959**

Plate III, fig. 2

Rectuvigerina phlegeri Le Calvez, 1959, Rev. Travaux Inst. Pêches Marit., Nantes, France, vol. 23, nº 3, p. 363, pl. 1, fig. 11.

Rectuvigerina phlegeri Le Calvez, Diz *et al.*, 2004, p. 275, pl. 2, fig. 7; Martins and Gomes, 2004, p. 138-139, fig. 2.77; Abu-Zied *et al.*, 2008, p. 65, pl. II, fig. 15; Milker and Schmiedl 2012, p. 83, fig. 20.18; Mendes et al., 2013, p. 108, pl. 1, fig. 14.

Family BULIMINIDAE Jones 1875

Genus BULIMINA d'Orbigny 1826

***Bulimina acanthia* Costa 1856**

Bulimina acanthia Costa, 1856, Accad. Pontaniana Napoli, Atti, Napoli, Italia, vol. 7, fasc. 2, p. 335, pl. 13, figs. 35, 36 and 36a.

Bulimina acanthia Costa, Ellis and Messina, 1942-2009, nº. 2.137-2.138; Colom, 1974, p. 105 and 115, fig. 16o-u.

***Bulimina aculeata* d'Orbigny 1826**

Plate II, fig. 17

Bulimina aculeata d'Orbigny, 1826, Ann. Sci. Nat., sér. 1, tom. 7, p. 269, nº 7; fig. in Parker, Jones & Brady, 1871, Ann. Mag. Nat. Hist., London, ser. 4, vol. 8, pl. 11, fig. 128.

Bulimina aculeata d'Orbigny, Boltovskoy *et al.*, 1980, p. 19-20, pl. 5, figs. 1-3; Levy *et al.*, 1995, p. 35, pl. 7, fig. 9; Martins and Gomes, 2004, p. 140-141, fig. 2.78; Milker and Schmiedl 2012, p. 83, fig. 20.19; Holbourn *et al.*, 2013, p. 88-89, figs. 1-3.

***Bulimina alazanensis* Cushman 1927**

Bulimina alazanensis Cushman, 1927, Jour. Pal. Menasha, Wis., U. S. A., vol. 1, p. 161, pl. 25, fig. 4.

Bulimina cf. *B. alazanensis* Cushman, Murray. 1971, .

Bulimina alazanensis Cushman, Debenay and Redois, 1997, p. 30-31, pl. 23, figs. 22 and 29; Martins and Gomes, 2004, p. 142-143, fig. 2.79; Holbourn *et al.*, 2013, p. 90-91, figs. 1-2.

***Bulimina elongata* d'Orbigny 1846**

Plate II, fig. 16

Bulimina elongata d'Orbigny, 1846, Foram. foss. Vienne, Paris, p. 187, pl. 11, figs. 19-20.

Bulimina elongata d'Orbigny var. *lappa* Cushman & Parker, Colom, 1974, p. 105 and 116, fig. 16v-a'; Martins and Gomes, 2004, p. 144-145, fig. 2.80.

Bulimina elongata d'Orbigny Colom, 1974, p. 105 and 116, fig. 16n; Jones, 1994, p. 55, pl. 51, figs. 1-2; Levy *et al.*, 1995, p. 35, pl. 7, fig. 10; Debenay *et al.*, 2001, p. 92-93, pl. IV, fig. 9; Diz and Francés, 2008, p. 184, pl. I, fig. 13; Mendes *et al.*, 2012, p. 38, fig. 3.9; Milker and Schmiedl, 2012, p. 83, fig. 20.21; Holbourn *et al.*, 2013, p. 94-95, figs. 1-2.

***Bulimina elegans* d'Orbigny 1826**

Bulimina elegans d'Orbigny, 1826, Ann. Sci. Nat., Paris, France, sér. 1, tom. 7, p. 270; fig. in Parker, Jones & Brady, 1865, Ann. Mag. Nat. Hist., London, England, vol. 16, ser. 3, pl. 2, fig. 64.

Bulimina elegans d'Orbigny, Ellis and Messina, 1942-2009, nº 2.239-2.241; Debenay *et al.*, 2001, p. 92-93, pl. IV, fig. 10.

***Bulimina exilis* (Brady 1884)**

Bulimina elegans d'Orbigny var. *exilis* Brady, 1884, Rept. Challenger Exp., London, England, Zool., pt. 22, vol. 9, p. 399, pl. 50, figs. 5-6.

Bulimina exilis (Brady), Levy *et al.*, 1994, p. 35, pl. 7, fig. 11; Jannink *et al.*, 1998, pl. 1, fig. 3; Martind and Gomes, 2004, p. 147-148, fig. 2.82.

***Bulimina gibba* Fornasini 1902**

Bulimina gibba Fornasini, 1902, Mem. Real. Accad. Sci. Ist. Bologna, ser. 5, vol. 8, p. 378, figs. 32 and 34.

Bulimina gibba Fornasini, Boltovskoy *et al.*, 1980, p. 20, pl. 5, figs. 7-9; Jones, 1994, p. 54, pl. 50, figs. 1-2; Diz and Francés, 2008, p. 184, pl. I, fig. 14; Milker and Schmiedl 2012, p. 83, fig. 20.22; Holbourn *et al.,* 2013, p. 96-97, figs. 1-3.

***Bulimina marginata* d'Orbigny 1826**

Plate II, fig. 18

Bulimina marginata d'Orbigny, 1826, Ann. Sci. Nat., Paris, France, sér. 1, tom. 7, p. 269, pl. 12, figs. 10-12.

Bulimina marginata d'Orbigny, Colom, 1974, p. 105 and 117, figs. 16d'-h' and 16k'-o'; Levy *et al.,* 1995, p. 35, pl. 7, fig. 12; Murray, 2003, p. 19, figs. 8.4 and 8.5; Martins and Gomes, 2004, p. 148-150, fig. 2.83; Milker and Schmiedl, 2012, p. 88-89, fig. 20.23; Holbourn *et al.*, 2013, p. 108-109, figs. 1-2.

***Bulimina striata* d'Orbigny 1843**

Plate II, fig. 19

Bulimina striata d'Orbigny, 1843, Guérin-Méneville, Icon. Règne animal Cuvier, Paris, p. 9, pl. 2, fig. 16, 16ª.

Bulimina striata d'Orbigny, Ellis and Messina, 1952-2009, nº 24.405-24.406; Levy *et al.*, 1994, p. 35, pl. 8, figs. 1-2.

Bulimina costata d'Orbigny, Colom, 1974, p. 105 and 116, figs. 16i-j, 16p'-r'; Abu-Zied *et al.*, 2008, p. 65, pl. II, figs. 8-9; Mojtahid *et al.*, pl. I, fig. 12.

***Bulimina* cf. *pseudoaffinis* Kleinpell 1938**

Bulimina pseudoaffinis Kleinpell, 1938, Amer. Assoc. Petrol. Geol., p. 257, pl. 9, fig. 9.

Bulimina pseudoaffinis Kleinpell, Ellis and Messina, 1942-2009, nº 25.576; Boltovskoy *et al.*, 1980, p. 21, pl. 5, figs. 18-19.

***Bulimina* sp**

Genus GLOBOBULIMINA Cushman 1927

***Globobulimina ovata* (d'Orbigny 1846)**

Plate II, fig. 15

Bulimina ovata d'Orbigny, 1846, Foram. Foss. Vienne, Paris, p. 185, pl. 11, figs. 13-14.

Praeglobobulimina ovata (d'Orbigny), Jones, 1994, p. 54, pl. 50, fig. 13.

Globobulimina ovata (d'Orbigny), Levy *et al.*, 1995, p. 36, pl. 8, fig. 4.

Family BULIMINELLIDAE Hofker 1951

Genus BULIMINELLA Cushman 1911

***Buliminella tenuata* (Cushman 1927)**

Plate III, fig. 1

Buliminella subfusiformis Cushman var. *tenuata* Cushman, 1927, California Univ. Scripps. Inst. Oceanogr., Bull., Berkeley, Califor., U. S. A., Tech. Ser., vol. 1, p. 149, pl. 2, fig.9.

Buliminella tenuata (Cushman), Martins and Gomes, 2004, p. 156-157, fig. 2.88.

***Buliminella* sp**

Family UVIGERINIDAE Haeckel 1894

Subfamily UVIGERININAE Haeckel 1894

Genus UVIGERINA d'Orbigny 1826

***Uvigerina mediterranea* Hofker 1932**

Uvigerina mediterranea Hofker, 1932, Staz. Zool. Napoli, Pubbl., Naples, Italy, vol. 12, fasc. 1, p. 118-119, fig. 32.

Uvigerina mediterranea Hofker, Colom, 1974, p. 108 and 122, fig. 19h-n; Levy *et al.*, 1995, p. 37-38, pl. 8, fig. 8; De Stigter *et al.*, 1998, pl. 3, fig. 1; Abu-Zied *et al.*, 2008, p. 65, pl. II, figs. 17-18; Frezza and Carboni, 2009, pl. 2, fig. 14; Mojtahid *et al.*, 2009, pl. II, fig. 30; Milker and Schmiedl, 2012, p. 83, fig. 20.28; Holbourn *et al.*, 2013, p. 596-597, fig. 1.

***Uvigerina peregrina* Cushman 1923**

Plate III, fig. 3

Uvigerina peregrina Cushman, 1923, U. S. Nat. Mus., Bull. Washington, nº 104, p. 166, pl. 42, figs. 7-10.

Uvigerina peregrina Cushman, Murray, 1971, p. 121, pl. 50, figs. 1-7; Boltovskoy *et al.*, 1980, p. 53, pl. 34, figs. 15-16; Levy *et al.*, 1995, p. 38, pl. 8, fig. 11; Jannink *et al.*, 1998, pl. 1, fig. 6; Debenay *et al.*, 2001; pl. IV, fig. 17; Mendes *et al.*, 2004, p. 189, pl. 2, fig. 12; Abu-Zied *et al.*, 2008, p. 65, pl. II, figs. 19-20; Frezza and Carboni, 2009, pl. 2, fig. 15; Milker and Schmiedl 2012, p. 83, fig. 20.29.

***Uvigerina* sp**

Subfamily ANGULOGERININAE Galloway 1933

Genus TRIFARINA Cushman 1923

***Trifarina bradyana* (Cushman 1932)**

Plate III, fig. 4

Angulogerina carinata Cushman var. *bradyana* Cushman, 1932, Contr. Cushman Lab. Foram. Res., Sharon, Mass. U. S. A., vol. 8, pt. 3, nº 121, p. 45, pl. 6, figs. 9-10.

Trifarina carinata Cushman var. *bradyana* Cushman, Levy et al., 1995, p. 39, pl. 8, fig. 14.

Trifarina bradyana (Cushman), Debenay and Redois, 1997, pl. 3, fig. 35; Martins and Gomes, 2004, p. 169, fig. 2.97.

***Trifarina carinata* (Cushman 1927)**

Plate III, fig. 5

Angulogerina carinata Cushman, 1927, California Univ. Scripps Inst. Oceanogr., Bull., Berkeley, Calif., U. S. A., Tech. Ser., vol. 1, p. 159, pl. 4, fig. 3.

Trifarina carinata (Cushman), Martins and Gomes, 2004, p. 172, fig. 2.99; Holbourn *et al.*, 2013, p. 562-563, figs. 1-2.

Family REUSSELLIDAE Cushman 1933

Genus REUSSELLA Cushman 1933

***Reussella spinulosa* Reuss 1850**

Plate III, fig. 6

Verneuilina spinulosa Reuss, 1850, K. Akad. Wiss. Wien, Math.-Nat. Cl., Denkschr., Wien, Österreich, Bd. 1, p. 374, pl. 47, fig. 12.

Reussella spinulosa (Reuss), Jones, 1994, p. 51, pl. 47, figs. 1-3; Milker and Schmiedl, 2012, p. 92, figs. 21.6-21.7.

Superfamily FURSENKOINACEA Loeblich and Tappan 1961

Family FURSENKOINIDAE Loeblich and Tappan 1961

Genus FURSENKOINA Loeblich and Tappan 1961

***Fursenkoina loeblichi* (Feyling-Hanssen 1954)**

Virgulina loeblichi Feyling-Hanssen, 1954, Norsk Geol. Tidsskr., Bergen, vol. 33, nº 3-4, p. 191, pl. 1, figs. 14-18, p. 192, text-fig. 3.

Virgulina loeblichi Feyling-Hanssen, Ellis and Messina, 1942-2009, nº 43.961.
Fursenkoina loeblichi (Feyling-Hanssen), Martins and Gomes, p. 173-174, fig. 2.100.

***Fursenkoina complanata* (Egger 1893)**

Plate III, fig. 7

Virgulina schreibersiana Czjzek var. *complanata* Egger, 1895, K. bayer. Akad. Wiss., math-physik. Cl., Abh., München, Deutschland, bd. 18, abth. 2, (1893), p. 292, pl. 8, figs. 91-92.
Fursenkoina schreibersiana (Czjzek), Murray, 1971, p. 185, pl. 77, figs. 7-10.
Stainforthia complanata (Egger), Martins and Gomes, 2004, p. 131-132, fig. 2.74; Diz and Francés, 2008, p. 185, pl. II, fig. 10; Milker and Schmiedl 2012, p. 83, fig. 20.16.
Fursenkoina complanata (Egger), Jones, 1994, p. 56, pl. 52, figs. 1-3; Mojtahid *et al.*, 2009, pl. I, fig. 11; Holbourn *et al.*, 2013, p. 258-259, figs. 1-2.

Superfamily DISCORBACEA Ehrenberg 1838
Family BAGGINIDAE Cushman 1927
Subfamily BAGGININAE Cushman 1927

Genus VALVULINERIA Cushman 1926

***Valvulineria bradyana* (Fornasini 1900)**

Plate III, fig. 8

Discorbina bradyana Fornasini, 1900, R. Accad. Sci. Ist. Bologna, Mem., Bologna, Italy, ser. 5, tom. 8 (1899-1900), p. 393, tf. 43.
Valvulineria bradyana (Fornasini), Colom, 1974, p. 83 and 137-138, fig. 10m-s; Martins and Gomes, 2004, p. 177-178, fig. 2.102; Frezza and Carboni, 2009, pl. 1, figs. 1-2; Mojtahid *et al.*, 2009, pl. I, fig. 5.

Family MISSISSIPPINIDAE Saidova 1981
Subfamily MISSISSIPPININAE Saidova 1981

Genus MISSISSIPINA Howe 1930

***Mississipina concentrica* (Parker and Jones 1864)**

Pulvinulina concentrica Parker and Jones, 1864, Linn. Soc. London, Trans., London, vol. 24, pt. 3, p. 470, pl. 48, fig. 14.

Pulvinulina concentrica Parker and Jones, Ellis and Messina, 1942-2009, nº 77.517.

Stomatorbina concentrica (Parker and Jones), Colom, 1974, p. 173 and 178, fig. 44q-u; Milker and Schmiedl, 2012, p. 95, figs. 21.24-21.25.

Mississipina concentrica (Parker and Jones), Jones, 1994, p. 104, pl. 105, fig. 1; Levy *et al.*, 1995, p. 40, pl. 9, fig. 6; Mendes *et al.*, 2004, p. 189, pl. 1, fig. 4.

Family DISCORBIDAE Ehrenberg 1838

Genus DISCORBIS Lamarck 1804

***Discorbis williamsoni* Chapman and Parr 1932**

Plate III, fig. 10

Discorbis williamsoni Chapman and Parr, 1932, Roy. Soc. Victoria, Proc. Melbourne, Australia, vol. 44, p. 226.

Discorbis nitida (Williamson), Colom, 1974, p. 125 and 129, fig. 21b-c.

Neoconorbina nitida (Williamson), Debenay *et al.*, 2001, p. 94-95, pl. V, figs. 9 and 12.

Discorbis williamsoni Chapman and Parr, Boltovskoy *et al.*, 1980, p. 28, pl. 12, figs. 5-12; Martins and Gomes, 2004, p. 183-184, fig. 2.107; Milker and Schmiedl, 2012, p.95 and 97, figs. 22.1-22.2.

Genus STREBLOIDES Bermúdez and Seiglie 1963

***Strebloides advenus* (Cushman 1922)**

Discorbis advena Cushman, 1922, Carnegie Inst. Washington, Publ. nº 311 (Dept. Marine Biol., Papers, vol. 17), Washington, D.C., U.S.A., p. 40.

Strebloides advenus (Cushman), Loeblich and Tappan, 1988, p. 559, pl. 608, figs. 1-5; Jones, 1994, p. 93, pl. 87, fig. 1a-c.

Family ROSALINIDAE Reiss 1963

Genus GAVELINOPSIS Hofker 1951

***Gavelinopsis praegeri* (Heron-Allen and Earland 1913)**

Plate III, fig. 9

Discorbina praegeri Heron-Allen and Earland, 1913, Roy. Irish Acad., Proc., Dublin, Ireland, vol. 31, sect. 3 (1911-15), p. 122, pl. 10, figs. 8-10.

Gavelinopsis praegeri (Heron-Allen and Earland), Murray, 1971, p. 133, pl. 55, figs. 1-5; Levy *et al.*, 1995, p. 41, figs. 7-8; Diz *et al.*, 2004, p. 273, pl. 2, fig. 9; Martins and Gomes, 2004, p. 185-186, fig. 2.108; Milker and Schmiedl, 2012, p. 97, figs. 22.3-22.4.

Genus NEOCONORBINA Hofker 1951

***Neoconorbina terquemi* (Rzehak 1888)**

Discorbina terquemi Rzehak, 1888, Verhandlugen der Geol. Bund., p. 226-229.

Neoconorbina terquemi (Rzehak), Jones, 1994, p. 94, pl. 88, figs. 5-8; Debenay *et al.*, 2001, pl. V, figs. 7-8; Abu-Zied *et al.*, 2008, p. 65, pl. II, figs. 26-27; Milker and Schmiedl, 2012, p. 97, figs. 22.5-22.6; Holbourn *et al.*, 2013, p. 360-361, figs. 1-3.

Genus ROSALINA d'Orbigny 1826

***Rosalina bradyi* (Cushman 1915)**

Discorbina globularis d'Orbigny var. *bradyi* Cushman, 1915,

Rosalina bradyi (Cushman), Jones, 1994, p. 93, pl. 86, fig. 8; Debenay *et al.*, 2001, pl. V, figs. 1-2; Abu-Zied *et al.*, 2008, p. 65, pl. II, figs. 28-29; Milker and Schmiedl, 2012, p. 98, figs. 22.11-22.14.

***Rosalina globularis* var. *anglica* (Cushman 1931)**

Discorbis globularis (d'Orbigny) var. *anglica* Cushman, 1931, W. S. Nat. Mus., Bull., Washington, D. C., U. S. A., nº 104, p. 23, pl. 4, fig. 10.

Discorbis globularis (d'Orbigny) var. *anglica* Cushman, Ellis and Messina, 1942-2009, nº 5.863.

Discorbinella globularis var. *anglica* (Cushman), Colom, 1974, p. 126-128, fig. 20m-r.

Rosalina anglica (Cushman), Debenay *et al.*, 2001, pl. V, figs. 10 and 14.

Rosalina globularis var. *anglica* (Cushman), Martins and Gomes, 2004, p. 191, fig. 2.112.

***Rosalina rugosa* d'Orbigny 1839**

Plate III, fig. 11

Rosalina rugosa d'Orbigny, 1839, Strasbourg, France, Levrault, tom. 5, pt. 5, p. 42, pl. 2, figs. 12-14.

Rosalina rugosa d'Orbigny, Ellis and Messina, 1942-2009, nº 19.243

Valvulineria rugosa (d'Orbigny), Jones, 1994, p. 93, pl. 87, fig. 3.

Rosalina rugosa d'Orbigny, Levy *et al.*, 1995, p. 41, pl. 9, fig. 10.

***Rosalina vilardeboana* d'Orbigny 1839**

Rosalina vilardeboana d'Orbigny, 1839, Strasbourg, France, Levrault, tom. 5, pt. 5, p. 44, pl. 6, figs. 13-15.

Rosalina vilardeboana d'Orbigny, Ellis and Messina, 1942-2009, nº 19.273.

Rosalina vilardeboana d'Orbigny, Jones, 1994, p. 93, pl. 86, fig. 9; Debenay *et al.*, 2001, pl. V, figs. 6 and 11.

Superfamily GLABRATELLACEA Loeblich and Tappan 1964

Family GLABRATELLIDAE Loeblich and Tappan 1964

Genus GLABRATELLA Doreen 1948

***Glabratella millettii* (Wright 1911)**

Plate IV, fig. 1

Discorbina millettii Wright, 1911, Proc. Belfast Nat. Field Club, Belfast, Ireland, ser. 2, vol. 6, appendix nº 2, p. 13, pl. 2, figs. 14-17.

Neoconorbina millettii (Wright), Debenay *et al.*, 2001, pl. V, fig. 5.

Discorbinoides millettii (Wright), Murray, 2003, p. 21, figs. 7.3-7.4.

Glabratella millettii (Wright), Murray, 1971, p. 139, pl. 58, figs. 1-4; Martins and Gomes, 2004, p. 193, fig. 2.114.

Superfamily DISCORBILLENACEA Sigal 1952

Family PARRELLOIDIDAE Hofker 1956

Genus CIBICIDOIDES Thalmann 1939

***Cibicidoides bradyi* (Trauth 1918)**

Truncatulina bradyi Trauth, 1918, K. Akad. Wiss. Wien, Math.-Naturw. Kl., Denkschr., Wien, sterreich, Bd., 95, p.235.

Truncatulina bradyi Trauth, Ellis and Messina, 1942-2009, nº 22.743.

Gyroidina bradyi (Trauth), Jones, 1994, p. 99, pl. 95, fig. 5.

Cibicidoides bradyi (Trauth), Martins and Gomes, 2004, p. 194-195, fig. 2.115; Holbourn *et al.*, 2013, p. 162-163, figs. 1-6.

***Cibicidoides pachyderma* (Rzehak 1886)**

Truncatulina pachyderma Rzehak, 1886, Naturf. Ver. Brünn, Verh., Brünn, Bd. 24 (1885), p. 87, pl. 1, fig. 5a-c.

Cibicidoides pachyderma (Rzehak), Jones, 1994, p. 98, pl. 94, fig. 9; Martins and Gomes, 2004, p. 196, fig. 2.116; Holbourn *et al.*, 2013, p. 198-199, figs. 1-3.

Cibicides pachydermus (Rzehak), Abu-Zied *et al.*, 2008, pl. III, figs. 3-5.

Family PSEUDOPARRELLIDAE Voloshinova 1952

Subfamily PSEUDOPARRELLINAE Voloshinova 1952

Genus EPISTOMINELLA Husezima and Maruhasi 1944

***Epistominella exigua* (Brady 1884)**

Plate IV, fig. 2

Pulvinulina exigua Brady, 1884, Rept. Challenger Exped., London, England, Zool., pt. 22, vol. 9, p. 696, pl. 103, figs. 13-14.

Epistominella exigua (Brady), Boltovskoy *et al.*, 1980, p. 31, pl. 14, figs. 14-17; Jannink *et al.*, 1998, pl. 1, fig. 4; Hayward *et al.*, 2002, p. 169, pl. I, figs. 28-30; Martins and Gomes, 2004, p. 197-199, fig. 2.117; Murray and Pudsey, 2004, p. 80, pl. 2, figs. 9 and 11; Duchemin *et al.*, 2007, p. 28, pl. 3, figs. 1-2; Holbourn *et al.*, 2013, p. 240-241, figs. 1-6.

***Epistominella vitrea* Parker 1953**

Epistominella vitrea Parker, 1953, Cushman Found. Foram., Spec. Pub., Washington, D. C., nº 2, p. 9, pl. 4, figs. 34-36.

Epistominella vitrea Parker, Murray, 1971, p. 131, pl. 54, figs. 1-6; Murray, 2003, p. 21, fig. 7.11-7.13; Martins and Gomes, 2004, p. 199-200, fig. 2.118; Duchemin *et al.*, 2007, p. 28, pl. 2, figs. 5-8; Mendes *et al.*, 2012, p. 38, fig. 4.1.

Family DISCORBINELLIDAE Sigal 1952

Subfamily DISCORBINELLINAE Sigal 1952

Genus DISCORBINELLA Cushman and Martin 1935

***Discorbinella berthelotti* (d'Orbigny 1839)**

Rosalina berthelotti d'Orbigny, 1839, Foram. Canaries, Béthune, Paris, France, tom. 2, pt. 2, Zool., p. 135, pl. 1, figs. 29-30.

Discorbis berthelotti (d'Orbigny), Boltovskoy *et al.*, 1980, p. 27, pl. 11, figs. 5-7.

Discorbinella berthelotti (d'Orbigny), Colom, 1974, p. 126 and 129, fig. 21l-n and 21t-w; Levy *et al.*, 1995, p. 42-43, pl. 10, figs. 1-2; Martins and Gomes, 2004, p. 201-202, fig. 2.119; Milker and Schmiedl, 2012, p. 104, fig. 23.29-23.30; Holbourn *et al.*, 2013, p. 230-231, figs. 1-3.

Superfamily PLANORBULINACEA Schwager 1877

Family PLANULINIDAE Bermúdez 1952

Genus HYALINEA Hofker 1951

***Hyalinea balthica* (Schröter 1783)**

Plate IV, fig. 3

Nautilus balthicus Schröter, 1783, Einleitung in die Conchylienkenntniss nach Linné, vol. 1, p. 20, pl. 1, fig. 2.

Hyalinea balthica (Schröter), Murray, 1971, p. 173, pl. 72, figs. 5-8; Colom, 1974, ; Levy *et al.*, 1995, p. 43-44, pl. 10, fig. 3; Martins and Gomes, 2004, p. 204-206, fig. 2.122; Abu-Zied *et al.*, 2008, p. 65, pl. II, fig. 30; Mojtahid *et al.*, 2009, pl. I, fig. 7; Milker and Schmiedl, 2012, p. 104 and 106, figs. 24.1-24.2; Holbourn *et al.*, 2013, p. 308-309, figs. 1-2.

Family CIBICIDIDAE Cushman 1927

Subfamily CIBICIDINAE Cushman 1927

Genus CIBICIDES de Montfort 1808

***Cibicides* cf. *ungerianus* (d'Orbigny 1846)**

Rotalina ungeriana d'Orbigny, 1846, Gide et Comp., Paris, France, p. 157, pl. 8, figs. 16-18.

Rotalina ungeriana d'Orbigny, Ellis and Messina, 1942-2009, nº 77.603-77.604.

Cibicides ungerianus (d'Orbigny), Martins and Gomes, 2004, p. 207-208, fig. 2.123.

Genus LOBATULA Fleming 1828

***Lobatula lobatula* (Walker and Jacob 1798)**

Plate IV, fig. 4

Nautilus lobatulus Walker and Jacob, 1798, Dillon and Keating, London, England, p. 642, pl. 14, fig. 36.

Cibicides lobatulus (Walker and Jacob), Murray, 1971, p. 175, pl. 73, figs. 1-7; Colom, 1974, p. 147-149 and 152-155, figs. 29a-k, 30, 31a-f and 32a-r; Murray, 2003, p. 21, fig.6.13-6.15; Holbourn et al., 2013, p. 152-153, figs. 1-3.

Lobatula lobatula (Walker and Jacob), Loeblich and Tappan, 1988, p. 583, pl. 637, figs. 10-13; Martins and Gomes, 2004, p. 211-213, fig. 2.126; Milker and Schmiedl, 2012, p. 107-108, figs. 24.17-24.20.

Family PLANORBULINIDAE Schwager 1877

Subfamily PLANORBULININAE Schwager 1877

Genus PLANORBULINA d'Orbigny 1826

***Planorbulina mediterranensis* d'Orbigny 1826**

Plate IV, fig. 5

Planorbulina mediterranensis d'Orbigny, 1826, Ann. Sci. Nat., Paris, France, vol. 7, p. 280, pl. 14, figs. 4-6.

Planorbulina mediterranensis d'Orbigny, Murray, 1971, p. 179, pl. 75, figs. 1-6; Colom, 1974, p. 158-159 and 169-170, figs. 39a-h and 40a-m; Levy *et al.*, 1995, p. 44-45, pl. 10, fig. 6; Martins and Gomes, 2004, p. 215-216, fig. 2.127; Mendes *et al.*, 2004, p. 189, pl. 1, fig. 5; Milker and Schmiedl, 2012, p. 108, figs. 24.21-24.24.

Superfamily ASTERIGERINACEA d'Orbigny 1839

Family ASTERIGERINATIDAE Reiss 1963

Genus ASTERIGERINATA Bermúdez 1949

***Asterigerinata mamilla* (Williamson 1858)**

Plate IV, fig. 6

Rotalina mamilla Williamson, 1858, Ray Soc., London, England, p. 54, pl. 4, figs. 109-111.

Discorbis mamilla (Williamson), Colom, 1974, p. 124 and 129, fig. 21x-y.

Asterigerinata mamilla (Williamson), Murray, 1971, p. 141, pl. 59, figs. 1-6; Levy *et al.*, 1995, p. 46, pl. 10, fig. 10; Martins and Gomes, 2004, p. 218-219, fig. 2.129.

Genus EOEPONIDELLA Wickenden 1949

***Eoeponidella pulchella* (Parker 1952)**

Pninaella pulchella Parker, 1952, Harvard Coll., Mus. Comp. Zoöl., Bull., Cambridge, Mass., vol. 106, nº 9, p. 420, pl. 6, figs. 18-20.

Eoeponidella pulchella (Parker), Loeblich and Tappan, 1988, p. 607, pl. 675, figs. 8-11; Diz et al., 2004, p. 273, pl. 2, fig. 14; Martins and Gomes, 2004, p. 219-220, fig. 2.130.

Family NONIONIDAE Schultze 1854

Subfamily NONIONINAE Schultze 1854

Genus HAYNESINA Banner and Culver 1978

***Haynesina depressula* (Walker and Jacob 1798)**

Nautilus depressulus Walker and Jacob, 1798, in Kanmacher, F., *Adams' essays on the microscope*, London, England, Dillon and Keating, Ed. 2, p. 641, pl. 14, fig. 33.

Haynesina depressula (Walker and Jacob), Debenay *et al.*, 2001, pl. VI, fig. 13; Frezza and Carboni, 2009, pl. 2, fig. 6; Milker and Schmiedl, 2012, p. 112, figs. 25.17-25.18.

***Haynesina germanica* (Ehrenberg 1840)**

Plate V, fig. 1

Nonionina germanica Ehrenberg, 1840, K. Preuss. Akad. Wiss. Berlin, Ber., Berlin, Deutschland, p. 23. Figure in Ehrenberg C. G., 1841, K. Akad. Wiss. Berlin, Physik-Math. Kl., Abh., Berlin, Deutschland, Jahrg. Pl. 2, fig. 1.

Haynesina germanica (Ehrenberg), Jones, 1994, p. 107, pl. 109, figs. 6-7?; Alve and Murray, 1999, p. 191, pl. I, figs. 1-2; Debenay *et al.*, 2001, pl. VI, fig. 11; Martins and Gomes, 2004, p. 221-222, fig. 2.131; Diz and Francés, 2008, p. 185, pl. II, fig. 5.

***Haynesina* sp**

Genus NONION de Montfort 1808

***Nonion fabum* (Fichtel and Moll, 1798)**

Plate V, fig. 2

Nautilus faba Fichtel and Moll, 1798, Vienne: Anton Pichler, p. 103, pl. 19, figs. a-c.

Nonion fabum (Fichtel and Moll), Jones, 1994, p. 108, pl. 109, figs. 12-13; Debenay and Redois, 1997, p. 36-37, pl. 4, figs. 3-6; Martins and Gomes, 2004, p. 223-224, fig. 2.132; Mendes *et al.*, 2004, p. 189, pl. I, fig. 10; Duchemin *et al.*, 2005, p. 218, pl. 2, fig. 15; Milker and Schmiedl 2012, p. 109, fig. 25.22, 25.23 and 25.24.

Genus NONIONELLA Cushman 1926

***Nonionella iridea* Heron-Allen and Earland 1932**

Nonionella iridea Heron-Allen and Earland, 1932, Cambridge, England, Univ. Press, vol. 4, p. 438, figs. 14-16.

Nonionella iridea Heron-Allen and Earland, Gooday and Hughes, 2002, p. 105, pl. I, figs. c-d; Murray, 2003, p. 24, figs. 9.2-9.3; Martins and Gomes, 2004, p. 227-228, fig. 2.135; Mendes *et al.*, 2004, p. 189, pl. 2, fig. 6; Duchemin *et al.*, 2005, p. 218, pl. 2, figs. 18-19.

***Nonionella stella* (Cushman and Moyer 1930)**

Plate V, fig. 3

Nonionella miocenica Cushman var. *stella* Cushman and Moyer, 1930, Contr. Cushman Lab. Foram. Res., Sharon, Mass., U. S. A., vol. 6, pt. 3, nº 93, p. 56, pl. 7, fig. 17.

Nonionella stella (Cushman and Moyer), Diz *et al.*, 2004, p. 273, pl. 2, fig. 15; Martins and Gomes, 2004, p. 229-230, fig. 2.136; Diz and Francés, 2008, p. 185, pl. II, fig. 8; Mendes *et al.*, 2013, p. 108, pl. 2, fig. 7.

***Nonionella turgida* (Williamson 1858)**

Plate V, fig. 4

Rotalina turgida Williamson, 1858, Ray Soc., London, England, p. 50, pl. 4, figs. 95-97.

Nonionella turgida (Williamson), Levy *et al.*, 1995, p. 46-47, pl. 10, fig. 11; Debenay *et al.*, 2001, pl. VI, fig. 14; Murray, 2003, p. 24, figs. 9.4-9.5; Martins and Gomes, 2004, p. 231-232, fig. 2.137; Duchemin *et al.*, 2005, p. 218, pl. 2, fig. 20; Abu-Zied *et al.*, 2008, p. 65, pl. III, figs. 12-13; Frezza and Carboni, 2009, pl. 2, figs. 7-8; Mojtahid *et al.*, 2009, pl. I, fig. 6; Milker and Schmiedl, 2012, p. 113, figs. 26.1-26.6; Holbourn *et al.*, 2013, p. 372-373, figs. 1-2.

***Nonionella* sp**

Subfamily ASTRONONIONINAE Saidova 1981

Genus ASTRONONION Cushman and Edwards 1937

***Astrononion stelligerum* (d'Orbigny 1839)**

Nonionina stelligera d'Orbigny, 1839, Foram. Canaries, Paris, p. 128, pl. 3, figs. 1-2.

Nonionina stelligera d'Orbigny, Ellis and Messina, 1942-2009, nº 79.975-79.977.

Astrononion stelligerum (d'Orbigny), Jones, 1994, ; Levy *et al.*, 1995, p. 47, pl. 11, fig. 2; Milker and Schmiedl, 2012, p. 115, figs. 26.7-26.8.

Subfamily PULLENIINAE Schwager 1877

Genus MELONIS de Monfort 1808

***Melonis affinis* (Reuss 1851)**

Nonionina affinis Reuss, 1851, Deutsch. Geol. Ges., Zeitschr., Berlin, Deutschland, Bd. 3, p. 72, pl. 5, fig. 32.

Nonionina affinis Reuss, Ellis and Messina, 1942-2009, nº 14.069.

Melonis affine (Reuss), Boltovskoy *et al.*, 1980, p. 38, pl. 21, figs. 5-7.

Melonis affinis (Reuss), Jones, 1994, p. 107-108, pl. 109, figs. 8-9; Abu-Zied *et al.*, 2008, p. 65, pl. III, figs. 14-15; Milker and Schmiedl, 2012, p. 115, figs. 26.9-26.10.

Superfamily CHILLOSTOMELLACEA Brady 1881

Family HETEROLEPIDAE Gonzáles-Donoso 1969

Genus HETEROLEPA Franzenau 1884

***Heterolepa pseudoungerianus* (Cushman 1922)**

Truncatulina pseudoungeriana Cushman, 1922, U. S. Geol. Surv., prof. Pap., Washington, D. C., U. S. A., nº 129-E, p. 97, pl. 20, fig. 9.

Cibicides pseudoungerianus (Cushman), Murray, 1971, p. 177, pl. 74, figs. 1-6.

Heterolepa pseudoungeriana (Cushman), Levy *et al.*, 1995, p. 49, pl. 11, figs. 5-6.

Heterolepa pseudoungerianus (Cushman), Martins and Gomes, 2004, p. 244-245, fig. 2.145.

Family GAVELINELLIDAE Hofker 1956

Subfamily GAVELINELLINAE Hofker 1956

Genus GYROIDINA d'Orbigny 1826

***Gyroidina umbonata* (Silvestri 1898)**

Plate V, fig. 5

Rotalia soldanii d'Orbigny var. *umbonata* Silvestri, 1898, Accad. Pont. Nouvi Lincei, Mem. Roma, Italia, vol. 15, p. 329, pl. 6, fig. 14a-c.

Gyroidina niponica Ishizaki, 1944, Nat. Hist. Soc. Taiwan, Trans., Taihoku, Taiwan (Formosa), vol. 34, nº 244, p. 102, pl. 3, fig. 3a-c (in Ellis and Messina, 1942-2009, nº 38.475).

Gyroidina umbonata (Silvestri), Levy *et al.*, 1995, p. 50, pl. 11, fig. 10; Debenay and Redois, 1997, p. 32, pl. 4, figs. 10-11; Martins and Gomes, 2004, p. 247-248, fig. 2.147; Duchemin *et al.*, 2007, p. 28, pl. 2, figs. 2-4; Mojtahid *et al.*, 2009, pl. I, fig. 8.

Genus HANSENISCA n. gen.

***Hansenisca soldanii* (d'Orbigny 1826)**

Gyroidina neosoldanii Brotzen, Murray, 1971, p. 197, pl. 83, figs. 1-5.

Gyroidinoides neosoldanii (Brotzen), Levy *et al.*, 1995, p. 50, pl. 11, fig. 8.

Gyroidinoides soldanii (d'Orbigny), Jones, 1994, p. 106, pl. 107, figs. 6-7; Holbourn *et al.*, 2013, p. 278-279, figs. 1-3.

Gyroidina soldanii (d'Orbigny), Colom, 1974, p. 163-164, fig. 42m-n.

Hansenisca soldanii (d'Orbigny), Loeblich and Tappan, 1988, p. 639, pl. 719, figs. 5-9; Martins and Gomes, 2004, p. 248-249, fig. 2.148.

Genus HANZAWAIA Asano 1944

***Hanzawaia nitidula* (Bandy 1953)**

Cibicidina basiloba (Cushman) var. *nitidula* Bandy, 1953, Jour. Pal. Tulsa, Okla., vol. 27, nº 2, p. 178, pl. 22, fig. 3.

Cibicidina basiloba (Cushman) var. *nitidula* Bandy, Ellis and Messina, 1942-2009, nº 41.876.

Hanzawaia nitidula (Bandy), Martins and Gomes, 2004, p. 250-251, fig. 2.149.

Family TRICHOHYALIDAE Saidova 1981

Genus BUCCELLA Andersen 1952

***Buccella frigida* (Cushman)**

Pulvinulina frigida Cushman, 1922, Contr. Canadian Biol. Fish., 1921 (1922), nº 9, p. 12 [144]. Lectotype, Andersen, 1952, J. Washington Acad. Sci., vol. 42, p. 147, text-fig. 6.

Buccella frigida (Cushman) emend. Andersen, Ellis and Messina, 1942-2009, nº 41.821-41.822.

Buccella peruviana f. *frigida* (Andersen), Boltovskoy *et al.*, 1980, p. 19, pl. 4, figs. 9, 14-15 and 20-22.

Buccella frigida (Cushman), Murray, 1971, p. 129, pl. 53, figs. 1-5; Jones, 1994, p. 105, pl. 105, figs. 8-9.

Superfamily ROTALIACEA Ehrenberg 1839

Family ROTALIIDAE Ehrenberg 1839

Subfamily AMMONIINAE Saidova 1981

Genus AMMONIA Brünnich 1772

***Ammonia beccarii* (Linné 1758)**

Plate V, fig. 6

Nautilus beccarii Linné, 1758, impensis L. Salvii, Holmiae, Suecia, t. 1, p. 710, pl. 1, fig. 1a-c.

Ammonia beccarii (Linné), Murray, 1971, p. 151, pl. 62, figs. 1-7; Levy *et al.*, 1995, p. 51, pl. 12, fig. 1; Martins and Gomes, 2004, p. 253, fig. 2.150.

Family ELPHIDIIDAE Galloway 1933

Subfamily ELPHIDIINAE Galloway 1933

Genus CRIBRONONION Thalmann 1947

***Cribrononion gerthi* (Van Voorthuysen 1957)**

Plate V, fig. 7

Elphidium gerthi Van Voorthuysen, 1957, Geol. Stichting Med., Haarlem, Netherlands, vol. 11, p. 32, pl. 23, fig. 12a-b.

Elphidium gerthi Van Voorthuysen, Murray, 1971, p. 161, pl. 67, figs. 1-7; Murray, 2003, p. 21, fig. 7.8; Mendes *et al.*, 2012, p. 38, fig. 4.8.

Cribroelphidium gerthi (Van Voorthuysen), Diz and Francés, 2008, p. 185, pl. II, fig. 1.

Cribrononion gerthi (Van Voorthuysen), Levy *et al*., 1995, p. 51, pl. 12, fig. 2; Debenay *et al.*, 2001, p. 96-97, pl. VI, fig. 15; Martins and Gomes, 2004, p. 257-258, fig. 2.152;

Genus ELPHIDIUM de Monfort 1808

***Elphidium advenum* (Cushman 1922)**

Polystomella advena Cushman, 1922, Carnegie Inst. Washington, Publ. nº 311 (Dept. Marine Biol., Papers, vol. 17), Washington, D. C., U. S. A., p. 56, pl. 9, figs. 11-12.

Elphidium advenum (Cushman), Jones, 1994, p. 108, pl. 110, fig. 1; Mojtahid *et al.*, 2009, pl. II, fig. 19; Milker and Schmiedl, 2012, p. 119, figs. 27.7-27.8.

***Elphidium complanatum* (d'Orbigny 1839)**

Polystomella complanata d'Orbigny, 1839, Béthune, Paris, France, tome 2, pt. 2, Zool., p. 129, pl. 2, figs. 35-36.

Elphidium complanatum (d'Orbigny), Colom, 1974, p. 143, figs. 26e-j and 26m-n; Martins and Gomes, 2004, p. 259-260, fig. 2.153; Milker and Schmiedl, 2012, p. 120, figs. 27.9-27.10.

***Elphidium crispum* (Linné 1758)**

Nautilus crispus Linné, 1758, Holmiae, Suecia, imprensis L. Salvii, tomus 1, p. 709, pl. 1.

Nautilus crispus (Linné), Murray, 1971, p. 155, pl. 64, figs. 1-6; Colom, 1974, p. 135 and 143, fig. 27; Jones, 1994, p. 109, pl. 110, figs. 6-7; Levy *et al.*, 1995, p. 51, pl. 12, fig. 5; Martins and Gomes, 2004, p. 261-262, fig. 2.154; Milker and Schmiedl, 2012, p. 120, figs. 27.13-27.14; Holbourn *et al.*, 2013, p. 236-237, figs. 1-3.

***Elphidium cuvillieri* Levy 1966**

Plate V, fig. 8

Elphidium cuvillieri Levy, 1966, Vie et Milieu, Paris, tome 17, fasc. 1a, p. 5-6, pl. 1, fig. 6, pl. 2.

Cribroelphidium cuvillieri (Levy), Debenay *et al.*, 2001, pl. VI, fig. 18.

Elphidium cuvillieri Levy, Mendes *et al.*, 2012, p. 38, fig. 4.6.

***Elphidium discoidale* (d'Orbigny 1839)**

Polystomella discoidalis, d'Orbigny, 1839, A. Bertrabd, Paris, France, p. 56 (plates published separately), vol. 8, pl. 6, figs. 23-24.

Elphidium discoidale (d'Orbigny), Boltovskoy *et al.*, 1980, p. 29, pl. 13, figs. 5-7; Martins and Gomes, 2004, p. 262-263, fig. 2.155.

***Elphidium excavatum* (Terquem 1876)**

Plate V, fig. 9

Polystomella excavata Terquem, 1876, Soc. Dunkerquoise, Mém., vol. 19, p. 429, pl. 2, fig. 2.

Cribroelphidium excavatum (Terquem), Debenay *et al.*, 2001, pl. VI, fig. 5.

Elphidium excavatum (Terquem), Murray, 1971, p. 159, pl. 66, figs. 1-7; Boltovskoy *et al.*, 1980, p. 29, pl. 13, figs. 8-11; Alve and Murray, 1999, p. 191, pl. I, figs. 8-10; Murray, 2003, p. 21, figs. 7.6-7.7; Mendes *et al.*, 2012, p. 38, fig. 4.7.

***Elphidium macellum* (Fichtel and Moll 1798)**

Plate V, fig. 10

Nautilus macellus Fichtel and Moll, 1798, *Testac. Microsc.*, p. 66, var. α, pl. 10, figs. e-g, var. β, pl. 10, figs. h-k.

Elphidium macellum (Fichtel and Moll), Boltovskoy *et al.*, 1980, p. 30, pl. 14, figs. 1-6; Jones, 1994, p. 109, pl. 110, figs. 8 and 11; Mojtahid *et al.*, 2009, pl. II, fig. 18; Milker and Schmiedl, 2012, p. 122, figs. 27.21-27.22; Holbourn *et al.*, 2013, p. 238-239, figs. 1-2.

***Elphidium magellanicum* Heron-Allen and Earland 1932**

Elphidium magellanicum Heron-Allen and Earland, 1932, *'Discovery' Rep.*, vol. 4, p. 440, pl. 16, figs. 26-28.

Cribroelphidium magellanicum (Heron-Allen and Earland), Debenay *et al.*, 2001, pl. VI, fig. 7.

Elphidium magellanicum Heron-Allen and Earland, Murray, 1971, p. 163, pl. 68, figs. 1-7; Boltovskoy *et al.*, 1980, p. 30, pl. 14, figs. 7-10; Murray, 2003, p. 21, figs. 7.9-7.10.

VIII.2. Plates

PLATE I

1. *Bigenerina nodosaria* d'Orbigny, scale bar 100 μm.

2. *Textularia conica* d'Orbigny, scale bar 50 μm.

3. *Textularia deltoidea* Reuss, scale bar 50 μm.

4. *Adelosina laevigata* d'Orbigny, scale bar 100 μm.

5. *Quinqueloculina lata* Terquem, scale bar 10 μm.

6. *Quinqueloculina stalkeri* Loeblichi & Tappan, scale bar 50 μm.

7. *Sigmoilopsis schlumbergeri* (Silvestri), scale bar 50 μm.

8. *Oolina hexagona* (Williamson), scale bar 50 μm.

9. *Fissurina fimbriata* (Brady), scale bar 10 μm.

10. *Fissurina orbignyana* Seguenza, scale bar 50 μm.

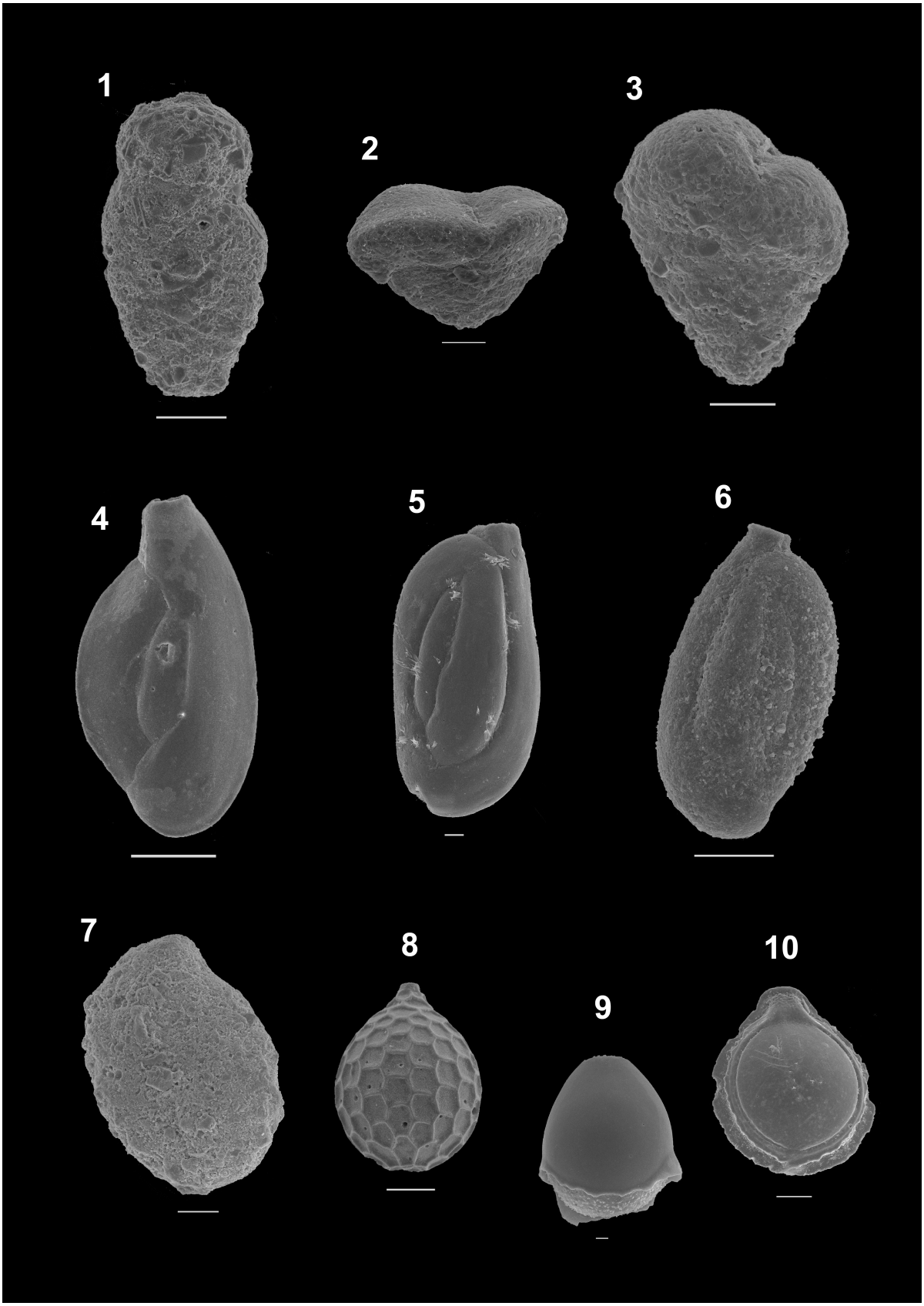
1
2
3
4
5
6
7
8
9
10

PLATE II

1. *Lamarckina haliotidea* (Heron-Allen & Earland),ventral side, scale bar 350 μm.

2. *Rubratella intermedia* Grell,ventral side, scale bar 10 μm.

3. *Bolivina albatrossi* Cushman, scale bar 50 μm.

4. *Brizalina dilatata* (Reuss), scale bar 50 μm.

5. *Bolivina ordinaria* Phleger & Parker: **a)** frontal view, **b)** lateral view, scale bar 50 μm.

6. *Bolivina pseudoplicata* Heron-Allen & Earland, scale bar 50 μm.

7. *Bolivina seminuda* Cushman, scale bar 100 μm.

8. *Bolivina subspinescens* Cushman, scale bar 10 μm.

9. *Brizalina spathulata* (Williamson), scale bar 50 μm.

10. *Brizalina subaeraniensis* (Cushman), scale bar 100 μm.

11. *Bolivina striatula* Cushman, scale bar 50 μm.

12. *Cassidulina laevigata* d'Orbigny, scale bar 50 μm.

13. *Cassidulina minuta* Cushman, scale bar 50 μm.

14. *Stainforthia fusiformis* (Williamson), scale bar 50 μm.

15. *Globobulimina ovata*, scale bar 100 μm.

16. *Bulimina elongata* d'Orbigny, scale bar 50 μm.

17. *Bulimina aculeata* d'Orbigny, scale bar 50 μm.

18. *Bulimina marginata* d'Orbigny, scale bar 50 μm.

19. *Bulimina striata* d'Orbigny, scale bar 50 μm.

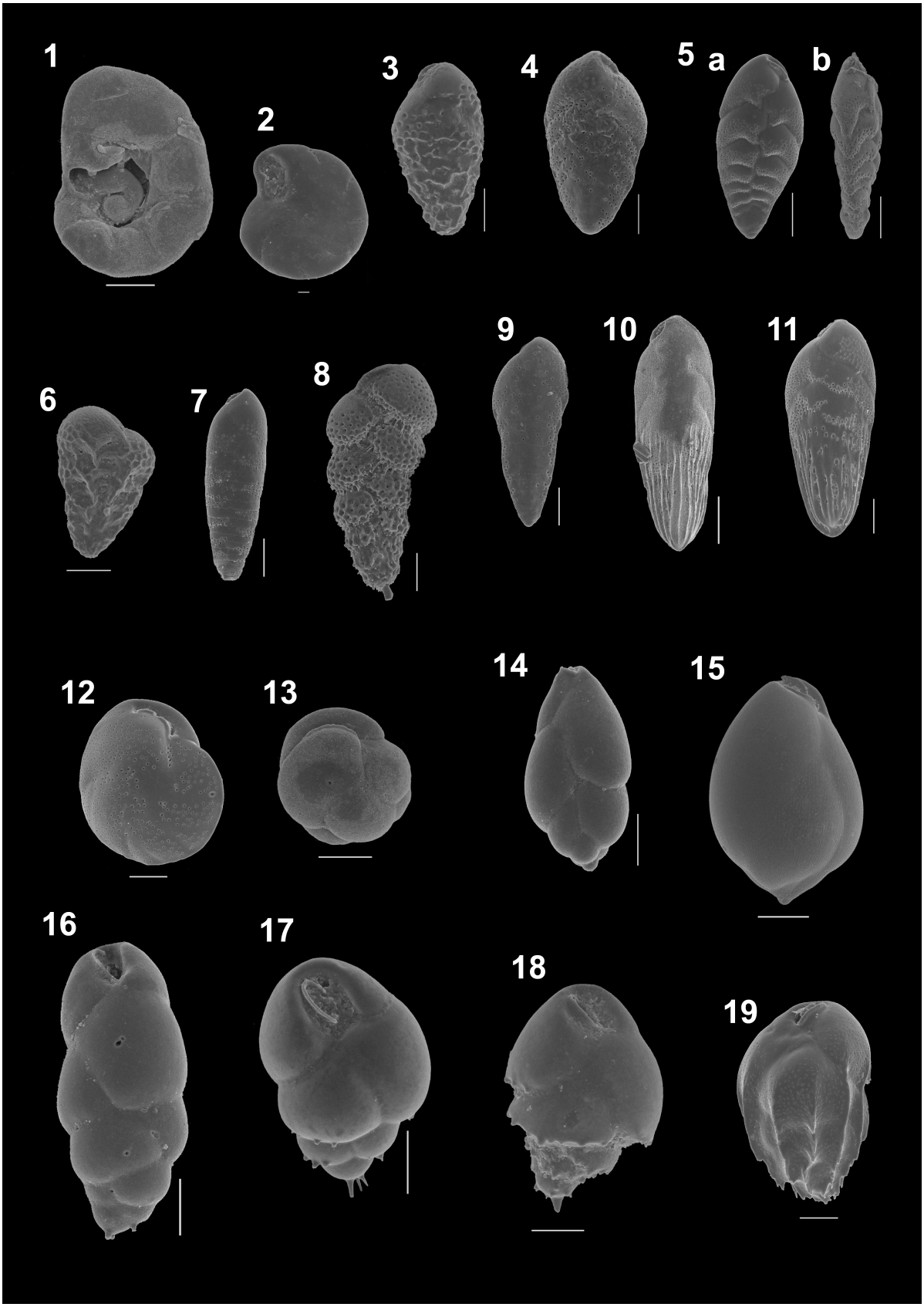
1
2
3
4
5 a
b
6
7
8
9
10
11
12
13
14
15
16
17
18
19

PLATE III

1. *Buliminella tenuata* (Cushman), scale bar 50 μm.

2. *Rectuvigerina phlegeri* Le Calvez, scale bar 100 μm.

3. *Uvigerina peregrina* Cushman, scale bar 200 μm.

4. *Trifarina bradyana* (Cushman), scale bar 50 μm.

5. *Trifarina carinata* (Cushman), scale bar 50 μm.

6. *Reussella spinulosa* (Reuss), scale bar 50 μm.

7. *Fursenkoina complanata* (Egger), scale bar 50 μm.

8. *Valvulineria bradyana* (Fornasini): **a)** dorsal side, scale bar 50 μm, **b)** ventral side, scale bar 100 μm.

9. *Gavelinopsis praegeri* (Heron-Allen and Earland), ventral side, scale bar 50 μm.

10. *Discorbis williamsoni* Chapman and Parr, ventral side, scale bar 50 μm.

11. *Rosalina rugosa* d'Orbigny: **a)** dorsal side, scale bar 100 μm, **b)** ventral side, scale bar 50 μm.

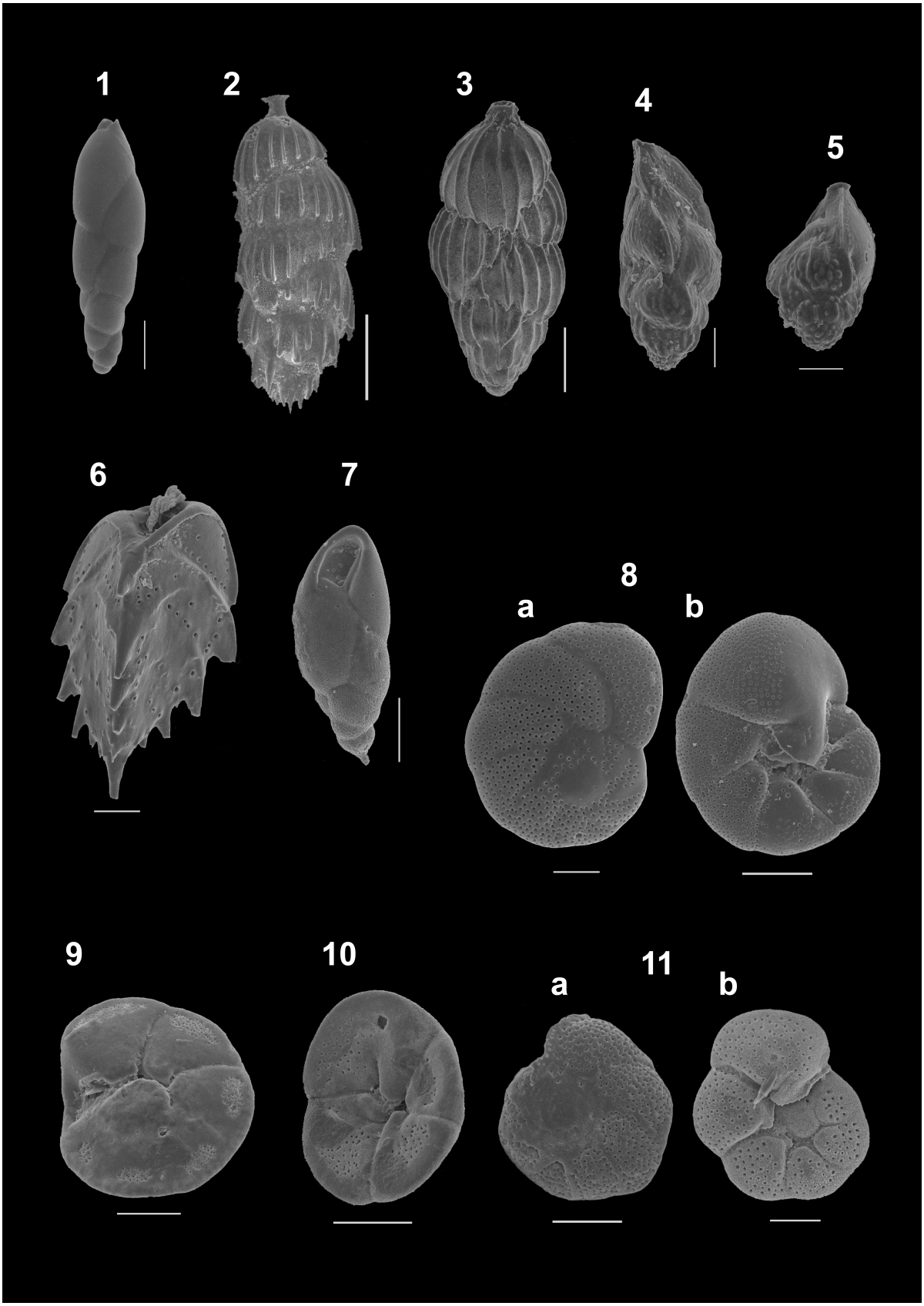
1
2
3
4
5
6
7
8
a
b
9
10
11
a
b

PLATE IV

1. *Glabratella millettii* (Wright), ventral side, scale bar 50 μm.

2. *Epistominella exigua* (Brady): **a)** dorsal side, **b)** ventral side, scale bar 10 μm.

3. *Hyalinea balthica* (Schröter), scale bar 50 μm.

4. *Lobatula lobatula* (Walker and Jacob): **a)** dorsal side, **b)** ventral side, scale bar 100 μm.

5. *Planorbulina mediterranensis* d'Orbigny: **a)** dorsal side, **b)** ventral side, scale bar 100 μm **c)** apertures, scale bar 50 μm.

6. *Asterigerinata mamilla* (Williamson): **a)** dorsal side, **b)** ventral side, scale bar 50 μm.

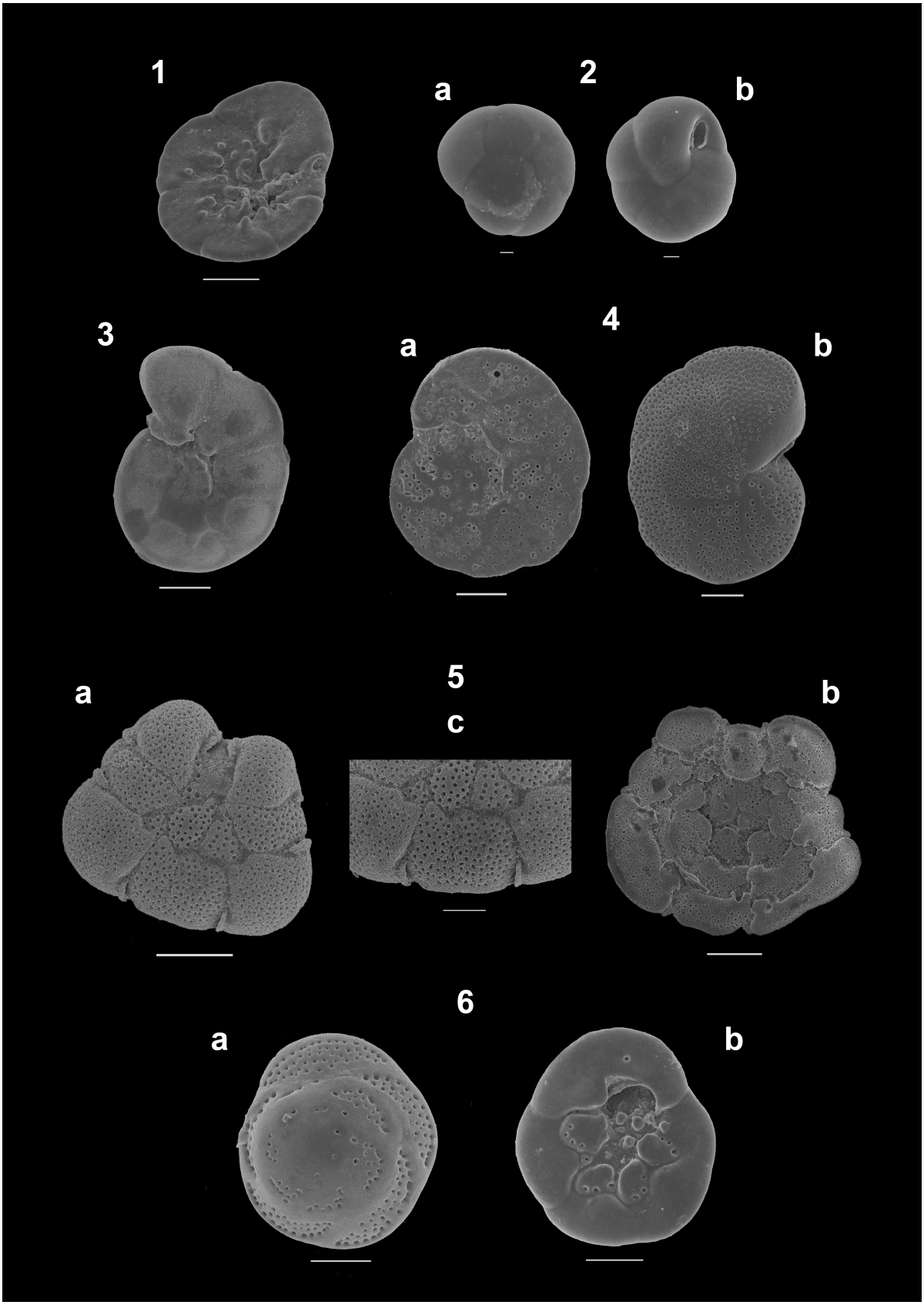
1
2
a
b
3
4
a
b
a
5
c
b
6
a
b

PLATE V

1. *Haynesina germanica* (Ehrenberg), scale bar 50 μm.

2. *Nonion fabum* (Fichtel and Moll), scale bar 100 μm.

3. *Nonionella stella* (Cushman and Moyer), ventral side, scale bar 50 μm.

4. *Nonionella turgida* (Williamson): **a)** dorsal side, **b)** ventral side, scale bar 100 μm.

5. *Gyroidina umbonata* (Silvestri): **a)** dorsal side, **b)** ventral side, scale bar 50 μm.

6. *Ammonia beccarii* (Linné), ventral side, scale bar 100 μm.

7. *Cribrononion gerthi* (Van Voorthuysen): **a)** apertural view, **b)** lateral view, scale bar 50 μm.

8. *Elphidium cuvillieri* Levy, scale bar 100 μm.

9. *Elphidium excavatum* (Terquem), scale bar 100 μm.

10. *Elphidium macellum* (Fichtel and Moll), scale bar 100 μm.

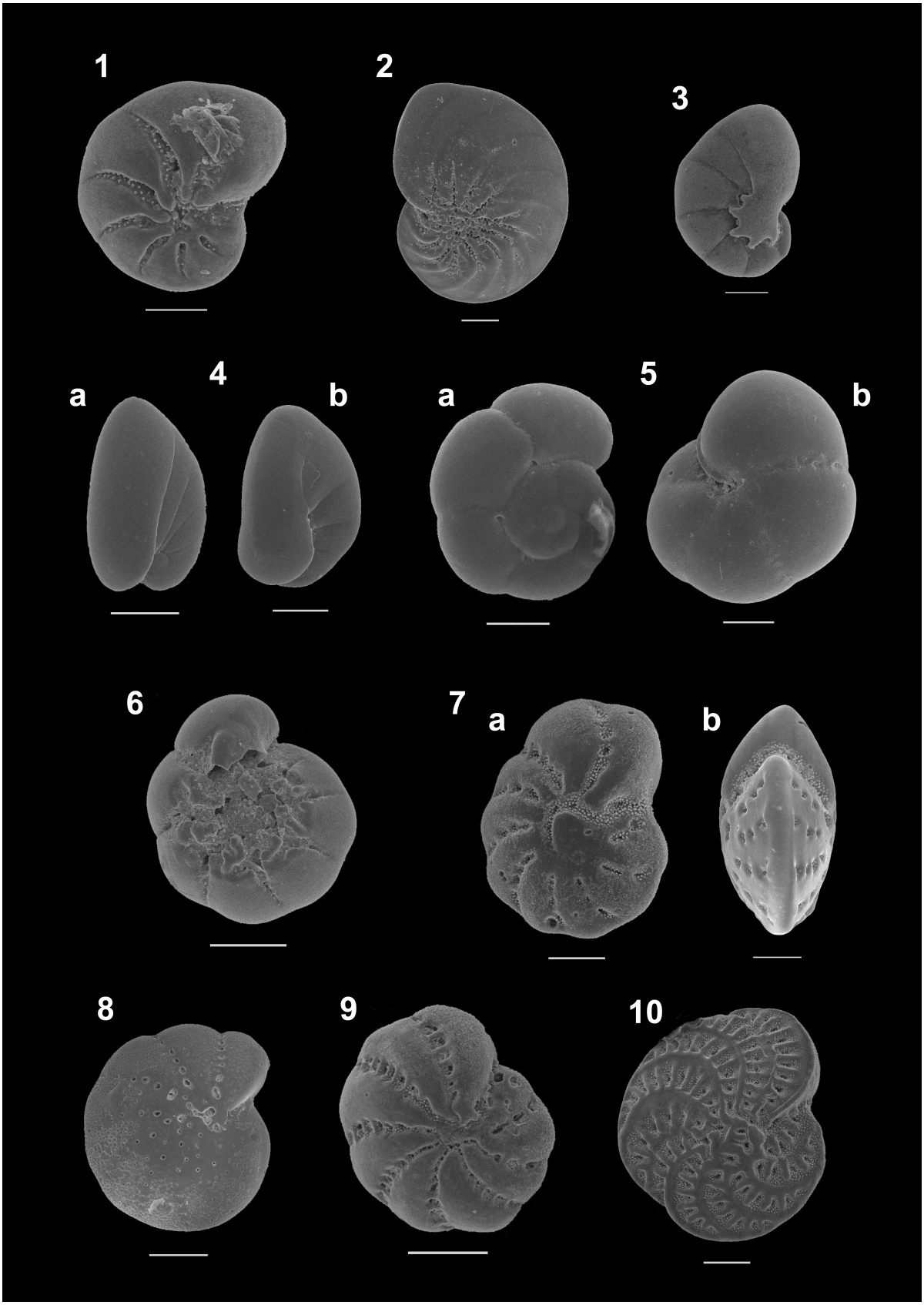
1
2
3
a
4
b
a
5
b
6
7
a
b
8
9
10

REFERENCES

Abrantes, F., Lebreiro, S., Rodrigues, T., Gil, I., Bartels-Jónsdóttir, H., Oliveira, P., Kissel, C., Grimalt, J. O. (2005). Shallow-marine sediment cores record climate variability and earthquake activity off Lisbon (Portugal) for the last 2000 years. *Quaternary Science Reviews*, 24, 2477-2494.

Abu-Zied, R. H., Rohling, E. J., Jorissen, F. J., Fontanier, C., Casford, J. S. L., Cooke, S. (2008). Benthic foraminiferal response to changes in bottom-water oxygenation and organic carbon flux in the eastern Mediterranean during LGM to Recent times. *Marine Micropaleontology*, 67, 46-68.

Alarcão, J. (1987). "Portugal Romano". Coleção História Mundi, Editorial Verbo, Lisboa (in Portuguese).

Alarcão, J. (1990). "Portugal: das origens à Romanização". *In*: Nova História de Portugal (coord. Joel Serrão e A. H. Oliveira Marques), vol. I. Editorial Presença, Lisboa (in Portuguese).

Alcoforado, M. J., Nunes, M. F., Garcia, J. C., Taborda, J. P. (2000). Temperature and precipitation reconstruction in southern Portugal during the late Maunder Minimum (1675–1715). *The Holocene*, 10, 333-340.

Alley, R. B., Clark, P. U. (1999). The deglaciation of the northern hemisphere: a global perspective. *Annual Reviews of Earth and Planetary Sciences*, 27, 149–182.

Alve, E. (1991). Benthic foraminifera in sediment cores reflecting heavy metal pollution in Sørfjord, western Norway. *Journal of Foraminiferal Research*, 21(1), 1-19.

Alve, E. (2003). A common opportunistic foraminiferal species as an indicator of rapidly changing conditions in a range of environments. *Estuarine, Coastal and Shelf Science*, 57, 501-514.

Alve, E., Murray, J. (1999). Marginal marine environments of the Skagerrak and Kattegat: a baseline study of living (stained) benthic foraminiferal ecology. *Palaeogeography, Palaeoclimatology, Palaeoecology*, 146, 171-193.

Alves, E., Rocha, J. S., Barbosa, A. E. (2001). "Estudo das condições ambientais no estuário do rio Guadiana e zonas adjacentes. 2a fase: Componente fluvial". Relatório 221/01-NHE, Laboratório Nacional de Engenharia Civil, Lisboa (in Portuguese).

Alves, M., Gaillard, F., Sparrow, M., Knoll, M., Giraud, S. (2002). Circulation patterns and transport of the Azores Front-Current System. *Deep-Sea Research II*, 49, 3983–4002.

Alves, T. M., Gawthorpe, R. L., Hunt, D. W., Monteiro, J. H. (2003). Cenozoic tectono-sedimentary evolution of the western Iberian margin. *Marine Geology*, 195, 75–108.

Alt-Epping, U., Stuut, J.-B. W., Hebbeln, D., Schneider, R. (2009). Variations in sediment provenance during the past 3000 years off the Tagus River, Portugal. *Marine Geology*, 261, 82-91.

Anderson, R. S., Jiménez-Moreno, G., Carrión, J. S., Pérez-Martínez, C. (2011). Postglacial history of alpine vegetation, fire, and climate from Laguna de Río Seco, Sierra Nevada, southern Spain. *Quaternary Science Reviews*, 30, 1615-1629.

Araújo, M. F., Jouanneau, J.-M., Valério, P., Barbosa, T., Gouveia, A., Weber, O., Oliveira, A., Rodrigues, A., Dias, J. M. A. (2002). Geochemical tracers on the northern Portuguese estuarine sediments on the shelf. *Progress in Oceanography*, 52, 277-297.

Baldy, P., Boillot, G., Dupeuple, P.-A., Malod, J., Moita, I., Mougenout, D. (1977). Carte géologique du plateau continental sud-portugais et sud-espagnol (Golfe de Cadix). *Bulletin de la Société Géologique de France*, (7), t. XIX, 703-724.

Barber, D. C., Dyke, A., Hillaire-Marcel, C., Jennings, A. E., Andrews, J. T., Kerwin, M. W., Biladeau, G., McNeeley, R., Southon, J., Morehead, M. D., Gagnon, J.-M. (1999). Forcing of the cold event of 8,200 years ago by catastrophic drainage of Laurentide lakes. *Nature*, 400, 344–348.

Bard, E. (2002). Climate shock: Abrupt changes iver millennial time scales. *Physics Today*, 55(12), 32, doi: 10.1063/1.1537910.

Bard, E., Raisbeck, G. M., Jouzel., J (2007). Letter to the editor. *Quaternary Science Reviews*, 26, 2301-2308.

Bard, E., Hamelin, B., Delanghe-Sabatier, D. (2010). Deglacial Meltwater Pulse 1B and Younger Dryas Sea Levels Revisited with Boreholes at Tahiti. *Science*, 327, 1235-1237.

Barmawidjaja, D. M., Jorissen, F. J., Puskaric, S., Van der Zwaan, G. J. (1992). Microhabitat selection by benthic foraminifera in the northern Adriatic Sea. *Journal of Foraminiferal Research*, 22(4), 297-317.

Barmawidjaja, D. M., Van der Zwaan, G. J., Jorissen, F. J., Puskaric, S. (1995). 150 years of eutrophication in the northern Adriatic Sea: Evidence from a benthic foraminiferal record. *Marine Geology*, 122, 367-384.

Barriendos, M. (1997). Climatic variations in the Iberian peninsula during the late Maunder minimum (AD 1675–1715): an analysis of data from rogation ceremonies. *The Holocene*, 7, 105–111.

Bartels-Jonsdóttir, H. B., Knudsen, K. L., Abrantes, F., Lebreiro, S., Eiríksson, J. (2006). Climate variability during the last 2000 years in the Tagus Prodelta, western Iberian Margin: Benthic foraminifera and stable isotopes. *Marine Micropaleontology*, 59, 83-103.

Berglund, B. E. (2003). Human impact and climate changes – synchronous events and a causal link?. *Quaternary International*, 105, 7-12.

Bernárdez P., González-Álvares, R., Francés, G., Prego, R., Bárcena, M. A., Romero, O. E. (2008). Late Holocene history of the rainfall in the NW Iberian peninsula – Evidence from a marine record. *Journal of Marine Systems*, 72, 366-382.

Bernhard, J. M., Sen Gupta, B. K. (1999). "Foraminifera of oxygen-depleted environments". *In*: Modern Foraminifera (Sen Gupta, Ed.). Kluwer Academic Publishers, Dordrecht/Boston/London.

Blaauw, M., Heegaard, E. (2012). "Estimation of age-depth relationships". *In*: Tracking Environmental Change Using Lake Sediments (Birks, H. J. B., Lotter, A. F., Juggins, S., Smol, J. P., (Eds.), vol. 5 – "Developments in Paleoenvironmental Research". Springer Science and Business Media B. V.

Boltovskoy, E., Giussani, G., Watanabe, S, Wrigh, W. (1980). "Atlas of Benthic Shelf Foraminifera of the Southwest Atlantic". Dr. W. Publishers, The Hague-Boston-London.

Bond, G., Broecker, W., Johnsen, S., McManus, J., Labeyrie, L., Jouzel, G., Bonani, G. (1993). Correlations between climate records from North Atlantic sediments and Greenland ice. *Nature*, 365, 143–147.

Bond, G., Showers, W., Cheseby, M., Lotti, R., Almasi, P., deMenocal, P. (1997). A pervasive millennial-scale cycle in the North Atlantic Holocene and Glacial climates. *Science*, 278, 1257-1266.

Boone, J. L. and Worman, F. S. (2007). Rural settlement and soil erosion from the late Roman Period through the medieval Islamic Period in the lower Alentejo of Portugal. *Journal of Field Archaeology*, 32, 115-132.

Borges Coelho, A. (2008). "Portugal na Espanha Árabe". Editorial Caminho, Lisboa (in Portuguese).

Boski, T., Moura, D., Veiga-Pires, C., Camacho, S., Duarte, D., Scott, D. B., Fernandes, S. G. (2002). Postglacial sea-level rise and sedimentary response in the Guadiana Estuary, Portugal/Spain border. *Sedimentary Geology*, 150, 103-122.

Boski, T., Camacho, S., Moura, D., Fletcher, W., Wilamowski, A., Veiga-Pires, C., Correia, V., Loureiro, C., Santana, P. (2008). Chronology of the sedimentar processes during the postglacial sea level rise in two estuaries of the Algarve coast, Southern Portugal. *Estuarine, Coastal and Shelf Science*. 77, 230-244.

Bradley, R. S. (2003). "Climate of the Last Millennium". Personal communication at the HOLOCENE Working Group Workshop, Bjerknes Centre for Climate Research.

Broecker, W. S. (1994). Massive iceberg discharges as triggers for global climate change. *Nature*, 372, 421–424.

Broecker, W. S. (1997). Thermohaline circulation, the Achilles heel of our climate system: will man-made CO2 upset the current balance?. *Science*, 278, 1582–1588.

Broecker, W. S., Andree, M., Wolfli, W., Oeschger, H., Bonani, G., Kennett, J., Peteet, D. (1988). The chronology of the last deglaciation: implications to the cause of the Younger Dryas event. *Paleoceanography*, 3, 1–19.

Büngten, U., Tegel, W., Nicolussi, K., McCormik, M., Frank, D., Trouet, V., Kaplan, J. O., Herzig, F., Heussner, K.-U., Wanner, H., Luterbacher, J., Esper, J. (2011). 2500 Years of European climate variability and human susceptibility. *Science*, 311, 578-582.

Burdloff, D., Araújo, M. F., Jouanneau, J. M., Mendes, I., Monge Soares, A. M., Dias, J. M. A. (2008). Sources of organic carbon in the Portuguese continental shelf sediments during the Holocene period. *Applied Geochemestry*, 23, 2857-2870.

Buzas, M. A. (1990). Another look at confidence limits for species proportions. *Journal of Paleontology*, 64, 842-843.

Cacho, I., Grimalt, J. O., Canals, M. (2002). Response of the Western Mediterranean Sea to rapid climatic variability during the last 50,000 years: a molecular biomarker approach. *Journal of Marine Systems*, 32-34, 253-272.

Carrión, J. S. (2002). Patterns and processes of Late Quaternary environmental change in a montane region of southwestern Europe. *Quaternary Science Reviews*, 21, 2047-2066.

Carrión, J. S. and Dupré, M. (1997). Late quaternary vegetational history at Navarrés, eastern Spain. A two-core approach. *New Phytologist*, 134, 177–191.

Carrión, J. S., Munuera, M., Dupré, M., Andrade, A. (2001). Abrupt vegetation changes in the Segura Mountains of southern Spain throughout the Holocene. *Journal of Ecology*, 89, 783-797.

Carrión, J. S., Yll, E. I., Willis, K. J., Sánchez, P. (2004). Holocene forest history of the eastern plateaux in the Segura Mountains (Murcia, southeastern Spain). *Review of Palaeobotany and Palynology*, 132, 219-236.

Carrión, J. S., Fuentes, N., González-Sampériz, P., Sánchez Quirante, L., Finlayson, J. C., Fernández, S., Andrade, A. (2007). Holocene environmental change in a montane region of southern Europe with a long history of human settlement. *Quaternary Science Reviews*, 26, 1455-1475.

Carrión, J. S., Fernández, S., González-Sampériz, P., Gil-Romera, G., Badal, E., Carrión-Marco, Y., López-Merino, L., López-Sáez, J. A., Fierro, E., Burjachs, F. (2010a). Expected trends and surprises in the Lateglacial and Holocene vegetation history of the Iberian Peninsula and Balearic Islands. *Review of Palaeobotany and Palynology*, 162(3), 458-475.

Carrión, J. S., Fernández, S., Jiménez-Moreno, G., Fauquette, S., Gil-Romera, G., González-Sampérez, P., Finlayson, C. (2010b). The historical origins of aridity and vegetation degradation in southeastern Spain. *Journal of Arid Environments*, 74, 731-736.

Casana, J. (2008). Mediterranean valleys revisited: Linking soil erosion, land use and climate variability. *Geomorphology*, 101, 429-442.

Castro-Díez, Y., Pozo-Vázquez, D., Rodrigo, F. S., Esteban-Parra, M. J. (2002). NAO and winter temperature variability in Southern Europe. *Geophysical Research Letters*, 29(8), 1160-1163.

Chapman, M. R., Shackelton, N. L. (2000). Evidence of 550-year and 1000-year cyclicities in North Atlantic circulation patterns during the Holocene. *The Holocene*, 10, 287-291.

Chester, D. K. (2012). Pleistocene and Holocene geomorphological development in the Algarve, southern Portugal. *Geomorphology*, 153-154, 17-28.

Chester, D. K., James, P. A. (1999). Late Pleistocene and Holocene landscape development in the Algarve region, Southern Portugal. *Journal of Mediterranean Archaeology*, 12, 169-196.

Ciavola, P., Taborda, R., Ferreira, Ó., Dias, J. A. (1997). Field measurements of longshore sand transport and control processes on a steep meso-tidal beach in Portugal. *Journal of Coastal Research*, 13(4), 1119-1129.

Colom, G. (1974). "Foraminiferos ibericos: Introducción al estudio de las espécies bentónicas recientes". Patrono Juán de la Cierva, Barcelona (in Spanish).

Cook, E. R., DÁrrigo, R., Mann, M. E. (2002). A well-verified, multiproxy reconstruction of the winter North Atlantic Oscillation Index since A.D. 1400. *Journal of Climate*, 15, 1754-1764.

Corella, J. P., Stefanova, V., El Anjoumi, A., Rico, E., Giralt, S., Moreno, A., Plata-Montero, A., Valero-Garcés, B. L. (2013). A 2500-year multi-proxy reconstruction of climate change and human activities in northern Spain: The Lake Arreo record. *Palaeogeography, Palaeoclimatology, Palaeoecology*, 386, 555-568.

Costa, M., Silva, R., Vitorino, J. (2001). "Contribuição para o estudo do clima de agitação marítima na costa portuguesa". *In*: 2as Jornadas Portuguesas de Engenharia Costeira e Portuária. International Navigation Association PIANC, Sines (in Portuguese).

Corredeira, C., Araújo, M. F., Jouanneau, J.-M. (2008). Copper, lead and zinc impact in SW Iberian shelf sediments: An assessment of recent historical changes in Guadiana river basin. *Geochemical Journal*, 42, 319-329.

Corte-Real, J., Qian, B., Xu, H. (1998). Regional climate change in Portugal: Precipitation variability associated with large-scale atmospheric circulation. *International Journal of Climatology*, 18, 619-635.

Cravo, A., Madureira, M., Felícia, H., Rita, F., Bebianno, M. J. (2006). Impact of outflow from the Guadiana River on the distribution of suspended particulate matter and nutrients in the adjacent coastal zone. *Estuarine, Coastal and Shelf Science*, 70, 63-75.

Criado-Aldeanueva, F., García-Lafuente, J., Vargas, J. M., del Río, J., Vásquez, A., Reul, A., Sánxhez, A. (2006). Distribution and circulation of water masses in the Gulf of Cadiz from in situ observations. *Deep-Sea Research II*, 53, 1144-1160.

Crockett, J. S., Nittrouer, C. A. (2004). The sandy inner shelf as a repository for muddy sediment: an example from Northern California. *Continental Shelf Research*, 24, 55-73.

Cunha, F. R. (1983). "O ambiente climático Algarvio no conjunto de Portugal Continental". *In*: Seminário "O Papel da Universidade no processo de regionalização e desenvolvimento regional". Universidade do Algarve, Faro (in Portuguese).

Dabrio, C. J., Zazo, C., Goy, J. L., Sierro, F. J., Borja, F., Lario, J., González, J. A., Flores, J. A. (2000). Depositional history of estuarine infill during the last postglacial transgression (Gulf of Cadiz, Southern Spain). *Marine Geology*, 162, 381-404.

Dansgaard, W., Johnsen, S. J., Clausen, H. B., Dahl-Jensen, D., Gundestrup, N. S., Hammer, C. U., Hvidberg, C. S., Steffensen, J. P., Sveinbjörnsdottir, A. E., Jouzel, J., Bond, G. (1993). Evidence for general instability of past climate from a 250-kyr ice-core record. *Nature*, 364, 218-220.

De Rijk, S., Jorissen, F. J., Rohling, E. J., Troelska, S. R. (2000). Organic flux controlo n bathymetric zonation of Mediterranean benthic foraminiferal. *Marine Micropaleontology*, 40, 151-166.

De Stigter, H. C., Jorissen, F. J., Van der Zwaan, G. J. (1998). Bathymetric distribution and microhabitat partitioning of live (Rose Bengal stained) foraminifera along a shelf to bathyal transect in the southern Adriatic Sea. *Journal of Foraminiferal Research*, 28(1), 40-65.

Debenay, J.-P., Redois, F. (1997). Recent foraminifera of the northern continental shelf of Senegal. *Revue de Micropaléontologie*, 40(1), 15-38.

Debenay, J.-P., Tsakiridis, E., Soulard, R., Grossel, H. (2001). Factors determining the distribution of foraminiferal assemblages in Port Joinville Harbour (Ile d'Yeu, France): the influence of pollution. *Marine Micropaleontology*, 43, 75-118.

Delgado, J., Boski, T., Nieto, J. M., Pereira, L., Moura, D., Gomes, A., Sousa, C., García-Tenorio, R. (2012). Sea-level rise and anthropogenic activities recorded in the late Pleistocene/Holocene sedimentary infill of the Guadiana Estuary (SW Iberia). *Quaternary Science Reviews*, 33, 121-141.

deMenocal, P., Ortiz, J., Guilderson, T., Sarnthein, M. (2000). Coherent high- and low-climate variability during the Holocene Warm Period. *Science*, 288, nº 5474, 2198-2202.

Dermody, B. J., de Boer, H. J., Bierkens, M. F. P., Weber, S. L., Wassen, M. J., Dekker, S. C. (2012). A seesaw in Mediterranean precipitation during the Roman Period linked to millennial-scale changes in the North Atlantic. *Climate of the Past*, 8, 637-651.

Désprat, S., Sánchez Goñi, M. F., Loutre, M.-F. (2003). Revealing climatic variability of the last three millennia in northwestern Iberia using pollen influx data. *Earth and Planetary Science Letters*, 213, 63-78.

Désprat, V., Combourieu-Nebout, N., Essallami, L., Sicre, M. A., Dormoy, I., Peyron, O., Siani, G., Roumazeilles, V. B., Turon, J. L. (2013). Deglacial and Holocene vegetation and climatic changes in the southern Central Mediterranean from a direct land-sea correlation. *Climate of the Past*, 9, 767-787.

Devy-Vareta, N. (1985). Para uma geografia histórica da floresta portuguesa: as matas medievais e a 'Coutada Velha' do Rei. *Revista da Faculdade de Letras do Porto – Geografia*, vol. 1, 47-67 (in Portuguese).

Dias, J. M. A. (1987). "Dinâmica sedimentar e evolução recente da plataforma continental Portuguesa setentrional". PhD Thesis, Universidade de Lisboa (in Portuguese).

Dias, J. M. A., Nittrouer, C. A. (1984). Continental shelf sediments of northern Portugal. *Continental Shelf Research*, 3, 147–165.

Dias, J. M. A., Boski, T., Rodrigues, A., Magalhães, F. (2000). Coast line evolution in Portugal since the Last Glacial Maximum until present - a synthesis. *Marine Geology*, 170, 177-186.

Dias, J. M. A., González, R., Garcia, C., Díaz del Río, V. (2002a). Sediment distribution patterns on the Galicia-Minho continental shelf. *Progress in Oceanography*, 52, 215–231.

Dias, J. M. A., Jouanneau, J.-M., González, R., Araújo, M. F., Drago, T., Garcia, C., Oliveira, A., Rodrigues, A., Vitorino, J., Weber, O. (2002b). Present day sedimentary processes on the northern Iberian shelf. *Progress in Oceanography*, 52, 249-259.

Dias, J. M. A., González, R., Ferreira, Ó. (2004). Natural versus anthropic causes in variations of sand export from river basins: an example from the Guadiana River Mouth (Southwestern Iberia). *Polish Geological Institute Special Papers*, 11, 95–102.

Dinis, J. L., Henriques, V., Freitas, M. C., Andrade, C., Costa, P. (2006). Natural to anthropogenic forcing in the Holocene evolution of three coastal lagoons (Caldas da Rainha valley, western Portugal). *Quaternary International*, 150, 41–51.

Díz, P., Francés, G. (2008). Distribution of live benthic foraminifera in the Ría de Vigo (NW Spain). *Marine Micropaleontology*, 66, 165-191.

Díz, P., Francés, G., Rosón, G. (2006). Effects of contrasting upwelling- downwelling on benthic foraminiferal distribution in the Ría de Vigo (NW Spain). *Journal of Marine Systems*, 60, 1-18.

Díz, P., Francés, G., Pelejero, G., Grimalt, J. O., Vilas, F. (2002). The last 3000 years in the Ría de Vigo (NW Iberian Margin): climatic and hydrological signals. *The Holocene*, 12, 459-468.

Díz, P., Francés, G., Costas, S., Souto, C., Alejo, I. (2004). Distribution of benthic foraminifera in coarse sediments, Ría de Vigo, NW Iberian Margin. *Journal of Foraminiferal Research*, 34, 258-275.

Donnici, S., Barbero, R. S. (2002). The benthic foraminiferal communities of the northern Adriatic continental shelf. *Marine Micropaleontology*, 44, 93-123.

Dorado Valiño, M., Valdeolmillos Rodríguez, A., Ruiz Zapata, M. B., Gil García, M. J., Bustamante Gutiérrez, I. (2002). Climatic changes since the Late-glacial/Holocene transition in La Mancha Plain (South-central Iberian Peninsula, Spain) and their incidence on Las Tablas de Daimiel marshlands. *Quaternary International*, 93-94, 73-84.

Drago, T., Araújo, F., Valério, P., Weber, O., Jouanneau, J.-M. (1999). Geomorphological control of fine sedimentation on the northern Portuguese shelf. *Boletín Instituto Español de Oceanografia*, 15(1/4), 111–122.

Domínguez-Castro, F., Santisteban, J. I., Barriendos, M., Mediavilla, R. (2008). Reconstruction of drought episodes for central Spain from rogation ceremonies recorded at the Toledo Cathedral from 1506 to 1900: A methodological approach. *Global and Planetary Change*, 63, 230-242.

Dubrulle, C., Jouanneau, J. M., Lesueur, P., Bourillet, J. F., Weber, O. (2007). Nature and ratesof fine-sedimentation on a mid-shelf: 'La Grande Vasière' (Bay of Biscay, France). *Continental Shelf Research*, 27, 2099-2115.

Duchemin, D., Jorissen, F. J., Andrieux-Loyer, F., Le Loc'h, F., Hily, C., Philippon, X. (2005). Living benthic foraminifera from 'La Grande Vasière', French Atlantic continental shelf: Faunal composition and microhabitats. *Journal of Foraminiferal Research*, 35(3), 198-218.

Duchemin, G., Fontanier, C., Jorissen, F. J., Barras, C., Griveaud, C. (2007). Living small-sized (63-150 m) foraminifera from mid-shelf to mid-slope environments in the Bay of Biscay. *Journal of Foraminiferal Research*, 37(1), 12-32.

Duchemin, G., Jorissen, F. J., Le Loc'h, F., Andrieux-Loyer, F., Hily, C., Thouzeau, G. (2008). Seasonal variability of living benthic foraminifera from the outer continental shelf of the Bay of Biscay. *Journal of Sea Research*, 59, 297-319.

Duplessy, J. C., Labeyrie, L., Arnold, M., Paterne, M., Duprat, J., van Weering, T. C. E. (1992). Changes in surface salinity of the North Atlantic Ocean during the last deglaciation. *Nature*, 358, 485–488.

Eddy, J. A. (1976). The Maunder Minimum. *Science*, 192, nº 4245, 1189–1202.

Edwards, B. D. (2002). Variations in sediment texture on the northern Monterey Bay National Marine Sanctuary continental shelf. *Marine Geology*, 181, 83-100.

Eiríksson, J., Bartels-Jonsdóttir, H. B., Cage, A. G., Gudmundsdóttir, E. R., Klitgaard-Kristensen, D., Marret, F., Rodrigues, T., Abrantes, F., Austin, W. E. N., Jiang, H., Knudsen, K.-L., Sejrup, H.-P. (2006). Variability of the North Atlantic Current during the last 2000 years based on shelf bottom water and sea surface temperatures along an open ocean/shallow marine transect in western Europe. *The Holocene*, 16, 1017-1029.

Ellis, B. F., Messina, A. R. (1942-2009). "Catalogue of Foraminifera". Bulletin of the American Museum of Natural History, Micropaleontological Press.

Ernst, S., Duijnstee, I., Van der Zwaan, B. (2002). The dynamics of the benthic foraminiferal microhabitat: recovery after experimental disturbance. *Marine Micropaleontology*, 46, 343-361.

Eynaud, F., de Abreu, L., Voelker, A., Schönfeld, J., Salgueiro, E., Turon, J.-L., Penaud, A., Toucanne, S., Naughton, F., Sánchez Goñi, M. F., Malaizé, B., Cacho, I. (2009). Position of the Polar Front along the western Iberian margin during key cold episodes of the last 45 ka. *Geochemestry, Geophysics, Geosystems*, 10(7), DOI: 10.1029/2009GC002398.

Fabião, C. (1993). "O Passado Proto-Histórico e Romano". *In*: História de Portugal (coord. José Mattoso), vol. I – "Antes de Portugal". Editorial Estampa, Lisboa (in Portuguese).

Fairbanks, R. G. (1989). A 17,000-year glacio-eustatic sea level record: influence of glacial melting rates on the Younger Dryas event and deep-ocean circulation. *Nature*, 342, 637-642.

Fairbanks, R. G. (1990). The age and origin of the ‘‘Younger Dryas climate event’’ in Greenland ice cores. *Paleoceanography*, 5, 937–948.

Fatela, F., Taborda, R. (2002). Confidence limits of species proportion in microfossil assemblages. *Marine Micropaleontology*, 45, 169-174.

Faust, D., Zielhofer, C., Escudero, R. B., Diaz del Olmo, F. (2004). High-resolution fluvial record of late Holocene geomorphic change in northern Tunisia: climatic or human impact. *Quaternary Science Reviews*, 23, 1757-1775.

Fernández-Salas, L. M., Rey, J., Perez-Vásquez, E., Ramirez, J. L., Hernández-Molina, F. J., Somoza, L., De Andrés, J. R., Lobo, F. J. (1999). Morphology and characterization of the relict facies on the internal continental shelf in the Gulf of Cadiz between Ayamonte and Huelva (Spain). *Boletín del Instituto Español de Oceanografia*, 15, 123-132.

Fischer, W. (1987). “Report of the sixth session of the Committee for the development and management of the fishery resources of the Gulfs”. FAO Fisheries and Aqualculture Report/372. Food and Agriculture Organization of the United Nations, Rome.

Fiúza, A. (1983). “Upwelling patterns off Portugal”. *In*: Coastal Upwelling (E. Suess, Thiede, J., Ed.). Plenum Publishing Corporation.

Fleming, K., Johnston, P., Zwartz, D., Yokoyama, Y., Lambeck, K., Chappell, J. (1998). Refining the eustatic sea-level curve since the Last Glacial Maximum using far- and intermediate-field sites. *Earth and Planetary Science Letters*, 163, 327-342.

Fletcher, W., Sánchez Goñi, M. F. (2008). Orbital- and sub-orbital-scale climate impacts on vegetation of the western Mediterranean basin over the past 48,000 yr. *Quaternary Research*, 70, 451-464.

Fletcher, W., Boski, T., Moura, D. (2007). Palynological evidence for environmental and climatic change in the lower Guadiana Valley, Portugal, during the last 13 000 years. *The Holocene*, 17(4), 481-494.

Fletcher, W., Debret, M., Sánchez Goñi, M. F. (2012). Mid-Holocene emergency of a low-frequency millennial oscillation in western Mediterranean climate: Implications for past dynamics of the North Atlantic atmospheric westerlies. *The Holocene*, 23(2), 153-166.

Folk, R. L. (1954). The distinction between rain size and mineral composition in sedimentary-rock nomenclature. *Journal of Geology*, 62/4, 344-359.

Folkard, A. W., Davis, P. A., Fiúza, A. F. G., Ambar, I. (1997). Remotely sensed sea surface thermal patterns in the Gulf of Cádiz and the Strait of Gibraltar: variability, correlations, and relationships with the surface wind field. *Journal of Geophysical Research*, 102(C3), 5669–5683.

Fontanier, C., Jorissen, F. J., Licari, L., Alexandre, A., Anschutz, P., Carbonel, P. (2002). Live benthic foraminiferal faunas from the Bay of Biscay: faunal density, composition, and microhabitats. *Deep-Sea Research I*, 49, 751-785.

Fontanier, C., Jorissen, F. J., Chaillou, G., David, C., Anschutz, P., Lafon, V. (2003). Seasonal and interannual variability of benthic foraminiferal faunas at 550 m depth in the Bay of Biscay. *Deep-Sea Research I*, 50, 457-494.

Frezza, V., Carboni, G. (2009). Distribution of recent foraminiferal assemblages near the Ombrone River mouth (Northern Tyrrhenian Sea, Italy). *Revue de Micropaléontologie*, 52, 43-66.

Gamito, T. J. (2007). "O Algarve e o Magrebe". Universidade do Algarve, Faro (in Portuguese).

García-Lafuente, J., Ruiz, J. (2007). The Gulf of Cadiz pelagic ecosystem: A review. *Progress in Oceanography*, 74, 228-251.

García- Lafuente, J., Delgado, J., Criado-Aldeanueva, F., Bruno, M., del Río, J., Vargas, J. M. (2006). Water mass circulation on the continental shelf of the Gulf of Cadiz. *Deep-Sea Research II*, 53, 1182-1197.

Garel, E., Ferreira, Ó. (2011). Monitoring estuaries using non-permanent stations: practical aspects and data examples. *Ocean Dynamics*, 61, 891-902.

Garel, E., Pino, L., Santos, A., Ferreira, Ó. (2009). Tidal and river discharge forcing upon water and sediment circulation at a rock-bound estuary (Guadiana Estuary, Portugal). *Estuarine, Coastal and Shelf Science*, 84, 269-281.

Gil, I. M., Abrantes, F., Hebbeln, D. (2006). The North Atlantic Oscillation forcing throughout the last 2000 years: Spatial variability as revealed by high-resolution marine diatom records from N and SW Europe. *Marine Micropaleontology*, 60, 113-129.

Gil-Romera, G., Carrión, J. S., Pausas, J. G., Sevilla-Callejo, M., Lamb, H. F., Fernández, S., Burjachs, F. (2010). Holocene fire activity and vegetation response in South-Eastern Iberia. *Quaternary Science Reviews*, 29(9-10), 1082-1092.

Giraudi, C., Mercuri, A. M., Seu, D. (2012). Holocene paleoclimatic in the northern Sahara margin (Jefara Plain, northwestern Libya). *The Holocene*, 23(3), 339-352.

Goineau, A., Fontanier, C., Jorissen, F., Buscail, R., Kerhervé, P., Cathalot, C., Pruski, A. M., Lantoine, F., Bourgeois, S., Metzger, E., Legrand, E., Rabouille, C. (2012). Temporal variability of live (stained) benthic foraminiferal faunas in a river-dominated shelf – Faunal response to rapid changes of the river influence (Rhône prodelta, NW Mediterranean). *Biogeosciences*, 9, 1367-1388.

González, R. and Dias, J. M. A. (2006). Sediment dispersal patterns on the northern Gulf of Cadiz Shelf: Which areas are influenced by anthropogenic sand starvation?. *Journal of Coastal Research*, SI 39, 572-577.

González, R., Dias, J. A., Ferreira, O. (2001). Recent rapid evolution of the Guadiana Estuary (Southwestern Iberian Peninsula). *Journal of Coastal Research*, SI 34, 516-524.

González, R., Dias, J. M. A., Lobo, F., Mendes, I. (2004). Sedimentological and paleoenvironmental characterisation of transgressive sediments on the Guadiana Shelf (Northern Gulf of Cadiz, SW Iberia). *Quaternary International*, 120, 133-144.

González, R., Araújo, M. F., Burdloff, D., Cachão, M., Cascalho, J., Corredeira, C., Dias, J. M. A., Fradique, C., Ferreira, J., Gomes, C., Machado, A., Mendes, I., Rocha, F. (2007). Sediment and pollutant transport in the Northern Gulf of Cadiz: A multi-proxy approach. *Journal of Marine Systems*, 68, 1-23.

González-Álvarez, R., Bernárdez, P., Pena, L. D., Francés, G., Prego, R., Diz, P., Vilas, F. (2005). Paleoclimatic evolution of the Galician continental shelf (NW of Spain) during the last 3000 years: from a storm regime to present conditions. *Journal of Marine Systems*, 54, 245-260.

Gooday, A. J., Rathburn, A. E. (1999). Temporal variability in living deep-sea benthic foraminifera: a review. *Earth-Science Reviews*, 46, 187-212.

Goodess, C. M., Jones, P. D. (2002). Links between circulation and changes in the characteristics of Iberian rainfall. *International Journal of Climatology*, 22, 1593-1615.

Goy, J. L., Zazo, C., Dabrio, C. J., Lario, J., Borja, F., Sierro, F. J., Flores, J. A. (1996). Global and regional factors controlling changes of coastlines in Southern Iberia (Spain) during the Holocene. *Quaternary Science Reviews*, 15, 773-780.

Gràcia, E., Dañobeitia, J., Vergés, J., Bartolomé, R., Córdoba, D. (2003). Crustal architecture and tectonic evolution of the Gulf of Cadiz (SW Iberian margin) at the convergence of the Eurasian and African plates. *Tectonics*, 22 (4), 1033.

Grimm, E. C. (1987). CONISS: A FORTRAN 77 program for stratigraphically constrained cluster analysis by the method of incremental sum of squares. *Computers & Geosciences*, 13(1), 13-35.

Grimm, E. C. (2004). TILIA ver. 2.0.2: A pollen program for analysis and display. Illinois State Museum, Springfield, IL, U.S.A.

Grootes, P. M., Stuiver, M., White, J. W. C., Johnsen, S., Jouzel, J. (1993). Comparison of oxygen isotope records from the GISP2 and GRIP Greenland ice cores. *Nature*, 366, 552-554.

Gutiérrez-Mas, J. M., Domínguez, S., López, F. (1994). Present-day sedimentation patterns of the Gulf of Cadiz northern shelf from heavy mineral analysis. *Geo-Marine Letters*, 14, 52–58.

Gutiérrez-Mas, J. M., Hernández-Molina, F. J., López-Aguayo, F. (1996). Holocene sedimentary dynamics on the Iberian continental shelf of the Gulf of Cadiz (SW Spain). *Continental Shelf Research*, 16(13), 1635–1653.

Gutiérrez-Mas, J. P. M., Sánchez, A., Dominguez, S., Muñoz-Perez, J. J. (2003). Multicycle sediments on the continental shelf of Cadiz (SW Spain). *Estuarine, Coastal and Shelf Science*, 57, 667-677.

Hammer, Ø., Harper, D. A. T., Ryan, P. D. (2008). PAST – PAlaeontological STatistics, ver. 1.81, http://folk.uio.no/ohammer/past/.

Hanebuth, T., Stattegger, K. (2004). Depositional sequences on a late Pleistocene-Holocene tropical siliciclastic shelf (Sunda Shelf, southeast Asia). *Journal of Asian Earth Sciences*, 23(1), 113-126.

Hanebuth, T., Stattegger, K., Grootes, P. M. (2000). Rapid flooding of the Sunda shelf: A late-glacial sea-level record. *Science*, 288, 1033-1035.

Hayward, B. W., Sabaa, A. T., Grenfell, H. R., Neil, H., Bostock, H. (2013). Ecological distribution of recent deep-water foraminifera around New Zealand. *Journal of Foraminiferal Research*, 43(4), 415-442.

Hedberg H. D. (Ed.) (1976). "International stratigraphic guide". John Wiley & Sons, New York.

Hijma, M. P., Cohen, K. M. (2010). Timing and magnitude of the sea-level jump precluding the 8200 yr event. *Geology*, 38, 275-278.

Holbourn, A., Henderson, A. S., MacLeod, N. (2013). "Atlas of Benthic Foraminifera". Wiley-Blackwell, John Wiley & Sons, Ltd., Publication.

Hughes, M. K. and Diaz, H. F. (Eds.) (1994). "The Medieval Warm Period". Kluwer, Dordrecht.

Hurrell, J. W. (1995). Decadal trends in the North Atlantic Oscillation: Regional temperatures and Precipitation. *Science*, 269, 676-679.

Hurrell, J. W., Van Loon, H. (1997). Decadal variations in climate associated with the North Atlantic Oscillation. *Climate Change*, 36, 301-326.

Hurrell, J. W., Deser, C. (2010). North Atlantic climate variability: The role of the North Atlantic Oscillation. *Journal of Marine Systems*, 79, 231-244.

Hurrell, J. W., Kushnir, Y., Ottersen, G., Visbeck, M. (2003). An overview of the North Atlantic Oscillation. *Geophysical Monograph Series*, American Geophysical Union, 134, 1-35.

Jalut, G., Amat, A. E., Bonnet, L., Gauquelin, T., Fontugne, M. (2000). Holocene climatic changes in the Western Mediterranean, from south-east France to south-east Spain. *Palaeogeography, Palaeoclimatology, Palaeoecology*, 160, 255-290.

Jalut, G., Dedoubat, J. J., Fontugne, M., Otto, T. (2009). Holocene circum-Mediterranean vegetation changes: Climate forcing and human impact. *Quaternary International*, 200, 4-18.

Jannink, N. T., Zachariasse, W. J., Van der Zwaan, G. J. (1998). Living (Rose Bengal stained) benthic foraminiferal from the Pakistan continental margin (northern Arabian Sea). *Deep-Sea Research I*, 45, 1483-1513.

Jiménez-Moreno, G., Anderson, R. S. (2012). Holocene vegetation and climate change recorded in alpine bog sediments from the Borreguilles de la Virgen, Sierra Nevada, southern Spain. *Quaternary Research*, 77, 44-53.

Jorissen, F. J. (1987). The distribution of benthic foraminifera in the Adriatic Sea. *Marine Micropaleontology*, 12, 21-48.

Jorissen, F. J. (1999). Benthic foraminiferal succession across Late Quaternary Mediterranean sapropels. *Marine Geology*, 153, 91-101.

Jorissen, F. J., Barmawidjaja, D. M., Puskaric, S., Van der Zwaan, G. J. (1992). Vertical distribution of benthic foraminifera in the northern Adriatic Sea: The relation with the organic flux. *Marine Micropaleontology*, 19(1-2), 131-146.

Jorissen, F. J., De Stigter, H. C., Widmark, J. G. V. (1995). A conceptual model explaining benthic foraminiferal microhabitats. *Marine Micropaleonotlogy*, 26, 3-15.

Jouanneau, J. M., Garcia, C., Oliveira, A., Rodrigues, A., Dias, J. A., Weber, O. (1998). Dispersal and deposition of suspended sedimento n the shelf off the Tagus and Sado estuaires, S.W. Portugal. *Progress in Oceanography*, 42, 233-257.

Jouanneau, J. M., Weber, O., Drago, T., Rodrigues, A., Oliveira, A., Dias, J. M. A., Garcia, C., Schmidt, S., Reyss, J. L. (2002). Recent sedimentation and sedimentary budgets on the western Iberian shelf. *Progress in Oceanography*, 52, 261-275.

Jones, R. W. (1994). "The Challenger Foraminifera". Oxford University Press, London.

Kaal, J., Carrión-Marco, Y., Asouti, E., Seijo, M. M., Martínez-Cortizas, A., Casáis, M. C., Boado, F. C. (2011). Long-term deforestation in NW Spain: linking the Holocene fire history to vegetation change and human activities. *Quaternary Science Reviews*, 30, 161-175.

Kineke, G. C., Sternberg, R. W., Trowbridge, J. H., Geyer, W. R. (1996). Fluid-mud processes on the Amazon continental shelf. *Continental Shelf Research*, 16, 667–696.

Krebs, C. J. (1989). "Ecological Methodology". Harper Collins Publishers.

Lambeck, K., Chappell, J. (2001). Sea level change through the last glacial cycle. *Science*, 292, 679-686.

Lantzsch, H., Hanebuth, T. J. J., Bender, V. B. (2009a). Holocene evolution of mud depocentres on a high-energy, low-accumulation shelf (NW Iberia). *Quaternary Research*, 72, 325-336.

Lantzsch, H., Hanebuth, T. J. J., Bender, V. B., Krastel, S. (2009b). Sedimentary architecture of a low-accumulation shelf since the Late Pleistocene (NW Iberia). *Marine Geology*, 259, 47-58.

Lantzsch, H., Hanebuth, T. J. J., Henrich, R. (2010). Sediment recycling and adjustment of deposition during deglacial drowning of a low-accumulation shelf (NW Iberia). *Continental Shelf Research*, 30, 1665-1679.

Lario, J., Zazo, C., Goy, J. L., Dabrio, C. J., Borja, F., Silva, P. G., Sierro, F., González, A., Soler, V., Yll, E. (2002). Changes in sedimentation trends in SW Iberian Holocene estuaries (Spain). *Quaternary International*, 93-94, 171-176.

Lebreiro, S. M, Francés, G., Abrantes, F. F. G., Díz, P., Bartels-Jonsdóttir, H. B., Stroynowski, Z. N., Gil, I. M., Pena, L. D., Rodrigues, T., Jones, P. D., Nombela, M. A., Alejo, I., Briffa, K. R., Harris, I., Grimalt, J. O. (2006). Climate change and coastal hydrographic response along the Atlantic Iberian margin (Tagus Prodelta and Muros Ría) during the last two millennia. *The Holocene*, 16, 1003-1015.

Leorri, E., Cearreta, A., Milne, G. (2012). Field observations and modelling of Holocene sea-level changes in the Southern Bay of Biscay: implication for understanding current rates of relative sea-level change and vertical land motion along the Atlantic coast of SW Europe. *Quaternary Science Reviews*, 42, 59-73.

Lesueur, P., Tastet, J. P., Marambat, L. (1996). Shelf mud fields formation within historical times: examples from offshore the Gironde estuary, France. *Continental Shelf Research*, 16(14), 1849-1870.

Lesueur, P., Jouanneau, J.-M., Boust, D., Tastet, J.-P., Weber, O. (2001). Sedimentation rates and fluxes in the continental shelf mud fields in the Bay of Biscay (France). *Continental Shelf Research*, 21, 1383-1401.

Lesueur, P., Tastet, J.-P., Weber, O. (2002). Origin and morphosedimentary evolution of fine-grained modern continental shelf deposits: the Gironde mud fields (Bay of Biscay, France). *Sedimentology*, 49, 1299-1320.

Levy, A., Mathieu, R., Poignant, A., Rosset-Moulinier, M., Ubaldo, M., Ambroise, D. (1993). Recent foraminifera from the continental margin of Portugal. *Micropaleontology*, 39, 75-87.

Levy, A., Mathieu, R., Poignant, A., Rousset-Moulinier, M., Ubaldo, M., Lebreiro, S. (1995). "Foraminifères actuels de la Marge Continentale Portugaise – Inventaire et Distribuition". Memórias do Instituto Geológico e Mineiro, Lisboa.

Lobo, F. J., Hernández-Molina, F. J., Somoza, L., Díaz del Río, V., Dias, J. M. A. (2001). The sedimentar record of the post-glacial transgression on the Gulf of Cadiz continental shelf (Southwest Spain). *Marine Geology*, 178, 171-195.

Lobo, F. J., Dias, J. M. A., González, R., Hernández-Molina, F. J., Morales, J. A., Díaz del Río, V. (2003). High-resolution seismic stratigraphy of a narrow, bedrock-controlled estuary: the Guadiana estuary system, SW Iberia. *Journal of Sedimentary Research*, 73, 973-986.

Lobo, F. J., Sánchez, R., González, R., Dias, J. M. A., Hernández-Molina, F. J., Fernández-Salas, L. M., Díaz del Río, V., Mendes, I. (2004). Contrasting styles of the Holocene highstand sedimentation and sediment dispersal systems in the northern shelf of the Gulf of Cadiz. *Continental Shelf Research*, 24, 461-482.

Lobo, F. J., Fernández-Salas, L. M., Hernández-Molina, F. J., González, R., Dias, J. M. A., Díaz del Río, V., Somoza, L. (2005). Holocene highstand deposits in the Gulf of Cadiz, SW Iberian Peninsula: A high-resolution record of hierarchical environmental changes. *Marine Geology*, 219(2-3), 109-131.

Loeblich, A. R., Tappan, H. (1987). "Foraminiferal genera and their classification". Van Nostrand Reinhold, New York.

Long, A. (2001). Mid-Holocene sea-level change and coastal evolution. *Progress in Physical Geography*, 25, 399-408.

López-Galindo, A., Rodero, J., Maldonado, A. (1999). Surface facies and sediment dispersal patterns: southeastern Gulf of Cadiz, Spanish continental margin. *Marine Geology*, 155, 83-98.

Loureiro, J. J. M., Nunes, M. N. F., Machado, M. L. R. (1986). "A Bacia Hidrográfica do Rio Guadiana". *In*: Monografias Hidrológicas dos Principais Cursos de Água de Portugal Continental. M.P.A.T., S.E.A.R.N. Direção-Geral dos Recursos e Aproveitamentos, pp. 341-407 (in Portuguese).

Loureiro, N. S., Coutinho, M. A. (1995). Rainfall changes and rainfall erosivity increase in the Algarve (Portugal). *Catena*, 24, 55-67.

Luterbacher, J., Xoplaki, E., Dietrich, D., Jones, P. D., Davies, T. D., Portis, D., Gonzalez-Rouco, J. F., von Storch, H., Gyalistras, D., Casty, C., Wanner, H. (2002). Extending North Atlantic Oscillation reconstructions back to 1500. *Atmospheric Science Letters*, doi:10.1006/asle.2001.0044.

Macedo, M. C. (1999). "Conchas Marinhas de Portugal". Editorial Verbo, Lisboa.

Machado, A., Rocha, F., Araújo, M. F., Vitali, F., Gomes, C., Dias, J. A. (2005). Geochemical characterization of surficial sediments from the southwestern Iberian continental shelf. *Ciencias Marinas*, 31(1B), 161-177.

Machado, A., Rocha, F., Gomes, C., Dias, J. (2007). Distribution and Composition of Suspended Particulate Matter in Guadiana Estuary (Southwestern Iberian Peninsula). *Journal of Coastal Research*, SI 50 (ICS 2007 Proceedings, Australia), 1040-1045.

Macias, S., Torres, C. (Coord.) (1998). "Portugal Islâmico: Os últimos sinais do Mediterrâneo". Museu Nacional de Arqueologia, Lisboa (in Portuguese).

Magalhães, F. (2001). "Os sedimentos da plataforma continental Portuguesa: contrastes espaciais, perspectiva temporal, potencialidades económicas". PhD Thesis, Universidade de Lisboa (in Portuguese).

Magalhães, N. (2002). "O Legado Arquitectónico Islâmico no Algarve". Instituto Português de Património Arquitectónico, Direção-Geral de Faro (in Portuguese).

Magny, M., Miramont, C., Sivan, O. (2002). Assessment of the impact of climate and anthropogenic factors on Holocene Mediterranean vegetation in Europe on the basis of palaeohydrological records. *Palaeogeography, Palaeoclimatology, Palaeoecology*, 186, 47-59.

Magny, M., Bégeot, C., Guiot, J., Peyron, O. (2003). Contrasting patterns of hydrological changes in Europe in response to Holocene climate cooling phases. *Quaternary Science Reviews*, 22, 1589-1596.

Magny, M., Vannière, B., Zanchetta, G., Fouache, E., Touchais, G., Petrika, L., Coussot, C., Walter-Simonnet, A.-V., Arnaud, F. (2009). Possible complexity of the climatic event around 4300-3800 cal. BP in the central and western Mediterranean. *The Holocene*, 19(6), 823-833.

Maldonado, A., Nelson, H. N. (1999). Interaction of tectonic and depositional processes that control the evolution of the Iberian Gulf of Cadiz margin. *Marine Geology*, 155, 217-242.

Mann, M. E., Bradley, R. S., Hughes, M. K. (1999). Northern hemisphere temperatures during the last millennium: inferences, uncertainties and limitations. *Geophysical Research Letters*, 26, 759–762.

Mann, M. E. (2002). "Little Ice Age". *In*: Encyclopedia of Global Environmental Change (Michael MacCracken and John Perry, Eds.), vol. 1 – "The Earth System: physical and chemical dimensions of global environmental change". John Wiley & Sons, Ltd.

Mann, M. E., Jones, P. D. (2003). Global surface temperatures over the past two millennia. *Geophysical Research Letters*, 30(15), DOI: 10.1029/2003GL017814.

Marquer, L., Pomel, S., Abichou, A., Schulz, E., Kaniewski, D., Van Campo, E. (2008). Late Holocene high resolution paleoclimatic reconstrction inferred from Sebkha Mhabeul, southeast Tunisia. *Quaternary Research*, 70, 240-250.

Martín-Puertas C., Valero-Garcés, B. L., Brauer, A., Mata, M. P., Delgado-Huertas, A., Dulski, P. (2009). The Iberian-Roman Humid Period (2600-1600 cal yr BP) in the Zoñar Lake varve record (Andalucía, southern Spain). *Quaternary Research*, 71, 108-120.

Martin-Vide, J., Lopez-Bustins, J.-A. (2006). The Western Mediterranean Oscillation and rainfall in the Iberian Peninsula. *International Journal of Climatology*, 26, 1455-1475.

Martínez-Cortizas, A., Costa-Casais, M., López-Sáez, J. A. (2009). Environmental change in NW Iberia between 7000 and 500 cal BC. *Quaternary International*, 200, 77-89.

Martins, V., Gomes, V. (2004). "Foraminíferos da Margem Continental NW Ibérica, Sistemática, Ecologia e Distribuição". Agenda Comum – Comunicação Lda. (in Portuguese).

Martins, V., Jouanneau, J.-M., Weber, O., Rocha, F. (2006). Tracing the late Holocene evolution of the NW Iberian upwelling system. *Marine Micropaleontology*, 59, 35-55.

Martins, V., Dubert, J., Jouanneau, J.-M., Weber, O., Ferreira da Silva, E., Patinha, C., Alveirinho Dias, J. M., Rocha, F. (2007). A multiproxy approach of the Holocene evolution of shelf-slope circulation on the NW Iberian Continental Shelf. *Marine Geology*, 239, 1-18.

Martins, R., Azevedo, M. R., Mamede, R., Sousa, B., Freitas, R., Rocha, F., Quintino, V., Rodrigues, A. M. (2012). Sedimentary and geochemical characterization and provenance of the Portuguese continental shelf soft-bottom sediments. *Journal of Marine Systems*, 91, 41-52.

Mattoso, J. (1995). "Identificação de um país: Ensaio sobre as origens de Portugal, 1096-1325. II – Composição". Editorial Estampa, Lisboa (in Portuguese).

Mattoso, J. (1998). A nobreza medieval portuguesa no contexto peninsular. *Revista da Faculdade de Letras do Porto – História*, série II, vol. 15, nº 2 (in Portuguese).

Mayewski, P. A., Meeker, L. D., Whitlow, S., Twickler, M. S., Morrison, M. C., Bloomfield, R., Bond, G. C., Alley, R. B., Gow, A. J., Grootes, P. M., Meese, D. A., Ram, M., Taylor, K. C., Wumkes, W. (1994). Changes in atmospheric circulation and ocean ice cover over the North-Atlantic during the last 41,000 years. *Science*, 263, 1747–1751.

Mayewski, P. A., Rohling, E. E., Stager, J. C., Karlén, W., Maasch, K. A., Meeker, L. D., Meyerson, E. A., Gasse, F., van Kreveld, S., Holmgren, K., Lee-Thorp, J., Rosqvist, G., Rack, F., Staubwasser, M., Schneider, R. R., Steig, E. J. (2004). Holocene climate variability. *Quaternary Research*, 62, 243-255.

Medialdea, T., Vegas, R., Somoza, L., Vázquez, J. T., Maldonado, A., Díaz-del-Río, V., Maestro, A., Córdoba, D., Fernández-Puga, M. C. (2004). Structure and evolution of the "Olistostrome" complex of the Gibraltar Arc in the Gulf of Cádiz (eastern Central Atlantic): evidence from two long seismic cross-sections. *Marine Geology*, 209 (1–4), 173-198.

Mendes, I., González, R., Dias, J. M. A., Lobo, F., Martins, V. (2004). Factors influencing recente benthic foraminifera distribution on the Guadiana shelf (Southwestern Iberia). *Marine Micropaleontology*, 51, 171-192.

Mendes, I., Rosa, F., Dias, J. A., Schönfeld, J., Ferreira, Ó., Pinheiro, J. (2010). Inner shelf paleoenvironmental evolution as a function of land-ocean interactions in the vicinity of the Guadiana River, SW Iberia. *Quaternary International*, 221, 58-67.

Mendes, I., Alveirinho Dias, J., Schönfeld, J., Ferreira, Ó. (2012a). Distribution of living benthic foraminiferal on the northern Gulf of Cadiz continental shelf. *Journal of Foraminiferal Research*, 42(1), 18-38.

Mendes, I., Dias, J. A., Schönfeld, J., Ferreira, Ó., Rosa, F., González, R., Lobo, F. J. (2012b). Natural and human-induced Holocene paleoenvironmental changes on the Guadiana shelf (northern Gulf of Cadiz). *The Holocene*, 22(9), 1011-1024.

Mendes, I., Dias, J. A., Schönfeld, J., Ferreira, Ó., Rosa, F., Lobo, F. J. (2013). Living, dead and fossil benthic foraminifera on a river dominated shelf (northern Gulf of Cadiz) and their use for paleoenvironmental reconstruction. *Continental Shelf Research*, 68, 91-111.

Mighall, T.M., Martínez Cortizas, A., Biester, H., Turner, S. E. (2006). Proxy climate and vegetation changes during the last five millennia in NW Iberia: Pollen and non-pollen palynomorph data from two ombrotrophic peat bogs in the North Western Iberian Peninsula. *Review of Palaeobotany and Palynology*, 141, 203-223.

Mil-Homens, M., Stevens, R. L., Abrantes, F., Cato, I. (2006). Heavy metal assessment for surface sediments from three areas of the Portuguese continental shelf. *Continental Shelf Research*, 26, 1184–1205.

Milker, Y., Schmiedl, G. (2012). A taxonomic guide to modern benthic shelf foraminifera of the western Mediterranean Sea. *Palaeontologica Electronica*, vol. 15, Issue 2; 16A.

Milker, Y., Schmiedl, G., Betzler, C., Römer, M., Jaramillo-Vogel, D., Siccha, M. (2009). Distribution of recent benthic foraminifera in shelf carbonate environments of the Western Mediterranean Sea. *Marine Micropaleontology*, 73, 207-225.

Mohamed, K. J., Rey, D., Rubio, B., Vilas, F., Frederichs, T. (2010). Interplay between detrital and diagenetic processes since the last glacial maximum on the northwest Iberian continental shelf. *Quaternary Research*, 73, 507-520.

Moita, I. (1985). Notícia explicativa da carta dos sedimentos superficiais do Cabo de S. Vicente ao Rio Guadiana, pp. SED 7 and 8. Instituto Hidrográfico, Lisboa (in Portuguese).

Mojtahid, M., Jorissen, F., Lansard, B., Fontanier, C., Bombled, B., Rabouille, C. (2009). Spatial distribution of live benthic foraminifera in the Rhône prodelta: Faunal response to a continental-marine organic matter gradient. *Marine Micropaleontology*, 70, 177-200.

Mojtahid, M., Jorissen, F. J., Garcia, J., Schiebel, R., Michel, E., Eynaud, F., Gillet, H., Cremer, M., Diz Ferreiro, P., Siccha, M., Howa, H. (2013). High resolution Holocene record in the southeastern Bay of Biscay: Global versus regional climate signals. *Palaeogeography, Palaeoclimatology, Palaeoecology*, 377, 28-44.

Monteiro, J. H., Dias, J. A., Gaspar, L. C., Possolo, A. M. (1982). "Recent marine sediments of the Portuguese Continental Shelf". *In*: Seminar on Actual Problems of Oceonography in Portugal, Lisboa.

Morales, J. A. (1997). Evolution and fácies architecture of the mesotidal Guadiana River delta (S.W. Spain-Portugal). *Marine Geology*, 138, 127-148.

Morales, J. A., Delgado, I., Gutiérrez-Mas, J. M. (2006). Sedimentary characterization of bed types along the Guadiana estuary (SW Europe) before the construction of the Alqueva dam. *Estuarine, Coastal and Shelf Science*, 70, 117-131.

Morellón, M., Valero-Garcés, B., Moreno, A., González-Sampériz, P., Mata, P., Romero, O., Maestro, M., Navas, A. (2008). Holocene paleohydrology and climate variability in northeastern Spain: The sedimentar record of Lake Estanya (Pre-Pyrenean range). *Quaternary International*, 181, 15-31.

Moreno, A., Pérez, A., Frigola, J., Nieto-Moreno, V., Rodrigo-Gámiz, M., Martrat, B., González-Sampériz, P., Morellón, M., Martín-Puertas, C., Corella, J. P., Belmonte, A., Sancho, C., Cacho, I., Herrera, G., Canals, M., Grimalt, J. O., Jiménez-Espejo, F., Martínez-Ruiz, F., Vegas-Vilarrúbia, T., Valero-Garcés, B. L. (2012). The Medieval Climate Anomaly in the Iberian Peninsula reconstructed from marine and lake records. *Quaternary Science Reviews*, 43, 16-32.

Morigi, C., Jorissen, F. J., Gervais, A., Guichard, S., Borsetti, A. M. (2001). Benthic foraminiferal faunas in surface sediments off NW Africa: relationship with organic flux to the ocean floor. *Journal of Foraminiferal Research*, 31(4), 350-368.

Morigi, C., Jorissen, F. J., Fraticelli, S., Horton, B. P., Principi, M., Sabbatina, A., Capotondi, L., Curzi, P. V., Negri, A. (2005). Benthic foraminiferal evidence for the formation of the Holocene mud-belt and bathymetrical evolution in the central Adriatic Sea. *Marine Micropaleontology*, 57, 25-49.

Mörner, N. A. (1993). Global change: the last millennia. *Global and Planetary Change*, 7(1/3), 211–217.

Moura, D., Veiga-Pires, C., Albardeiro, L., Boski, T., Rodrigues, A. L., Tareco, H. (2007). Holocene sea level fluctuations and coastal evolution in the central Algarve (Southern Portugal). *Marine Geology*, 237, 127-142.

Muñoz-Sobrino, C., Ramil-Rego, P., Gómez-Orellana, L., Díaz Varela, R. A. (2005). Palynological data on major Holocene climatic events in NW Iberia. Boreas, 34, 381–400.

Murray, J. (1971). "An Atlas of British Recent Foraminiferids". Heinemann Educational Books, London.

Murray, J. W. (1991). "Ecology and Palaeoecology of Benthic Foraminifera". Longman Scientific & Technical.

Murray, J. (2003). An illustrated guide to the benthic foraminifera of the Hebridean Shelf, West of Scotland, with notes on their mode of life. *Palaeontologica Electronica*, 5(1).

Murray, J. (2006). "Ecology and applications of benthic foraminifera". Cambridge University Press, Cambridge.

Nagy, J., Alve, E. (1987). Temporal changes in foraminiferal faunas and impact of pollution in Sandebukta, Oslo Fjord. *Marine Micropaleontology*, 12, 109-128.

Naughton, F., Sánchez Goñi, M. F., Désprat, V., Turon, J.-L., Duprat, J., Malaizé, B., Joli, C., Cortijo, E., Drago, T., Freitas, M. C. (2007a). Present-day and past (last 25 000 years) marine pollen signal off western Iberia. *Marine Micropaleontology*, 62, 91-114.

Naughton, F., Sánchez-Goñi, M. F., Drago, T., Freitas, M. C., Oliveira, A. (2007b). Holocene chnages in the Douro Estuary (Northwestern Iberia). *Journal of Coastal Research*, 23(3), 711-720.

Nelson, C. H., Baraza, J., Maldonado, A., Rodero, J., Escutia, C., Barber, J. H. Jr.ª (1999). Influence of the Atlantic inflow and Mediterranean outflow currents on Late Quaternary sedimentary facies of the Gulf of Cadiz continental margin. *Marine Geology*, 155, 99-129.

Nizou, J., Hanebuth, T. J. J., Heslop, D., Schwenk, T., Palamenghi, L., Stuut, J.-B., Henrich, R. (2010). The Senegal River mud belt: A high-resolution archive of paleoclimatic change and coastal evolution. *Marine Geology*, 278, 150-164.

Nittrouer, C. A., Wright, L. D. (1994). Transport of particles across continental shelves. *Revues of Geophysics*, 32, 85.

Nocete, F., Álex, E., Nieto, J. M., Sáez, R., Bayona, M. R. (2005). An archaeological approach to regional environmental pollution in the south-western Iberian Peninsula related to Third Millennium BC mining and metallurgy. *Journal of Archaeological Science*, 32, 1566-1576.

Oberle, F. K. J., Hanebuth, T. J. J., Baasch, B., Schwenk, T. (2014). Volumetric budget calculation of sediment and carbon storage and export for a late Holocene mid-shelf mudbelt system (NW Iberia). *Continental Shelf Research*, 76, 12-24.

Oliveira Marques, A. H. (1987). "Portugal na crise dos séculos XIV e XV". *In*: Nova História de Portugal (coord. Joel Serrão e A. H. Oliveira Marques), vol. IV. Editorial Presença, Lisboa (in Portuguese).

Oliveira Marques, A. H. (1993). "Portugal: das Invasões Germânicas à Reconquista". *In*: Nova História de Portugal (coord. Joel Serrão e A. H. Oliveira Marques), vol. II. Editorial Presença, Lisboa (in Portuguese).

Paiva, P., Jouanneau, J.-M., Araújo, F., Weber, O., Rodrigues, A., Dias, J. M. A. (1997). Elemental distribution in a sedimentary deposit on the shelf off the Tagus estuary (Portugal). *Water, Air, and Soil Pollution*, 99, 507–514.

Pessanha, L. E., Pires, H. O. (1981). "Elementos sobre o clima de agitação marítima na costa sul do Algarve". Instituto Nacional de Meteorologia e Geofísica, Lisboa (in Portuguese).

Pires, H. O. (1998). "Project INDIA, Preliminary report on Wave Climate at Faro". Instituto de Meteorologia, Lisboa (in Portuguese).

Portela, L. I. (2004). Sediment Delivery from the Guadiana Estuary to the Coastal Ocean. *Journal of Coastal Research*, SI 39 (ICS 2004 Proceedings, Brazil), 1819-1823.

Portela, L. I. (2008). Sediment transport and morphodynamics of the Douro River Estuary. *Geo-Marine Letters*, 28, 77-86.

Powers, M. C. (1953). A new roundness scale for sedimentary particles. *Journal of Sedimentary Petrology*, 23, 117–119.

Prieto, L., Navarro, G., Rodríguez-Galvéz, S., Huertas, I. E., Naranjo, J. M., Ruiz, J. (2009). Oceanographic and metereological forcing of the pelagic ecosystem on the Gulf of Cadiz shelf (SW Iberian Peninsula). *Continental Shelf Research*, 29, 2122-2137.

Relvas, P., Barton, E. D. (2002). Mesoscale patterns in the Cape São Vicente (Iberian Peninsula) upwelling region. *Journal of Geophysical Research*, 107(C10), 28, 1-23.

Relvas, P., Barton, E. D., Dubert, J., Oliveira, P. B., Peliz, Á., da Silva, J. C. B., Santos, A. M. P. (2007). Physical oceanography of the western Iberia ecosystem: Latest views and challenges. *Progress in Oceanography*, 74, 149-173.

Ribeiro, O. (1945). 'Portugal, o Mediterrâneo e o Atlântico: Estudo Geográfico'. Coleção Universitas, nº 5, Coimbra Editora, Coimbra (in Portuguese).

Ribeiro, O. (1987). 'A Formação de Portugal'. Instituto de Cultura e Língua Portuguesa, Lisboa (in Portuguese).

Rodero, J., Pallarés, L., Maldonado, A. (1999). Late Quaternary seismic facies of the Gulf of Cadiz Spanish margin: depositional processes influenced by sea-level change and tectonic controls. *Marine Geology*, 155, 131-156.

Rodriguez-Puebla, C., Encinas, A. H., Nieto, S., Garmendia, J. (1998). Spatial and temporal patterns of anual precipitation variability over the Iberian Peninsula. *International Journal of Climatology*, 18, 299-316.

Rosa, F., Dias, J. A., Mendes, I., Ferreira, Ó. (2011). Mid to late Holocene constraints for continental shelf mud deposition in association with river input: the Guadiana Mud Patch (SW Iberia). *Geo-Marine Letters*, 31, 109-121.

Rosa, F., Rufino, M. M., Ferreira, Ó., Matias, A., Brito, A. C., Gaspar, M. B. (2013). The influence of coastal processes on inner shelf sediment distribution: The Eastern Algarve Shelf (Southern Portugal). *Geologica Acta*, vol. 11, nº 1, 59-73.

Rossi, V., Vaiani, S. C. (2008). Benthic foraminiferal evidence of sediment supply changes and fluvial drainage reorganization in Holocene deposits of the Po Delta, Italy. *Marine Micropaleontology*, 69, 106-118.

Roque, C. (1998). "Análise Morfosedimentar da sequência deposicional do Quaternário Superior da Plataforma Continental Algarvia entre Faro e a foz do Guadiana". Master Thesis, Universidade de Lisboa (in Portuguese).

Roussiez, V., Aloisi, J.-C., Monaco, A., Ludwig, W. (2005). Early muddy deposits along the Gulf of Lions shoreline: A key for a better understanding of land-to-sea transfer of sediments and associated pollutant fluxes. *Marine Geology*, 222-223, 345-358.

Ruddiman, W. F., McIntyre, A. (1981). The North Atlantic Ocean during the last deglaciation. *Palaeogeography, Palaeoclimatology Palaeoecology*, 35, 145–214.

Ruiz, F., González-Regalado, M. L., Pendón, J. G., Abad, M., Olías, M., Muñoz, J. M. (2005). Correlation between foraminifera and sedimentary environments in recente estuaries of Southwestern Spain: Applications to Holocene reconstructions. *Quaternary International*, 140-141, 21-36.

Ruiz, J., Navarro, G. (2006). Upwelling spots and vertical velocities in the Gulf of Cadiz: An approach for their diagnose by combining temperature and ocean colour remote sensing. *Deep-Sea Research II*, 53, 1282-1293.

Sarnthein, M. (1971). Oberflächensedimente im Persischen Golf und Golf von Oman, 11. Quantitative Komponentenanalyse der Grobfraktion. *"Meteor" Forschungs-Ergebnisse*, 5, 1-113.

Schilman, B., Bar-Matthews, M., Almogi-Labin, A., Luz, B. (2001). Global climate instability reflected by Eastern Mediterranean marine records during the late Holocene. *Palaeogeography, Palaeoecology, Palaeoecology*, 176, 157-176.

Schmiedl, G., de Bovée, F., Buscail, R., Charrière, B., Hemleben, C., Medernach, L., Picon, P. (2000). Trophic control of benthic foraminiferal abundance and microhabitat in the bathyal Gulf of Lions, western Mediterranean Sea. *Marine Micropaleontology*, 40, 167-188.

Schneider, H. E., Cailleux, A. (1959). Signification géomorphologique des formes des grains de sable des Etats-Unis. *Geomorphology*, 3, 114–125.

Schneider, H., Höfer, D., Trog, C., Busch, S., Schneider, M., Baadi, J., Daut, G., Mäusbacher, R. (2010). Holocene estuary development in the Algarve Region (Southern Portugal) – A reconstruction of sedimentological and ecological evolution. *Quaternary International*, 221, 141-158.

Sen Gupta, B (1999). "Modern Foraminifera" (B. Sen Gupta, Ed.). Kluwer Academic Publishers, Dordrecht/Boston/London.

Serrão, J. V. (1986). "O Terceiro Liberalismo (1851-1890)". *In*: História de Portugal, vol. IX. Editorial Verbo, Lisboa (in Portuguese).

Sierro, F. J., Flores, J. A., Baraza, J. (1999). Late glacial to recent paleoenvironmental chenages in the Gulf of Cadiz and formation of sandy contourite layers. *Marine Geology*, 155, 157-172.

Silva, K. A., Corliss, B., Rathburn, A. E., Thunell, R. C. (1996). Seasonality of living benthic foraminifera from the San Pedro Basin, California borderland. *Journal of Foraminiferal Research*, 26(1), 71-93.

Shakun, J. D., Carlson, A. E. (2010). A global perspective on Last Glacial Maximum to Holocene climate change. *Quaternary Science Reviews*, 29, 1801-1816.

Smith, D. E., Harrison, S., Firth, C. R., Jordan, J. T. (2011). The early Holocene sea level rise. *Quaternary Science Reviews*, 30, 1846-1860.

Soares; A. M., Matos Martins, J. M. (2010). Radiocarbon dating of marine samples from Gulf of Cadiz: The reservoir effect. *Quaternary International*, 221, 9-12.

Sommerfield, C., Nittrouer, C., 1999. Modern accumulation rates and a sediment budget for the Eel shelf: a flood-dominated depositional environment. *Marine Geology*, 154, 227–241.

Sommerfield, C. K., Wheatcroft, R. A. (2007). Late Holocene sediment accumulation on the northern California shelf: Oceanic, fluvial, and anthropogenic influences. *Geological Society of America Bulletin*, 119(9-10), 1120-1134.

Somoza, L., Hernández-Molina, F. J., De Andrés, J. R., Rey, J. (1997). Continental shelf architecture and sea-level cycles: Late Quaternary high-resolution stratigraphy of the Gulf of Cadiz (Spain). *Geo-Marine Letters*, 17, 133–139.

Strabo – Geographica, III, 1, 9. Translation by Velozo, F., J. and Cardoso, J. (1965). Primeira Contribuição para uma Nova Edição Crítica. Colecção Amphitheatrum nº IX, Centro de Estudos Humanísticos, Universidade do Porto, Porto (in Portuguese).

Stuiver, M., Reimer, P. J. (1993). Extended 14C database and revised CALIB radiocarbon calibration program. *Radiocarbon*, 35, 215-230.

Stuiver, M., Grootes, P.M., Brazunias, T.F. (1995). The GISP2 $d^{18}O$ record of the past 16,500 years and the role of the Sun, ocean and volcanoes. *Quaternary Research*, 44, 341–354.

Stuiver, M., Reimer, P. J., Reimer, R. W. (2005). CALIB Radiocarbon calibration ver. 5.0.1, http://calib.qub.ac.uk/calib/.

Teixeira, S. B., Gaspar, P., Rosa, M. (2005). "Holocene sea-level índex points on the Quarteira Coast (Algarve, Portugal)". *In*: Coastal Hope Proceedings (M. C. Freitas and T. Drago, Eds.), Lisbon.

Telford, R. J., Heegaard, E., Birks, H. J. B. (2004). All age-depth models are wrong: but how badly?. *Quaternary Science Reviews*, 23, 1-5.

Thorndycraft, V. R., Benito, G. (2006). Late Holocene fluvial chronology of Spain: The role of climatic variability and human impact. *Catena*, 66, 34-41.

Torelli, L., Sartori, R., Zitellini, N. (1997). The giant chaotic body in the Atlantic Ocean off Gibraltar: new results from a deep seismic reflection survey. *Marine and Petroleum Geology*, 14(2), 125-138.

Trigo, R. M., Pozo-Vásquez, V., Orborn, T. J., Castro-Díez, Y., Gámiz-Fortis, S., Esteban-Parra, J. (2004). North Atlantic Oscillation influence on precipitation, river flow and water resources in the Iberian Peninsula. *International Journal of Climatology*, 24, 925-944.

Trouet, V., Esper, J., Graham, N. E., Baker, A., Scource, J. D., Frank, D. C. (2009). Persistent positive North Atlantic Oscillation mode dominated the Medieval Climate Anomaly. *Science*, 324, 78-80.

Trouet, V., Scource, J. D., Raible, C. C. (2012). North Atlantic storminess and Atlantic Meridional Overturning Circulation during the last Millennium: Reconciling contradictory proxy records of NAO variability. *Global and Planetary Change*, 84-85, 48-55.

Ulses, C., Estournel, C., Durrieu de Madron, X., Palanques, A. (2008). Suspended sediment transport in the Gulf of Lions (NW Mediterranean): Impacto f extreme storms and floods. *Continental Shelf Research*, 28(15), 2071-2091.

van Andel, T. H., Heath, G. R., Moore, T. C. (1975). Cenozoic history and palaeoceanography of the central equatorial Pacific ocean. *Memoir of the Geological Society of America*, 143, 1-134.

Vanney, J., Mougenot, D. (1981). "La plate-forme continentale du Portugal et les provinces adjacentes: Analyse geomorphologique". Memórias dos Serviços Geológicos de Portugal, 28.

Villanueva, P. G., Cervera, J. L. C. (1999a). Distribution of Planorbulinacea (benthic foraminifera) assemblages in surfasse sediments on the northern Gulf of Cadiz. *Boletín Instituto Español de Oceanografía*, 15, 181-190.

Villanueva, P. G., Cervera, J. L. C. (1999b). The recent Uvigerinids (benthic foraminifera) in the northeastern Gulf of Cadiz. *Boletín Instituto Español de Oceanografía*, 15, 191-202.

Vis, G.-J., Kasse, C., Vanderbergh, J. (2008). Late Pleistocene and Holocene palaeogeography of the Lower Tagus Valley (Portugal): effects of relative sea level, valley morphology and sediment supply. *Quaternary Science Reviews*, 27, 1682-1709.

Visbeck, M. H., Hurrell, J. W., Polvani, L., Cullen, H. M. (2001). "The North Atlantic Oscillation: Past, present, and future". *In*: PNAS (Proceedings of the National Academy of Sciences of the U.S.A), vol. 98, nº 23, 12876-12877.

Vargas, J. M., García-Lafuente, J., Delgado, J., Criado, F. (2003). Seasonal and wind-induced variability of Sea Surface Temperature patterns in the Gulf of Cadiz. *Journal of Marine Systems*, 38, 205-219.

Wanner, H., Beer, J., Bütikofer, J., Crowley, T. J., Cubasch, U., Flückiger, J., Goosse, H., Grosjean, M., Joos, F., Kaplan, J. O., Küttel, M., Müller, S. A., Prentice, I. C., Solomina, O., Stocker, T. F., Tarasov, P., Wagner, M., Widmann, M. (2008). Mid- to Late Holocene climate change: an overview. *Quaternary Science Reviews*, 27, 1791-1828.

Wanner, H., Solomina, O., Grosjean, M., Ritz, S., Jetel, M. (2011). Structure and origin of Holocene cold events. *Quaternary Science Reviews*, 30, 3109-3123.

Zazo, C., Dabrio, C. J., Goy, J. L., Lario, J., Cabero, A., Silva, P. G., Bardaji, T., Mercier, N., Borja, F., Roquero, E. (2008). The coastal archives of the last 15 ka in the Atlantic-Mediterranean Spanish linkage area: Sea level and climate changes. *Quaternary International*, 181, 72-87.

Zielhofer, C., Faust, D., Diaz del Olmo, F., Escudero, R. B. (2002). Sedimentation and soil formation phases in the Ghardimaou Basin (northern Tunisia) during the Holocene. *Quaternary International*, 93-94, 109-125.

APPENDICES

Appendix A: **Vibrocore1** - Relative abundances (%) of taxa with more than one specimen for all sampled levels (cm), number of taxa with one specimen and total of specimens counted in each sample. In bold are the main species (> 5% in at least one sample) identified in vibrocore 1.

Core levels	**3-4**	**9-10**	**19-20**	**28-30**	**38-40**	**48-50**	**58-60**	**68-70**	**78-80**	**88-90**	**98-100**	**108-110**	**116-118**	**128-130**
Number of taxa with one specimen	17	14	15	14	14	11	14	7	11	16	12	12	13	13
Total (n)	624	395	365	387	419	342	435	419	345	562	378	357	419	348
Taxa														
Abditodentrix asketocomptella														
Adelosina laevigata														
Adelosina cf. *granulocostata*														
Ammoglobigerina globigeriniformis	0.3													
Ammonia beccarii	1.1	2.0	1.4	2.1	1.7	2.0	1.8	3.3	2.9	1.2	0.8	0.6	1.0	2.6
Amphycorina scalaris					0.5								0.5	
Amphycorina separans							0.5			0.5				
Asterigerinata mamila			0.5			0.6								
Bolivina alata	0.3												0.5	
Bolivina albatrossi	0.2			0.8				0.5						
Bolivina difformis		0.8		0.5	0.5	0.6				0.4		0.6		
Bolivina inflata														
Bolivina ordinaria	14.3	12.4	16.4	14.0	12.6	15.2	16.1	15.3	8.1	12.1	12.7	10.4	12.9	9.8
Bolivina pseudoplicata							0.7							
Bolivina seminuda				0.5		0.6		0.5						
Bolivina striatula	5.9	3.3	9.3	8.5	9.5	6.7	4.6	5.5	5.8	1.4	3.2	7.8	10.0	5.7
Bolivina subspinescens	1.3	2.0	1.1	1.8	2.9	2.9	4.1	2.9	1.7	1.2	2.1	4.5	1.7	3.4
Bolivina tortuosa var. *atlantica*								0.5						
Bolivina cf. *acerosa*	0.6	1.5	1.1	0.8					2.0	0.7		0.8		
Bolivina cf. *plicata*														
Bolivina cf. *skagerrakensis*		0.5	0.5	1.3										
Bolivina sp	0.9	1.0			1.2	0.9	1.8	0.5	0.6	1.6	0.5	2.0		
Brizalina dilatata	16.3	19.5	16.7	12.1	14.6	10.8	17.7	16.0	16.8	18.7	11.9	14.8	15.3	19.3

(Cont.)

Core levels	**3-4**	**9-10**	**19-20**	**28-30**	**38-40**	**48-50**	**58-60**	**68-70**	**78-80**	**88-90**	**98-100**	**108-110**	**116-118**	**128-130**
Taxa														
Brizalina spathulata	2.2	1.5	1.4	1.0	1.4	0.9	2.1	1.4	2.9	1.4	0.8	2.2	0.7	1.4
Brizalina subaeraniensis	1.1				1.0	4.4	3.0		2.3	0.5	1.9	1.4	1.2	1.7
Buccella frigida														
Bulimina acanthia														
Bulimina aculeata	2.1	1.0	0.8	3.1	1.0		1.4		2.6	1.6	2.6		1.0	2.3
Bulimina elegans					0.5	0.6					0.8			
Bulimina elongata	1.0	1.0		0.8	1.0	0.6	1.1		1.2	0.5	1.6	0.6	1.0	1.4
Bulimina gibba						0.6	0.5	0.7						
Bulimina marginata	7.4	9.4	6.8	9.6	9.3	8.2	3.0	11.5	9.3	8.7	8.7	10.6	8.1	7.5
Bulimina striata					1.2	0.6	0.7	0.5	1.7		0.5	0.6		1.1
Bulimina cf. *pseudoaffinis*	0.6	0.5			0.7		0.7			0.4	0.5	0.8		
Cassidulina crassa													0.7	0.6
Cassidulina laevigata	13.8	13.9	14.0	13.7	13.4	14.3	16.1	11.9	13.9	14.4	19.8	11.8	14.3	15.2
Cassidulina minuta	5.4	7.8	9.9	8.3	5.3	6.4	6.7	5.3	5.8	8.2	9.3	7.3	8.8	4.9
Cassidulina teretis			0.5		0.7			0.7	1.7		0.8	1.1	2.1	2.3
Cassidulinoides bradyi										0.4	0.5			
Cibicides cf. *ungerianus*														
Cibicidoides bradyi														
Cibicidoides pachyderma														
Cribrononion gerthi	2.1	2.5	1.6	2.3	5.5	2.9	2.8	4.1	1.4	1.8	3.2	3.4	2.1	4.9
Discorbinella berthelotti				0.8		0.6	0.5	0.5				0.6		0.9
Discorbis williamsoni														
Elphidium advenum														
Elphidium complanatum														
Elphidium crispum														
Elphidium cuvillieri														
Elphidium discoidale														

(Cont.)

Core levels	**3-4**	**9-10**	**19-20**	**28-30**	**38-40**	**48-50**	**58-60**	**68-70**	**78-80**	**88-90**	**98-100**	**108-110**	**116-118**	**128-130**
Taxa														
Elphidium excavatum										0.7				
Elphidium macellum														
Eoeponidella pulchella														
Epistominella exigua	11.1	4.6	4.1	5.4	3.1	4.7	3.0	2.4	6.4	6.2	1.3	1.4	3.3	1.1
Epistominella vitrea							0.5	0.5	2.3	0.9	1.3		1.4	
Fissurina annectens														
Fissurina fimbriata	0.3				0.7			0.5		0.5	1.1			
Fissurina laevigata														
Fissurina sp										0.4				
Fursenkoina complanata	0.5	1.5	1.6			0.6				1.1	1.6	0.6		0.6
Gavelinopsis praegeri														
Globocassidulina subglobosa								0.5			0.5		0.5	
Gyroidina umbonata	1.4	0.8	1.9	1.3				0.5	1.7	1.1	2.6	2.0	1.2	
Haynesina depressula														
Haynesina germanica														
Haynesina sp														
Heterolepa pseudoungerianus														
Hyalinea balthica	1.6	3.3	2.7	2.3	3.3	5.3	3.2	3.1	1.4	2.7	1.3	3.9	3.1	3.4
Lagena sulcata										0.4				
Lamarckina haliotidea														
Lobatula lobatula														
Nonion fabum	0.3	1.8	0.5	1.6	2.4	2.0		2.4	0.9	1.8		1.7	0.7	1.1
Nonionella iridea	0.5		0.5						0.6					
Nonionella stella														
Nonionella turgida														
Nonionella sp														
Planorbulina mediterranensis														

(Cont.)

Core levels	**3-4**	**9-10**	**19-20**	**28-30**	**38-40**	**48-50**	**58-60**	**68-70**	**78-80**	**88-90**	**98-100**	**108-110**	**116-118**	**128-130**
Taxa														
Quinqueloculina lata														
Quinqueloculina seminulum														
Quinqueloculina stalkeri	0.3													
Quinqueloculina venusta														
Rectuvigerina phlegeri	1.9	1.0					0.5		1.2	0.4	0.8		0.5	
Reussella spinulosa														
Rosalina bradyi														
Rosalina globularis var. *anglica*														
Rosalina rugosa														
Rosalina vilardeboana														
Rubratella intermedia														
Stainforthia feylingi														
Stainforthia fusiformis														
Stainforthia sp														
Textularia candeiana									0.9			0.8		
Textularia deltoidea	0.3													
Trifarina bradyana														
Trifarina carinata				0.8	0.5	1.2	0.9			1.1	0.8	0.8	0.5	2.0
Uvigerina mediterranea		0.5	0.5	0.8	1.2		1.6	1.7		1.1	1.9	2.0	1.4	2.3
Uvigerina peregrina	0.6			0.5	1.2	2.6		1.0	0.6	0.5				0.6
Uvigerina spp (juv.)				0.8				0.5		2.7				
Valvulineria bradyana	1.4	2.3	1.6	0.8							1.3	1.7	2.4	

Core levels	**138-140**	**148-150**	**158-160**	**168-170**	**178-180**	**186-188**	**198-200**	**208-210**	**220-222**	**240-242**	**270-272**
Number of taxa with one specimen	11	11	18	14	19	20	27	21	20	16	26
Total (n)	445	295	295	356	328	296	302	296	348	317	300
Taxa											
Abditodentrix asketocomptella						0.7					
Adelosina laevigata											
Adelosina cf. *granulocostata*											
Ammoglobigerina globigeriniformis											
Ammonia beccarii	1.6	3.1	4.4	4.5	8.2	15.2	11.9	11.1	8.6	17.4	9.7
Amphycorina scalaris											
Amphycorina separans											
Asterigerinata mamila	0.4	0.7	4.4	9.3	10.1	12.2	12.9	16.2	25.3	18.3	25.0
Bolivina alata											
Bolivina albatrossi											
Bolivina difformis											0.7
Bolivina inflata					0.6						
Bolivina ordinaria	8.8	11.5	21.0	19.9	14.3	3.7	6.6	9.8	12.9	16.7	13.7
Bolivina pseudoplicata			1.4	0.6	2.4	5.7	5.0	5.4	2.6	2.5	3.0
Bolivina seminuda											
Bolivina striatula	4.5	3.1		0.6	1.2			0.7	0.6		1.0
Bolivina subspinescens	2.9	1.0								0.6	
Bolivina tortuosa var. *atlantica*											
Bolivina cf. *acerosa*											
Bolivina cf. *plicata*								1.0			
Bolivina cf. *skagerrakensis*											
Bolivina sp	0.7										
Brizalina dilatata	23.1	18.6	14.2	10.1	7.3	8.1	4.3	5.1	2.3	1.9	1.7

(Cont.)

Core levels	**138-140**	**148-150**	**158-160**	**168-170**	**178-180**	**186-188**	**198-200**	**208-210**	**220-222**	**240-242**	**270-272**
Taxa											
Brizalina spathulata	1.1			0.6	0.9		1.0			0.6	
Brizalina subaeraniensis	2.2	3.4	4.4	1.1	0.9				0.6		
Buccella frigida			2.4	0.6	3.7		1.3	0.7			
Bulimina acanthia						0.7	0.7				1.3
Bulimina aculeata	1.3	4.1			0.6				1.7		
Bulimina elegans		0.7	0.7	1.1	0.6		1.0		1.4	0.9	3.0
Bulimina elongata	0.4	2.4	1.0	3.1	0.6	1.0	0.7	2.0	6.3	6.9	5.3
Bulimina gibba						1.7			2.6	0.9	1.0
Bulimina marginata	5.8	3.1	1.4	1.1	0.9	0.7			0.6		
Bulimina striata	1.6							0.7			
Bulimina cf. *pseudoaffinis*			0.7								
Cassidulina crassa		1.4		0.8	0.6		1.3	1.0	0.6		
Cassidulina laevigata	20.0	19.0	16.9	16.0	6.1	5.4	3.0	4.4	3.2	4.4	4.3
Cassidulina minuta	3.1	2.7	4.1	4.2	1.8	4.4	2.3	4.4	0.9	0.9	1.7
Cassidulina teretis	0.9	4.1		1.4	2.1		1.3				1.0
Cassidulinoides bradyi											
Cibicides cf. *ungerianus*					1.2	0.7	1.3	1.0			
Cibicidoides bradyi											
Cibicidoides pachyderma											
Cribrononion gerthi	5.6	8.5	7.5	7.0	15.5	20.9	20.5	19.9	6.0	4.1	7.3
Discorbinella berthelotti	1.6	0.7	1.0								
Discorbis williamsoni											
Elphidium advenum											
Elphidium complanatum				0.6				0.7		0.6	
Elphidium crispum							0.7	1.0			
Elphidium cuvillieri				0.6		0.7			1.1	2.2	1.7
Elphidium discoidale							1.0				

(Cont.)

Core levels	138-140	148-150	158-160	168-170	178-180	186-188	198-200	208-210	220-222	240-242	270-272
Taxa											
Elphidium excavatum											
Elphidium macellum						0.7					
Eoeponidella pulchella									0.6		
Epistominella exigua	1.1		0.7		1.2		2.6		2.3		2.7
Epistominella vitrea		1.0	1.7	2.0	1.5	1.7		1.0			
Fissurina annectens											0.7
Fissurina fimbriata											
Fissurina laevigata							0.7				
Fissurina sp											0.7
Fursenkoina complanata									0.6		
Gavelinopsis praegeri					1.2	0.7	2.6	0.7	0.6	0.6	1.7
Globocassidulina subglobosa	0.4					2.0	1.7		0.9		
Gyroidina umbonata											
Haynesina depressula			0.7	0.6					0.6		
Haynesina germanica						0.7			0.6	0.9	1.3
Haynesina sp							1.0				
Heterolepa pseudoungerianus				0.8	1.5	1.7	1.3	1.0		1.3	1.0
Hyalinea balthica	5.6	2.4	0.7	0.6	0.9						
Lagena sulcata											
Lamarckina haliotidea											
Lobatula lobatula								1.0			
Nonion fabum	2.0	1.7	2.7	2.8	0.9		0.7		0.6	0.9	
Nonionella iridea				0.8	0.6						
Nonionella stella					1.5				4.6	2.5	
Nonionella turgida				0.6						0.6	
Nonionella sp	0.4				0.9						0.7
Planorbulina mediterranensis											

(Cont.)

Core levels	138-140	148-150	158-160	168-170	178-180	186-188	198-200	208-210	220-222	240-242	270-272
Taxa											
Quinqueloculina lata							0.7				
Quinqueloculina seminulum										0.9	
Quinqueloculina stalkeri											
Quinqueloculina venusta											
Rectuvigerina phlegeri				2.2					0.9		
Reussella spinulosa											
Rosalina bradyi											
Rosalina globularis var. *anglica*											
Rosalina rugosa		0.7									
Rosalina vilardeboana										0.6	
Rubratella intermedia											
Stainforthia feylingi					0.6						
Stainforthia fusiformis				0.6	0.6			0.7	3.4	5.0	
Stainforthia sp											
Textularia candeiana					2.1	1.4		2.0	0.9	0.6	
Textularia deltoidea										0.9	
Trifarina bradyana						1.4					
Trifarina carinata		2.0		1.1	0.6		2.3	1.4	0.6	0.6	1.3
Uvigerina mediterranea	1.3	0.7	2.0								
Uvigerina peregrina	0.7					0.7					
Uvigerina spp (juv.)											
Valvulineria bradyana				0.8		0.7	0.7				

Core levels	**284-286**	**308-310**	**320-322**	**328-330**	**366-368**	**376-378**
Number of taxa with one specimen	30	23	19	19	25	40
Total (n)	295	307	305	303	312	303
Taxa						
Abditodentrix asketocomptella						
Adelosina laevigata						1.3
Adelosina cf. *granulocostata*						0.7
Ammoglobigerina globigeriniformis						
Ammonia beccarii	2.4	10.7	13.1	10.2	3.2	1.0
Amphycorina scalaris						
Amphycorina separans						
Asterigerinata mamila	25.1	23.8	19.3	21.1	25.6	19.1
Bolivina alata						
Bolivina albatrossi						
Bolivina difformis			1.6	0.7	1.0	1.3
Bolivina inflata						0.7
Bolivina ordinaria	10.8	6.5	3.9	5.9	15.1	5.9
Bolivina pseudoplicata	4.4	5.9	8.5	3.3	4.2	5.6
Bolivina seminuda						
Bolivina striatula	1.0					1.0
Bolivina subspinescens						
Bolivina tortuosa var. *atlantica*						
Bolivina cf. *acerosa*						
Bolivina cf. *plicata*	0.7	1.0			3.2	
Bolivina cf. *skagerrakensis*						
Bolivina sp						
Brizalina dilatata	2.7	1.6	2.3		0.6	1.3

(Cont.)

Core levels	284-286	308-310	320-322	328-330	366-368	376-378
Taxa						
Brizalina spathulata						
Brizalina subaeraniensis					0.6	
Buccella frigida	2.7	2.6		0.7		
Bulimina acanthia						
Bulimina aculeata	1.4					1.3
Bulimina elegans	1.7	1.6	1.6	1.3		
Bulimina elongata	2.7	3.9	10.8	6.6	1.3	
Bulimina gibba		0.7	2.3	1.0	0.6	1.0
Bulimina marginata						
Bulimina striata						
Bulimina cf. *pseudoaffinis*					0.6	
Cassidulina crassa		0.7	1.0	0.7	0.6	1.3
Cassidulina laevigata	3.1	2.0	0.7	0.7		2.0
Cassidulina minuta	0.7	0.7		2.0	1.9	3.3
Cassidulina teretis				0.7		0.7
Cassidulinoides bradyi						
Cibicides cf. *ungerianus*		2.3		2.0	1.3	
Cibicidoides bradyi				0.7		
Cibicidoides pachyderma		0.7				
Cribrononion gerthi	10.5	7.8	10.8	10.6	9.6	8.6
Discorbinella berthelotti					0.6	
Discorbis williamsoni				0.7		
Elphidium advenum				0.7		
Elphidium complanatum		0.7		2.3		
Elphidium crispum				0.7		
Elphidium cuvillieri		0.7	0.7		2.6	
Elphidium discoidale						

(Cont.)

Core levels	284-286	308-310	320-322	328-330	366-368	376-378
Taxa						
Elphidium excavatum	2.4	2.3		2.0	2.6	
Elphidium macellum	0.7	0.7	1.0	1.0	0.6	1.0
Eoeponidella pulchella			0.7			1.3
Epistominella exigua	1.7	0.7				2.3
Epistominella vitrea					4.2	
Fissurina annectens						
Fissurina fimbriata						
Fissurina laevigata						
Fissurina sp				0.7		0.7
Fursenkoina complanata		0.7	1.3			
Gavelinopsis praegeri	2.0	5.2	0.7	4.0	2.6	3.3
Globocassidulina subglobosa		1.0		1.7	1.0	2.6
Gyroidina umbonata						0.7
Haynesina depressula						
Haynesina germanica		2.3	1.0		1.6	
Haynesina sp						
Heterolepa pseudoungerianus	0.7		1.0	1.3	1.3	3.0
Hyalinea balthica						
Lagena sulcata						
Lamarckina haliotidea				1.0	0.6	0.7
Lobatula lobatula						
Nonion fabum	0.7					
Nonionella iridea						0.7
Nonionella stella	1.7		2.0			1.0
Nonionella turgida						
Nonionella sp	0.7			0.7	0.6	1.3
Planorbulina mediterranensis	1.0		1.3	0.7		

(Cont.)

Core levels	284-286	308-310	320-322	328-330	366-368	376-378
Taxa						
Quinqueloculina lata	1.0			1.0		2.3
Quinqueloculina seminulum			1.6			
Quinqueloculina stalkeri						
Quinqueloculina venusta	0.7					
Rectuvigerina phlegeri						
Reussella spinulosa			0.7			
Rosalina bradyi		0.7				
Rosalina globularis var. *anglica*					1.0	
Rosalina rugosa						
Rosalina vilardeboana			0.7		0.6	
Rubratella intermedia		0.7				
Stainforthia feylingi				0.7		
Stainforthia fusiformis	2.0		3.6	1.0		6.3
Stainforthia sp	1.0					1.0
Textularia candeiana	0.7		0.7			0.7
Textularia deltoidea						
Trifarina bradyana	0.7			1.3		
Trifarina carinata	2.4	4.9	1.0	4.6	1.6	2.0
Uvigerina mediterranea						
Uvigerina peregrina						
Uvigerina spp (juv.)						
Valvulineria bradyana					1.0	

Appendix B: **Vibrocore 6** - Relative abundances (%) of taxa with more than one specimen for all sampled levels (cm), number of taxa with one specimen and total of specimens counted in each sample. In bold are the main species (> 5% in at least one sample) identified in vibrocore 6.

Core levels	**4-5**	**9-10**	**39-40**	**52-54**	**58-60**	**68-70**	**82-84**	**88-90**	**100-102**	**110-112**	**118-120**	**128-130**
Number of taxa with one specimen	25	12	21	14	9	19	14	15	28	15	15	16
Total (n)	411	362	382	377	343	315	383	401	452	354	313	318
Taxa												
Ammonia beccarii	2.7	3.9	1.8	1.6	2.6	2.2	2.6	0,5	4.0	3.4	2.2	1,9
Amphicoryna catesbyi												
Amphicoryna scalaris				0.8				0,7		0.6		
Asterigerinata mamilla			1.0	1.3	1.5	1.9			0.7	1.1	1.9	2,8
Bolivina cf. *acerosa*	0.5	0.8	0.5	0.8	0.6	0.6			0.4			0,9
Bolivina difformis							0.5					
Bolivina inflata												
Bolivina ordinaria	17.3	25.1	26.2	25.7	26.2	31.1	32.1	35,9	26.8	22.3	25.9	28,6
Bolivina plicata												
Bolivina pseudoplicata				0.5	0.6	0.6	1.0	0,7	1.1	0.8	1.6	1,3
Bolivina seminuda	1.2					0.6			1.8	0.8		
Bolivina striatula							0.5	0,7	0.4	0.6	0.6	1,6
Brizalina dilatata	11.4	9.1	7.9	12.2	8.7	9.8	11.2	15,7	8.2	4.5	9.6	10,1
Brizalina spathulata	3.2	3.9	2.4	2.1	2.6	1.3		1,0	1.1	0.6	1.0	0,6
Brizalina subaeraniensis						1.3	0.5	0,5		0.6	1.3	
Buccella frigida												
Bulimina aculeata	5.4	1.9		2.9	3.2		3.1	0,7	3.5	3.4	4.2	0,6
Bulimina alazanensis	0.7											
Bulimina elegans							0.5	1,2				0,6
Bulimina elongata	0.7	4.1	4.2	4.5	4.7	3.5	2.3	3,0	2.7	2.3	1.6	1,6
Bulimina exilis		1.1			0.6		1.6	1,7	0.4	1.4		
Bulimina gibba	1.7	3.0	1.6	0.5	1.2		1.3	0,5	0.7	0.8	0.6	0,9
Bulimina marginata	3.2	3.0	2.4	2.7	2.3	3.2	3.9	5,2	2.0	3.4	4.2	2,2
Bulimina striata												
Bulimina cf. *pseudoaffinis*			0.8		0.9							

(Cont.)

Core levels	**4-5**	**9-10**	**39-40**	**52-54**	**58-60**	**68-70**	**82-84**	**88-90**	**100-102**	**110-112**	**118-120**	**128-130**
Taxa												
Bulimina sp			0.5									
Buliminella tenuata									1.5	0.6		
Buliminella sp												
Cassidulina crassa					0.6							
Cassidulina laevigata	9.5	13.0	12.8	9.3	10.2	8.3	12.0	9.0	5.3	9.0	7.0	9.7
Cassidulina minuta	5.1	1.4	2.9	4.2	3.5	5.4	2.9	1.7	2.9	1.1	3.5	2.2
Cassidulina teretis	2.4	0.8	1.3	3.2	2.3	1.0	1.8	0.7	1.1	2.0	0.6	0.9
Cassidulinoides bradyi						0.6						
Cibicides cf. *ungerianus*											1.0	
Cibicidoides pachyderma												
Cribrononion gerthi		2.5	5.0	2.7	5.0	6.7	3.9	1.2	5.3	5.1	5.8	7.2
Discorbinella berthelotti			0.5				0.5					
Discorbis williamsoni												
Elphidium cuvillieri	0.5	3.3	3.7	1.1	1.5	2.2	0.5	1.2	1.1	1.1	1.3	1.3
Elphidium discoidale		0.6										
Elphidium excavatum	3.2	0.8		1.1								
Elphidium macellum				0.5						1.1		
Eoeponidella pulchella												
Epistominella exigua	9.2		3.7	4.5	4.1	1.9	4.4	5.5	9.3	2.8	1.9	2.2
Epistominella vitrea		1.7										
Fissurina laevigata				0.8					0.4			
Fissurina lucida						0.6				0.6		0.6
Fissurina marginata												
Fissurina orbygniana										0.6		
Fissurina staphyllearia			0.5									
Fissurina sp				0.8			0.8					

(Cont.)

Core levels	**4-5**	**9-10**	**39-40**	**52-54**	**58-60**	**68-70**	**82-84**	**88-90**	**100-102**	**110-112**	**118-120**	**128-130**
Taxa												
Fursenkoina complanata	1.7	1.1		1.9	2.0	0.6	0.5	2.5	2.7	2.3	1.9	3.1
Fursenkoina loeblichi	0.5								0.4			
Gavelinopsis praegeri			0.8	0.5			0.8			2.5	1.3	2.8
Globobulimina ovata											0.6	
Globocassidulina subglobosa		0.6			0.6	0.6	0.5		0.4			
Gyroidina umbonata			0.5	0.5	0.9	1.0			0.7			
Haynesina depressula												
Haynesina germanica												
Haynesina sp												
Heterolepa pseudoungerianus			0.5			0.6						
Hopkinsina atlantica	0.5											
Hyalinea balthica										0.6	0.6	
Lagena semistriata												
Lamarckina haliotidea												
Lobatula lobatula			0.5			0.6				0.8		0.6
Neoconorbina terquemi												
Nonion fabum	2.4	3.0	5.2	2.4	2.0	3.5	2.3	2.7	1.8	4.2	2.2	3.1
Nonionella sp	0.7						0.5					
Nonionella iridea									0.7			
Nonionella turgida	1.2								0.4			
Planorbulina mediterranensis											0.6	
Quinqueloculina lata					0.9							
Rectuvigerina phlegeri	4.1	3.3		3.2	2.3	1.3	1.8	2.0	2.7	6.5	4.5	2.8
Rosalina bradyi												
Rosalina globularis var. *anglica*												
Rosalina rugosa												0.6
Rosalina vilardeboana												

(Cont.)

Core levels	**4-5**	**9-10**	**39-40**	**52-54**	**58-60**	**68-70**	**82-84**	**88-90**	**100-102**	**110-112**	**118-120**	**128-130**
Taxa												
Rubratella intermedia												
Sigmoilinita tenuis												
Sigmoilopsis schlumbergeri										1.4	1.0	0.9
Spiroplectammina wrighti										0.6		0.6
Stainforthia feylingi		0.6										
Stainforthia fusiformis	0.5											
Stainforthia sp									1.1			
Strebloides advenus									0.4			
Textularia agglutinans					0.6							
Textularia candeiana									0.4	3.1	1.0	0.6
Textularia deltoidea									0.4		0.6	
Trifarina bradyana												0.6
Trifarina carinata	1.5	2.5	2.1	1.6	2.6	1.0	0.5	0.7	0.9	2.3	3.5	0.9
Uvigerina mediterranea								0.5			0.6	
Uvigerina peregrina		0.6										
Valvulineria bradyana	2.9	5.0	5.2	2.4	2.6	1.9	1.0			0.8	1.0	

Core levels	**143.5-145**	**153-155**	**161-163**	**171-173**	**183-185**	**193-195**	**203-205**	**213-215**	**221-223**	**231-233**	**241-243**
Number of taxa with one specimen	19	23	18	18	17	21	21	22	22	18	27
Total (n)	370	400	308	344	382	442	353	338	389	323	299
Taxa											
Ammonia beccarii	1.6	4.8	3.9	4.4	2.6	3.4	3.4	1.5	2.8	4.3	2.7
Amphicoryna catesbyi	0.5				0.5						
Amphicoryna scalaris											
Asterigerinata mamilla	2.4	7.0	10.1	11.3	9.9	8.1	13.0	20.7	10.5	17.0	19.7
Bolivina cf. *acerosa*	0.5		1.0	1.2	0.8		1.1	0.9		0.6	
Bolivina difformis						0.5	0.6				
Bolivina inflata											
Bolivina ordinaria	42.4	22.3	21.4	19.2	22.3	24.4	18.1	23.4	29.0	20.4	26.4
Bolivina plicata											
Bolivina pseudoplicata		1.5	2.6	2.3	2.1	1.8	2.3	3.8	2.8	2.2	2.0
Bolivina seminuda	0.5		0.6		0.5						
Bolivina striatula		0.5	1.0	0.6		0.5	0.6				
Brizalina dilatata	9.7	8.8	8.8	8.4	9.9	12.7	5.7	6.5	8.5	4.3	5.4
Brizalina spathulata	0.5	1.0	1.3	2.0	2.6	2.3	1.7	1.5	1.5	0.9	0.7
Brizalina subaeraniensis	1.1	0.5			0.5				0.8	0.6	
Buccella frigida				0.6		0.5	0.6				
Bulimina aculeata	1.9		2.3	1.7	1.0	1.6	1.4		0.5		
Bulimina alazanensis											
Bulimina elegans	0.8	0.5	1.0		1.0	0.9		0.9	1.3		
Bulimina elongata	2.4	3.5		3.5	2.1	1.1	2.8	3.3	2.1	2.5	3.3
Bulimina exilis				0.6							
Bulimina gibba	0.5				0.8		0.6		0.5	0.9	
Bulimina marginata	2.2	1.0		1.5	1.3	1.4	2.3				
Bulimina striata					0.5						
Bulimina cf. *pseudoaffinis*	0.8					0.5	0.6		0.8		

(Cont.)

Core levels	**143.5-145**	**153-155**	**161-163**	**171-173**	**183-185**	**193-195**	**203-205**	**213-215**	**221-223**	**231-233**	**241-243**
Taxa											
Bulimina sp		0.8		0.6							
Buliminella tenuata		0.5			0.5						
Buliminella sp											
Cassidulina crassa	6.2	8.8	7.8	6.1	6.0	6.1	7.6	2.7	5.9	4.6	4.3
Cassidulina laevigata	1.9	1.8	1.9	2.0		2.3	2.8	2.4	2.3	0.9	2.0
Cassidulina minuta	0.8	1.0	0.6	1.5	1.6	1.1	0.8	0.6	0.5	1.5	1.3
Cassidulina teretis						0.5					
Cassidulinoides bradyi	0.5			0.6		0.5					
Cibicides cf. *ungerianus*					0.5			0.6			
Cibicidoides pachyderma	2.7	7.5	6.8	6.7	9.7	6.1	10.5	11.8	7.7	7.4	7.4
Cribrononion gerthi		0.8	1.9	1.7	0.5	0.5	1.4	0.6	0.8	1.2	1.0
Discorbinella berthelotti				0.6							
Discorbis williamsoni	0.8	3.0	1.0	1.2	1.0	2.3	2.5	1.5	0.8	2.5	0.7
Elphidium cuvillieri											
Elphidium discoidale											
Elphidium excavatum		1.0		0.6	0.5			0.6			1.7
Elphidium macellum						0.5				0.6	1.0
Eoeponidella pulchella	3.0	2.8	2.6	0.9	1.6	0.5	0.8	0.9	2.3	1.2	
Epistominella exigua											
Epistominella vitrea											
Fissurina laevigata										0.9	
Fissurina lucida									0.5		
Fissurina marginata											
Fissurina orbygniana											
Fissurina staphyllearia											
Fissurina sp		0.8		0.6							

(Cont.)

Core levels	**143.5-145**	**153-155**	**161-163**	**171-173**	**183-185**	**193-195**	**203-205**	**213-215**	**221-223**	**231-233**	**241-243**
Taxa											
Fursenkoina complanata	1.4	0.8	1.6	0.9		0.5	1.1	0.6	2.1	0.9	1.3
Fursenkoina loeblichi					0.5						
Gavelinopsis praegeri	2.2	2.0	1.9	1.2	1.6	0.9	0.8	0.6	0.5	2.5	
Globobulimina ovata											
Globocassidulina subglobosa		0.8				0.5	0.8	0.6	1.3		
Gyroidina umbonata											
Haynesina depressula											
Haynesina germanica						0.7					
Haynesina sp											0.7
Heterolepa pseudoungerianus		1.0						0.6			
Hopkinsina atlantica											
Hyalinea balthica											
Lagena semistriata	0.5										
Lamarckina haliotidea											
Lobatula lobatula					0.5		0.8				
Neoconorbina terquemi											
Nonion fabum	0.8	3.5	5.2	4.4	3.9	3.8	3.4	1.2	3.1	5.9	4.3
Nonionella sp											
Nonionella iridea											0.7
Nonionella turgida											
Planorbulina mediterranensis											
Quinqueloculina lata											
Rectuvigerina phlegeri	2.2	2.3	2.9	3.5	2.9	2.9	2.5	2.1	3.3	5.6	3.3
Rosalina bradyi		0.5									
Rosalina globularis var. *anglica*											
Rosalina rugosa						0.9			1.0	0.9	
Rosalina vilardeboana											

(Cont.)

Core levels	**143.5-145**	**153-155**	**161-163**	**171-173**	**183-185**	**193-195**	**203-205**	**213-215**	**221-223**	**231-233**	**241-243**
Taxa											
Rubratella intermedia					0.8						
Sigmoilinita tenuis				0.6							
Sigmoilopsis schlumbergeri	1.4	1.0	1.0		0.8	0.7					
Spiroplectammina wrighti											
Stainforthia feylingi						0.5					
Stainforthia fusiformis		0.5									
Stainforthia sp										0.6	
Strebloides advenus											
Textularia agglutinans											
Textularia candeiana	1.4			0.6	1.6	0.5					
Textularia deltoidea			0.6								
Trifarina bradyana			0.6								
Trifarina carinata	1.1	1.5	1.6	2.9	1.8	3.8	2.5	3.3	1.0	3.1	1.0
Uvigerina mediterranea							0.6				
Uvigerina peregrina			0.6					0.6			
Valvulineria bradyana		1.5	1.3	1.2	0.5						

Core levels	**253-255**	**261-263**	**271-273**	**281-283**	**293-295**
Number of taxa with one specimen	16	18	21	15	19
Total (n)	371	365	435	349	362
Taxa					
Ammonia beccarii	3.5	1.4	1.1	1.4	1.9
Amphicoryna catesbyi					
Amphicoryna scalaris					
Asterigerinata mamilla	28.0	26.0	23.2	30.9	29.6
Bolivina cf. *acerosa*		0.5	0.7	0.6	0.8
Bolivina difformis			0.5		
Bolivina inflata		0.8			
Bolivina ordinaria	25.9	28.2	28.7	20.1	23.2
Bolivina plicata	0.5	0.8			
Bolivina pseudoplicata	2.2	2.5	5.1	3.7	5.8
Bolivina seminuda					
Bolivina striatula	0.5		1.6		
Brizalina dilatata	2.4	2.5	2.5	3.2	0.6
Brizalina spathulata	0.5				0.6
Brizalina subaeraniensis	1.1				
Buccella frigida					0.6
Bulimina aculeata	0.8	0.8	1.1		
Bulimina alazanensis					
Bulimina elegans	1.1		0.5	0.9	0.6
Bulimina elongata	4.9	3.6	3.4	4.0	5.0
Bulimina exilis			0.5		
Bulimina gibba	0.5	2.5	0.9	1.4	0.8
Bulimina marginata					
Bulimina striata					
Bulimina cf. *pseudoaffinis*			0.7	0.9	

(Cont.)

Core levels	253-255	261-263	271-273	281-283	293-295
Taxa					
Bulimina sp					
Buliminella tenuata					
Buliminella sp					
Cassidulina crassa					
Cassidulina laevigata	2.4	3.8	1.1	0.9	1.1
Cassidulina minuta	1.9	2.5	2.1	0.9	3.0
Cassidulina teretis	0.8	0.5	0.7	1.1	
Cassidulinoides bradyi					
Cibicides cf. *ungerianus*					
Cibicidoides pachyderma					
Cribrononion gerthi	6.7	7.1	7.6	9.2	4.4
Discorbinella berthelotti	0.5	1.1	0.9		1.4
Discorbis williamsoni					
Elphidium cuvillieri	1.1	0.8	1.6	1.1	
Elphidium discoidale					
Elphidium excavatum					
Elphidium macellum			0.5	0.6	
Eoeponidella pulchella					
Epistominella exigua					
Epistominella vitrea					
Fissurina laevigata					
Fissurina lucida					
Fissurina marginata					
Fissurina orbygniana					
Fissurina staphyllearia					
Fissurina sp			0.9		

(Cont.)

Core levels	**253-255**	**261-263**	**271-273**	**281-283**	**293-295**
Taxa					
Fursenkoina complanata	0.5		0.5	1.1	0.6
Fursenkoina loeblichi					
Gavelinopsis praegeri		0.5	0.5		0.8
Globobulimina ovata					
Globocassidulina subglobosa	1.3				0.8
Gyroidina umbonata					
Haynesina depressula	1.1			1.1	0.8
Haynesina germanica			0.5		
Haynesina ***sp***		0.5			
Heterolepa pseudoungerianus			0.7	0.9	1.1
Hopkinsina atlantica					
Hyalinea balthica					
Lagena semistriata					0.6
Lamarckina haliotidea	0.5		0.5		
Lobatula lobatula		0.5			
Neoconorbina terquemi			0.5		
Nonion fabum	2.2	3.3	2.5	4.3	2.2
Nonionella sp					
Nonionella iridea					0.6
Nonionella turgida					
Planorbulina mediterranensis				0.9	
Quinqueloculina lata					
Rectuvigerina phlegeri	1.3	1.1	1.6	2.0	1.1
Rosalina bradyi					
Rosalina globularis var. *anglica*					0.6
Rosalina rugosa					1.7
Rosalina vilardeboana				1.4	0.6

(Cont.)

Core levels	253-255	261-263	271-273	281-283	293-295
Taxa					
Rubratella intermedia					
Sigmoilinita tenuis					
Sigmoilopsis schlumbergeri					
Spiroplectammina wrighti					
Stainforthia feylingi					
Stainforthia fusiformis					
Stainforthia sp					
Strebloides advenus					
Textularia agglutinans					
Textularia candeiana					
Textularia deltoidea					
Trifarina bradyana	0.5		0.7		
Trifarina carinata	2.7	3.6	1.4	3.2	4.1
Uvigerina mediterranea					
Uvigerina peregrina					
Valvulineria bradyana					

Appendix C: **Vibrocore 14** - Relative abundances (%) of taxa with more than one specimen for all sampled levels (cm), number of taxa with one specimen and total of specimens counted in each sample. In bold are the main species (> 5% in at least one sample) identified in vibrocore 14.

Core levels	**3-4**	**9-10**	**19-20**	**29-30**	**39-40**	**49-50**	**58-60**	**68-70**	**78-80**	**88-90**	**98-100**	**108-110**	**118-120**	**128-130**
Number of taxa with one specimen	20	13	24	22	18	9	20	27	20	15	10	19	17	16
Total (n)	321	322	340	306	376	283	324	304	318	330	407	304	393	417
Taxa														
Ammonia beccarii		2.8	0.6	2.6	1.6	0.7	2.2	1.3	0.6	0.6	1.0	0.7	1.3	1.9
Amphicoryna scalaris														
Amphicoryna separans														
Asterigenata mamilla	0.9	0.9	0.9	0.7				0.7		0.6	0.7		0.8	1.2
Bolivina albatrossi														
Bolivina difformis	0.6				0.5				0.9				0.5	
Bolivina inflata				1.0				0.7				0.7		
Bolivina ordinaria	25.5	17.7	17.6	16.3	14.1	18.0	20.7	16.8	15.4	13.9	16.5	16.1	19.8	18.5
Bolivina pseudoplicata					0.5	0.7		1.3	0.6		0.7	1.0	1.3	0.7
Bolivina seminuda	2.2	0.6		0.7	2.1					1.2	0.5		0.8	0.7
Bolivina striatula	1.2	5.0	2.1	2.0	0.8	0.7	0.6		2.5	0.6	1.5	2.3	0.8	2.9
Bolivina subspinescens	0.9	1.6	0.6							0.6				
Bolivina cf. *acerosa*				0.7										
Bolivina sp						1.1								
Brizalina dilatata	15.3	18.6	22.9	22.9	22.6	24.0	18.5	17.1	19.2	25.8	21.9	19.4	18.8	24.7
Brizalina spathulata	1.9	3.4	2.1		0.8	2.8	2.2	1.6	1.9	2.4	1.5	2.3	1.8	0.5
Brizalina subaeraniensis	1.2		1.2		1.6	0.7				0.9	0.5		0.8	1.2
Brizalina translucens	0.6													
Buccella frigida														
Bulimina aculeata	1.6	3.1	1.5		0.5		0.6	1.3	0.6	0.9	2.0	0.7	1.5	3.1
Bulimina elegans		0.6			0.8						0.5			
Bulimina elongata	0.6	1.2	0.9	2.0	4.5	3.2	0.9	2.6	1.9	1.2	0.7	1.6	1.8	1.7
Bulimina exilis		0.6		1.6	0.8			1.0						0.5
Bulimina gibba		0.9		1.6		1.1		0.7		0.6	1.0	1.0	0.8	1.0
Bulimina marginata	2.5	5.3	6.8	5.9	11.4	9.2	7.1	5.9	7.5	8.8	6.6	9.2	6.1	4.8

(Cont.)

Core levels	3-4	9-10	19-20	29-30	39-40	49-50	58-60	68-70	78-80	88-90	98-100	108-110	118-120	128-130
Taxa														
Bulimina striata			0.6										1.0	
Bulimina cf. *pseudoaffinis*			0.6						1.3	0.9	1.0			
Bulimina sp												1.0		
Buliminella tenuata	1.2													
Cassidulina crassa	0.6	0.6												
Cassidulina laevigata	6.2	10.6	11.2	12.7	12.2	15.9	16.4	16.1	15.1	12.4	14.3	9.5	14.5	13.7
Cassidulina minuta	6.2	2.5	5.0	4.6	4.3	4.2	7.4	6.3	8.5	6.7	7.6	5.9	4.8	2.6
Cassidulina teretis		2.2				0.7		3.0	3.8	3.0	1.5	4.3	2.3	0.7
Cibicides cf. *ungerianus*														
Cribrononion gerthi		4.3	5.3	5.2	3.5	2.5	4.9	3.6	3.5	3.6	2.9	7.9	6.9	6.2
Discorbinella berthelotti		0.6	0.9			0.7					1.0			
Discorbis williamsoni	0.6										0.5	1.0		
Elphidium cuvillieri											0.5			
Elphidium magellanicum			0.6											
Eoeponidella pulchella	0.6													
Epistominella exigua	8.1	2.2	3.8	2.3	1.1	2.8	3.4	1.3	1.6	1.8	3.7	2.6	1.3	2.9
Epistominella vitrea	3.1	1.6	2.4	1.0	0.8		2.2	4.3	2.8	2.4	2.5		0.8	
Fissurina annectens											0.5			0.5
Fissurina fimbriata									0.6				0.5	
Fissurina laevigata	0.6													
Fissurina lucida	0.6													
Fissurina marginata												0.7		
Fissurina sp									0.6					
Fursenkoina loeblichi	0.6			0.7										
Fursenkoina complanata	1.9	1.2			1.1		1.5	0.7	1.6	0.9	1.7	0.7		0.7
Globocassidulina subglobosa													0.8	
Gyroidina umbonata	0.6						0.9							

(Cont.)

Core levels	**3-4**	**9-10**	**19-20**	**29-30**	**39-40**	**49-50**	**58-60**	**68-70**	**78-80**	**88-90**	**98-100**	**108-110**	**118-120**	**128-130**
Taxa														
Hansenisca soldanii						0.7					0.7			
Hanzawaia nitidula														
Hyalinea balthica	0.9	0.9	0.6	1.0	1.9		0.9	1.6	1.3	0.9		1.0	1.8	
Haynesina depressula											0.5			
Heterolepa pseudoungerianus														
Melonis affinis														
Mississipina concentrica														
Neolenticulina peregrina														
Nonion fabum		0.9	1.5	2.3	1.9	3.2		1.6	0.6	2.1	0.7	1.3	2.8	1.7
Nonionella iridea	0.9							0.7						
Nonionella stella	0.6													
Rectuvigerina phlegeri	3.4	1.2	1.2	1.0	0.5		0.6				0.5	0.7	0.5	1.0
Stainforthia feylingi	0.6													
Textularia candeiana														
Textularia deltoidea														
Textularia sagittula														
Trifarina bradyana									0.6	1.2				
Trifarina carinata	0.9	1.2					0.9				0.5			1.7
Uvigerina mediterranea					1.1						0.7	0.7	1.0	0.7
Uvigerina peregrina		0.6	0.6				0.6		0.6					0.5
Uvigerina sp			0.6											
Valvulineria bradyana		2.8	1.2	4.2	4.3	3.9	0.6	1.0		1.2	0.7	1.6		

Core levels	**141-143**	**151-153**	**161-163**	**171-173**	**181-183**	**191-193**	**201-203**	**211-213**	**221-223**	**231-233**	**235-237**
Number of taxa with one specimen	9	18	10	22	18	14	22	19	25	18	19
Total (n)	387	306	338	362	300	322	368	353	331	350	449
Taxa											
Ammonia beccarii	1.6	1.6	2.4	2.2	1.7	1.2	2.4	0.8	2.1	1.1	1.8
Amphicoryna scalaris				0.6							
Amphicoryna separans				0.6							
Asterigenata mamilla	1.3	1.3		1.4	0.7		0.5		0.9	0.6	0.4
Bolivina albatrossi											0.4
Bolivina difformis											
Bolivina inflata											
Bolivina ordinaria	14.2	16.0	15.7	10.2	17.3	23.0	16.6	14.7	13.0	16.6	17.1
Bolivina pseudoplicata	0.8		0.9	0.6	2.0	0.6	1.4	0.6		1.4	1.1
Bolivina seminuda				0.8			0.5	1.1	0.6		
Bolivina striatula	1.8	1.6	2.4	2.5	2.7	3.1			2.4	2.0	1.3
Bolivina subspinescens		2.3		0.6	1.0		2.7	0.6	0.9	0.6	0.4
Bolivina cf. *acerosa*									0.9	0.6	
Bolivina sp	0.5								0.6		
Brizalina dilatata	23.0	23.5	25.1	16.0	21.3	20.5	20.9	19.8	19.3	24.0	25.6
Brizalina spathulata	1.3	2.3	2.4	2.5	2.0	2.8	1.4	2.5	1.2	1.4	2.9
Brizalina subaeraniensis	1.8	1.3	1.2	1.4	1.7	1.6	0.5	0.6	1.5	1.7	0.4
Brizalina translucens											
Buccella frigida										1.1	0.7
Bulimina aculeata	1.3	1.6	1.2	2.5	3.3		1.4	1.4	2.4	0.6	1.1
Bulimina elegans	1.0						0.5				
Bulimina elongata	1.3	2.0	1.5	0.8	1.7	0.9	0.5	0.6	2.1	1.1	2.0
Bulimina exilis	0.5		0.6					0.6	0.6		
Bulimina gibba	0.5		1.2	0.8	1.7	0.9	1.9	0.8			
Bulimina marginata	5.4	6.5	3.3	5.5	6.3	1.2	3.8	4.8	4.2	3.1	4.0

(Cont.)

Core levels	**141-143**	**151-153**	**161-163**	**171-173**	**181-183**	**191-193**	**201-203**	**211-213**	**221-223**	**231-233**	**235-237**
Taxa											
Bulimina striata				0.8			0.5	1.1			
Bulimina cf. *pseudoaffinis*				1.1		0.6			0.6	0.6	0.4
Bulimina sp											
Buliminella tenuata											
Cassidulina crassa										0.6	0.4
Cassidulina laevigata	14.0	12.7	11.8	13.5	9.3	13.0	12.5	15.0	10.9	11.4	12.0
Cassidulina minuta	7.0	2.3	5.3	4.7	3.0	2.5	5.4	5.1	4.8	5.1	3.8
Cassidulina teretis	1.6	0.7		1.9	1.7		1.4	2.3	0.9	2.0	2.7
Cibicides cf. *ungerianus*								0.6			
Cribrononion gerthi	9.3	5.9	9.2	4.1	5.0	5.6	6.5	5.7	6.9	7.7	5.6
Discorbinella berthelotti				0.6	0.7	1.6	1.1	1.4		1.1	1.3
Discorbis williamsoni											
Elphidium cuvillieri		1.0		0.8					0.6		
Elphidium magellanicum											
Eoeponidella pulchella								0.6			
Epistominella exigua	2.3	2.3	2.4	1.1	1.3	3.1	1.6	3.4	2.1	2.9	0.4
Epistominella vitrea						3.4			0.9		1.8
Fissurina annectens											
Fissurina fimbriata	0.5	0.7									0.4
Fissurina laevigata											
Fissurina lucida											
Fissurina marginata					0.7						
Fissurina sp							1.1	0.6			
Fursenkoina loeblichi					0.7						
Fursenkoina complanata	0.8			0.6	0.7	0.6	0.5	0.6	0.9	0.9	0.4
Globocassidulina subglobosa						0.9					
Gyroidina umbonata											0.4

(Cont.)

Core levels	141-143	151-153	161-163	171-173	181-183	191-193	201-203	211-213	221-223	231-233	235-237
Taxa											
Hansenisca soldanii										0.6	
Hanzawaia nitidula				0.6					0.6		
Hyalinea balthica		2.6	1.8	1.1	1.7	1.2	1.4	1.7	2.1	2.0	0.9
Haynesina depressula								0.8			
Heterolepa pseudoungerianus								0.6			
Melonis affinis								0.6			
Mississipina concentrica									0.6		
Neolenticulina peregrina											0.4
Nonion fabum	1.8	1.6	3.0	4.7	1.0	2.8	3.8	1.1	2.1	2.6	1.8
Nonionella iridea							0.5		0.9		
Nonionella stella											
Rectuvigerina phlegeri	1.3		0.6	1.9	3.0	1.2		2.8	2.4	0.9	0.9
Stainforthia feylingi											
Textularia candeiana			1.2	1.7		0.9			0.6		
Textularia deltoidea											0.4
Textularia sagittula			0.6								
Trifarina bradyana											
Trifarina carinata	0.5		1.5		0.7	1.2		0.6			0.7
Uvigerina mediterranea	1.3	1.6	0.9	1.9	0.7	0.9	0.8	0.6	0.9	0.6	0.9
Uvigerina peregrina		1.3	0.6	1.7	0.7		1.1		0.6		0.4
Uvigerina sp											
Valvulineria bradyana	0.8	1.3	0.6	2.2			0.5	0.6			